PRAIRIE ISLAND
NUCLEAR POWER PLANT

QUALIFICATION OF REACTOR PHYSICS METHODS
FOR
APPLICATION TO PI UNITS
NSPNAD-8101-A
Rev. 1

December 1982

NORTHERN STATES POWER COMPANY
NUCLEAR ANALYSIS DEPARTMENT



8702050373 870130
PDR ADOCK 05000282
P PDR

FEB 2 2 1983

UNITED STATES
NUCLEAR REGULATORY COMMISSION
WASHINGTON, D. C. 20555

FEB 17 1983

Docket Nos. 50-282
and 50-306

Mr. D. M. Musolf
Nuclear Support Services Department
Northern States Power Company
414 Nicollet Mall - 8th Floor
Minneapolis, Minnesota 55401

Dear Mr. Musolf:

The staff has completed the review of Technical Reports NSPNAD-8101P Rev. 1 and NSPNAD-8102P Rev. 1 (except for the COBRA-IIIC/MIT and a portion of the DYNODE P/3 Code) that was submitted by letter dated February 18, 1982 and revised by letter dated December 13, 1982. Our review of the COBRA-IIIC/MIT has progressed sufficiently to permit you to use the code for evaluating the thermal-hydraulic hot channel parameter for the Unit 2 Cycle 8 reload analysis. However, the mass and energy release data from the DYNODE P/3 Code serving as input to the CONTEMPT-LT Code for analyzing the containment pressure transient during a steam line break accident is not qualified since we have not reviewed DYNODE for this application.

We find the revised reports to be an acceptable method for analyzing future reloads and operation for the Prairie Island Nuclear Generating Plant, Unit Nos. 1 and 2 subject to these limitations and others listed in the conclusion of our safety evaluation.

A copy of the Safety Evaluation is enclosed.

Sincerely,

Robert A. Clark, Chief
Operating Reactors Branch #3
Division of Licensing

Enclosure:
Safety Evaluation

cc: See next page

Northern States Power Company

cc:

Gerald Charnoff, Esquire
Shaw, Pittman, Potts and Trowbridge
1800 M Street, N.W.
Washington, D. C. 20036

Mr. Louis J. Breimhurst
Executive Director
Minnesota Pollution Control Agency
1935 W. County Road B2
Roseville, Minnesota 55113

Mr. R. L. Tanner
County Auditor
Red Wing, Minnesota 55066

U. S. Environmental Protection Agency
Federal Activities Branch
Region V Office
ATTN: Regional Radiation
Representative
230 South Dearborn Street
Chicago, Illinois 60604

Mr. E. L. Watzl, Plant Manager
Prairie Island Nuclear Generating Plant
Northern States Power Company
Route 2
Welch, Minnesota 55089

Jocelyn F. Olson, Esquire
Special Assistant Attorney General
Minnesota Pollution Control Agency
1935 W. County Road B2
Roseville, Minneosta 55113

U.S. Nuclear Regulatory Commission
Resident Inspectors Office
Route #2, Box 500A
Welch, Minnesota 55089

Regional Administrator
Nuclear Regulatory Commission, Region III
Office of Executive Director for Operations
799 Roosevelt Road
Glen Ellyn, Illinois 60137



UNITED STATES
NUCLEAR REGULATORY COMMISSION
WASHINGTON, D. C. 20555

SAFETY EVALUATION BY THE OFFICE OF NUCLEAR REACTOR REGULATION OF THE REACTOR PHYSICS AND RELOAD SAFETY EVALUATION METHODS TECHNICAL REPORTS NSPNAD-8101P AND -8102P FOR THE NORTHERN STATES POWER COMPANY PRAIRIE ISLAND NUCLEAR GENERATING PLANT, UNIT NOS. 1 AND 2

TABLE OF CONTENTS

		Page No.
1.	Introduction	1
2.	Summary of Reports	1
	(A) Qualification of Reactor Physics Methods for Application to Prairie Island Units NSPNAD-8101P Rev. 1	1
	(B) Reload Safety Evaluation Methods for Application to Prairie Island Units NSPAD-8102P Rev. 1	3
3.	Discussion and Evaluation	6
	(A) Qualification of Reactor Physics Methods for Application to Prairie Island Units NSPNAD-8101P Rev. 1	6
	(B) Reload Safety Evaluation Methods for Application to Prairie Island Units NSPAD-8102P Rev. 1	10
	1. General Physics Methods (Section 2 NSPNAD-8102P Rev. 1)	11
	2. Safety Evaluation Methods (Section 3 NSPNAD-8101P Rev. 1)	12
4.	Conclusion	25
5.	Tables	27
6.	Figures	29
7.	References	80

1. Introduction

Northern States Power Company (NSP) the licensee, submitted two Technical Reports titled "Qualifications of Reactor Physics Methods for Application to PI Units NSPNAD-8101P Rev. 1" and "Reload Safety Evaluation Methods for Application to PI Units NSPNAD-8102P Rev. 1" by letter dated February 18, 1982 and revised by letter dated December 13, 1982. The licensee proposes to use these reports as guides to analyze future reloads and operations starting with Cycle 8 of Unit 2 (i.e., scheduled in August 1983) at the Prairie Island Nuclear Generating Plant, Unit Nos. 1 and 2. Report No. NSPNAD-8101P addresses the qualification of reactor physics methods that cover reactor model description, qualification and quantification of reliability factors as applied to operation and fuel reloads for the Prairie Island Nuclear Generating Plant, Unit Nos. 1 and 2. Report No. NSPNAD-8102P addresses methods for calculating specific physics parameters and their comparison to bounding values used in the postulated accident analysis. This report also gives the licensee's experience on the safety analysis and calculational results for the Prairie Island units. The Revision 1 of both reports issued by the licensee's letter dated December 13, 1982 includes all of the staff's comments which resulted from the review of the initial versions of these reports. The purpose of our review is to assure that the licensee has established acceptable methods for analyzing future reloads and operations at the Prairie Island Nuclear Generating Plant, Unit Nos. 1 and 2.

2. Summary of Reports

A. Qualification of Reactor Physics Methods for Application to Prairie Island Units NSPNAD-8101P Rev. 1

This report describes the reactor physics methods used by Northern States Power Company (NSP) for their analysis of the Prairie Island (PI) Nuclear Reactors. The report addresses the reactor model description, the qualification and quantification of reliability factors, and the application of the physics methods to both reactor operations and to reload safety evaluations.

The computer model used to analyze Prairie Island is the Advanced Recycle Methodology Program (ARMP) developed by Nuclear Associates International Corporation (NAI) under the sponsorship of Electric Power Research

Institute (EPRI). The ARMP computer system is composed of individual computer programs including the following physics related ones:

1. EPRI-CELL, a spectral code which is used to generate initial and burnup dependent nuclide concentrations and few group neutron cross sections.

2. PDQ7/HARMONY, a two-dimensional diffusion-depletion code which is used to calculate local peaking factors as well as for generating input data for the three-dimensional nodal code.

3. DP5, a three-dimensional nodal code which is a derivative of the EPRI-NODE-P code and is used to obtain core power distributions as well as core physics parameters such as control rod worths and reactivity coefficients.

4. CPM, a multi-group collision probability transport code which is used to provide lumped absorber data for burnable poisons and control rods.

5. CASMO II, a spectral code which is used to generate initial and burnup dependent nuclide concentrations and few group neutron cross sections.

Two models based on ARMP are used to analyze the Prairie Island reactors. The first is used for Cycles 3 through 6. The second model is identical to the first with the exception that the EPRI-CELL program is replaced with CASMO II which was developed by Studsvik Energiteknik AB. This model is used for Cycles 5 and 6 and will be used to analyze future cycles. These models are verified by benchmarking against Prairie Island measurements for several cycles of operation. Reliability factors, describing the allowances to be used in safety related calculations to assure conservatism, and uncertainty factors, describing the actual model accuracy, are evaluated by direct comparison of calculations to experimental data. The following physics parameters are addressed:

1. control rod worths (and critical boron concentrations),

2. isothermal temperature coefficient,

3. Doppler coefficient,

4. local, nodal and assembly power distributions,

5. burnup dependent isotopic compositions, and

6. delayed neutron parameters.

For each parameter addressed, the data base is presented, including comparisons between calculations and measurements as well as the uncertainty and reliability factors of the calculation. Conclusions are drawn regarding the suitability of the model to perform the calculations.

B. Reload Safety Evaluation Methods for Application to Prairie Island Units NSPNAD-8102P Rev. 1

This report describes the calculational methods for the specific physics parameters used in each cycle reload for accident analyses. Section 2 of this report describes the procedures of these calculational methods for each specific physics parameter. These specific physics parameters and their comparison to bounding values used in the accident analysis are as follows:

1. Moderator Temperature Coefficient

2. Power Reactivity Coefficient

3. Doppler Reactivity Coefficient

4. Boron Reactivity Coefficient

5. Shutdown Margin

6. Scram Reactivity

7. Nuclear Heat Flux Hot Channel Factor

8. Nuclear Enthalpy Rise Hot Channel Factor

9. Effective Delayed Neutron Fraction

10. Prompt Neutron Lifetime

Section 3 of the report describes the methods in which these physics parameters are applied to each accident or transient in order to determine whether or not any reanalysis is required. For each accident or transient, the following are considered in the application of these physics parameters:

1. Definition of Accident - a brief description of the causes and consequences.

2. Accident Analysis - a brief description of the methods employed and discussion of the sensitive physics parameters. Included is a list of the acceptance criteria.

3. Licensee's Safety Analysis Experience - a brief summary of the licensee's calculational experience and results of the comparison of their models to the Prairie Island Final Safety Analysis Report.

4. Cycle Specific Physics Calculations - a description of the specific physics calculations performed each cycle for the purposes of a reload safety evaluation.

5. Reload Safety Evaluation - A description of the comparison of the cycle specific physics characteristics and the bounding values used in the safety analysis. Specific application of the model reliability factors and biases are also addressed.

In addition, Section 3 of the licensee's report (NSPNAD-8102P Rev. 1) addresses the specific accidents and transients which are considered in the safety evaluation methods. These accidents and transients are as follows:

- Uncontrolled Rod Cluster Control Assembly (RCCA) Withdrawal from Subcritical

- Uncontrolled RCCA Withdrawal at Power

- Control Rod Misalignment

- Dropped Control Rod

- Uncontrolled Boron Dilution

- Startup of an Inactive Loop
- Feedwater System Malfunction
- Excessive Load Increase
- Loss of External Load
- Loss of Normal Feedwater
- Loss of Reactor Coolant Flow (Pump Trip)
- Loss of Reactor Coolant Flow (Locked Rotor)
- Fuel Handling Accident
- Main Steam Line Break
- Ejected Rod
- Loss of Coolant
- Fuel Misloading

The licensee's report also describes the computer programs that are used to simulate the response of the nuclear steam supply system (NSSS) and the thermal-hydraulic response of the hot coolant channel and hot spot in the core for the above listed transients and accidents when applicable. The computer programs that are used by the licensee in the analysis of these accidents and transients are as follows.

(a) DYNODE-P/3

The DYNODE-P Version 3 program is used to analyze the transient response of the Nuclear Steam Supply System (NSSS). This program provides a simulation of the core average power, the core average fuel temperature and the core average coolant channel thermal-hydraulic responses.

(b) COBRA-IIIC/MIT

The COBRA-IIIC/MIT is used to analyze the transient response of the hot channel in the core. This program provides a simulation of the thermal-hydraulic response of coolant channels and associated fuel rods within the core.

(c) CONTEMPT-LT

The CONTEMPT-LT program is used to compute the temperature-pressure response of the containment during a steam line break accident.

(d) TOODEE2

The TOODEE2 program is used to compare the temperature response of the hot fuel spot for certain accidents which include the hot fuel rod and the associated coolant channels. This program is used only if the COBRA-IIIC/MIT hot channel analysis shows a departure from nucleate boiling ratio (DNBR) that is less than the value corresponding to the 95% probability limit at a 95% confidence level.

3. Discussion and Evaluation

A. Qualification of Reactor Physics Methods for Application to Prairie Island Units NSPNAD-8101P Rev. 1

We have reviewed the information presented with regard to calculational methods and comparison of calculations and experiments. Although the ARMP computer system was used to analyze the Prairie Island cores, the report emphasizes the implementation of the NSP ARMP model since the detailed code descriptions are available in the EPRI ARMP documentation, "Advanced Recycle Methodology Program System Documentation," CCM-3 Research Project 118-1, September 1977. Therefore, we did not review the ARMP system, per se, but rather the qualification of its use in determining physics parameters for application to the Prairie Island cores.

Many of the computer programs used in the ARMP system are acceptable industry-wide codes and, therefore, require no additional review. These include the GAM, THERMOS, and CINDER programs which form the neutron cross

section generator, EPRI-CELL, as well as the two-dimensional diffusion-depletion program, PDQ7/HARMONY. We also find that the three-dimensional nodal code, DP5, is acceptably verified by comparisons to measured Prairie Island data over four cycles of operation. CASMO II is a suitable replacement for EPRI-CELL for future cycles although the data base for Cycles 5 and 6 is somewhat limited.

Control rod worth values are obtained from k-effectives and control rod positions computed by the nodal code. These are compared to worths obtained by measuring critical boron concentrations at various stages of rod insertion. The standard deviation of the differences between measured and calculated critical boron concentrations, hence control rod worths, is 1.0% for the CASMO/PDQ/DP5 model. For conservatism, however, a rod worth reliability factor of 10% is assumed. This is acceptable and is consistent with currently approved design methods.

Isothermal temperature coefficients are computed by varying the core average temperature in three-dimensional nodal calculations while holding all other parameters constant. These are compared to isothermal temperature coefficient measurements made with the plant reactivity computer. Based on these comparisons, we conclude that the NSP ARMP model predicts the isothermal temperature coefficient with a reliability of 2.9×10^{-5} $\Delta k/k$ per degree F when the appropriate bias is included. This represents a 95% probability at the 95% confidence level that the measured isothermal temperature coefficient is bounded by the predicted value. This is acceptable and is consistent with currently approved design methods.

The three-dimensional nodal code is used to calculate power coefficients as a function of power and exposure. The Doppler coefficient is then calculated by removing the moderator temperature coefficient component from the power coefficient. However, the uncertainty in the measurement of the Doppler coefficient with the plant reactivity computer is too large to quantify a reliability factor. However, U-238 resonance integrals calculated by CPM and by EPRI-CELL have been compared with experimental values obtained by AB Atomenergi and were well within the 4% experimental uncertainties associated with the measurements. Comparisons of temperature coefficients are also within the 10% experimental uncertainties associated with the measurements. A 10% reliability factor for the Doppler coefficient and a 20% reliability factor for the Doppler defect is, therefore, defined by the licensee. This is

acceptable since it is consistent with currently approved design methods. Also, comparisons of EPRI-CPM and CASMO calculations with experiments conducted in the KRITZ high temperature critical facility in Sweden corroborate the 10% reliability factor on the Doppler coefficient for the CASMO/PDQ/DP5 model.

Either of the spectral codes, EPRI-CELL or CASMO II, produces initial nuclide concentrations, depletion and fission product chain data, and tables of microscopic and macroscopic cross sections varying with burnup. Based on the good agreement between isotopic compositions calculated by both EPRI-CELL and CASMO and spent fuel isotopic data from Yankee Rowe and Saxton, we conclude that either method is acceptable for determining isotopic compositions.

Comparisons to measured data spanning Cycles 3 through 6 of Prairie Island operation are used to determine the uncertainties applicable to nodal power distributions. Since the reactor power distribution is not directly observable, the licensee's ARMP model has been used to calculate the actual incore detector signals in each of the instrumented locations. These measured reaction rates are local values measured at 61 axial locations in each instrument thimble. The three-dimensional calculational model using EPRI-CELL as the cross section generator were compared to reaction rate measurements over Cycles 3 through 6 for full power conditions representative of beginning, middle, and end of cycle. Calculations using CASMO II as the cross section code were compared to reaction rate measurements over Cycles 5 and 6 for full power conditions representative of beginning, middle, and end of cycle. The nuclear heat flux hot channel factor, F_Q, is defined as the maximum local fuel rod linear heat generation rate (LHGR) divided by the average fuel rod LHGR. It is computed by multiplying peak nodal values from the three-dimensional nodal DP5 results by the two-dimensional PDQ7 pin-to-box ratios. The calculated and measured reaction rates are local values and are, therefore, proportional to F_Q. The staff also agrees that the uncertainty determined from comparisons of measurements and calculations for the instrument thimble and detector is the same as the uncertainty that would be determined for a fuel pin if that pin could be instrumented. Therefore, the observed differences between calculated and measured flux detector reaction rates can be assumed to be the same as that which would be obtained between the calculated and measured local F_Q values and can be used to determine the calculational reliability factor for F_Q.

The calculational reliability factor for F_Q is defined as a single value, ΔF_Q, such that the calculated value of F_Q at any core location plus ΔF_Q has a 95% probability at a 95% confidence level of being conservative with respect to the measured F_Q at that location. A bounding reliability factor based on the value obtained at higher reaction rates has been used by the licensee. The reliability factors determined are .067 with a .007 bias using the EPRI-CELL model and .062 with a .015 bias using the CASMO II model. The derivation and use of this bounding calculational reliability factor for F_Q is acceptable.

The nuclear enthalpy rise hot channel factor, $F_{\Delta H}$, is defined as the ratio of the integral of linear power along the rod on which the minimum DNBR occurs to the core average integral power. It is calculated by multiplying the nodal assembly average power values by the PDQ7 peak pin-to-box ratios. As was the case with F_Q, the calculation reliability factor for $F_{\Delta H}$ is based on comparisons of measured and predicted in-core flux detector signals. For $F_{\Delta H}$, however, the measured rate is obtained by integrating the 61 measured axial locations for each instrument thimble. Unlike the case for F_Q, the $F_{\Delta H}$ values were found to exhibit no dependence on power. The reliability factors determined are .035 using the EPRI-CELL model and .044 using the CASMO II model. No calculational bias was observed. The reliability factor is applied as an additive factor to the calculated $F_{\Delta H}$ since it is derived from the differences of absolute reaction rates. We find the derivation and the use of the calculational reliability factor for $F_{\Delta H}$ is acceptable.

The determination of the reliability factors for the effective delayed neutron fraction, β_{eff}, is somewhat different than that for previous parameters since these values can be calculated but not measured. The licensee determines the calculational uncertainty for β_{eff} by considering the experimental and calculational uncertainties in its major components. The staff agrees with the assumed uncertainties and with the important components of β_{eff}. We, therefore, find the presented reliability factor of 4% for β_{eff} acceptable and appropriate for other delayed neutron parameters as well.

In conclusion, we have reviewed the report within the guidelines provided by Section 4.3 of the Standard Review Plan. Included in our review was the description of the experimental data base, the calculations performed, and the comparisons made to support the conclusions that the licensee's ARMP computer model is adequate to calculate steady-state physics parameters for Prairie Island reload cores.

Based on our review we conclude that the ARMP reactor physics methods used by the licensee and benchmarked against Prairie Island measurements over several cycles of operation are acceptable to be used in Prairie Island safety related calculations for the following parameters:

a) control rod worths

b) temperature coefficients

c) Doppler coefficients

d) burnup dependent isotopic compositions

e) power distributions....

f) critical boron concentrations

g) delayed neutron parameters

We also find the detailed discussion and evaluation of the uncertainty and reliability associated with each physics parameter acceptable. The application of the reliability factors and biases for each parameter is shown in Table 1.

We requested that the licensee continue the comparison of measured and calculated physics parameters during each cycle in order to provide continued assurance of the model applicability. This request was discussed with and agreed to by the licensee.

Based on the above evaluation, we find the report titled "Qualification of Reactor Physics Methods for Application to PI Units NSPNAD-8101P Rev.1" submitted by the licensee is an acceptable method for performing operations and fuel reload analyses for Prairie Island Nuclear Generating Plant, Unit Nos. 1 and 2.

B. Reload Safety Evaluation Methods for Application to Prairie Island Units NSPNAD-8102P Rev. 1

The licensee, in conjunction with Nuclear Associates, has developed various safety analyses for the Prairie Island Nuclear Generating Plant, Unit

Nos. 1 and 2. The licensee's report (NSPNAD-8102P Rev. 1) shows representative calculations applicable for operations and reload evaluations. Our evaluation covers the licensee's methodology used for performing general physics calculations shown in Section 2 titled "General Physics Methods" and the methodology for analyzing plant transients for a variety of reactor and balance-of-plant malfunctions shown in Section 3 titled "Safety Evaluation Methods". Specifically our review covers evaluations of the plant accidents listed in Section 2B of this evaluation (Page 3) and the computer codes used to analyze these accidents. More than 100 graphical comparisons in Section 3 of the licensee's report showing the results of calculations using Westinghouse FSAR models versus the results of the licensee's computer codes were also reviewed by the staff. Our specific discussion and evaluations of the topics covered in the licensee's report NSPNAD-8102P, Rev. 1 and listed in this evaluation, Section 2B (Page 3), is as follows:

1. General Physics Methods (Section 2 NSPNAD-8102P Rev. 1)

The calculational methods used to determine the important cycle specific safety-related physics parameters and the parameters themselves are described in Section 2, NSPNAD-8102P Rev. 1. The physics parameters described are:

a. Moderator Temperature Coefficent

b. Power Reactivity Coefficient

c. Doppler Reactivity Coefficient

d. Boron Reactivity Coefficient

e. Shutdown Margin

f. Scram Reactivity

g. Nuclear Heat Flux Hot Channel Factor

h. Nuclear Enthalpy Rise Hot Channel Factor

i. Effective Delayed Neutron Fraction

j. Prompt Neutron Lifetime

We have reviewed the definitions of these parameters and find them consistent with both the staff and industry-wide practice and, therefore, are acceptable. The calculational procedures used to calculate these physics parameters are consistent with currently approved methods and are acceptable.

2. Safety Evaluation Methods (Section 3, NSPNAD-8102P Rev. 1)

(a) Uncontrolled Rod Cluster Control Assemblies (RCCA) Withdrawal from a Subcritical Condition

The uncontrolled RCCA withdrawal from a subcritical condition is an Anticipated Operational Occurrence for which the fuel integrity must not be violated. Therefore, no centerline melt nor DNB must occur. The event is analyzed using input assumptions consistent with the Prairie Island FSAR and the licensee's DYNODE-P/3 computer code. The NSSS simulation incorporates point kinetics (including delayed neutrons and decay heat), fuel, clad, and gap heat conduction, and channel coolant thermal-hydraulics. Reactivity effects due to moderator and fuel temperature (Doppler) variation as well as those due to control rod scram are included. A comparison with the FSAR results show that the licensee's model predicts higher temperatures while the nuclear power between the two calculations agrees well. Based on these results, we find the licensee's methods acceptable for calculating the uncontrolled RCCA withdrawal transient from a subcritical condition if a cycle specific reanalysis is required.

Cycle specific physics calculations are performed at the most limiting core conditions during the cycle for the following parameters: (1) Doppler coefficient, (2) moderator temperature coefficient, (3) maximum reactivity insertion rate, (4) scram reactivity, and (5) effective delayed neutron fraction. Each of these parameters is adjusted to include the model reliability factors and biases derived in NSPNAD-8101P Rev. 1 which we find acceptable (note Section 3A of this SER). We find the key physics parameters selected to be appropriate for the transient. We also find the specific physics calculations performed each cycle to determine these key physics parameters acceptable. In addition, the determination of whether each parameter should be greater than or less than its corresponding value used in the reference analysis in order to be considered bounded, is acceptable.

(b) Uncontrolled Rod Cluster Control Assemblies (RCCA) Withdrawal at Power

The uncontrolled RCCA withdrawal from power is also an anticipated operational occurrence and, therefore, must not violate the fuel integrity. The reactivity insertion rate determines which protection system trip will initiate termination of the accident. Therefore, both a fast rate, which results in a high power trip, and a slow rate, which results in either an overtemperature trip or a high pressurizer level trip, are analyzed and compared to the Prairie Island FSAR results. For the fast reactivity rate, the licensee's calculation indicates a more severe temperature and pressure response but, in general, shows the same trends as the FSAR results. For the slow reactivity rate, the licensee's results predict a slower power ramp and slower pressure and temperature increases although the maximum values differ by only 3% or less. The minimum DNBR calculated by the licensee, however, is about 17% higher and, hence, less conservative, than the FSAR value. A further evaluation of the acceptability of the licensee's method for predicting minimum DNBR for this transient is made in our review of the COBRA-IIIC/MIT code discussed below (Note Page 23 of this SER).

Cycle specific physics calculations are performed at the most limiting core conditions during the cycle for the following parameters: (1) Doppler coefficient, (2) moderator temperature coefficient, (3) maximum reactivity insertion rate, (4) scram reactivity, and (5) nuclear enthalpy rise hot channel factor ($F_{\Delta H}$). Each of these parameters is adjusted to include the model reliability factors and biases derived in NSPNAD-8101P Rev. 1 which we find acceptable (note Section 3A of this SER). We find the key physics parameters selected to be appropriate for the transient. We also find the specific physics calculations performed for each cycle to determine these key physics parameters acceptable. In addition, the determination of whether each parameter should be greater than or less than its corresponding value used in the licensee's analysis in order to be considered bounded, is acceptable.

(c) Control Rod Misalignment

In this anticipated operational occurrence, one or more RCCAs are assumed to be displaced from the normally allowed position. Full power operation under these conditions could lead to a reduction in DNBR. The licensee has analyzed this occurrence using input consistent with the Prairie

Island FSAR and predicts a minimum DNBR of 1.47, about 6.5% higher than the FSAR result. Based on these results, we find the licensee's methods acceptable for calculating RCCA misalignment events when a cycle specific reanalysis is required.

The important cycle specific physics parameter is the nuclear enthalpy rise hot channel factor ($F_{\Delta H}$) and the maximum value is conservatively calculated with Bank D fully inserted and one RCCA of Bank D fully withdrawn.

We have reviewed the accident definition, the analytical methods and assumptions used, the important physics parameters selected, the specific physics calculations performed each cycle, and the bounding values used in the safety analysis, and find them to be acceptable.

(d) Control Rod Drop

For this anticipated operational occurrence a single RCCA is assumed to drop into a fully inserted position in the core. The drop may or may not result in a reactor trip. If the reactor is brought to full power with the fully inserted RCCA, a reduction in core thermal margins could result because of an increased hot channel peaking factor. The licensee's analysis shows a minimum DNBR of 1.934 as compared to the FSAR calculated value of 1.9. Although the licensee's results agree well with the FSAR analysis, they do not consider the concerns involving several aspects of the RCCA drop event which presently require operating restrictions on many Westinghouse-designed reactors including the Prairie Island units. This operating restriction, based on analyses of control rod drop events, is addressed in our letter dated November 28, 1979 to all affected licensees (Reference 1).

The most important cycle specific physics parameter is the resulting $F_{\Delta H}$ for the DNB evaluation, which is adjusted to include the model reliability factor derived in NSPNAD-8101P Rev. 1 which we find acceptable (note Section 3A of this SER).

We have reviewed the accident definition, the analytical methods and assumptions used, the important physics parameter selected, the specific physics calculations performed each cycle, and the bounding values used in the safety analysis, and find them acceptable with the above mentioned operating restrictions in effect.

(e) Control Rod Ejection

The RCCA ejection accident is analyzed by the licensee and compared to the results reported by Westinghouse (Reference 2) for zero power (BOL and EOL) and full power (BOL and EOL) initial conditions. A point kinetics model is used with reactivity feedbacks corrected by weighting factors to account for the spatial dimensions not included in the model. The thermal-hydraulic model includes a multi-nodal radial model of fuel, gap, and clad conduction, and a multi-nodal axial model of the coolant channel. The comparison shows that the licensee's results agree well for the zero power cases and are more conservative for the full power cases. We, therefore, find the licensee's method for analyzing this event to be acceptable.

(f) Fuel Handling Accident

The licensee has addressed the fuel handling accident related to sudden releases of gaseous fission products held in the voids between the fuel pellets and the cladding of one fuel assembly. If a fuel handling accident were to occur, the release would be in the containment or auxiliary building. Such a release would activate the special ventilation system containing an absolute and a charcoal filtration system. The licensee stated that, when calculating offsite exposure from a potential accident, the discharge to atmosphere is assumed to be at ground level from the auxiliary building to maximize the offsite doses. We find this acceptable. Other aspects of the methods used by the licensee for analyzing a potentional fuel handling accident were reviewed by the staff.

Radiological Consequences of Accidents For Which Fuel Failure is Predicted

Based on this review, the licensee has not furnished sufficient information related to extended fuel burnup and increased specific power of the fuel assemblies. Increases in burnup and fuel specific power beyond the traditional ranges covered in the Regulatory Guides and Standard Review Plan could affect the radiological consequences of some or all of the accidents for which fuel failures are predicted by changes in fuel failure rates, changes in total inventory and mix of radioisotopes in the fuel, the fraction of isotopes accumulated in the fuel-clad gaps, iodine spiking behavior, and the effect of fuel rod gas pressure on decontamination factors assumed for fuel handling accidents. The consequences of these effects due to burnup and fuel specific power must be demonstrated to be within the Standard Review Plan guidelines. The licensee stated that in order

to demonstrate that the offsite dose guidelines are met, the methods in NSPNAD-8102P Rev. 1 assume that the calculations used for the off-site doses in the FSAR are valid. These methods were reviewed and found acceptable by the staff prior to granting the operating license for those conditions of burnup and specific power expected. In addition, the licensee by letter dated December 13, 1982, has committed to evaluate the releases for burnups up to and beyond 37,000 MWD/MTU batch average exposure. The licensee at this time will also evaluate any increases in fuel assembly specific power levels from those previously analyzed. The results of these evaluations will be submitted for NRC staff review prior to June 1, 1983 and the licensee will include batch average burnup and specific power as bounding parameters in their methodology documents for every accident where fuel failure might be predicted to occur. The licensee does not plan to use the methodology in NSPNAD-8102P Rev. 1 before the Unit 2 Cycle 8 reload which is scheduled to begin in August 1983. Based on the licensee's commitment, we find that the methods for evaluating radiological consequences of accidents for which fuel failure can occur in NSPNAD-8102P Rev. 1 are adequately addressed and are acceptable.

(g) Nuclear Steam Supply System Transients and Malfunctions

The licensee, in conjunction with Nuclear Associates International (NAI), developed models for performing various safety analyses involving the plant transients and malfunctions for the Prairie Island Nuclear Generating Plant, Unit Nos. 1 and 2. These analyses include representative calculations for potential accidents of importance for a typical reload evaluation. The licensee's report (NSPNAD-8102P Rev. 1) addresses the methodology for analyzing plant transient behavior based on these models for a variety of reactor and balance of plant accidents. We have performed a detailed review of these results. The reactor and balance of plant accidents that appear in the licensee's report are as follows:

- Uncontrolled Boron Dilution
- Startup of an Inactive Loop
- Feedwater System Malfunction
- Excessive Load Increase
- Loss of External Load
- Loss of Normal Feedwater
- Loss of Reactor Coolant Flow - Pump Trip

- Loss of Reactor Coolant Flow - Locked Rotor
- Main Steam Line Break
- Loss of Coolant

In performing the transient analyses, the licensee utilized the DYNODE-P code under a license agreement with NAI, the developer of the DYNODE-P/3 code. Results calculated by the licensee using the DYNODE-P/3 code were compared with previous Westinghouse evaluations as documented in the Prairie Island FSAR. The licensee provided more than 100 graphical comparisons to illustrate the validity of the DYNODE-P/3 code.

Although the licensee did not include the analysis of the steam generator tube rupture event as part of the submittal in NSPNAD-8102P Rev. 1, a separate analysis was performed to gain confidence in the use of DYNODE-P/3 code. The report titled "Using RETRAN-02 and DYNODE-P to Analyze Steam Generator Tube Breaks", NSAC-47, issued in May 1982, was used as a basis for qualifying the DYNODE-P/3 code for analyzing a steam generator tube rupture event for the Prairie Island Plant. The staff considers the NSAC-47 report to be a significant milestone in establishing confidence in a methodology capable of performing post-accident analysis of an actual steam generator tube rupture event (a severe transient event for a PWR). The report shows that good agreement can be achieved between the analytical results and actual plant data obtained during the transient that occurred at Prairie Island Unit 1 on October 2, 1979. In addition, RETRAN-02 was also used in our evaluation of the DYNODE-P/3 code. The RETRAN code is a derivation of the RELAP code that the staff has found to be an adequate tool for audit calculations when properly used to model selected reactor plant transient behavior. RELAP has been used in both "conservative" and "best estimate" modes and the staff has confidence that RETRAN, because of its derivation, is also an adequate tool when properly used.

Based on the above, the staff reviewed the results from the NSAC-47 report and the results from RETRAN-02 and DYNODE-P/3 in assessing the steam generator tube rupture event. The objective of the staff was (1) to establish an analytical link between the results of RETRAN-02 and DYNODE-P/3 codes by means of the NSAC-47 report and (2) to use the NSAC-47 results to provide a link between both codes and the data obtained during the Prairie Island steam generator tube rupture event. The comparison of

the DYNODE-P/3 code results with RETRAN-02 results and with plant data* for the Prairie Island steam generator tube rupture event is shown in Figures 1 thru 14. This comparison of results and data for key operating parameters illustrates the qualification process used for DYNODE-P/3. In some cases the DYNODE-P/3 results are more conservative than the results from RETRAN-02. This was as expected since RETRAN-02 was developed to less conservative conditions (i.e., "best estimate") as compared to DYNODE-P/3. Based on the comparisons, we conclude that the DYNODE-P/3 results reasonably agree with the results given by RETRAN-02 and with the actual plant data obtained during the steam generator tube rupture event.

Following the review of the capability of the DYNODE-P/3 code to analyze the steam generator tube break event, a comparison audit of the DYNODE-P/3 code was made for eight selected malfunctions appearing in the licensee's report NSPNAD-8102P. This comparison audit compared the DYNODE-P/3 results generated by the licensee with the RETRAN-02 results generated by the NRC staff. The staff used the same initial system input conditions for RETRAN-02 as those used by the licensee for the DYNODE-P/3 code. The principal input parameters were reactor power level, coolant inlet enthalpy, core exposure (beginning or end of life) and trip set points (i.e., flow, temperature and pressure).

The eight accidents chosen for comparative technical audits were considered to be accidents which would encompass the range of technical severity of the types of calculations for which the licensee proposed to apply the DYNODE-P/3 code. The evaluation of DYNODE-P/3 for eight accidents that were audited by the staff is illustrated by the results shown in Figures 15 thru 50. In these examples the figures also show the FSAR results. Our evaluations of the transients (eight accidents) are as follows:

(1) Loss of Feedwater Heaters, Beginning of Life, Without Reactor Controllers Operating - Figures 15 thru 18

In this transient, the loss of feedwater heating causes an associated drop in core inlet temperature. In response to the drop in core average temperature, the doppler reactivity feedback attempts to drive the core power up until the core power matches the load demand and a new steady state level is reached. The RETRAN results show a higher increase

*The plant data were obtained from the Prairie Island plant computer which accumulated key data approximately 200 seconds preceding and following the reactor trip.

in power than the FSAR or DYNODE results for approximately the same decrease in core average temperature and the same doppler reactivity coefficient. This is due to the RETRAN calculations use a "best estimate" fuel cladding gap coefficient which is much larger than the conservatively small value used in the FSAR calculations. This larger coefficient causes a much faster response of the fuel temperature to the drop in the coolant temperature and hence a faster increase in power. Note the scaling on the plotted comparisons is somewhat deceiving and that the associated difference in peak power between the RETRAN and DYNODE calculations is only about 0.5%. The rest of the system parameters show reasonably good comparisons to the DYNODE results, given the difference in the power response. In this transient, the core power increase effect on DNBR is outweighed by the effect of the decrease in coolant temperature causing an increase in DNBR. Therefore, the minimum DNBR (MDNBR) occurs at the start of the transient and even though the RETRAN results are slightly more conservative than the DYNODE calculations, there will be no significant effect on MDNBR. On this basis, we conclude that DYNODE-P/3 is an acceptable tool for predicting the transient behavior of key parameters during this accident.

(2) Turbine Trip, Beginning of Life, with Reactor Controllers Operating - Figures 19 thru 23

The DYNODE results for this transient show good comparison to the FSAR results until the pressurizer relief valve setpoint is reached. The FSAR assumes an instantaneous opening of the relief valves which hold the pressure below the high pressure trip setpoint for approximately 10 seconds more. In the DYNODE analysis the reliefs are more realistically modeled with a 0.3 second opening delay and a two second stroke time. Note that even though the model is more realistic than the instantaneous opening used in the FSAR, the setpoints used in DYNODE, i.e., delay and stroke times, are conservative estimates of the actual times. This causes the DYNODE calculations to show a much faster pressurization rate after the relief valve setpoints are reached. The reactor trip setpoint is reached in approximately 2.5 seconds. The RETRAN results show a much slower initial pressurization rate which we attribute to the additional heat sink of the metal heat conductors. Therefore, the relief valve opening setpoint is reached approximately six seconds later in the transient. However, since the relief valves are modelled in RETRAN in the same way as they are in DYNODE, the time from when the relief setpoint

is reached to when the trip setpoint is reached, 3-4 seconds, is approximately the same as in the DYNODE analysis, as opposed to the ten seconds shown in the FSAR. The system behavior in general shows comparable trends between the RETRAN and DYNODE analysis. On this basis, we conclude that DYNODE-P/3 is an acceptable methodology for predicting the transient behavior of the key parameters during this accident.

(3) Turbine Trip, End of Life, With Reactor Controllers Operating - Figures 24 thru 28

This transient show similar behavior as in the beginning of core life with control case. In this case, however, both the RETRAN and FSAR analyses predict that the reactor does not trip whereas the DYNODE analysis shows a reactor trip on high pressure. In the FSAR, the pressure is held down due to the faster response of the relief valves. In the RETRAN case, the pressure is held below the trip setpoint due to the smaller initial pressurization rate. The results in general show comparable trends. We have concluded that DYNODE-P/3 adequately predicts the transient behavior for this accident.

(4) Turbine Trip, Beginning of Life, Without Reactor Controllers Operating - Figures 29 thru 33

In this case, the DYNODE results show good comparison to the FSAR since the relief valves are ignored in the analysis. The RETRAN results again show a smaller initial pressurization rate which causes the high pressure trip to occur slightly later. However, the system behavior shows similar trends. Also the RETRAN calculations do not predict an opening of the pressurizer safety valves. We have concluded that DYNODE-P/3 adequately predicts the transient behavior for this accident.

(5) Turbine Trip, End of Life, Without Reactor Controllers Operating - Figures 34 thru 38

This transient shows behavior similar to beginning of life without reactor controllers operating (Item 4 above) and the same concluding remark applies for this transient.

(6) Pump Trip, 1 of 2 Reactor Coolant Pumps - Figures 39 thru 42 and
(7) Pump Trip, 2 of 2 Reactor Coolant Pumps - Figures 43 thru 45

The following comments apply to both the 1 and 2 pump trip cases. The RETRAN results show very good comparison to the DYNODE calculations. The only differences are that in both cases the core power drops off much faster after the reactor trip signal in the RETRAN case. This is due to the fact that the RETRAN calculations use a best estimate trip curve with a greater total worth than the DYNODE or FSAR calculations. The DYNODE results in this case are therefore more conservative than the RETRAN results, as would be expected. We have concluded that DYNODE-P/3 adequately predicts the transient behavior for the key parameters for this accident.

(8) Main Steamline Break - Figures 46 thru 50

The RETRAN results show an associated cooldown rate of less than half of that predicted by DYNODE for the same break size. This slower cooldown is due to the fact that the RETRAN calculations include the effects of metal heat conductors. This large source of metal stored heat causes a much slower cooldown of the primary system. The pressurizer does not empty and the core just barely reaches criticality. The core goes critical much later in the transient and is quickly turned around by the high boron concentration of safety injection water causing a much lower peak heat flux and hence a larger margin of DNB. The DYNODE calculations are clearly much more conservative than the RETRAN results. On this basis, we have concluded that DYNODE-P/3 adequately predicts the transient behavior pertainng to the reactor and primary coolant system for the key parameters for this accident.

Based on our review, the qualification of the DYNODE-P/3 code is summarized as follows:

1. The license to operate the Prairie Island Nuclear Generating Plant, Unit Nos. 1 and 2 was predicated in part upon our acceptance of the transient results prepared by Westinghouse which appear in the Prairie Island Final Safety Analysis Report (FSAR). This acceptance of the transient results still applies since the plant has not been modified nor has the mode of operation changed in a manner that would affect the transient results.

2. The licensee's report NSPNAD-8102P Rev. 1 shows many comparisons of the transient results of the FSAR versus DYNODE-P/3 results. The DYNODE-P/3 code results show trends similar to those appearing in the FSAR for parameters important to reactor plant safety. Based on our review of these results, we have concluded that the DYNODE-P/3 code gives results that are either equivalent to or greater than the level of conservatism used in the FSAR for parameters important to reactor plant safety.

3. The staff spent many years developing and improving the RELAP codes and has used various versions of RELAP for audit calculations. As a result of this experience, we have gained confidence in the capability of the RELAP codes, when properly used, to model selected reactor plant transient behavior. Depending on the input assumptions and subroutines used, RELAP has been used in both "conservative" and "best estimate" modes. This level of confidence in RELAP also extends to RETRAN-02, which is derived from RELAP, and which has been designed for "best estimate" use by utilities. Our use of the RETRAN-02 code, as a means of auditing the results from the DYNODE-P/3 code shown in NSPNAD-8102P Rev. 1 was based on the staff's experience with and confidence in the RELAP and RETRAN codes. Our audit has shown that in all but one case, the DYNODE-P/3 code gives results that are equivalent to or greater than the level of conservatism given by RETRAN-02. In the case that exhibited a reduction in the level of conservatism, we determined that it has no safety significance to the reactor plant.

Based on the above evaluation we conclude that the DYNODE-P/3 code is an acceptable means for analyzing transients caused by a single steam generator tube rupture in a Westinghouse 2-loop reactor such as those existing at the Prairie Island facility. In addition, the DYNODE-P/3 code is acceptable for analyzing of transients caused by accidents described above and in the licensee's report, NSPNAD-8102P Rev. 1. This acceptance is contingent upon the completion of an audit of the licensee's administrative control procedures for the computer code quality assurance. The responsibility for this quality assurance audit is assigned to the NRC Region IV office. The Region IV audit will be initiated during January 1983 and is scheduled for completion by March 1983.

(h) Reactor Core Thermal-Hydraulic Hot Channel Analysis (COBRA-IIIC/MIT)

As shown in the NSPNAD-8102P Rev. 1 report, the licensee uses the COBRA-IIIC/MIT code to analyze the transient response of the hot channel in the core. The COBRA-IIIC/MIT code simulates the thermal-hydraulic response in the coolant channel of fuel rods within the core. The thermal-hydraulic hot channel analysis is performed for each transient to assure that the minimum DNBR is not reached. While we have not completed our review of the licensee's submittal dealing with the application of COBRA-IIIC/MIT for the analysis of the transient responses of the hot channels in the core, our review has progressed sufficiently to indicate that the results from COBRA-IIIC/MIT code gives a reasonable approximation, if not a conservative analysis of the limiting fuel assembly in the core. Consequently, we conclude that the licensee may use COBRA-IIIC/MIT for evaluating the thermal-hydraulic characteristics for the Prairie Island Unit 2 Cycle 8 reload analysis of the hot channel in order to assure that the minimum DNBR limit is not violated.

(i) Reactor Fuel Hot Spot Analyses for Certain Accidents - TOODEE2 Code

The TOODEE2 code developed by the NRC staff is a two dimensional, time dependent fuel element thermal analysis program. The primary object of this program is to calculate fuel element thermal response during post-LOCA refill and reflood in a PWR such as the facilities at Prairie Island. However, this code may also be used for certain non-LOCA transients with appropriate assumptions and input data. The code provides, as output, the fuel and cladding temperatures and the energy deposited into the fuel during transients.

The licensee's methodology in NSPNAD-8102P Rev. 1 applies the TOODEE2 code for analyzing non-LOCA transients including the postulated locked rotor and rod ejection accidents. The publicly-available version of the TOODEE2 code (NUREG-75/057) is used by the licensee to compute the transient temperature response of the hot channel for a number of transients and accidents. The code is used to demonstrate that coolability criteria continues to be satisfied when the hot channel condition analyzed by the COBRA-IIIC/MIT code yields an unfavorable DNBR. According to SRP 4.2, the fuel coolability criteria for non-LOCA accidents must include cladding embrittlement and violent expulsion of fuel. For cladding embrittlement, the Prairie Island FSAR uses a cladding maximum temperature

limit of 2700°F for some transients, e.g., locked rotor. For violent expulsion of fuel, a radially averaged enthalpy limit of 280 cal/g deposited into fuel is observed.

Since the TOODEE-2 code was originally not intended to be used for non-LOCA analyses, the licensee demonstrated that the results from TOODEE2 for limiting transients are indeed compatible to those previously analyzed in the FSAR.

For the two accidents analyzed in this manner, the results shown in NSPNAD-8102P Rev. 1 (Figures 3.12-6 for locked rotor; 3.15-2 and 3.15-4 for rod ejection) indicate that TOODEE2 calculations are consistent with the original calculations supporting the FSAR analyses. The initial and boundary conditions were taken from the FSAR. The transient conditions for power, core inlet flow, core inlet temperature, and pressure-dependent coolant saturation temperature were obtained from the DYNODE-P/3 code, which we find acceptable (note 3.8.2.(g)). For the cladding surface heat transfer coefficient, the licensee calculated the lowest value (with respect to time and axial location) of the Sandberg correlation used in the FSAR through an iterative process. When the lowest value of heat transfer coefficient was determined, this value was input to the TOODEE2 code as a constant for all time and axial locations to calculate the cladding surface temperature. This procedure was described in the licensee's letter dated January 4, 1983 (D. M. Musolf to NRR). Because of the assumption of cosine axial power shape, the highest cladding temperature always occurs at the core midplane of the hot channel, which reaches DNB first.

We have reviewed the NSP methodology of using TOODEE2 for non-LOCA transients and accidents identified in NSPNAD-8102P Rev. 1. Although only two accidents (locked rotor and rod ejection) were analyzed for benchmarking, we believe that TOODEE2 can be used for other similar events with conservative assumptions and appropriate initial as well as boundary conditions as described in the submittals. We, therefore, find the licensee's application of TOODEE2 acceptable for analyzing transient temperature response and energy deposited into the fuel at a hot channel for non-LOCA accidents such as those described in NSPNAD-8102P Rev. 1 in order to satisfy fuel coolability limits.

(j) Containment Temperature-Pressure Response During a Steam Line Break (CONTEMPT-LT)

The licensee calculated the containment response to postulated main steam line break (MSLB) accidents using the computer code CONTEMPT-LT/026 which requires the mass and energy release input data obtained from the DYNODE-P/3 computer code. The heat transfer correlations used in CONTEMPT-LT/026 by the licensee were taken from the Westinghouse Topical Report WCAP-8327, Containment Pressure Analysis Code (COCO) which we find acceptable for benchmark comparison. However, the correlations are more suitable for minimum containment pressure analyses following loss of coolant accidents rather than for the peak containment pressure analysis following MSLB accidents. Current guidelines in SRP Section 6.2.1.1.A, which refers to NUREG-0588 (Appendix B) recommends that the Uchida heat transfer correlation should be used for MSLB accidents while in the condensing mode, and that a natural convection heat transfer coefficient should be used in the non-condensing mode.

The CONTEMPT-LT/026 code calculates the containment pressure, temperature, thermodynamic state, and heat transfer as a function of time, following postulated pipe break accidents inside containment. As stated in Standard Review Plan (SRP) Section 6.2.1, the CONTEMPT-LT code has been found acceptable by the staff for use in containment analysis. However, our review of the mass and energy release data from the DYNODE-P/3 code that serve as input data to the CONTEMPT-LT code is not complete at this time. Consequently, we cannot make a finding that the DYNODE-P/3 code is qualified for use in conjunction with the CONTEMPT-LT code to perform the containment pressure transient analyses during the main steam line break accident described in the licensee's report, NSPNAD-8102P Rev. 1 Section 3.14. Therefore, staff acceptance of the licensee's method for analyzing the containment pressure transient resulting from the main steam line break accident is deferred until the staff has had an opportunity to complete its review.

4. Conclusion

Based on the above evaluation, we find the reactor model description, qualification, and quantification of reliability factors addressed in the licensee's report, NSPNAD-8101P Rev. 1 to be acceptable. Therefore, the methods described in NSPNAD-8101P Rev. 1 can be used by the licensee in performing operations and fuel reload analyses for the Prairie Island Nuclear Generating Plant, Unit Nos. 1 and 2.

Based on our evaluation, we find that the general physics calculational methods in Section 2 of the licensee's report, NSPNAD-8102P Rev. 1 are acceptable and that the licensee may use these calculational methods for performing operations and fuel reload analyses for the Prairie Island Nuclear Generating Plant, Unit Nos. 1 and 2.

Based on our evaluation, we also find analyses of postulated accidents described in Section 3 of the licensee's report, NSPNAD-8102P Rev. 1 acceptable contingent upon the following limitations.

1. Acceptance of the computer codes referenced in the licensee's report, NSPNAD-8102P Rev. 1 is limited to analyzing only the type of accidents listed and described in the report. Therefore, any use of these codes for licensing analysis beyond the type of accident discussed in the licensee's report, NSPNAD-8102P Rev. 1 must be accompanied by the applicable qualification information.

2. Acceptance of the control rod drop accident does not cover the analysis of the control rod drop events addressed in our letter dated November 28, 1979.

3. Acceptance of the methods of analysis for radiological consequences of any accident with predicted fuel failures is predicated upon the licensee submitting information on the release rates and effects on the mix of nuclides for burnups up to and beyond 37,000 MWD/MTU batch average exposure which is acceptable to the staff. This information will also include any increases in fuel assembly specific power from those previously analyzed.

4. Acceptance of the DYNODE-P/3 code is contingent upon achieving a a satisfactory resolution of findings resulting from audit of the licensee's administrative control procedures for the computer code quality assurance. However, an interim use of the DYNODE-P/3 code for the Prairie Island Unit 2 Cycle 8 reload analysis is acceptable since our audit findings revealed only minor discrepancies in the administrative control procedures for the computer code quality assurance. These discrepancies have no adverse effects on the safety level of plant operations.

5. The mass and energy release data from the DYNODE-P/3 code that serves as input data to the CONTEMPT-LT code is not qualified at this time for use in performing the containment pressure transient analysis for the main steam line break accident.

Date: FEB 17 1983

5. Tables

TABLE 1

RELIABILITY FACTORS FOR PRAIRIE ISLAND

PARAMETER	RELIABILITY FACTOR	BIAS	USED TO COMPARE TO SAFETY VALUE
F_Q^N	$RF_{FQ} = 0.062$	.015	$F_Q^N = (F_Q^N(\text{Model}) \cdot RF_{FQ} \cdot \text{Bias } F_Q) * (1 \cdot T)$
$F_{\Delta H}$	$RF_{F\Delta H} = 0.044$	.0	$F_{\Delta H} = (F_{\Delta H}(\text{Model}) \cdot RF_{F\Delta H} \cdot \text{Bias } F_{\Delta H}) * (1 \cdot T)$
Rod Worth	$RF_{Rod} = 0.10$	0	$\Delta\rho_{rod} = (\Delta\rho_{rod}(\text{Model}) \cdot \text{Bias}) * (1 \pm RF_{rod})$
Temperature Coefficient (pcm/°F)	$RF_M = 2.9$	-.03	$\alpha_M = \alpha_M(\text{Model}) \cdot \text{Bias}_M \pm RF_M$
Doppler Coefficient	$RF_D = 0.10$	0	$\alpha_D = (\alpha_D(\text{Model}) \cdot \text{Bias}_D) * (1 \pm RF_D)$
Doppler Defect	$RF_{DD} = 0.20$	0	$DD = (DD\ (\text{Model}) \cdot \text{Bias}_{DD}) * (1 \pm RF_{DD})$
Boron Worth	$RF_B = 0.10$	0	$\alpha_B = (\alpha_B(\text{Model}) \cdot \text{Bias}_B) * (1 \pm RF_B)$
Delayed Neutron Parameters	$RF_\beta = 0.04$	0	$\beta_{eff} = (\beta_{eff}(\text{Model}) \cdot \text{Bias}_\beta) * (1 \pm RF_\beta)$
	$RF_{\ell^*} = 0.04$	0	$\ell^* = (\ell^*(\text{Model}) \cdot \text{Bias}_{\ell^*}) * (1 \pm RF_{\ell^*})$

6. Figures

DRAFT

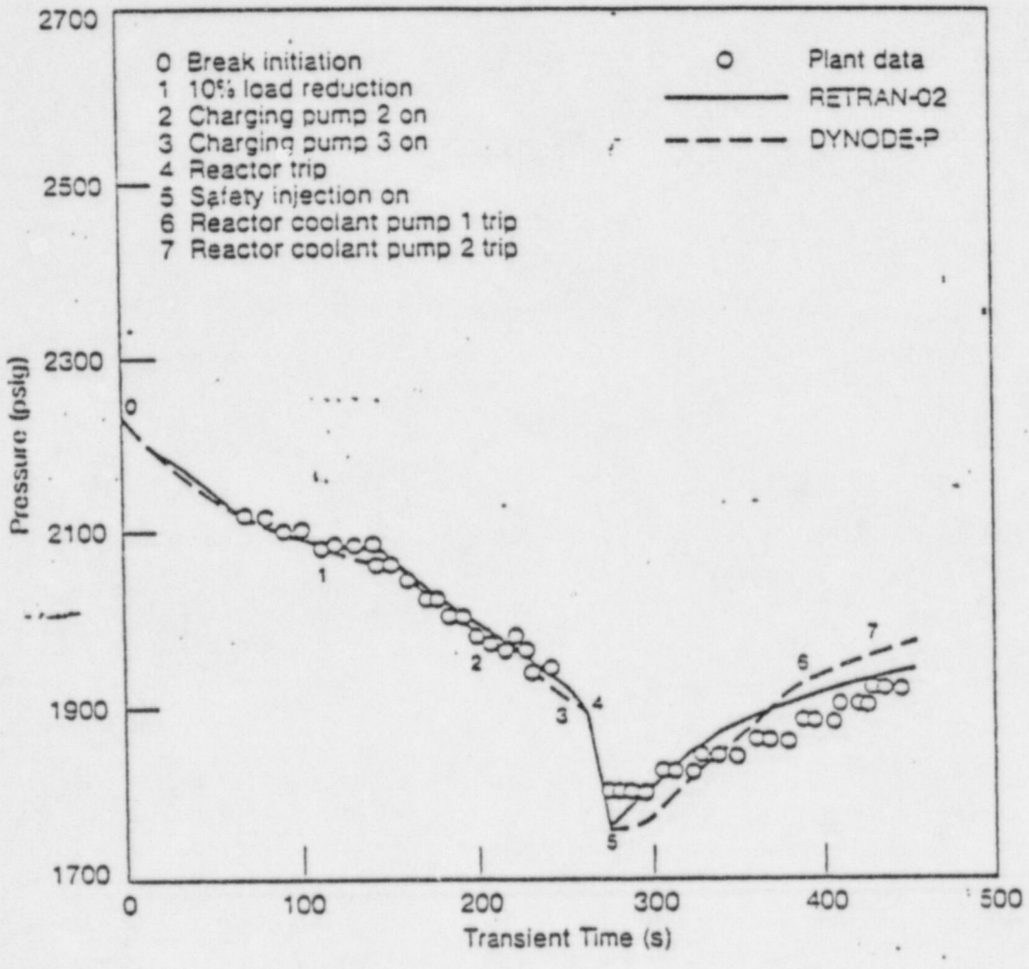


Figure 1. Reactor coolant system pressure.

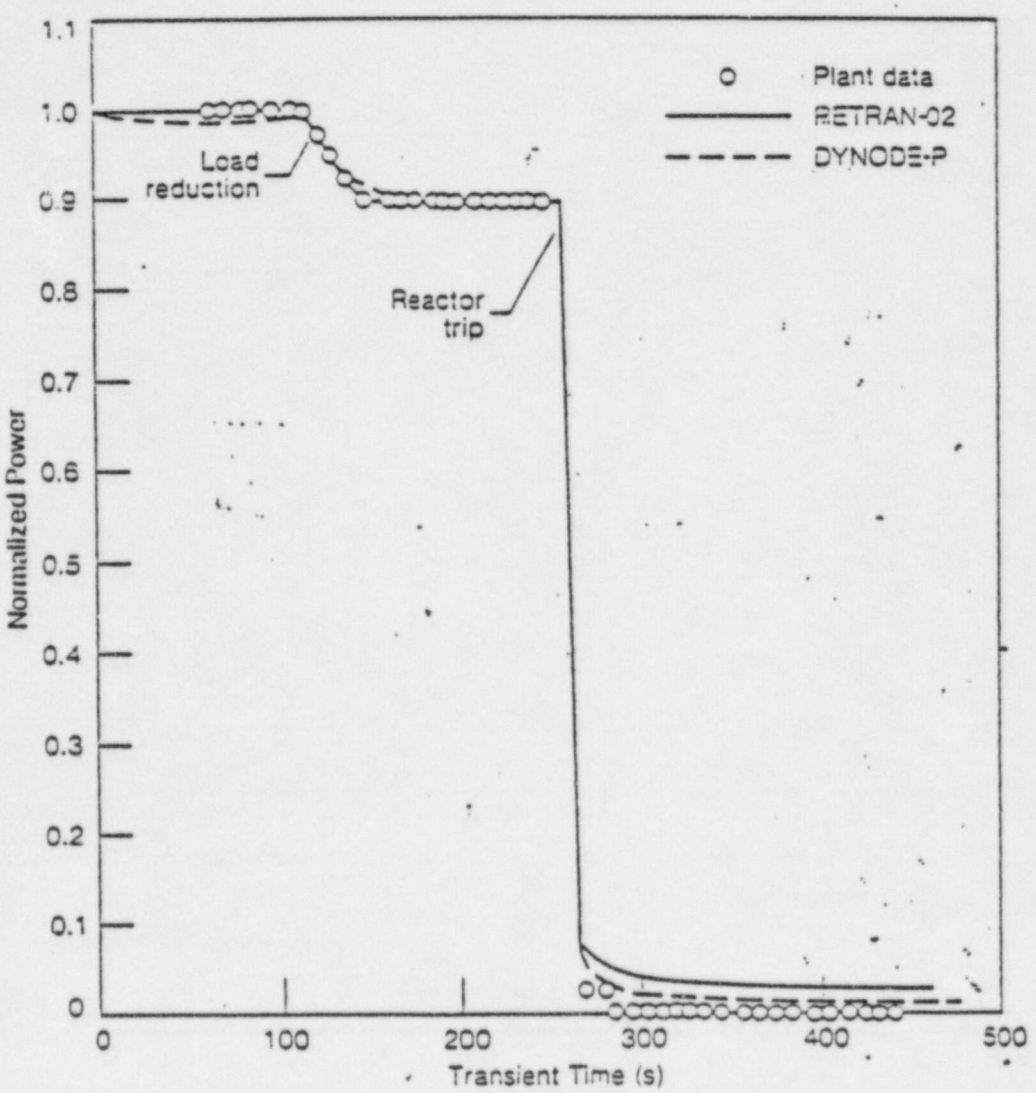


Figure 2. Normalized system power.

DRAFT

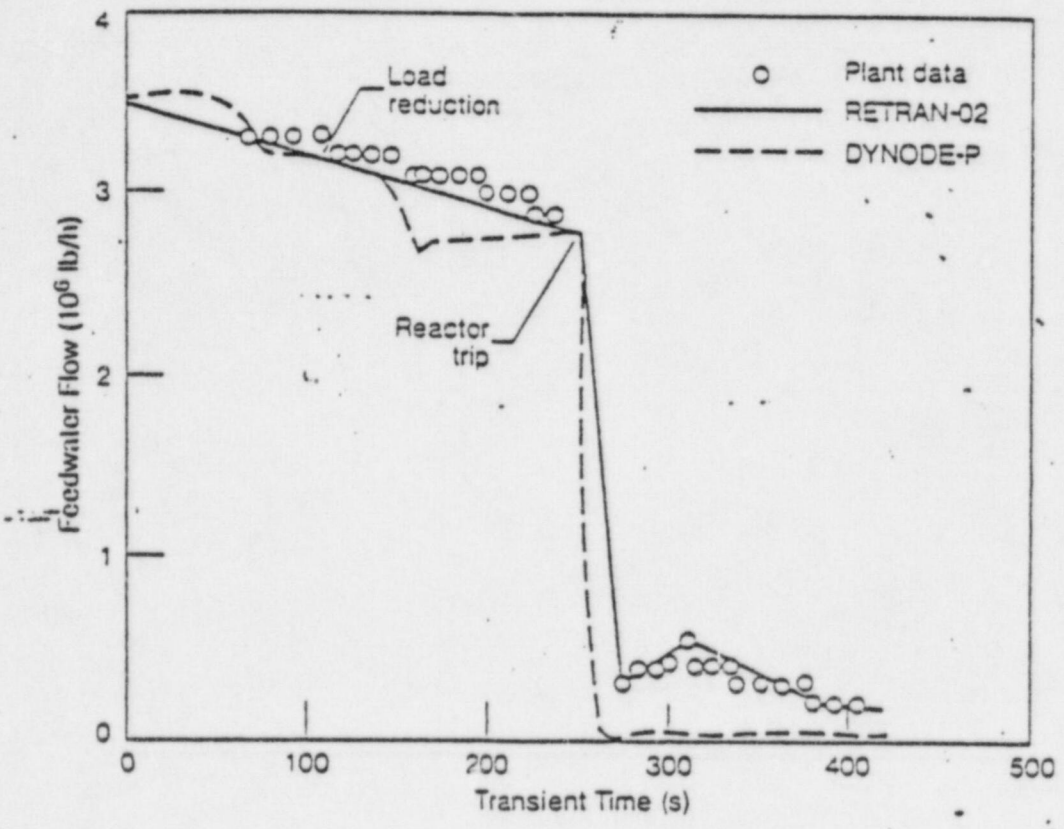


Figure 3. Loop A feedwater flow.

DRAFT

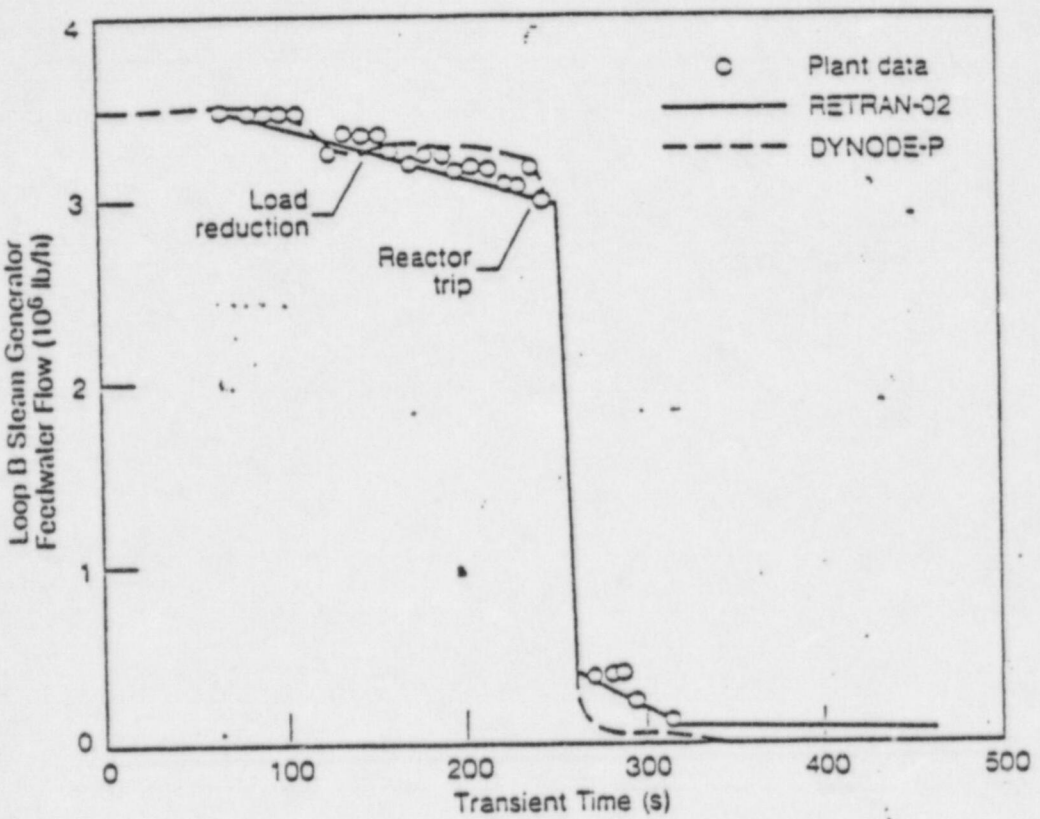


Figure 4. Loop B steam generator feedwater flow.

DRAFT

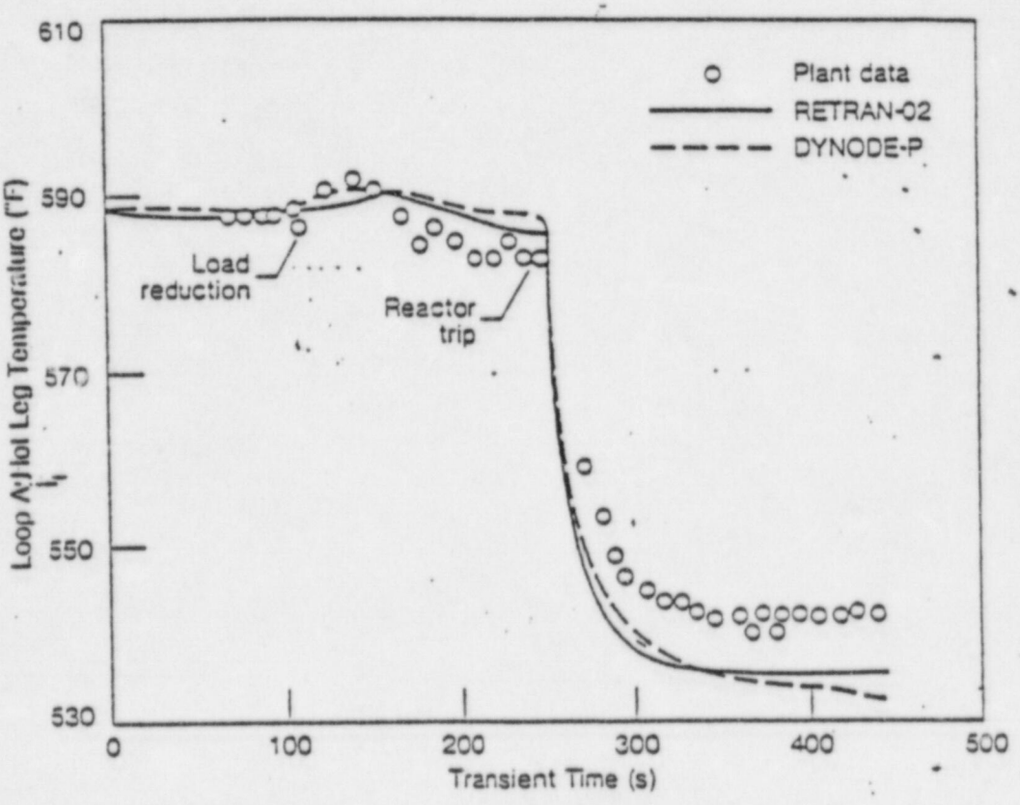


Figure 5. Loop A hot leg temperature.

DRAFT

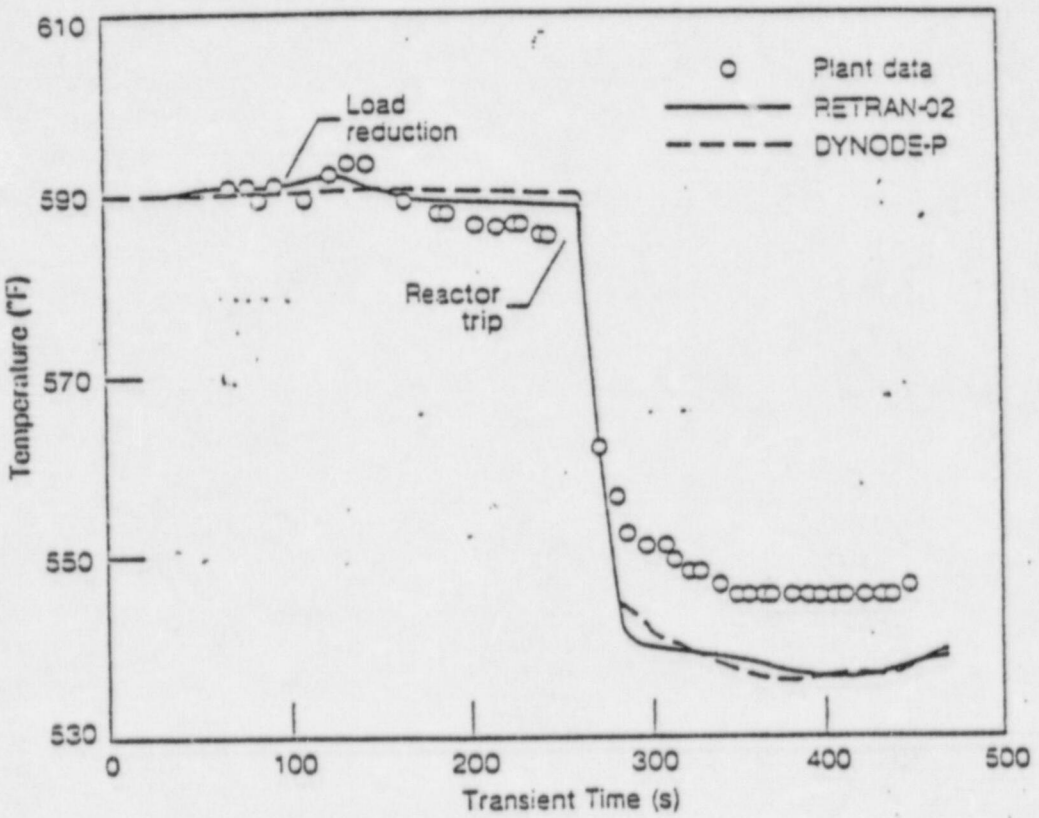


Figure 6. Hot leg temperature (Loop B).

DRAFT

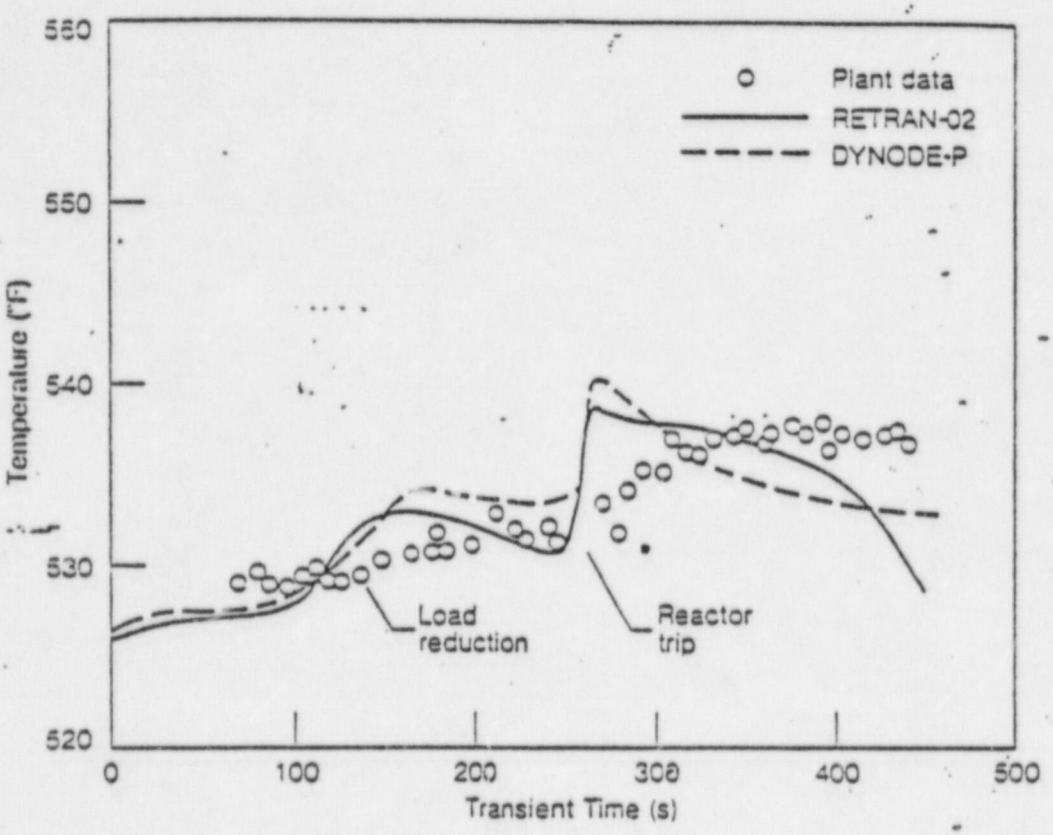


Figure 7. Loop A cold leg temperature.

DRAFT

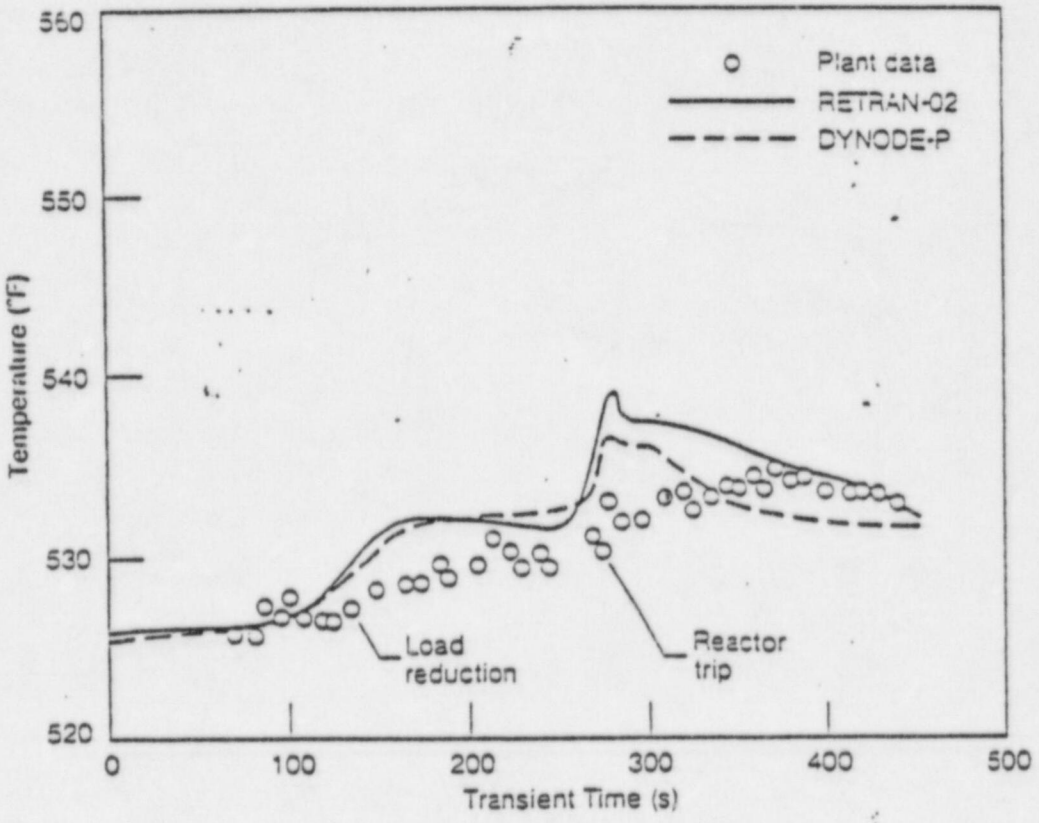


Figure 3. Loop B cold leg temperature.

DRAFT

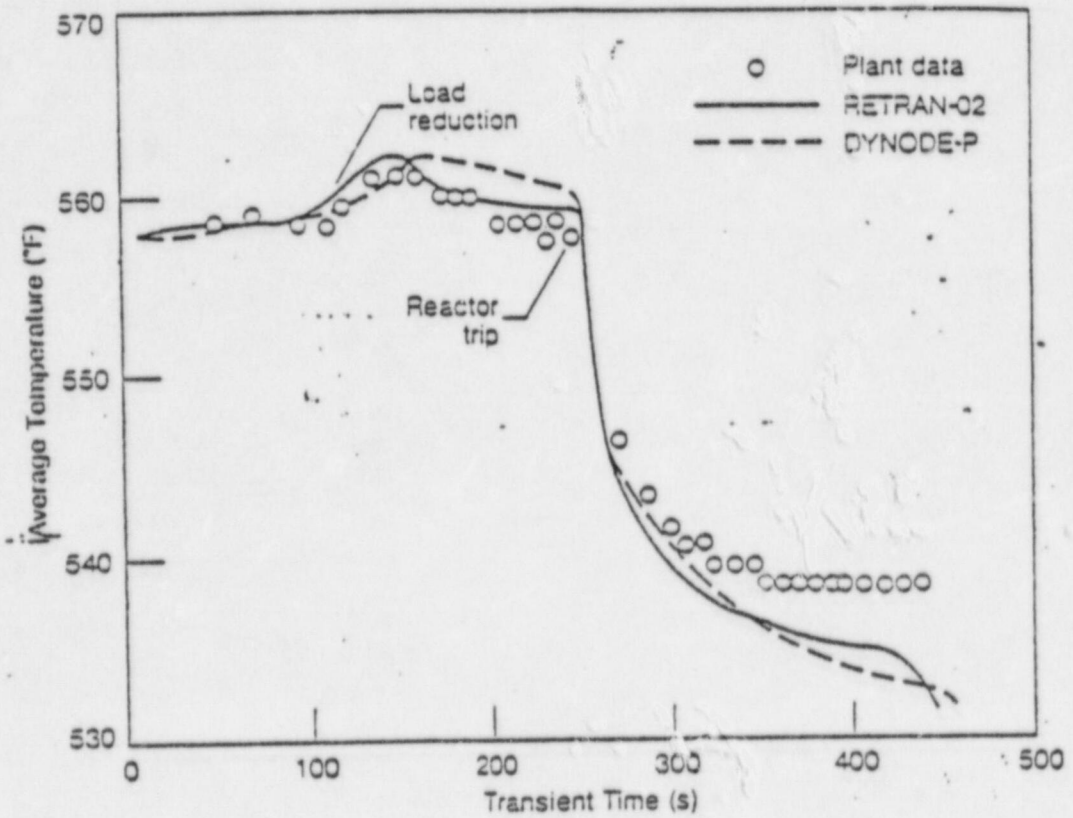


Figure 9. Loop A average temperature.

DRAFT

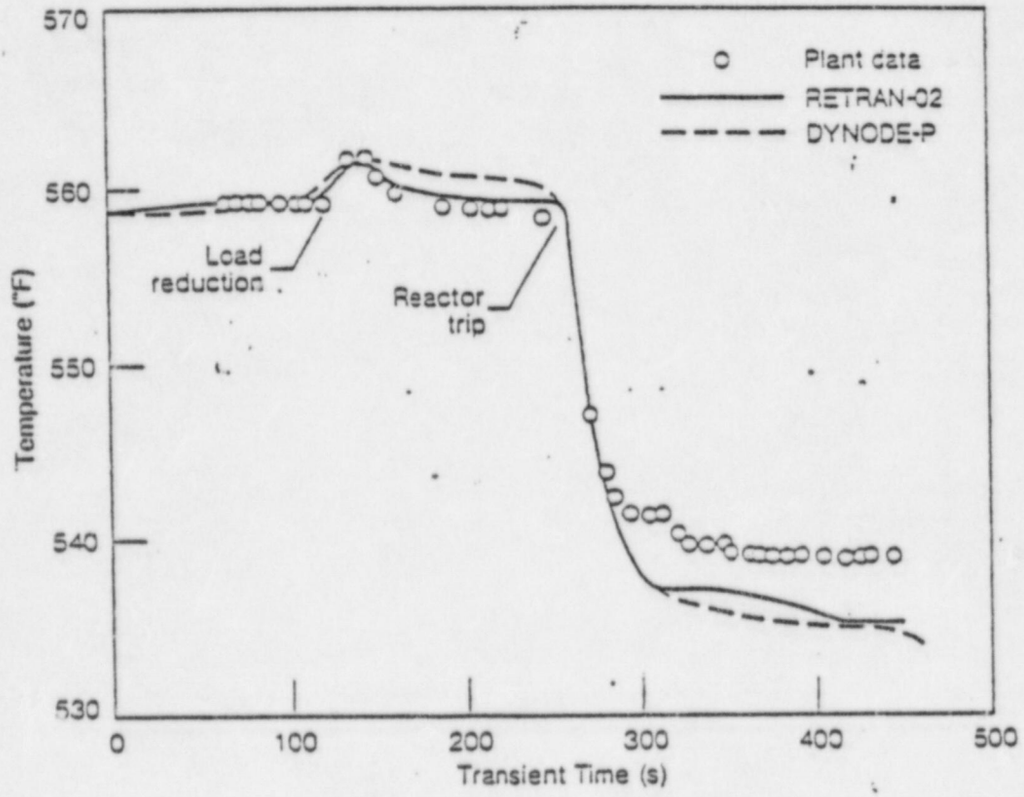


Figure 10. Loop B average temperature.

DRAFT

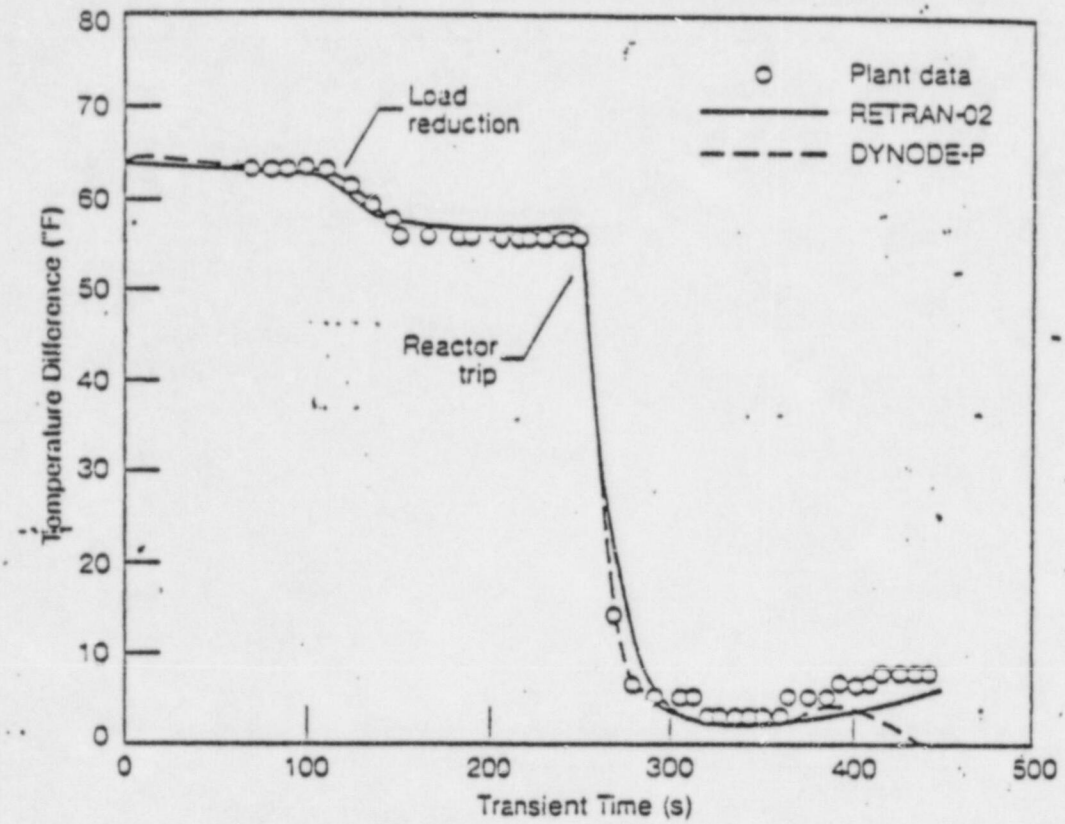


Figure 11. Loop A delta-T.

DRAFT

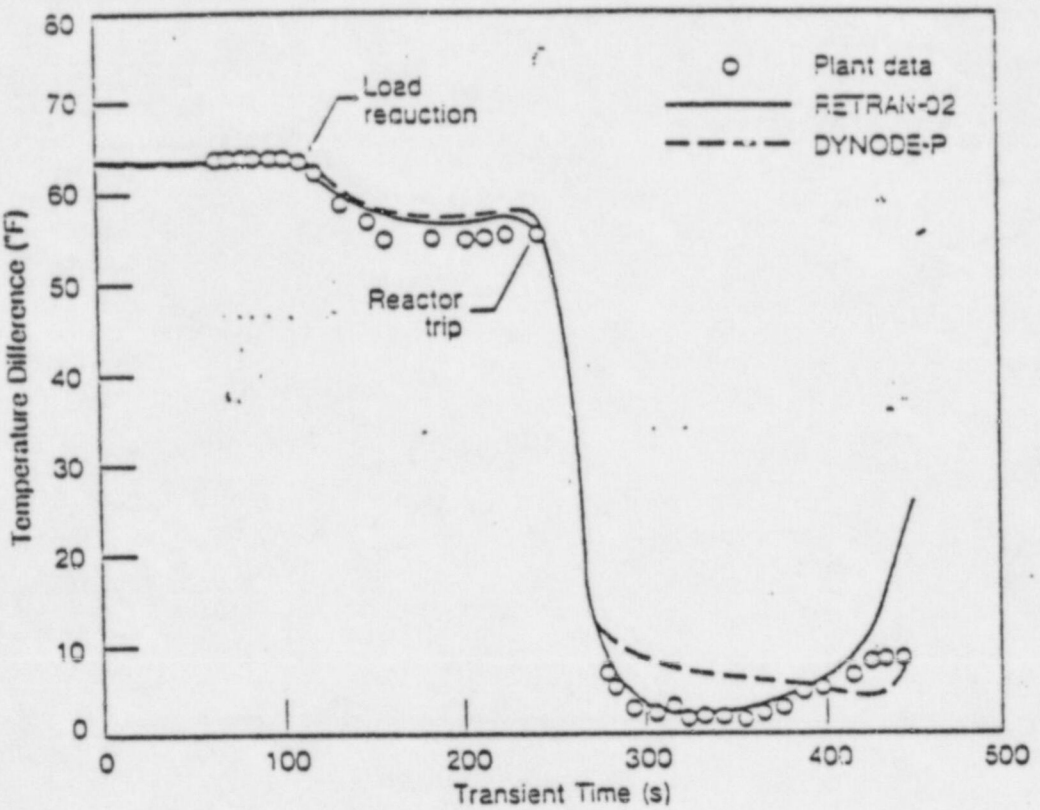


Figure 12. Loop B delta-T.

DRAFT

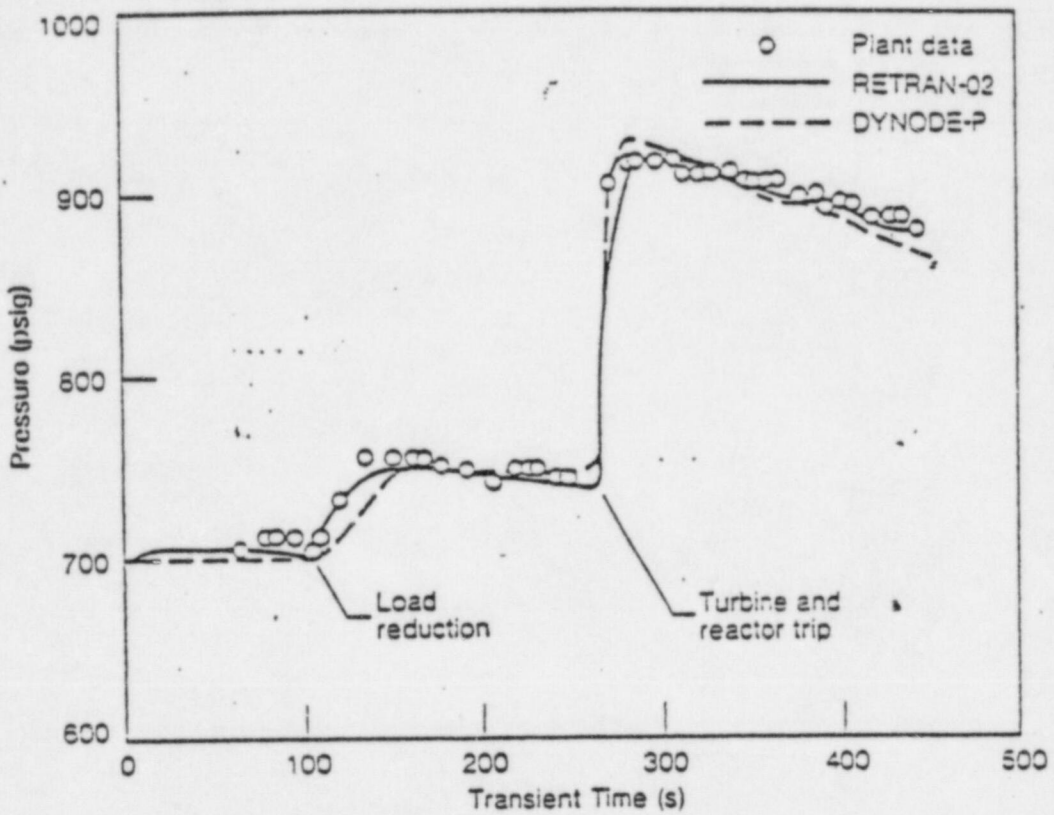


Figure 13. Steam generator pressure (Loop A).

DRAFT

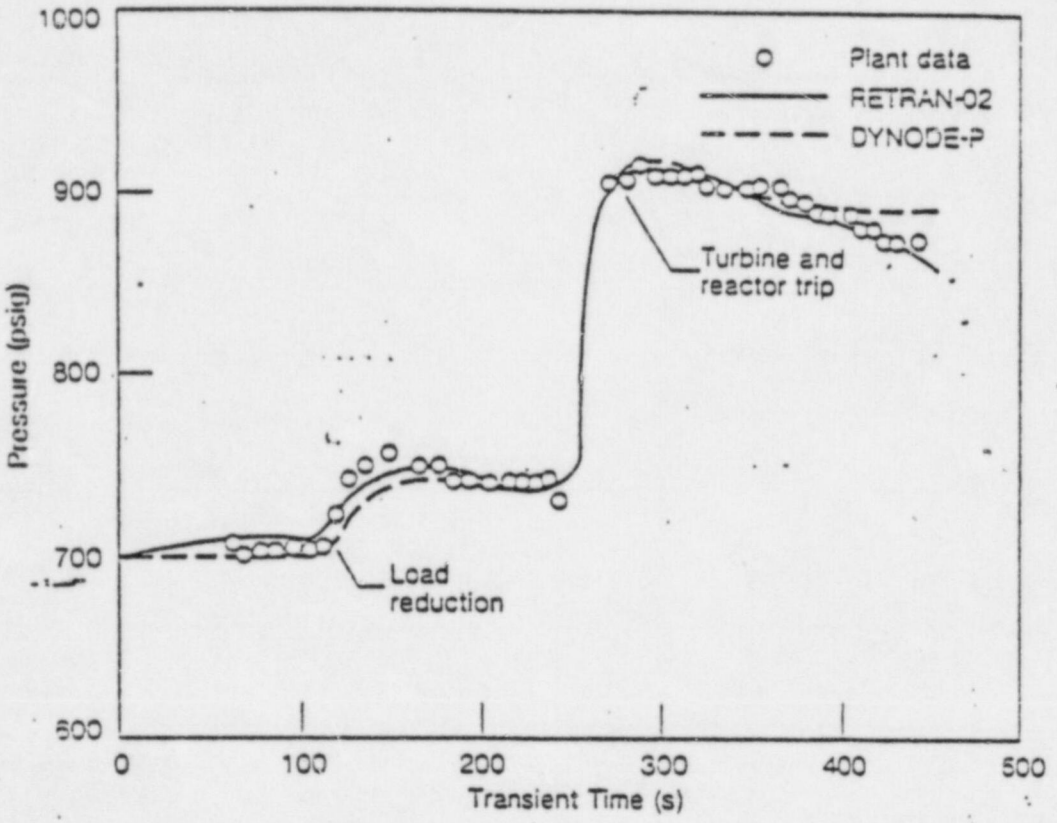


Figure 14. Steam generator pressure (Loop B).

FSAR Loss of Feedwater Heating
BOL Uncontrolled

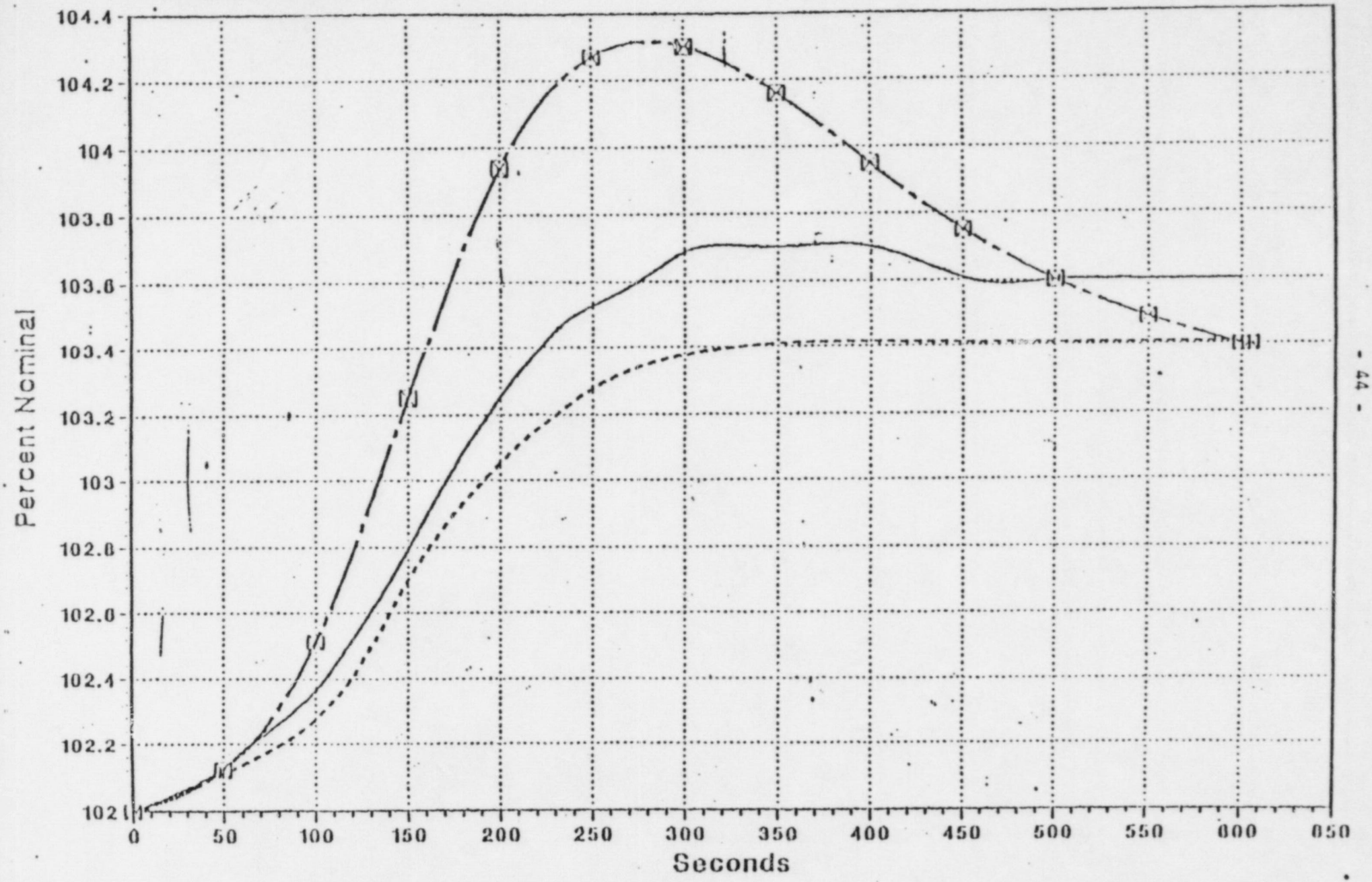


Figure 15

FSAR Loss of Feedwater Heating
BOL Uncontrolled

FSAR
NETRAN

Change in Pressurizer Pressure vs Time

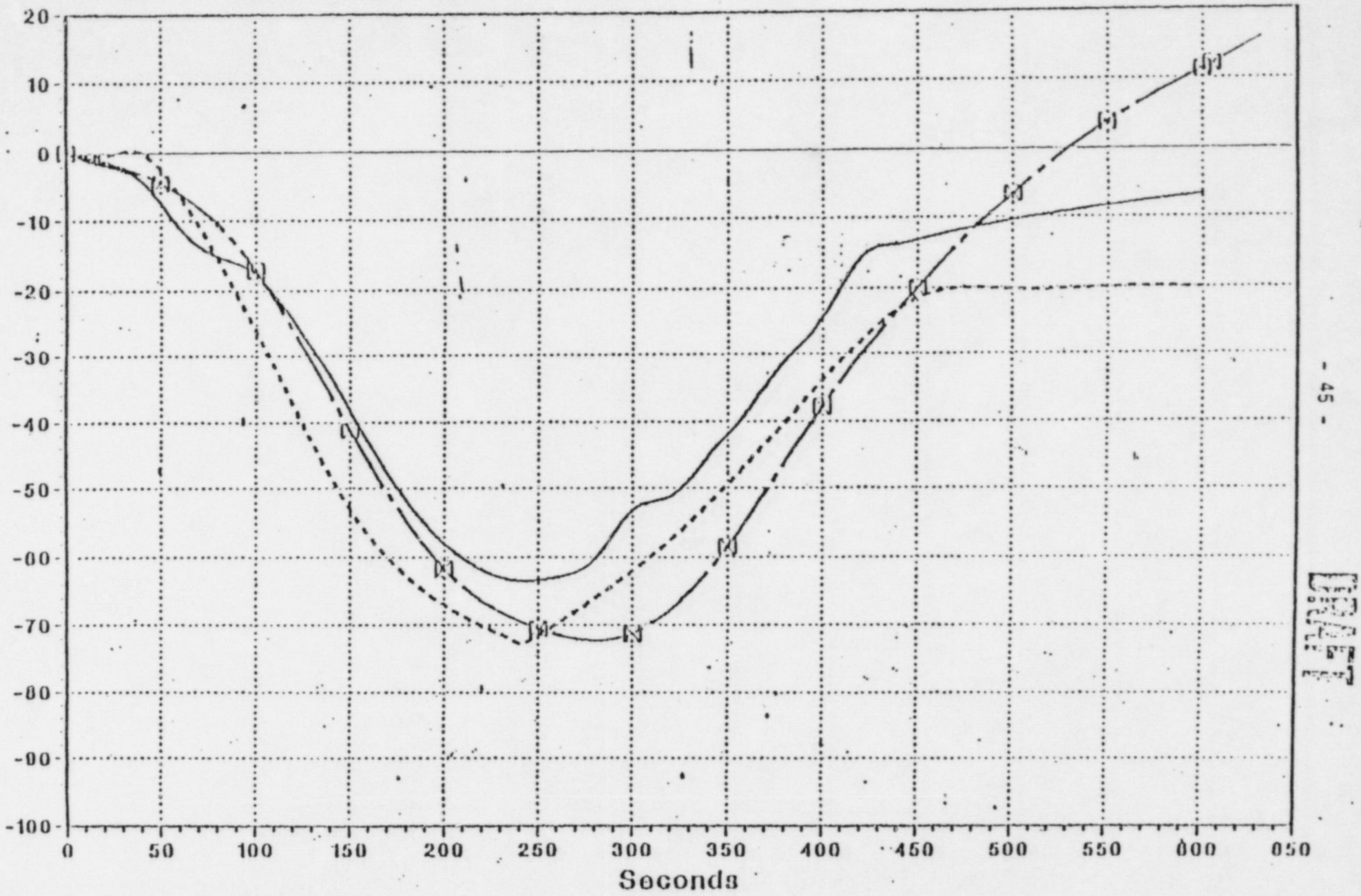


Figure 16

FSAR Loss of Feedwater Heating
BOL Uncontrolled

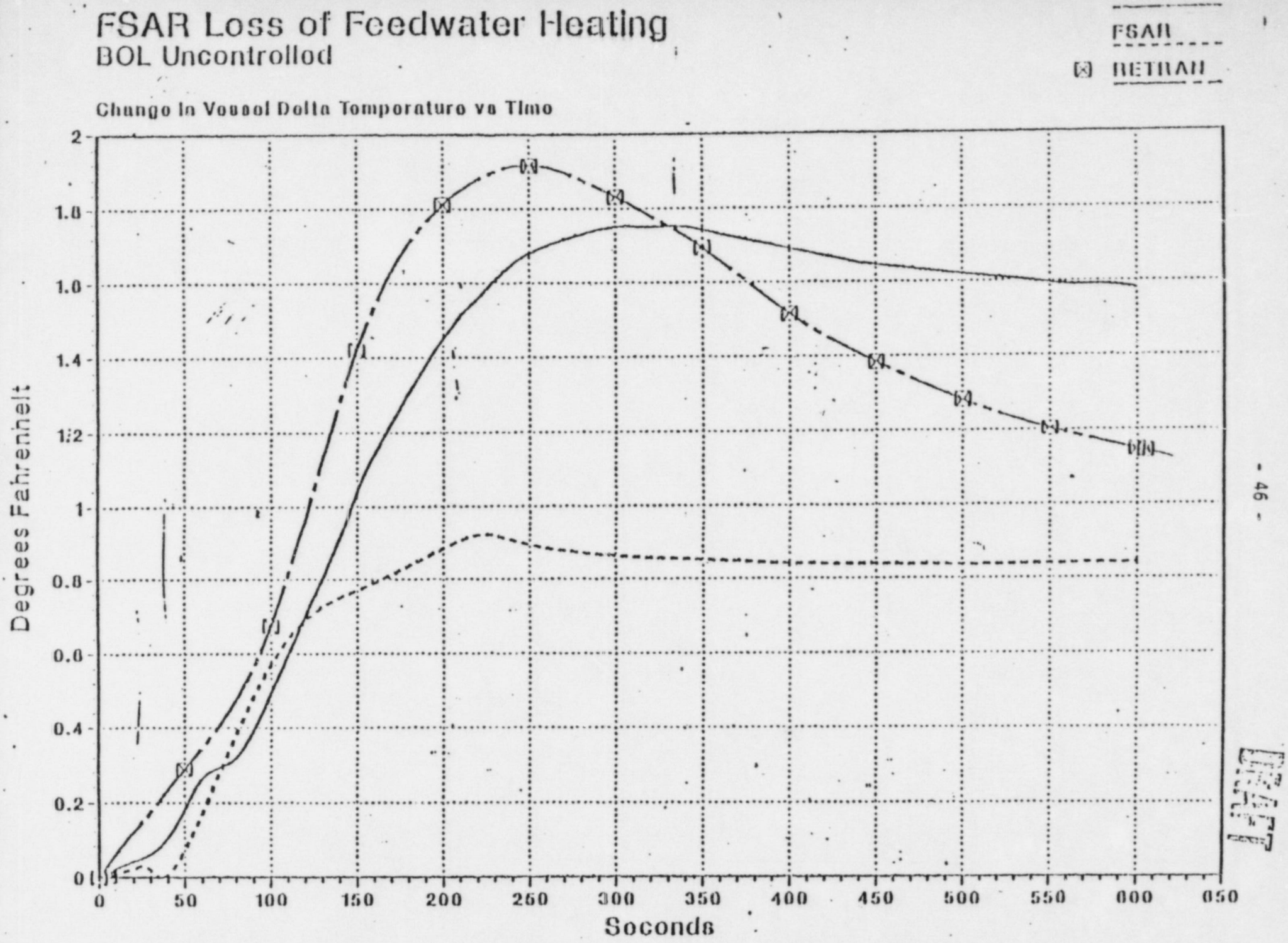


Figure 17

FSAR Loss of Feedwater Heating
BOL Uncontrolled

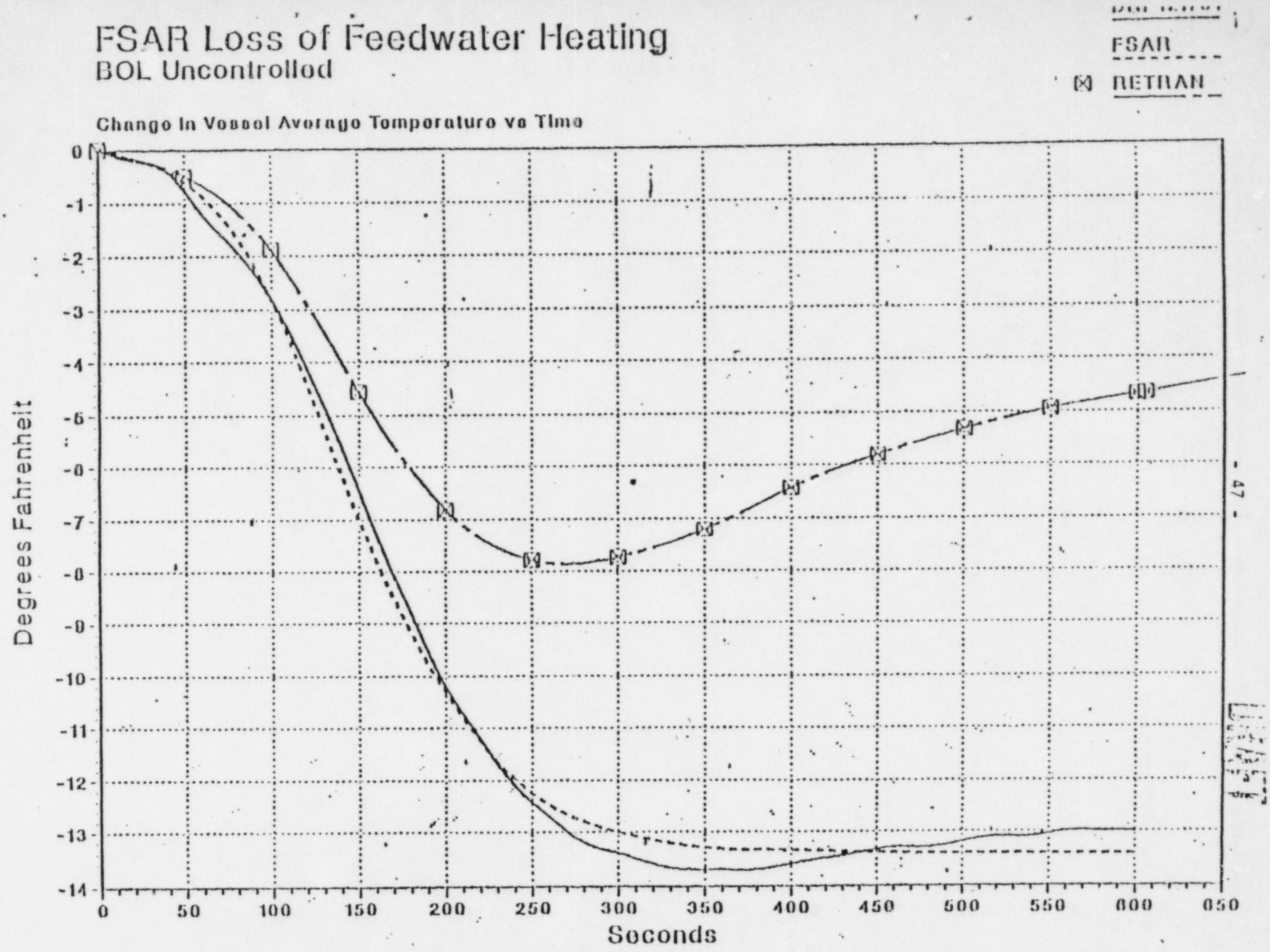


Figure 18

FSAR Turbine Trip
BOL with Control

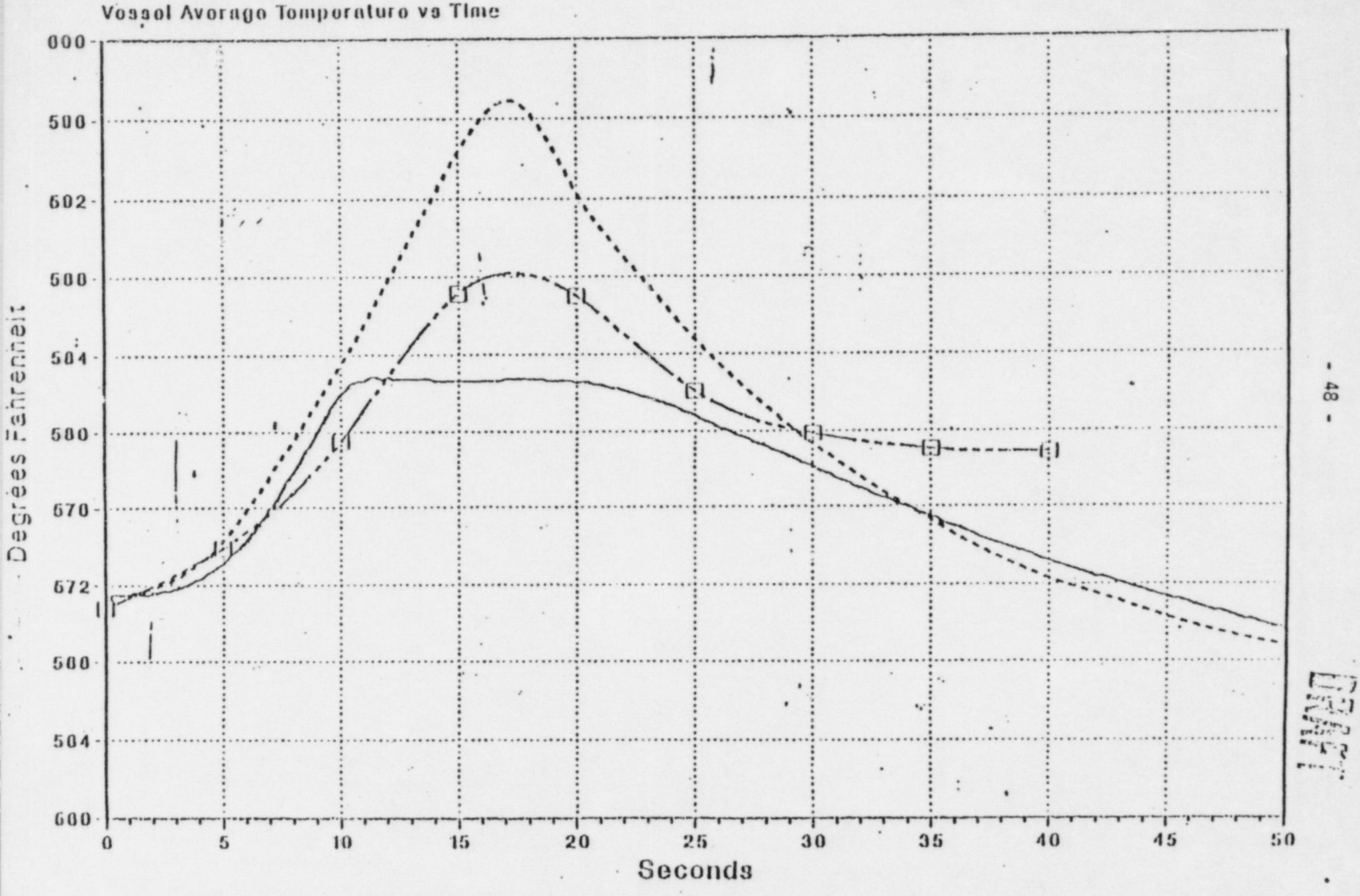


Figure 19

FSAR Turbine Trip
BOL with Control

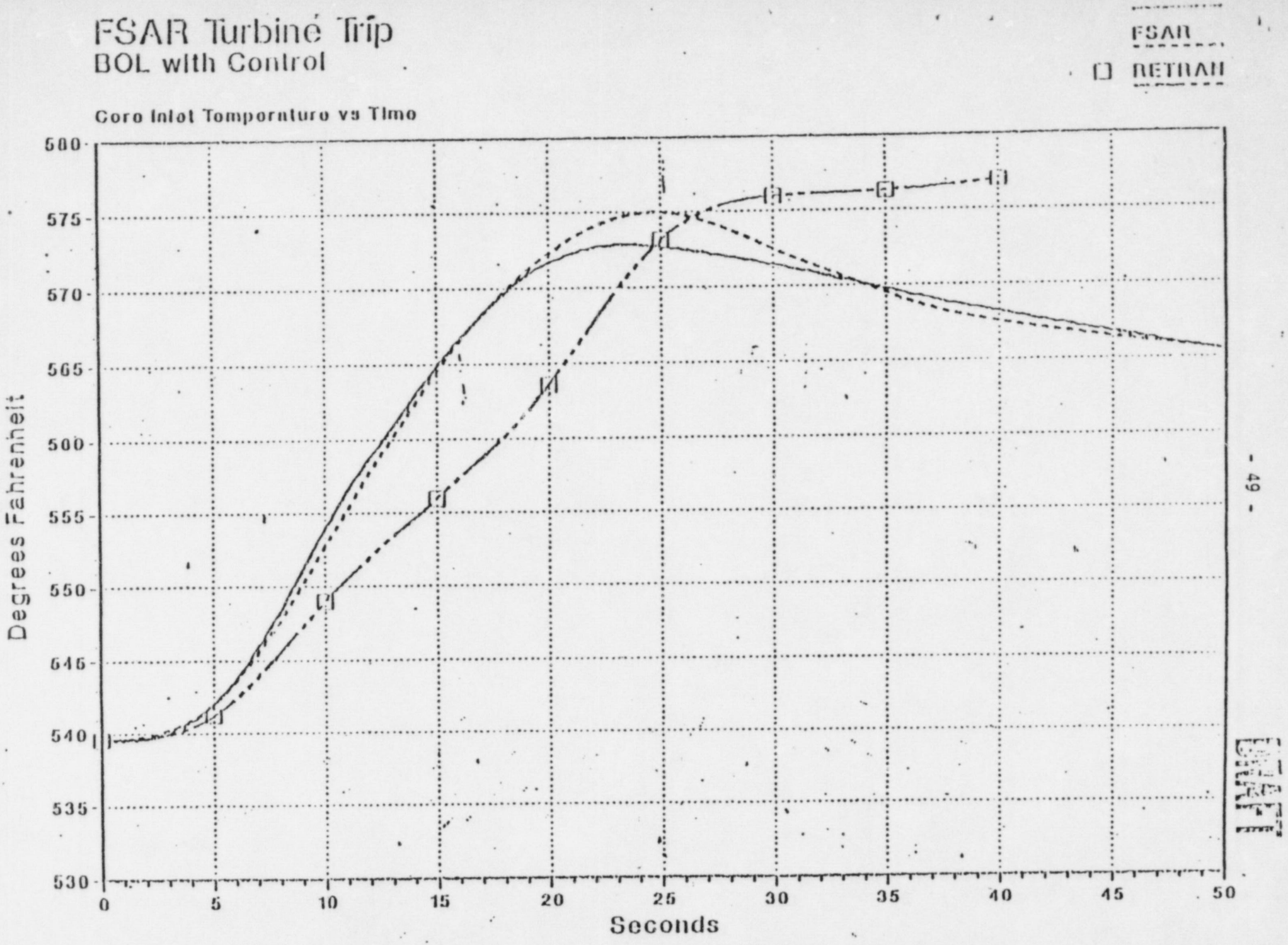


Figure 20

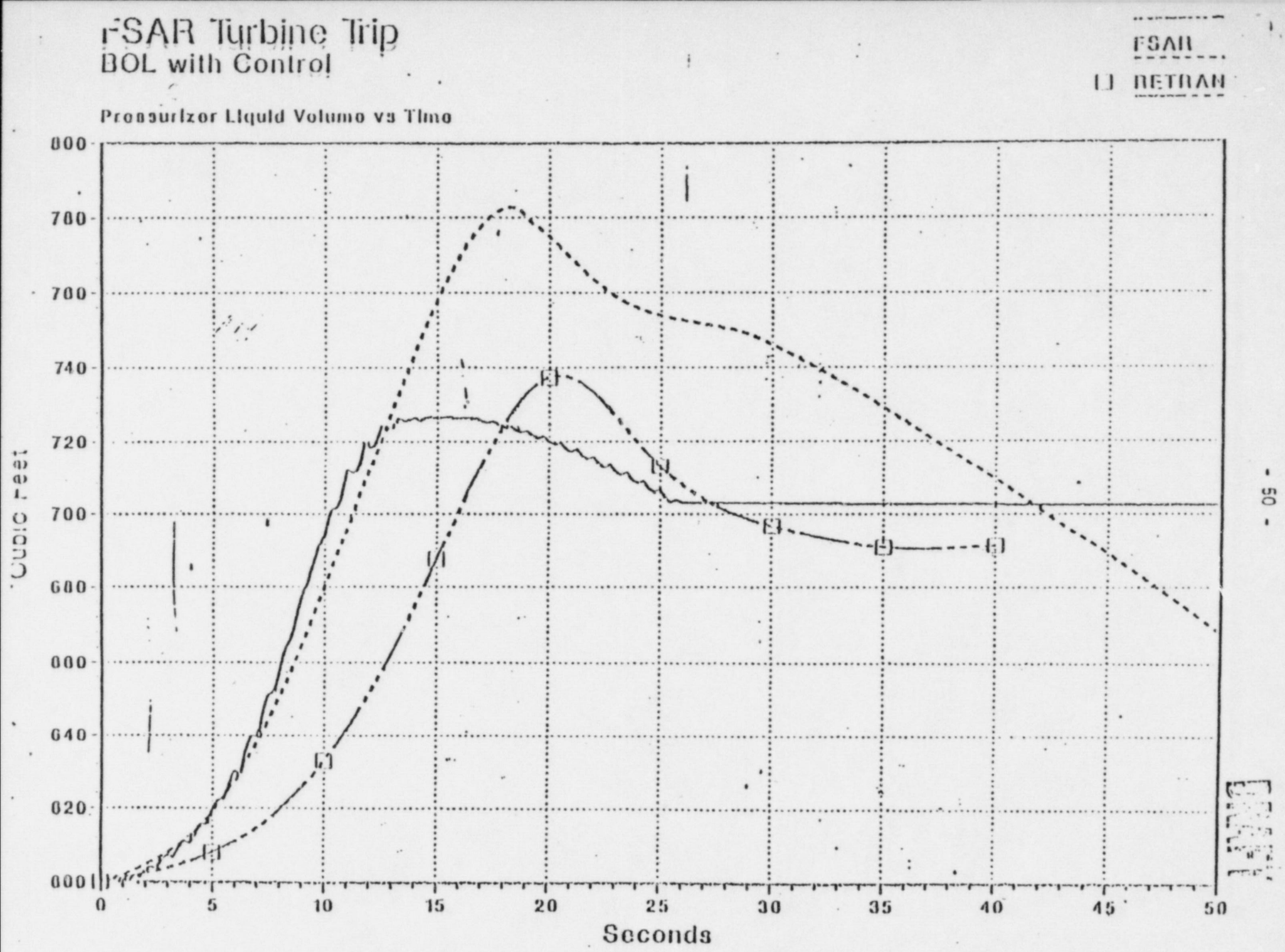

FSAR Turbine Trip
BOL with Control
FSAR
RETRAN
Pressurizer Liquid Volume vs Time
800
760
700
740
720
700
680
000
640
020
000
Cubic Feet
0
5
10
15
20
25
30
35
40
45
50
Seconds

Figure 21

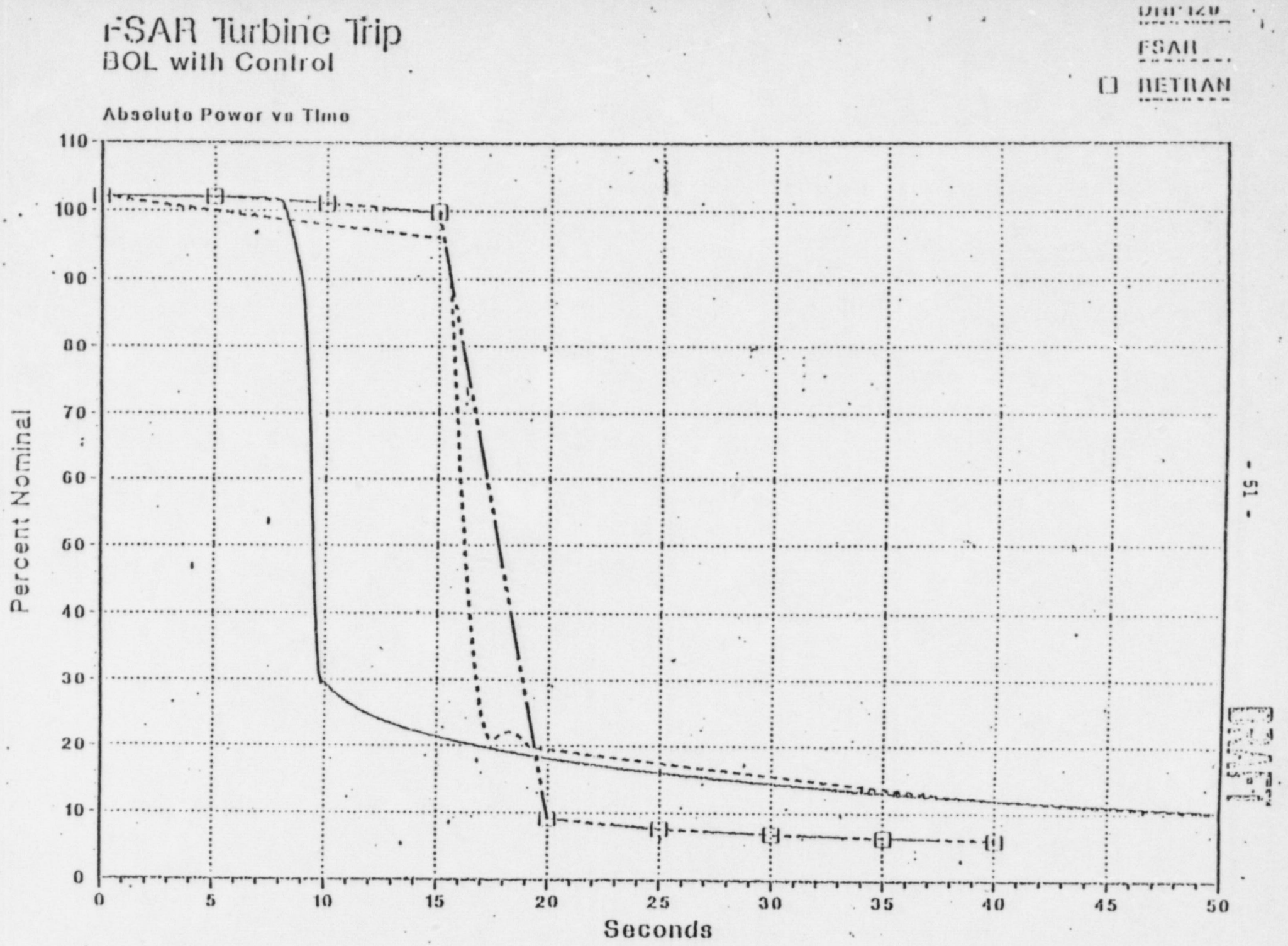

FSAR Turbine Trip
BOL with Control
Absolute Power vs Time
DIF120
FSAR
RETRAN
Percent Nominal
110
100
90
80
70
60
50
40
30
20
10
0
0
5
10
15
20
25
30
35
40
45
50
Seconds

Figure 22

FSAR Turbine Trip
BOL with Control

FSAR
RETRAN

Pressurizer Pressure vs Time

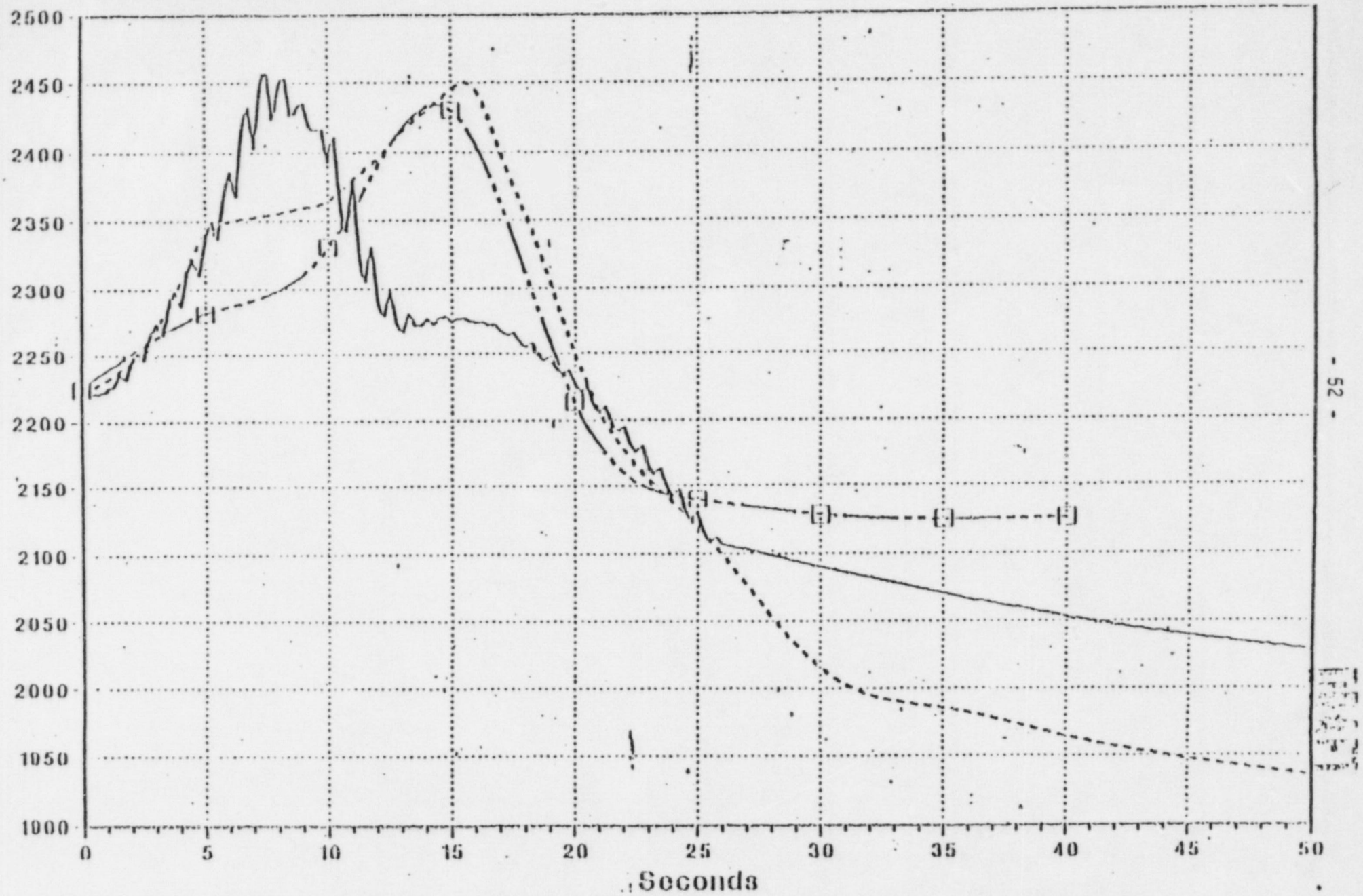


Figure 23

FSAR Turbine Trip
EOL with Control

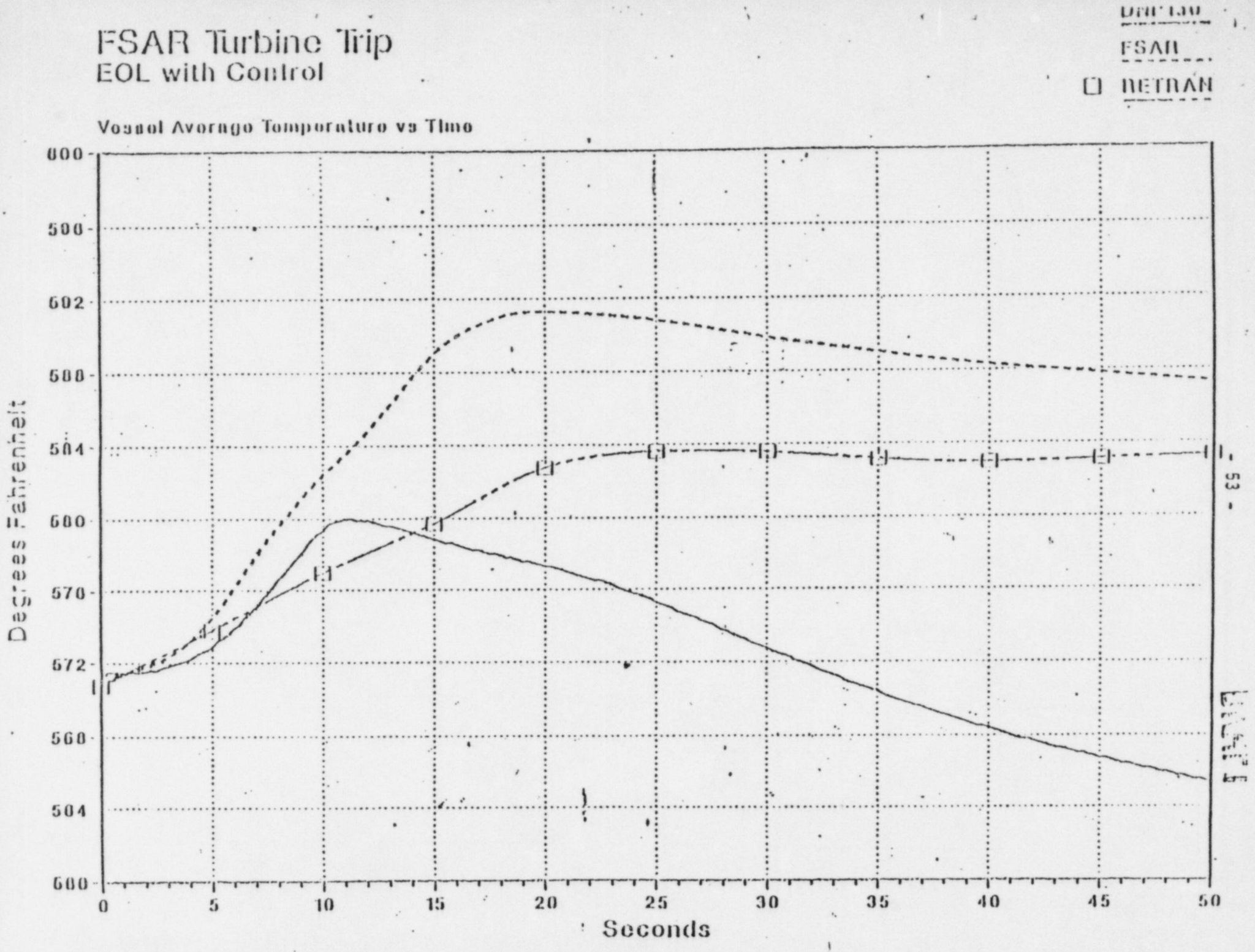


Figure 24

FSAR Turbine Trip
EOL with Control

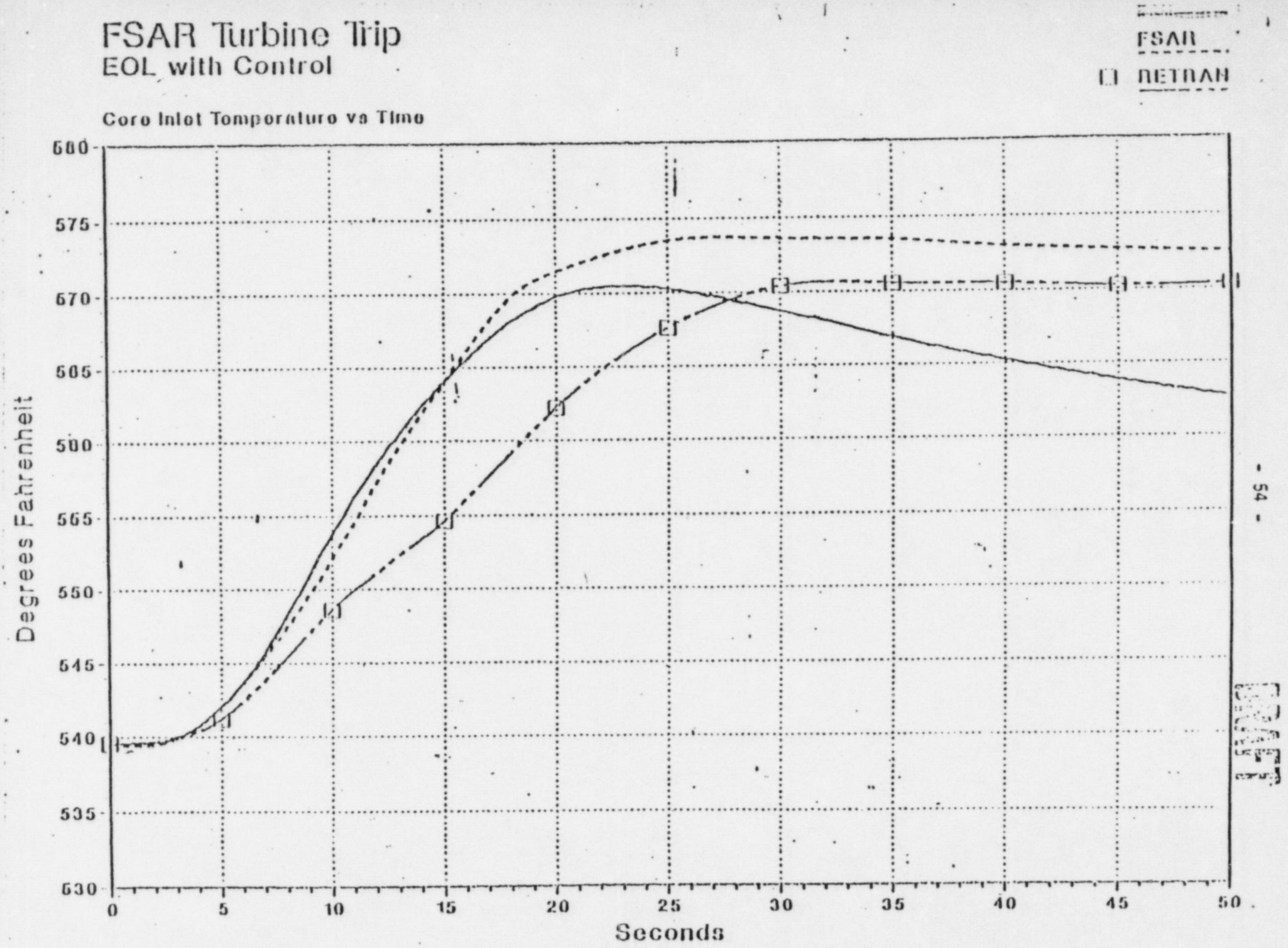


Figure 25

FSAR Turbine Trip
EOL with Control

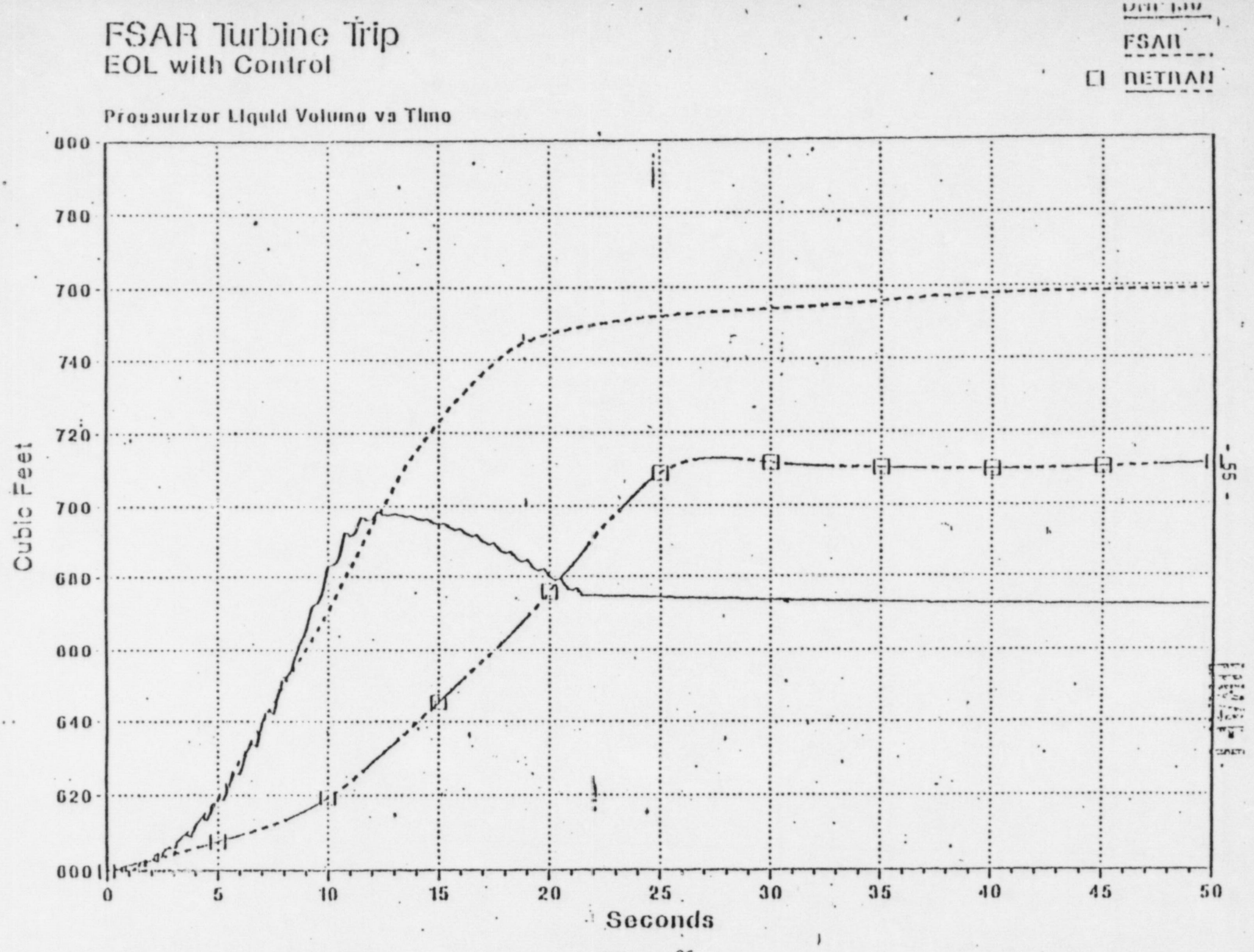


Figure 26

FSAR Turbine Trip
EOL with Control

FSAR
RETRAN

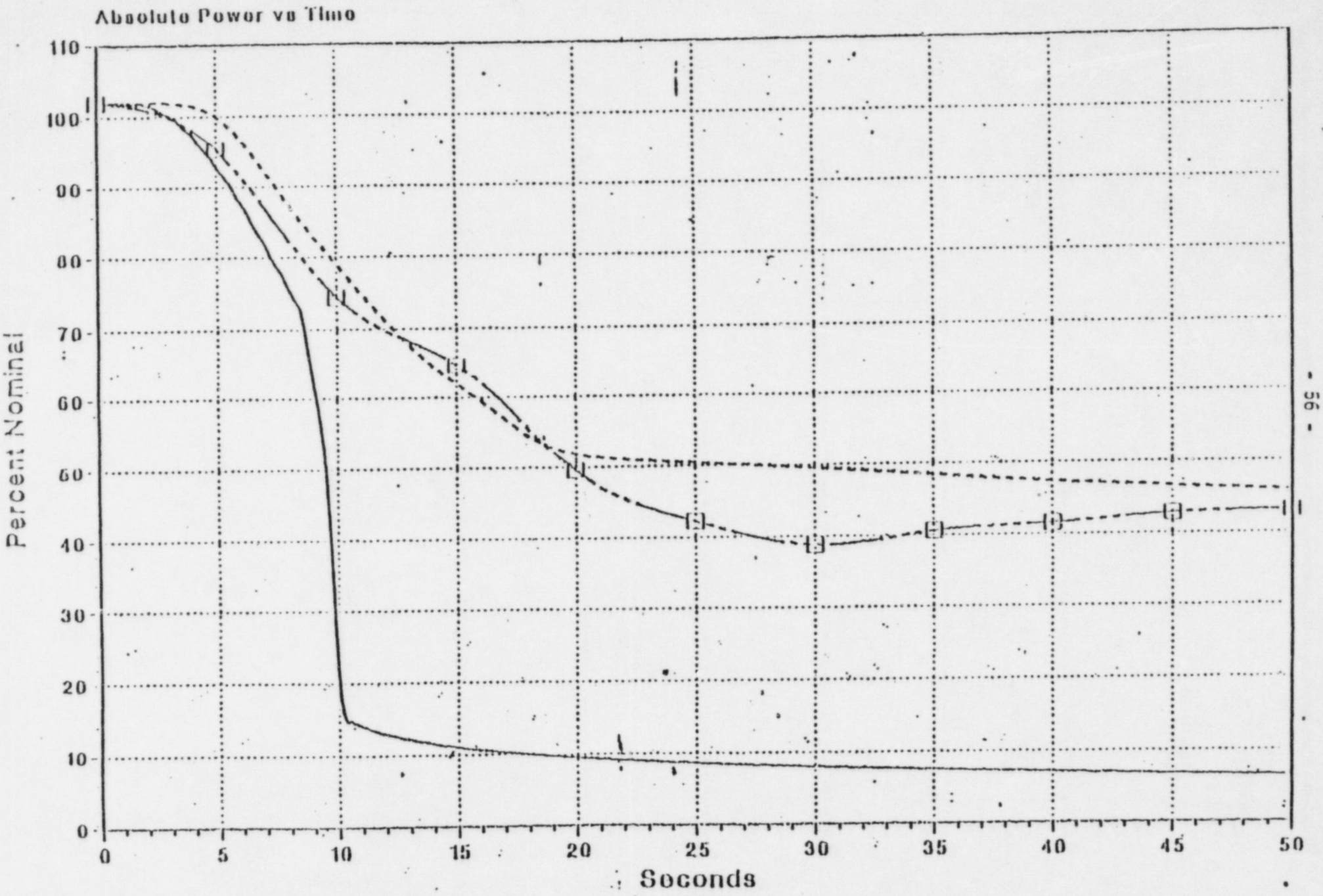


Figure 27

FSAR Turbine Trip
EOL with Control

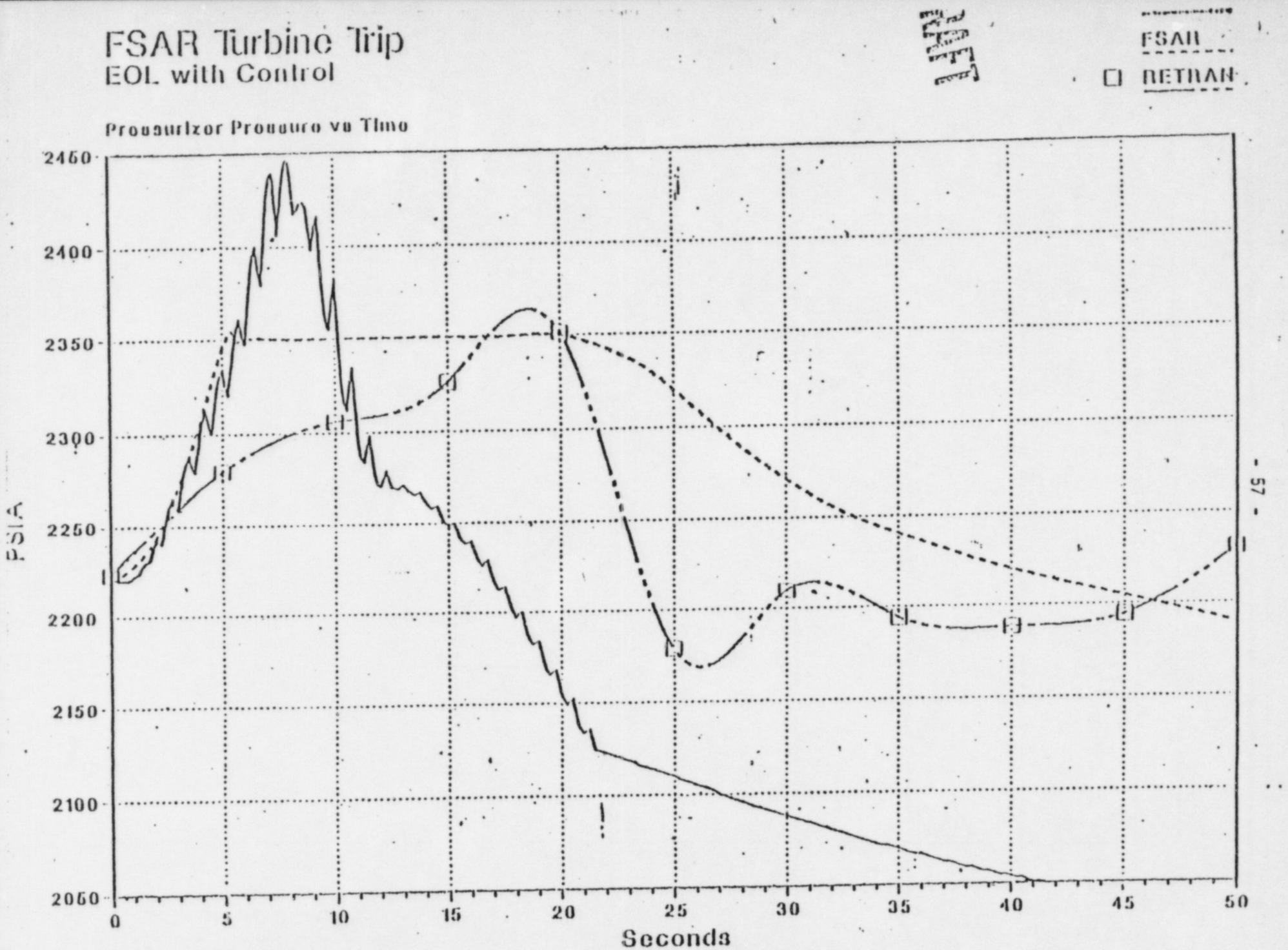


Figure 28

FSAR Turbine Trip
BOL Without Control

DNP131
FSAR
LI RETRAN

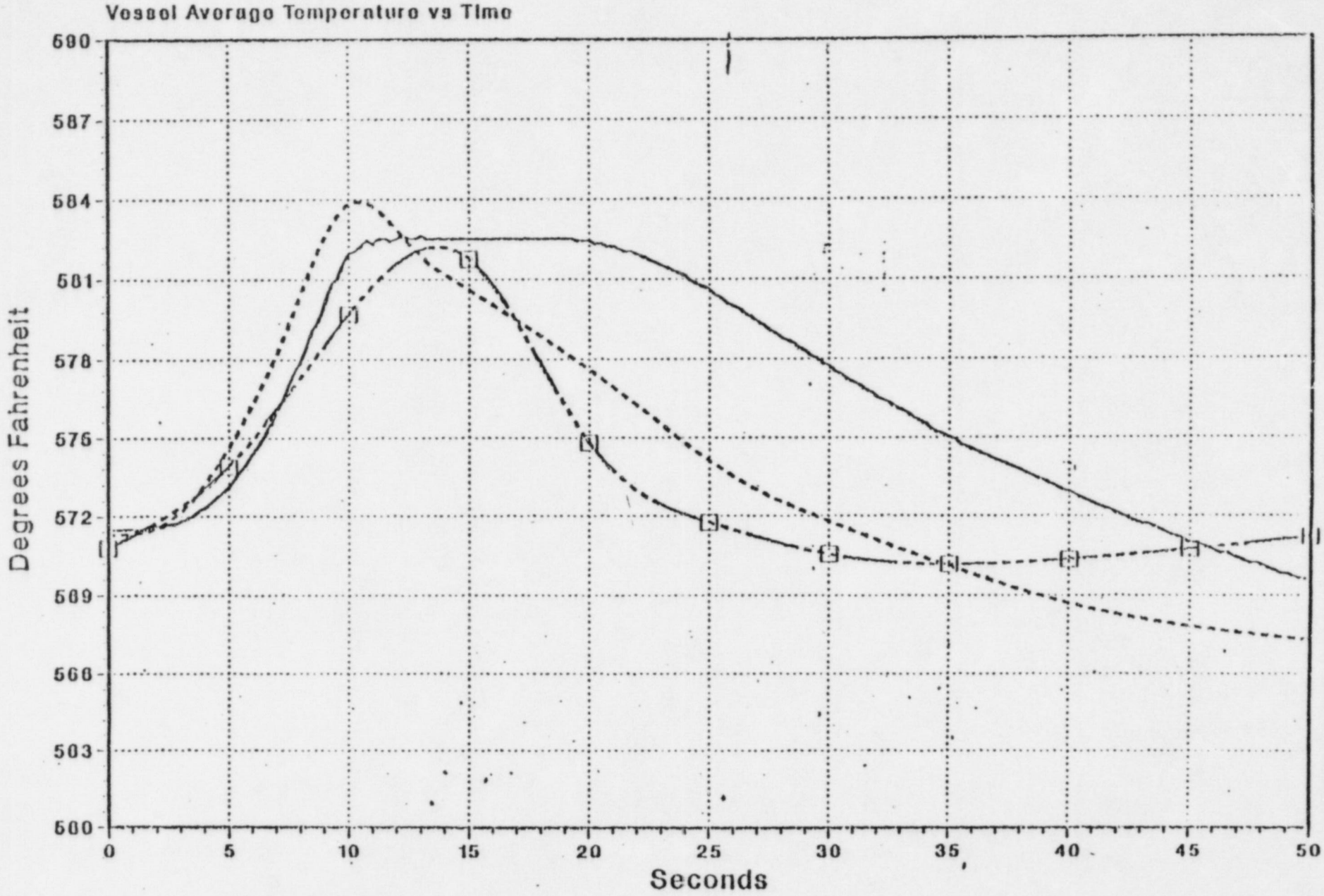


Figure 29

FSAR Turbine Trip
BOL without Control

DNP131
FSAR
RETRAN

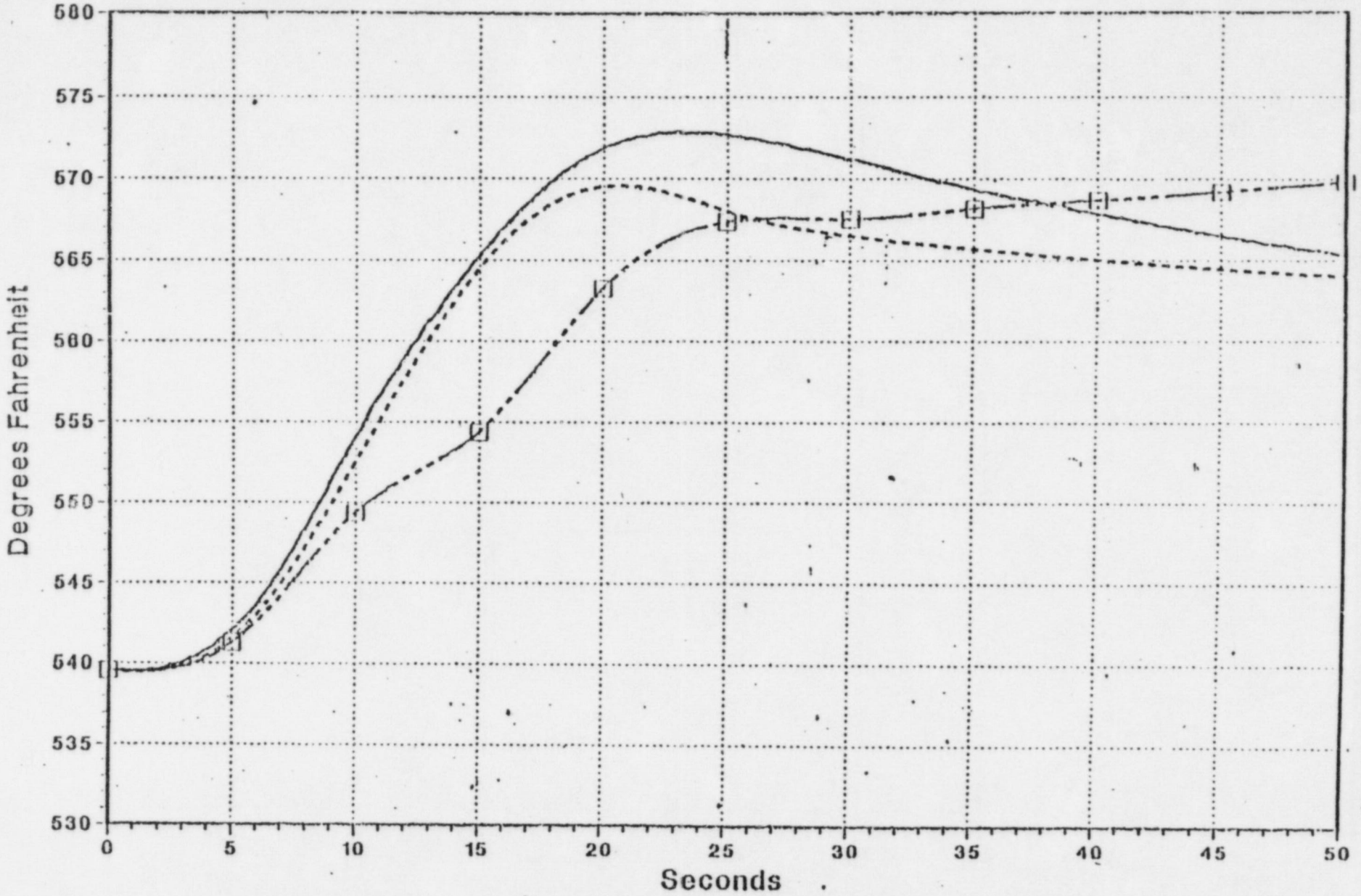


Figure 30

Prepared by NSP Safety Analysis 11/11/81

FSAR Turbine Trip
EOL without Control

DNP131
FSAR
RETRAN

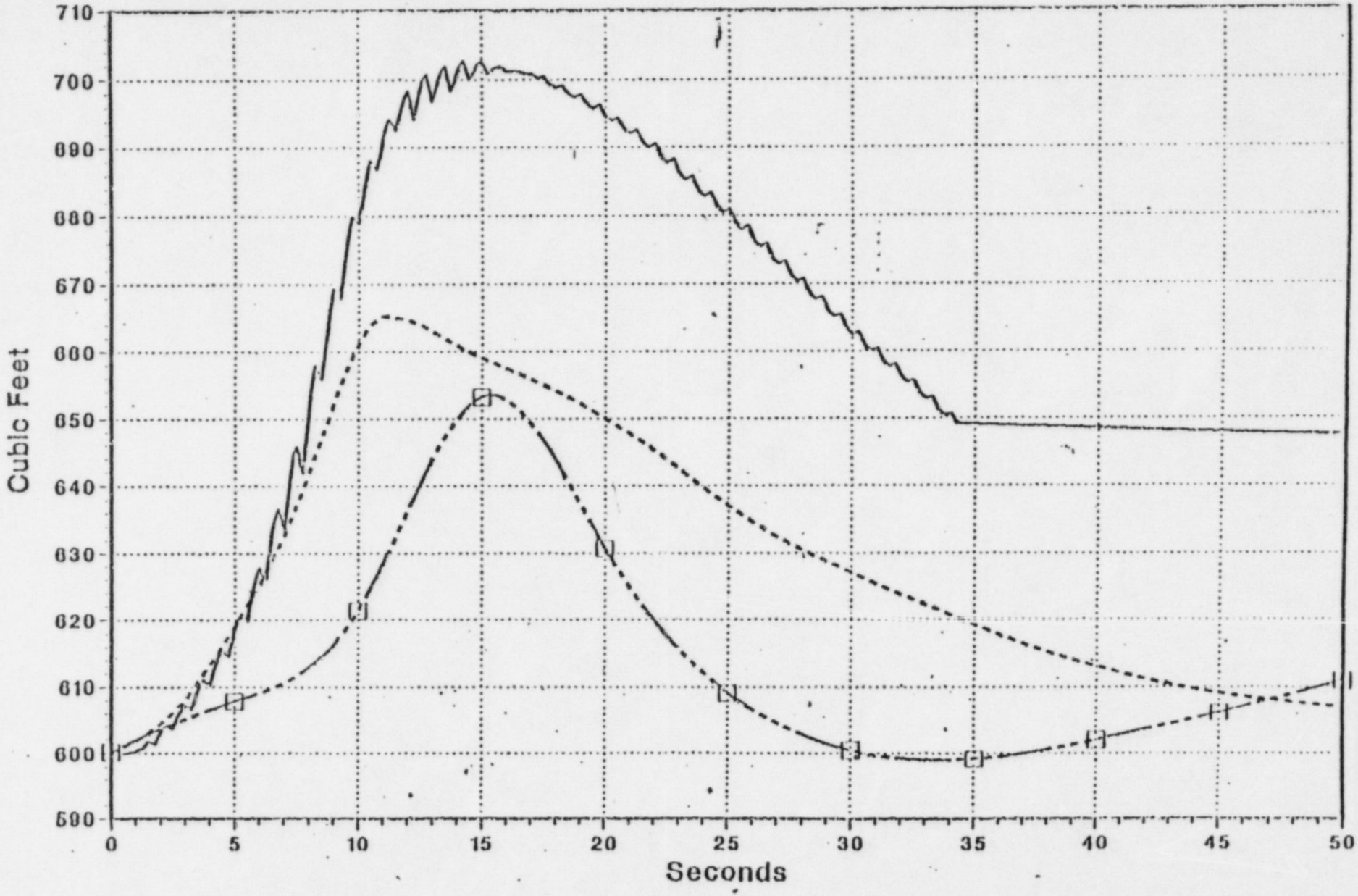
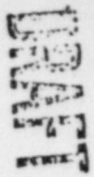


Figure 31

Prepared by NSP Safety Analysis 11/11/81

FSAR Turbine Trip
BOL without Control



DNP131
FSAR
RETRAN

Absolute Power vs Time

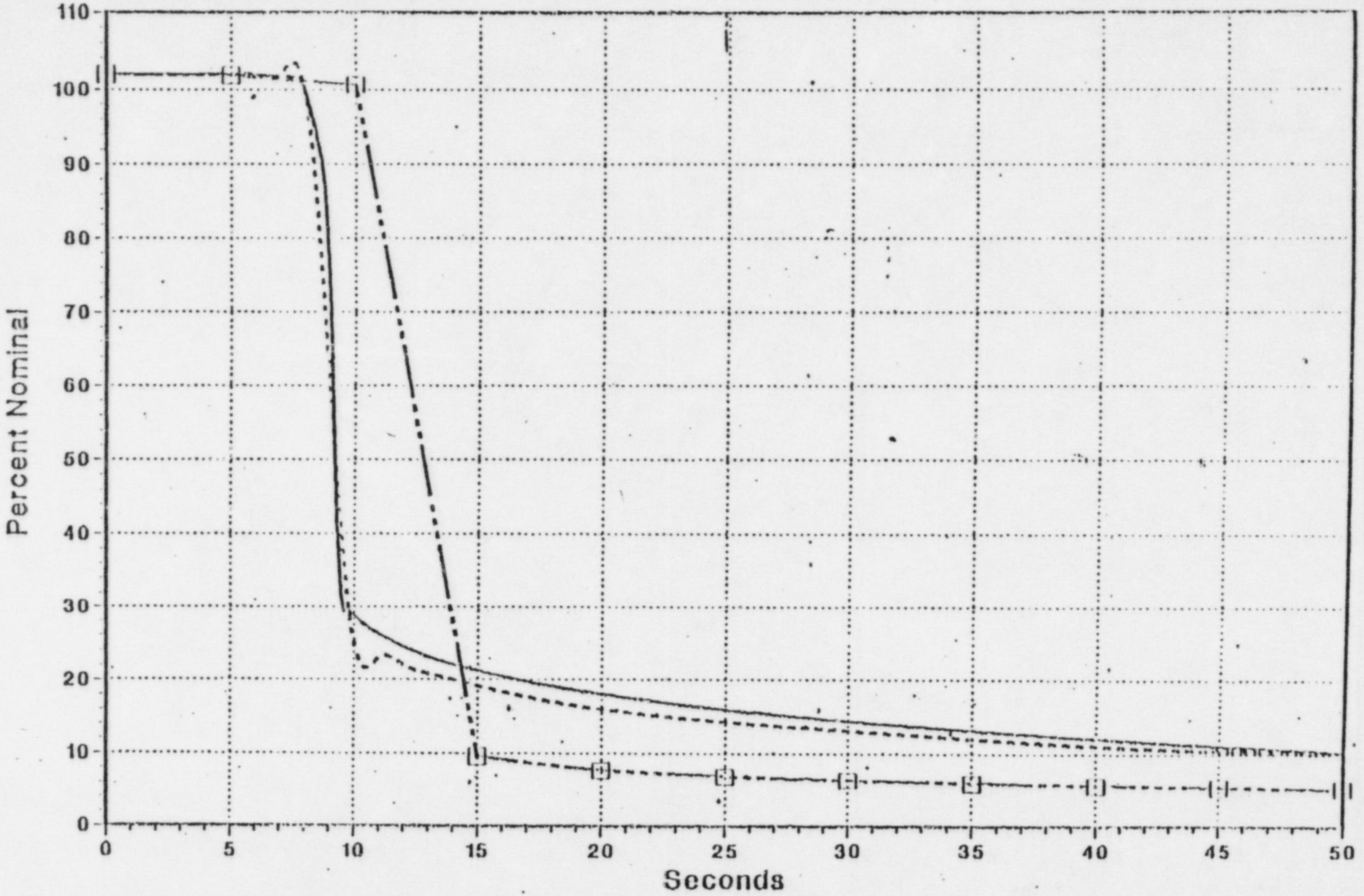


Figure 32

Prepared by NSP Safety Analysis 11/11/81

FSAR Turbine Trip
POL without Control

DNP131
FSAR
RETRAN

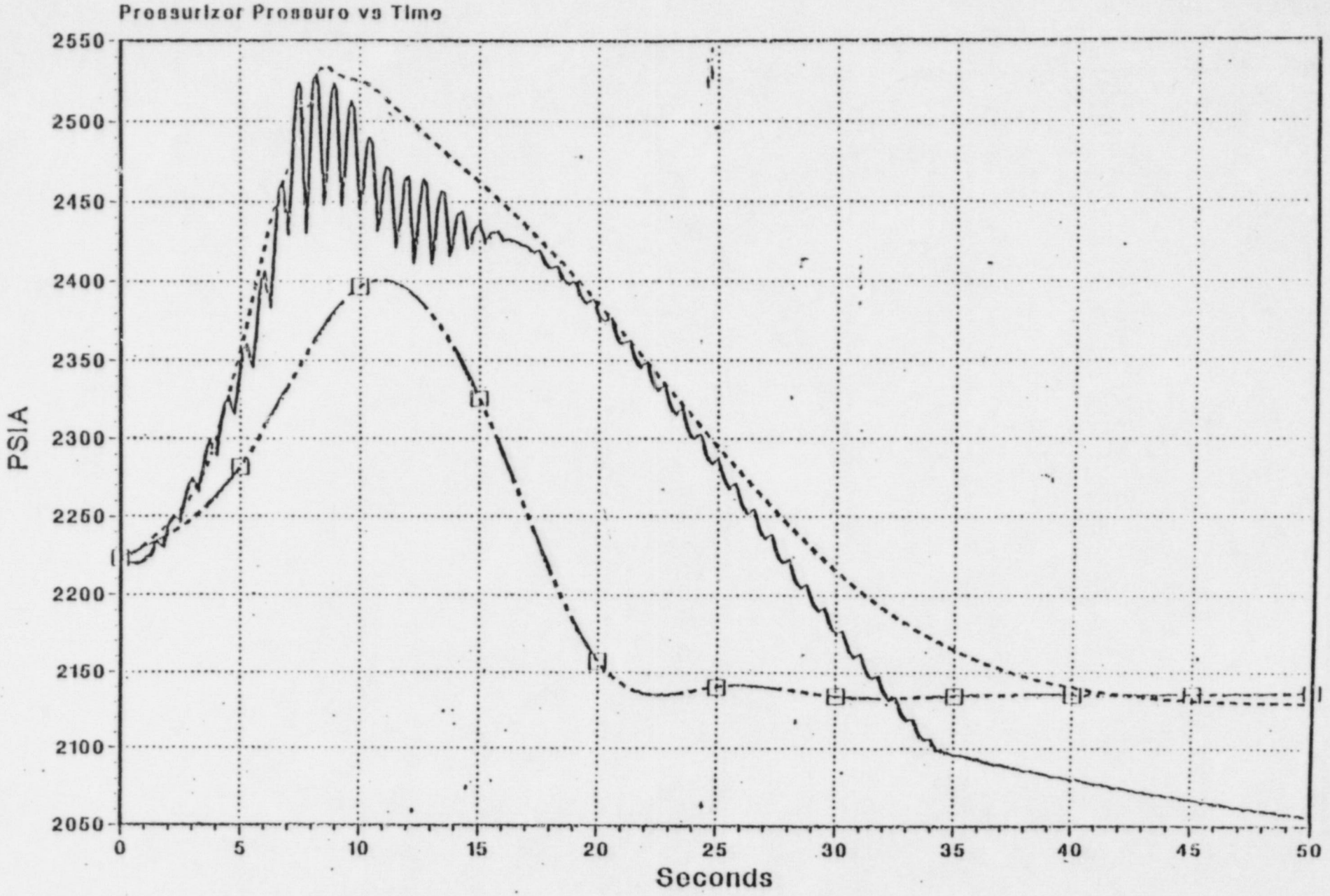


Figure 33

Prepared by NSP Safety Analysis 11/11/81

FSAR Turbine Trip
EOL without Control

DNP132
FSAR
RETRAN

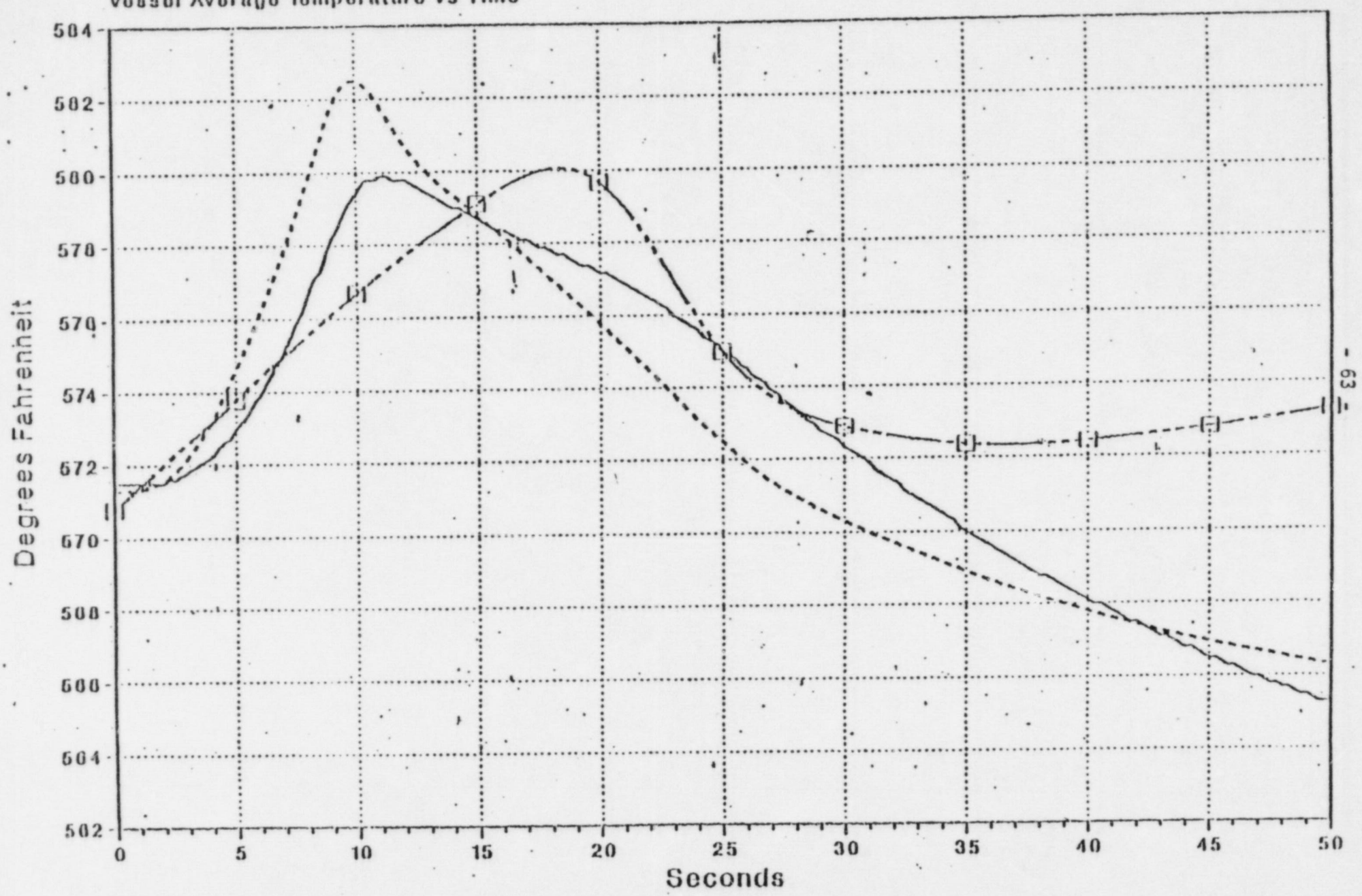


Figure 34

FSAR Turbine Trip
EOL without Control



DNP 1.3.2
FSAR
RETRAN

Core Inlet Temperature vs Time

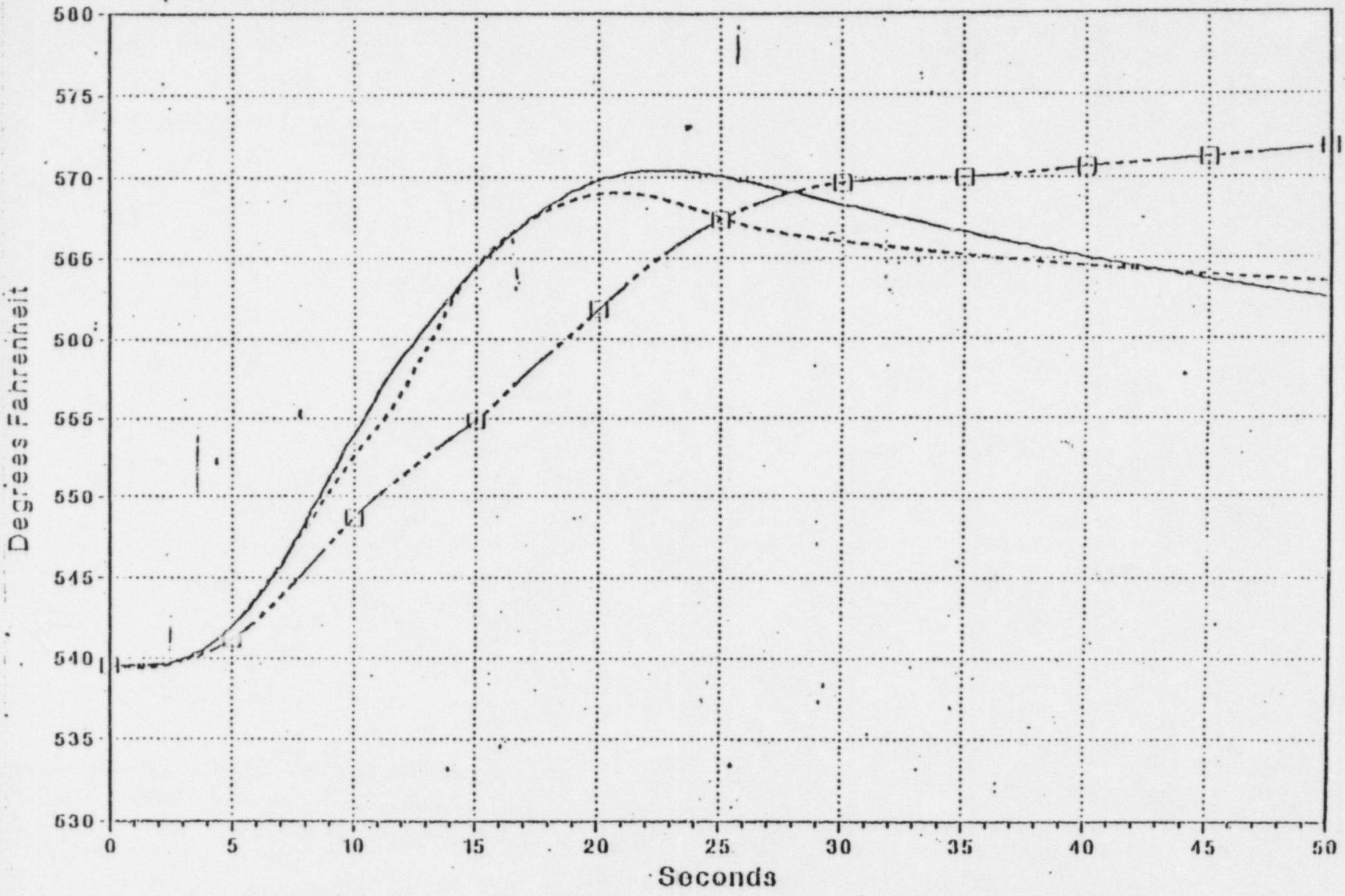
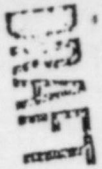


Figure 35

FSAR Turbine Trip
EOL without Control



FSAR
RETRAN

Pressurizer Liquid Volume vs Time

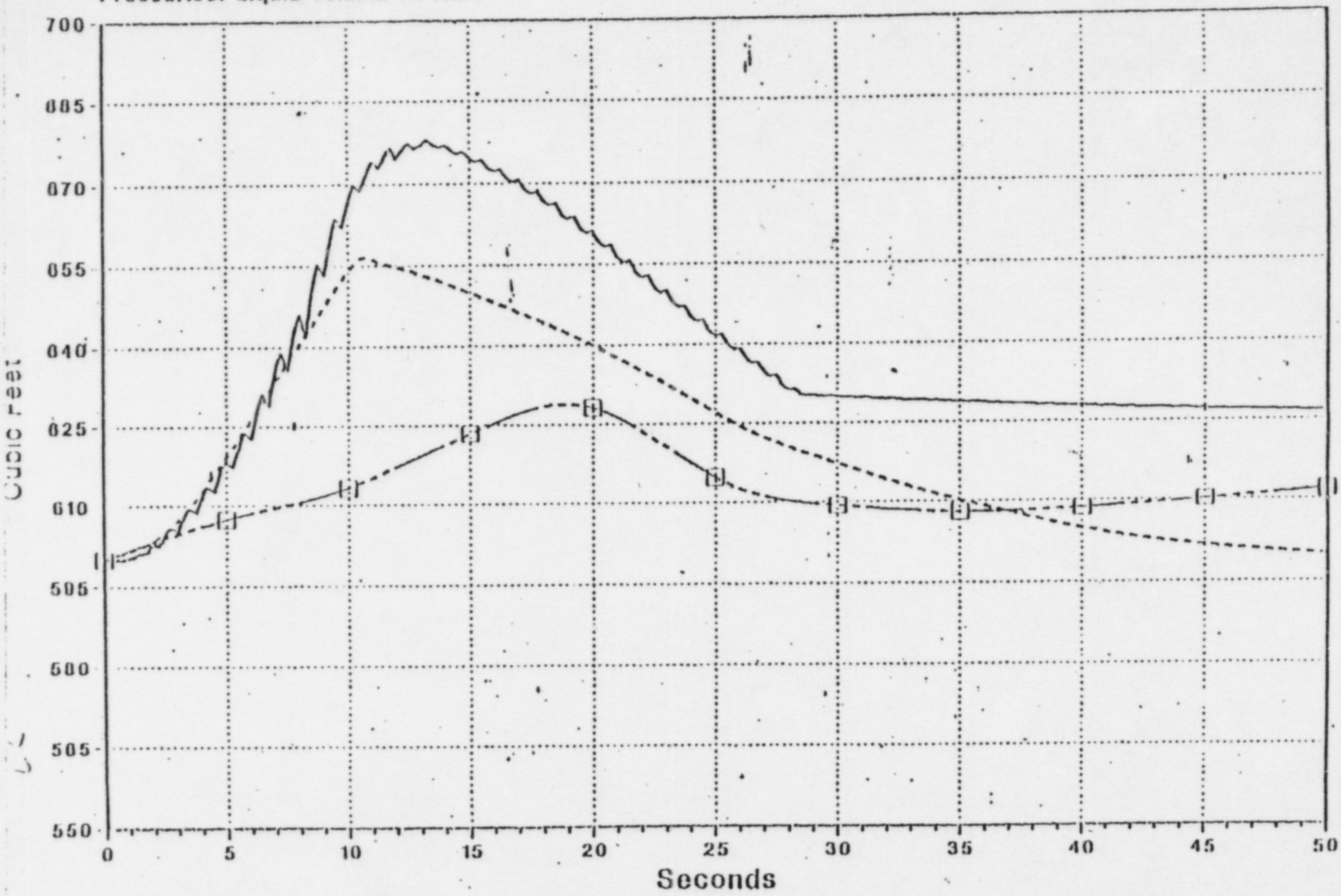


Figure 36

FSAR Turbine Trip
EOL without Control

DRAFT
FSAR
RETRAN

Absolute Power vs Time

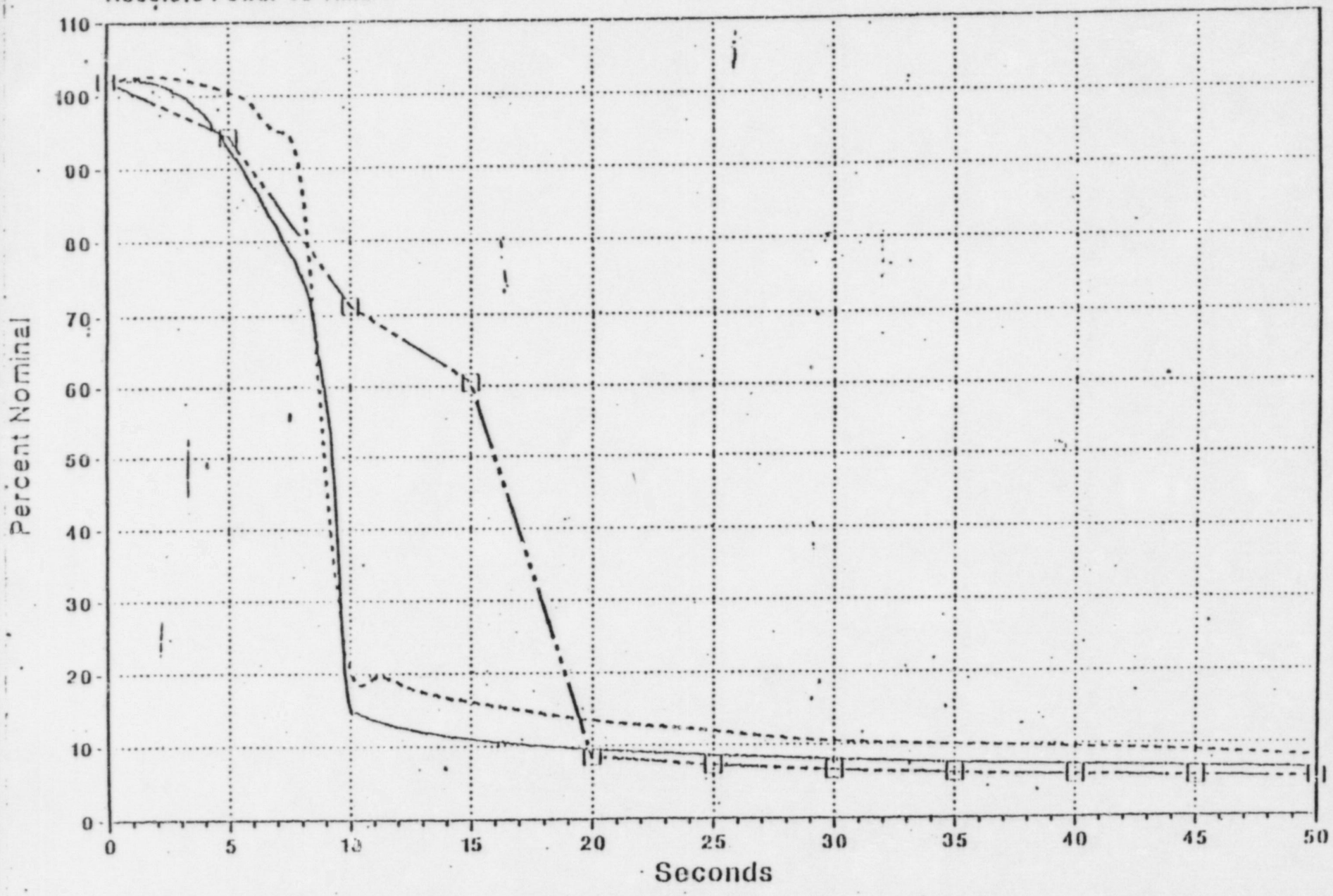


Figure 37

FSAR Turbine Trip
EOL without Control

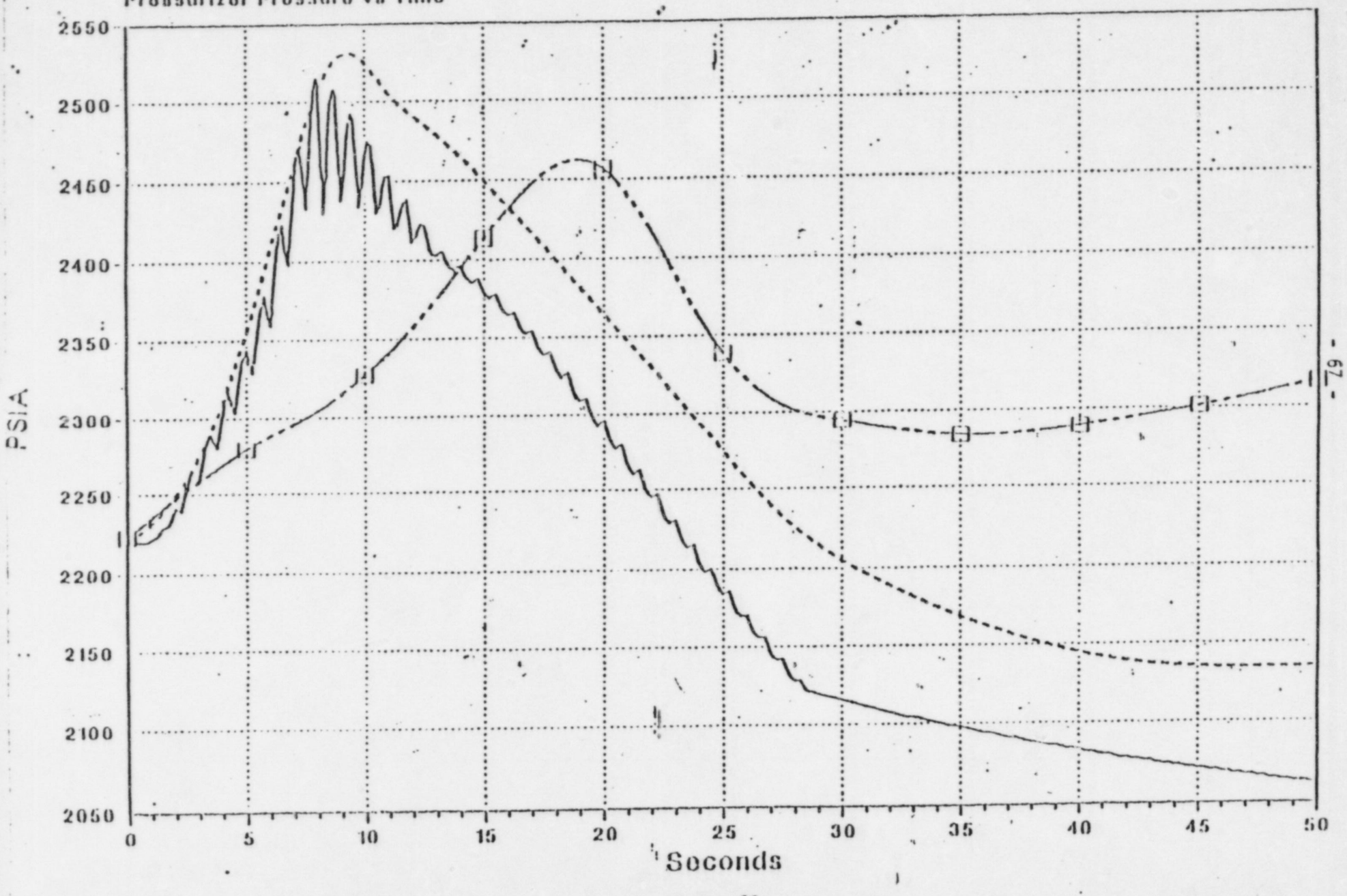


Figure 38

Fsar Loss of Flow
1/2 Pump Trip

DNP114
FSAR
[ ] RETRAN

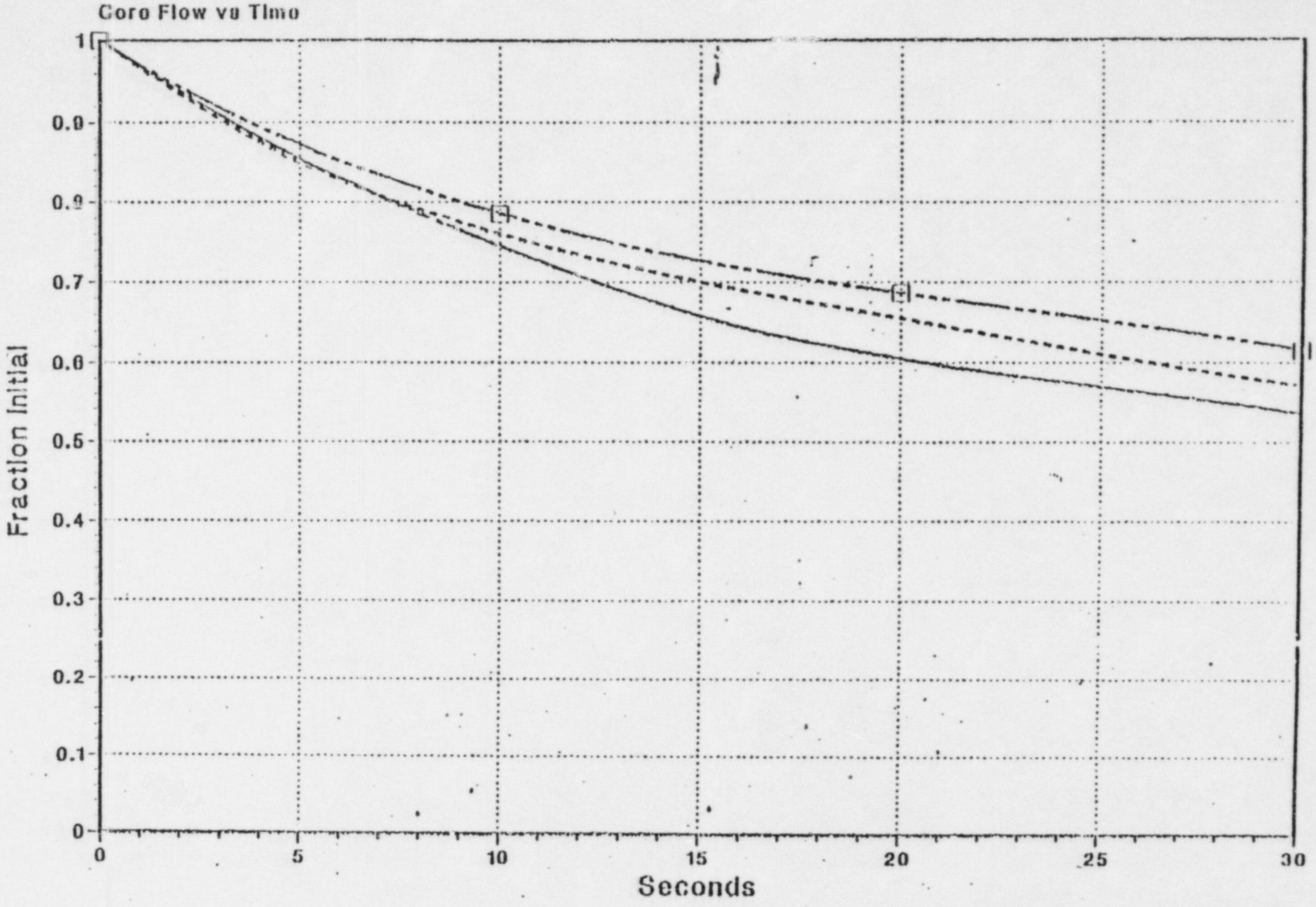


Figure 39

Fsar Loss of Flow
1/2 Pump Trip

DNP114
FSAR
RETRAN

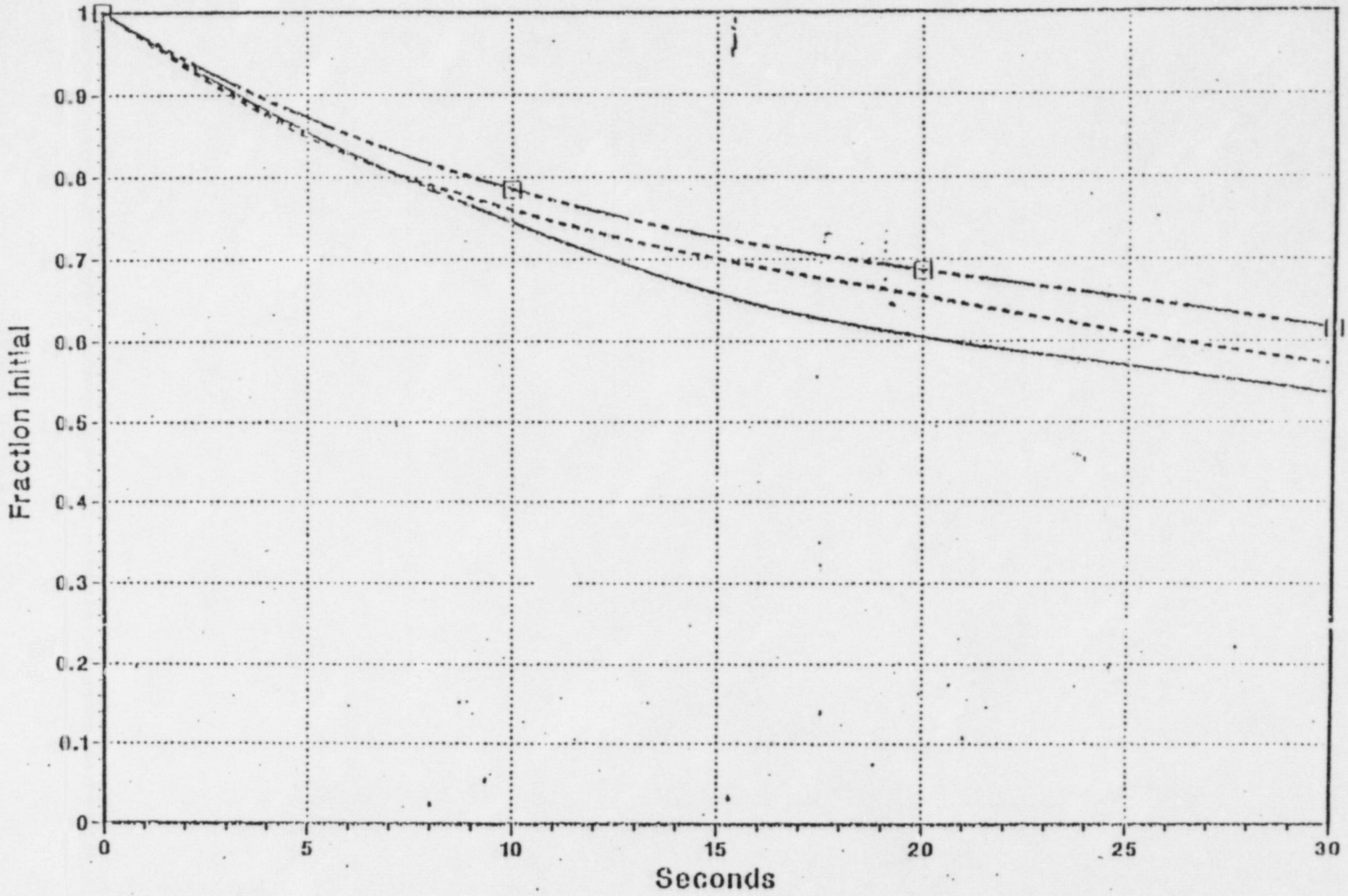


Figure 40

Fsar Loss of Flow
1/2 Pump Trip

DNP114
FSAR
RETRAN

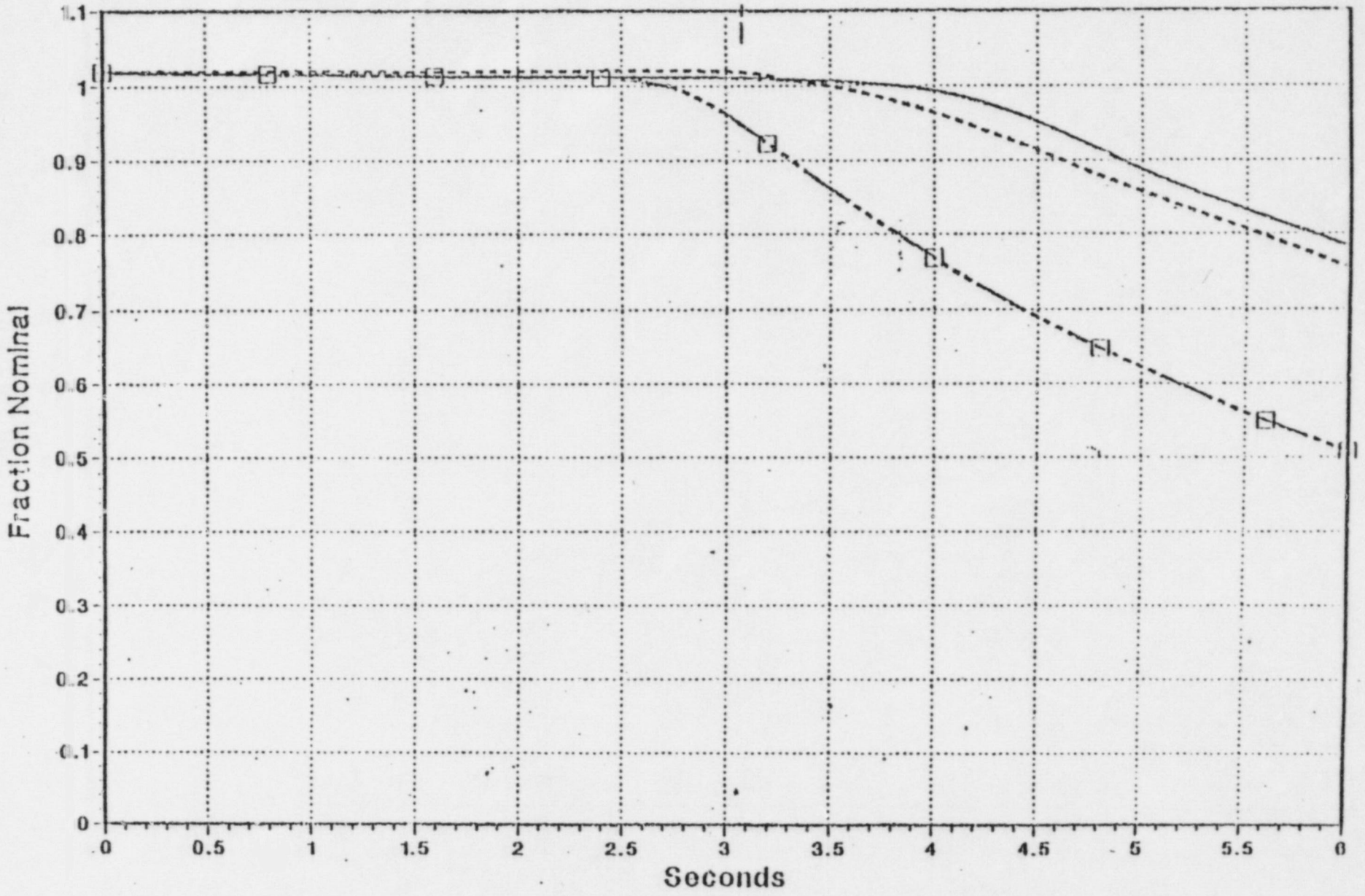


Figure 41

Fsar Loss of Flow
1/2 Pump Trip

DNP114
FSAR
RETRAN

Absolute Power vs Time

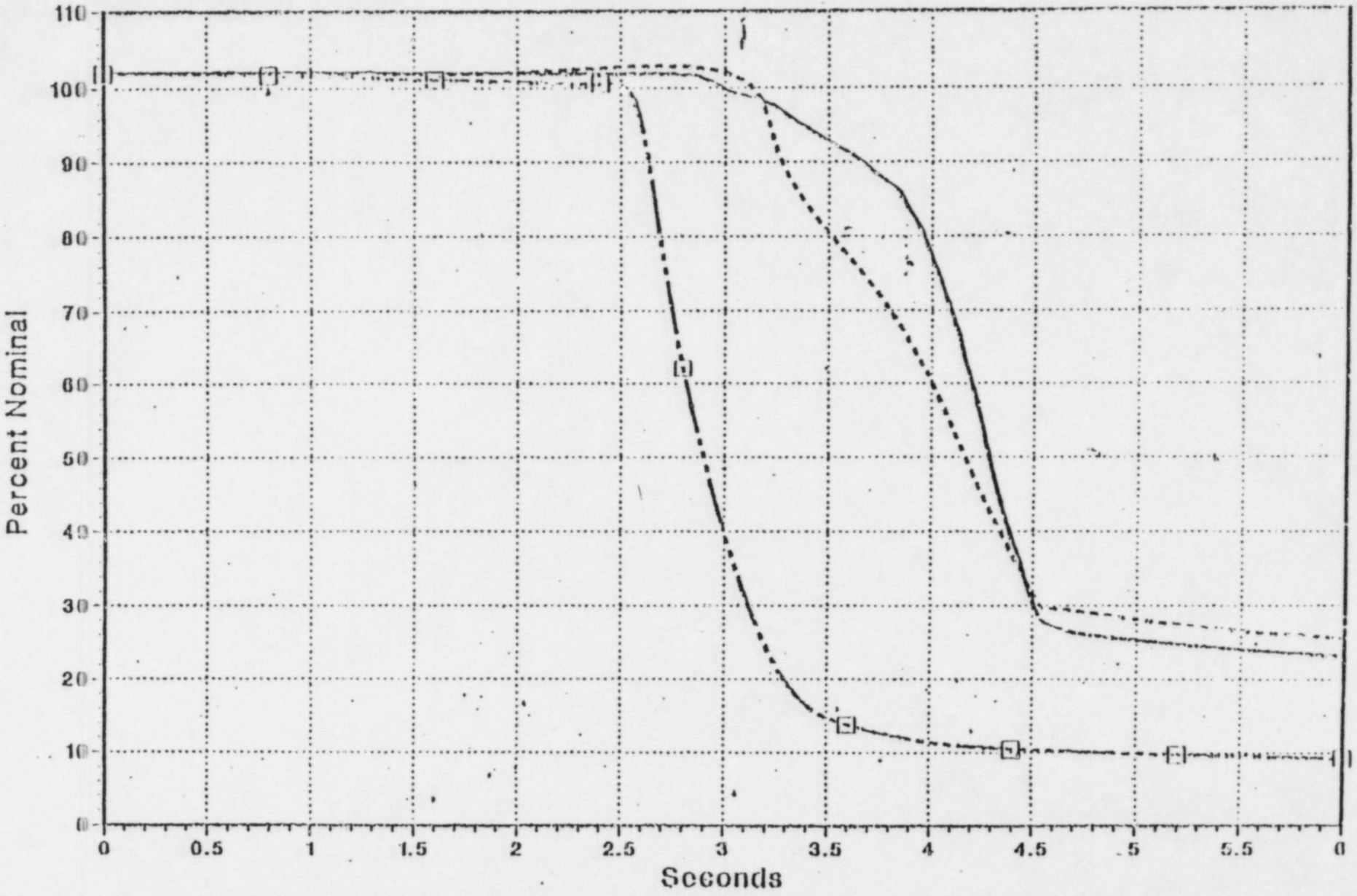


Figure 42

FSAR Loss of Flow
2 /2 Pump Trip

DNP113
FSAR
[ ] RETRAN

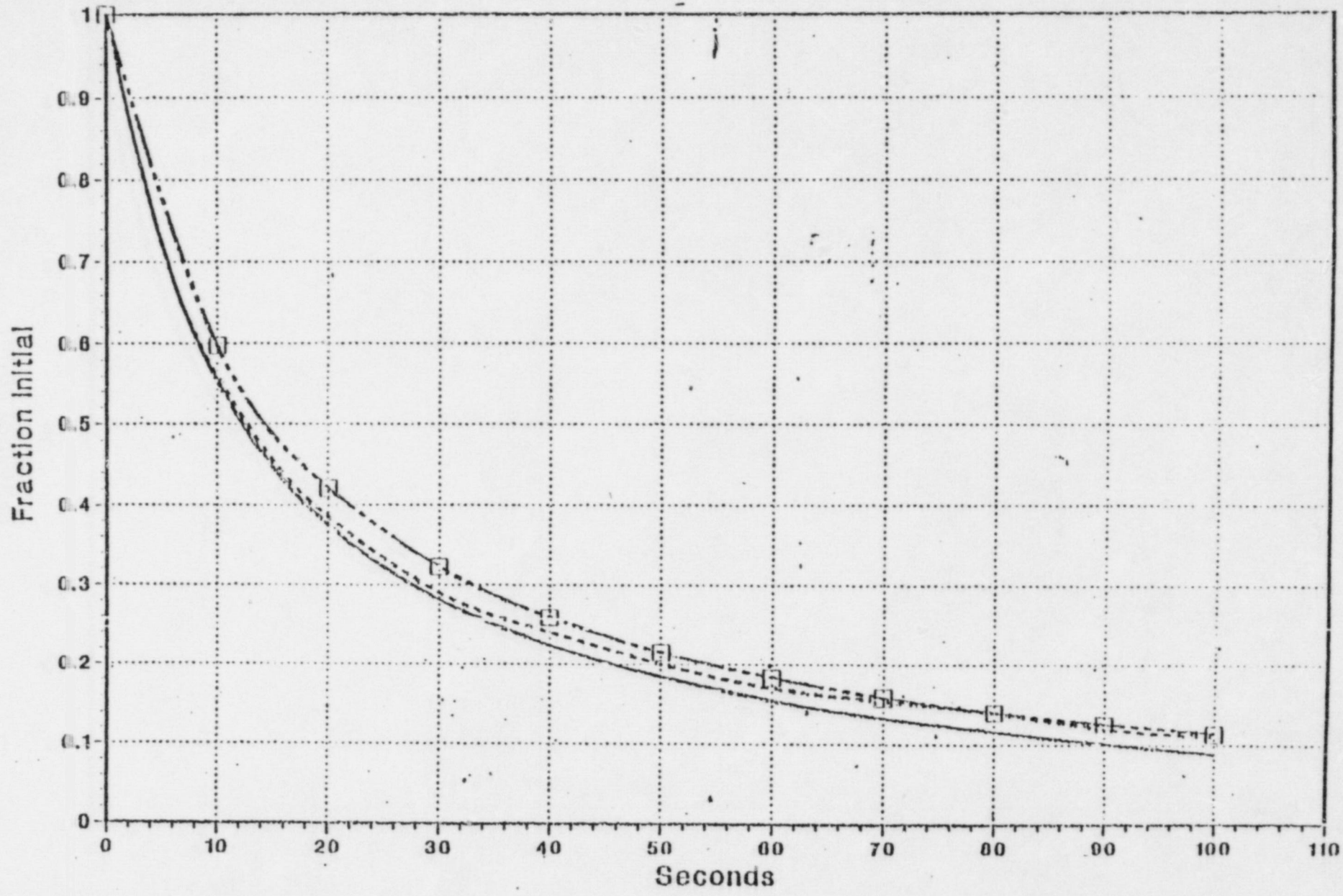


Figure 43

Prepared by NSP Safety Analysis 12/21/81

FSAR Loss of Flow
2/2 Pump Trip

DNP113
FSAR
RETRAN

Core Average Flux vs Time

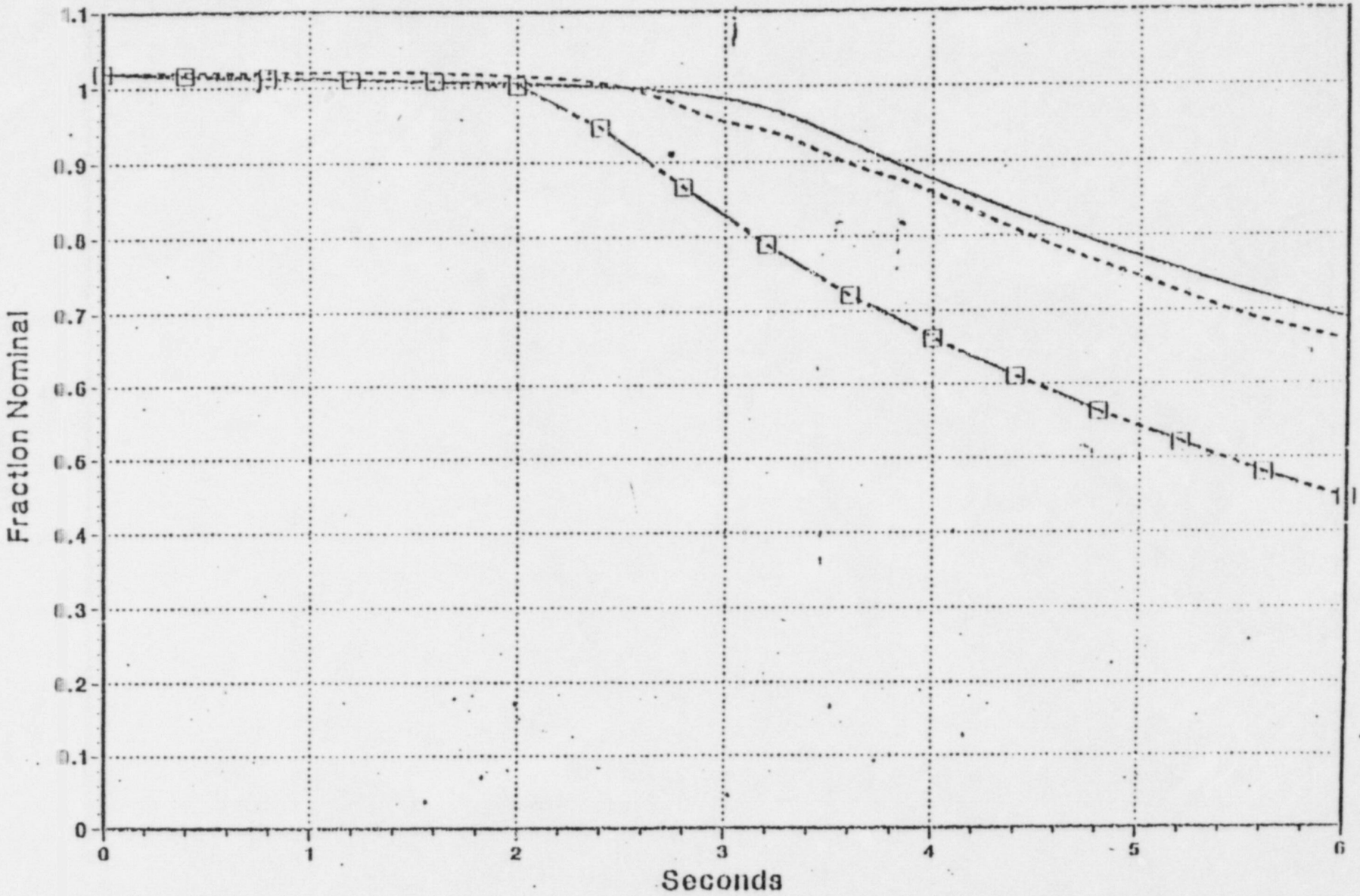


Figure 44

FSAR Loss of Flow
2/2 Pump Trip

DNP113
FSAR
RETRAN

Absolute Power vs Time

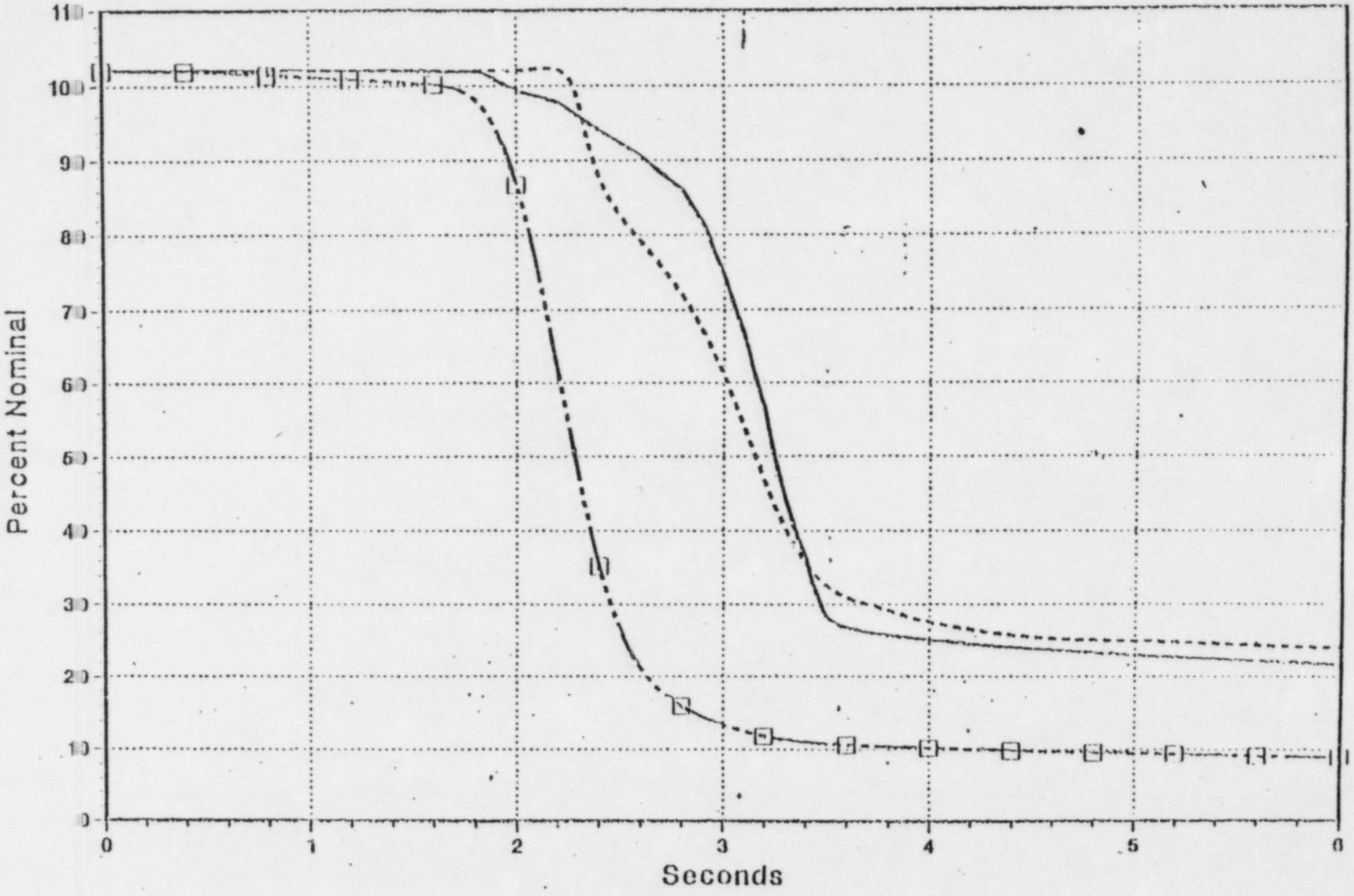


Figure 45

FSAR Steamline Break
Exit of S.G. with AC

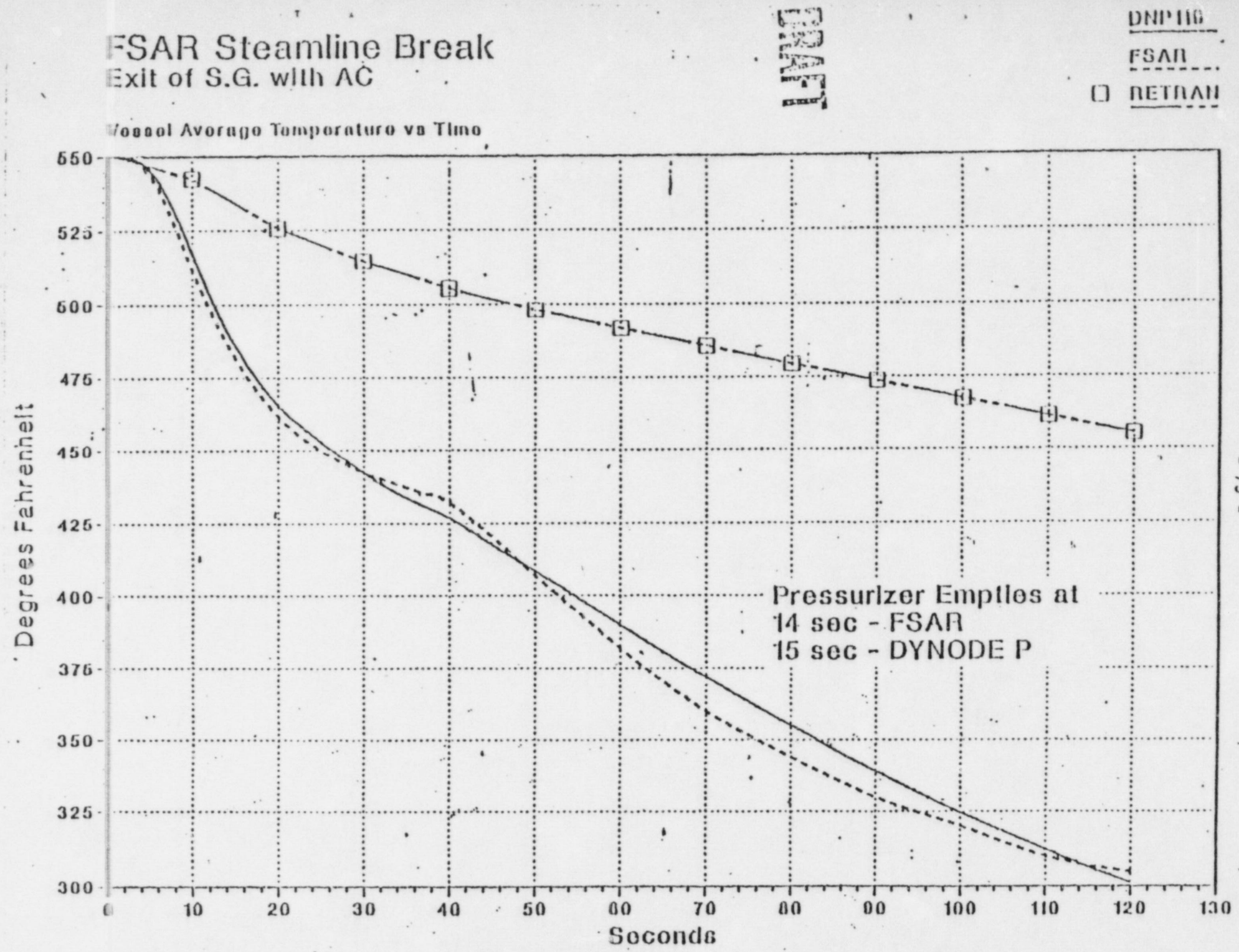


Figure 46

FSAR Steamline Break
Exit of S.G. with AC

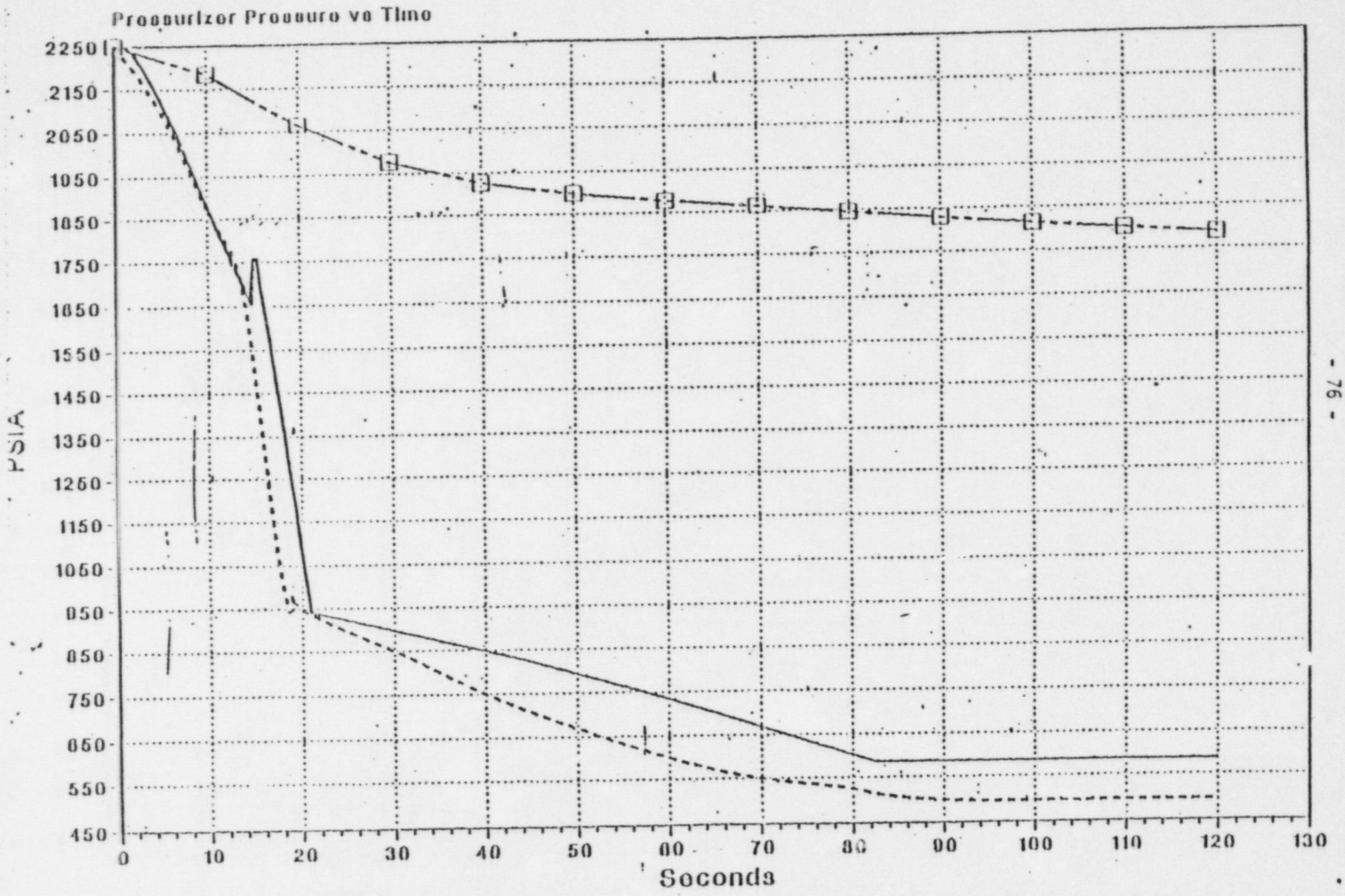


Figure 47

FSAR Steamline Break
Exit of S.G. with AC

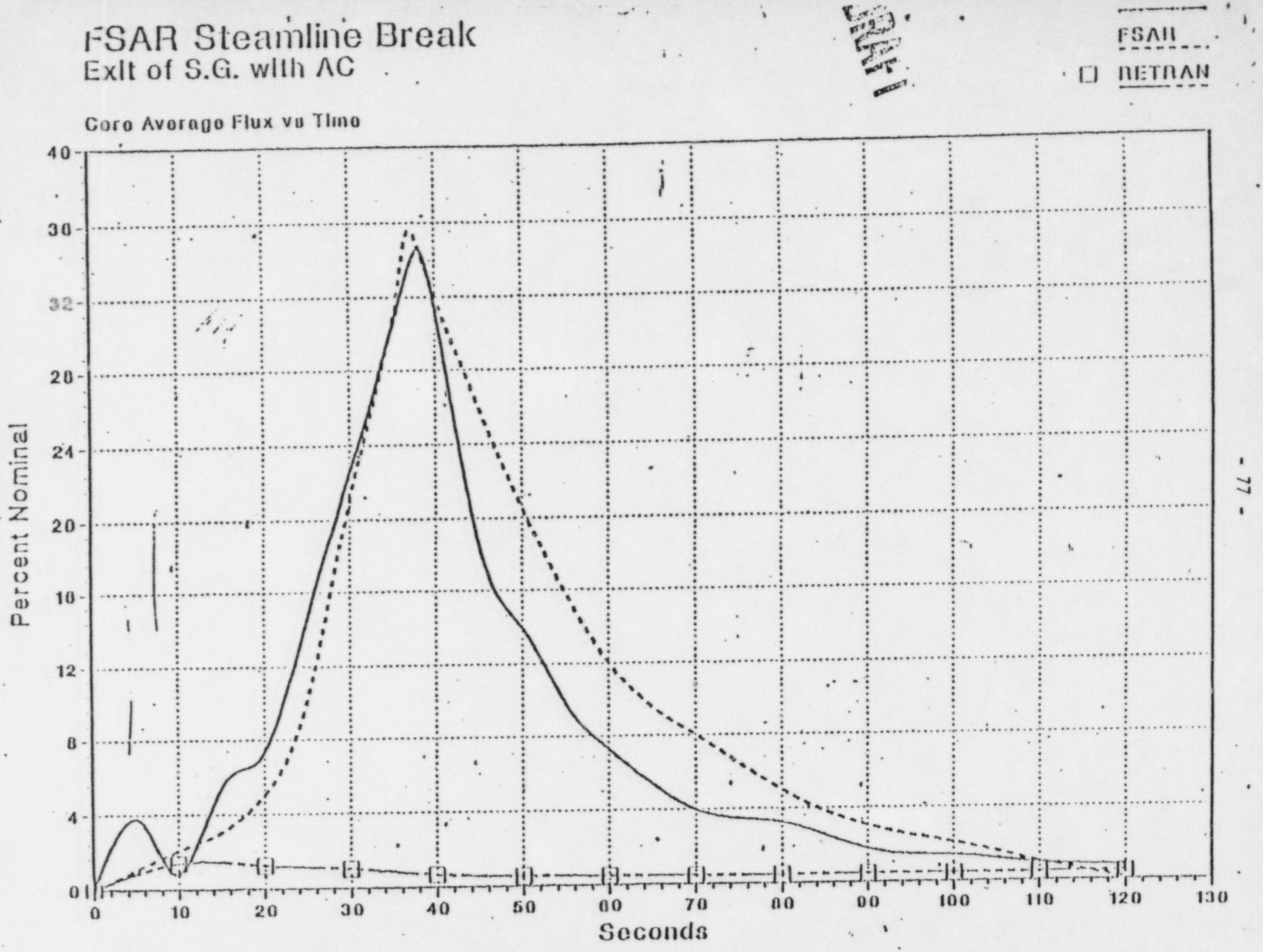


Figure 48

FSAR Steamline Break
Exit of S.G. with AC

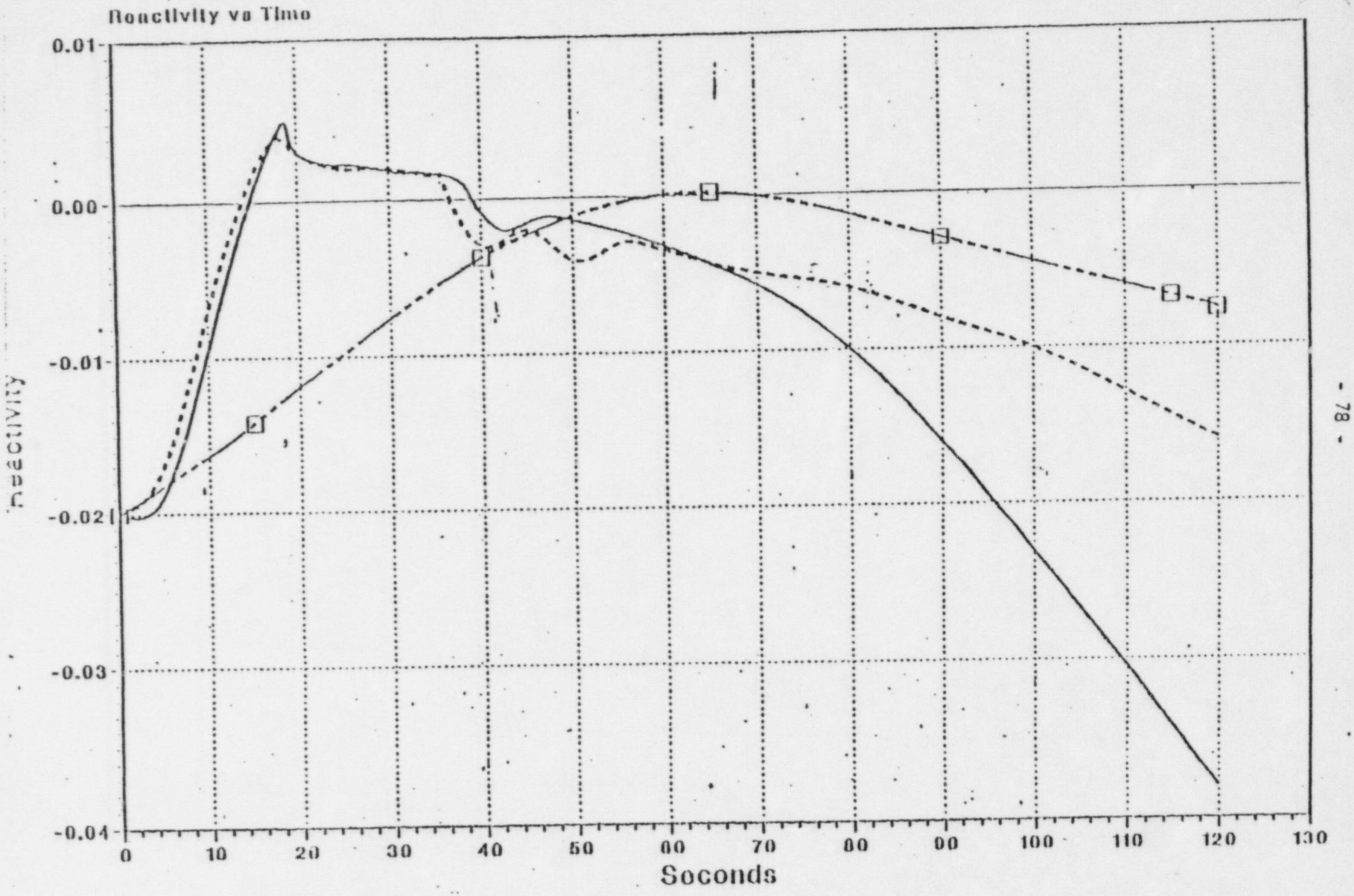


Figure 49

FSAR Steamline Break
Exit of S.G. with AC



DNP110
FSAR
RETRAN

Steam Release vs Time

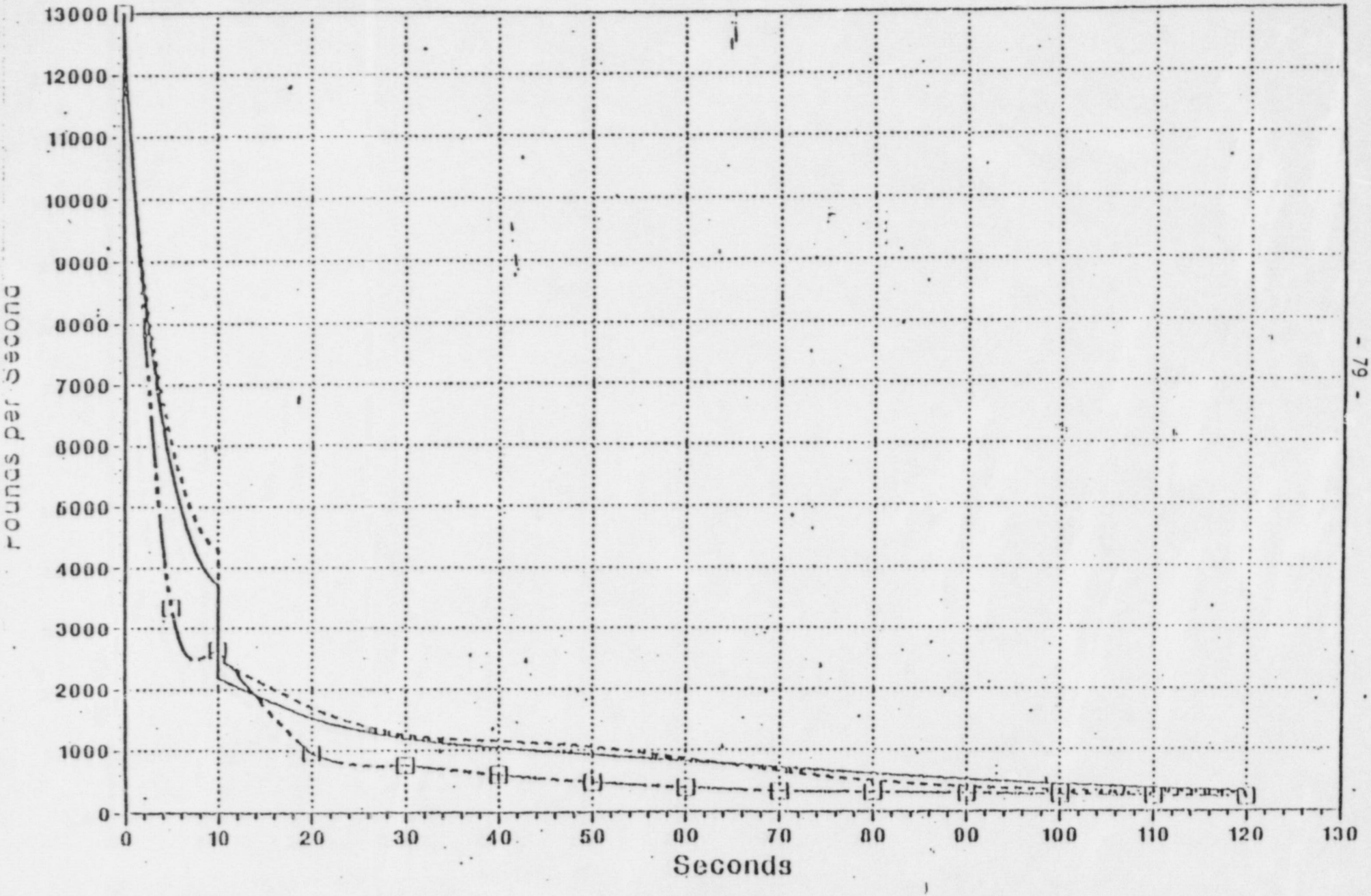


Figure 50

7. References

1. Memorandum from E. L. Jordan to Region Directors, "Analyses of Control Rod Drop Events on Westinghouse PWRs," November 28, 1979.

2. D. H. Risher, Jr., "An Evaluation of the Rod Ejection Accident in Westinghouse Pressurized Water Reactors Using Spatial Kinetics Methods," WCAP-7588, Rev. 1-A, January 1975.

Principal Contributors:
D. C. DiIanni
L. Kopp
E. H. Davidson
C. Y. Li
S. L. Wu
Yi-Hsiung Hsii
W. F. Pasedag

QUALIFICATION OF REACTOR PHYSICS METHODS

FOR

APPLICATION TO

PRAIRIE ISLAND

Revison 1

DECEMBER 1, 1982

PREPARED BY Richard L. Strong 12-8-82
DATE

REVIEWED BY Clifford Bowman 12-8-82
DATE

APPROVED BY _____
DATE

ABSTRACT

This document is a Topical Report describing the Northern States Power Company (NSP) qualification of reactor physics methods for application to the Prairie Island Units.

This document addresses the reactor model description, qualification and quantification of reliability factors and applications to operations and reload safety evaluations of the Prairie Island Units.

LEGAL NOTICE

This report was prepared by or on behalf of Northern States Power Company (NSP). Neither NSP, nor any person acting on behalf of NSP:

a. Makes any warranty or representation, express or implied, with respect to the accuracy, completeness, usefulness, or use of any information, apparatus, method or process disclosed or contained in this report, or that the use of any such information, apparatus, method, or process may not infringe privately owned rights; or

b. Assumes any liabilities with respect to the use of, or for damages resulting from the use of, any information, apparatus, method, or process disclosed in the report.

TABLE OF CONTENTS

		PAGE
1.0	INTRODUCTION	1-1
2.0	GENERAL CHARACTERISTICS OF THE NSP CALCULATIONAL MODELS	2-1
3.0	MODEL VERIFICATION & RELIABILITY FACTOR DETERMINATION	3-1
	3.1 Rod Worth Benchmarking	3-3
	3.2 Temperature Coefficient Benchmarking	3-6
	3.3 Doppler Coefficient	3-9
	3.4 Isotopics	3-14
	3.5 Power Distributions Reliability Factor Determination	3-24
	3.5.1 Local Power Distribution Reliability Factor on F_Q	3-24
	3.5.2 Integrated Power Distribution Reliability Factor on $F_{\Delta H}$	3-33
	3.6 Model Application to Plant Transient Tests	3-108
	3.7 Reliability Factors for Delayed Neutron Parameters	3-113
	3.8 Effective Neutron Lifetime	3-116
4.0	MODEL APPLICATIONS TO REACTOR OPERATIONS	4-1
	4.1 Power Distributions	4-1
	4.2 Isotopic Inventory	4-1
5.0	MODEL APPLICATIONS TO SAFETY EVALUATION CALCULATIONS	5-1
	5.1 Nuclear Heat Flux Hot Channel Factor F_Q^N	5-1
	5.2 Nuclear Enthalpy Rise Hot Channel Factor, $F_{\Delta H}$	5-2
	5.3 Rod Worths	5-3
	5.4 Moderator Coefficient (α_m)	5-3
	5.5 Fuel Temperature (Doppler) Coefficient (α_D)	5-4
	5.6 Boron Concentration Coefficient (α_B)	5-5
	5.7 Effective Delayed Neutron Fraction (β_{eff})	5-5

TABLE OF CONTENTS (continued)

		PAGE
5.8	Prompt Neutron Generation Time (ℓ^*)	5-5
5.9	Shutdown Margin (SDM)	5-6
5.10	Scram Worth Versus Time	5-8
6.0	REFERENCES	6-1
APPENDIX A	Statistical Methods for the Determination and Application of Uncertainties	A-1
A.1	Normal Distribution Statistics	A-2
A.2	Non-Normal Distribution Statistics	A-5
APPENDIX B	Auxiliary Computer Code Summary Description	B-1

LIST OF TABLES

TABLE	TITLE	PAGE
3.0.1	Reliability Factors for Prairie Island	3-2
3.1.1	Measured to Calculated Rod Worth Comparison	3-4
3.2.1	Measured to Calculated Isothermal Temperature Coefficients BOC, HZP	3-7
3.3.1	Resonance Integrals	3-11
3.3.2	Relative Differences in Resonance Integrals	3-12
3.3.3	Temperature Coefficient Comparisons to Experiment	3-13
3.4.1	Comparison Between EPRI-CELL and Saxton Experimental Data	3-16
3.4.2	Comparison Between CASMO and Saxton Experimental Data	3-17
3.5.1	Full Power State Points	3-38
3.6.1	Comparison of FSAR, Measured, Calculated Parameters for Rod Drop and Ejected Rod Tests Prairie Island Unit 1, Cycle 1.	3-110
4.1.1	Standard Deviation of Relative Detector Response Errors	4-3
A.1	Single-Sided Tolerance Factors	A-4

LIST OF FIGURES

FIGURE	DESCRIPTION	PAGE
2.0.1	Flowchart, EPRI-CELL/PDQ/DP5 Model	2-4
2.0.2	Flowchart, CASMO-II/PDQ/DP5 Model	2-5
3.4.1	Comparison of EPRI-CELL to Yankee Isotopic Ratios PU239/PU240	3-18
3.4.2	Comparison of EPRI-CELL to Yankee Isotopic Ratios PU240/PU241	3-19
3.4.3	Comparison of EPRI-CELL to Yankee Isotopic Ratios PU241/Pu242	3-20
3.4.4	Comparison of CASMO to Yankee Isotopic Ratios PU239/PU240	3-21
3.4.5	Comparison of CASMO to Yankee Isotopic Ratios PU240/Pu241	3-22
3.4.6	Comparison of CASMO to Yankee Isotopic Ratios PU241/PU242	3-23
3.5.1	Measured and Calculated Integrated Detector Response HFP BOC Cycle 3	3-40
3.5.2	Measured and Calculated Detector Response HFP BOC Cycle 3 Thimble G6	3-41
3.5.3	Measured and Calculated Detector Response HFP BOC Cycle 3 Thimble E6	3-42

LIST OF FIGURES (Continued)

FIGURE	DESCRIPTION	PAGE
3.5.4	Measured and Calculated Integrated Detector Response MOC Cycle 3	3-43
3.5.5	Measured and Calculated Detector Response MOC Cycle 3 Thimble G6	3-44
3.5.6	Measured and Calculated Detector Response MOC Cycle 3 Thimble I7	3-45
3.5.7	Measured and Calculated Integrated Detector Response EOC Cycle 3	3-46
3.5.8	Measured and Calculated Detector Response EOC Cycle 3 Thimble G6	3-47
3.5.9	Measured and Calculated Detector Response EOC Cycle 3 Thimble K4	3-48
3.5.10	Measured and Calculated Integrated Detector Response BOC Cycle 4	3-49
3.5.11	Measured and Calculated Detector Response BOC Cycle 4 Thimble G6	3-50
3.5.12	Measured and Calculated Detector Response BOC Cycle 4 Thimble E10	3-51
3.5.13	Measured and Calculated Integrated Detector Response MOC Cycle 4	3-52

LIST OF FIGURES (Continued)

FIGURE	DESCRIPTION	PAGE
3.5.14	Measured and Calculated Detector Response MOC Cycle 4 Thimble G6	3-53
3.5.15	Measured and Calculated Detector Response MOC Cycle 4 Thimble I5	3-54
3.5.16	Measured and Calculated Integrated Detector Response EOC Cycle 4	3-55
3.5.17	Measured and Calculated Detector Response EOC Cycle 4 Thimble G6	3-56
3.5.18	Measured and Calculated Detector Response EOC Cycle 4 Thimble J8	3-57
3.5.19	Measured and Calculated Integrated Detector BOC Cycle 5	3-58
3.5.20	Measured and Calculated Detector Response BOC Cycle 5 Thimble G6	3-59
3.5.21	Measured and Calculated Detector Response BOC Cycle 5 Thimble C8	3-60
3.5.22	Measured and Calculated Integrated Detector Response MOC Cycle 5	3-61
3.5.23	Measured and Calculated Detector Response MOC Cycle 5 Thimble H3	3-62

LIST OF FIGURES (Continued)

FIGURE	DESCRIPTION	PAGE
3.5.24	Measured and Calculated Detector Response MOC Cycle 5 Thimble D7	3-63
3.5.25	Measured and Calculated Integrated Detector Response EOC Cycle 5	3-64
3.5.26	Measured and Calculated Detector Response EOC Cycle 5 Thimble D5	3-65
3.5.27	Measured and Calculated Detector Response EOC Cycle 5 Thimble H8	3-66
3.5.28	Measured and Calculated Integrated Detector Response BOC Cycle 6	3-67
3.5.29	Measured and Calculated Detector Response BOC Cycle 6 Thimble G6	3-68
3.5.30	Measured and Calculated Detector Response BOC Cycle 6 Thimble J10	3-69
3.5.31	Measured and Calculated Integrated Detector Response MOC Cycle 6	3-70
3.5.32	Measured and Calculated Detector Response MOC Cycle 6 Thimble G6	3-71
3.5.33	Measured and Calculated Detector Response MOC Cycle 6 Thimble G11	3-72
3.5.34	Measured and Calculated Integrated Detector Response EOC Cycle 6	3-73

LIST OF FIGURES (Continucd)

FIGURE	DESCRIPTION	PAGE
3.5.35	Measured and Calculated Detector Response EOC Cycle 6 Thimble G6	3-74
3.5.36	Measured and Calculated Detector Response EOC Cycle 6 Thimble K7	3-75
3.5.37	Measured and Calculated Integrated Detector Response BOC Cycle 5 CASMO/PDQ/DP5 Model	3-76
3.5.38	Measured and Calculated Detector Response BOC Cycle 5 CASMO/PDQ/DP5 Model Thimble G6	3-77
3.5.39	Measured and Calculated Detector Response BOC Cycle 5 CASMO/PDQ/DP5 Model Thimble C8	3-78
3.5.40	Measured and Calculated Integrated Detector Response MOC Cycle 5 CASMO/PDQ/DP5 Model	3-79
3.5.41	Measured and Calculated Detector Response MOC Cycle 5 CASMO/PDQ/DP5 Model Thimble H3	3-80
3.5.42	Measured and Calculated Detector Response MOC Cycle 5 CASMO/PDQ/DP5 Model Thimble D7	3-81
3.5.43	Measured and Calculated Integrated Detector Response EOC Cycle 5 CASMO/PDQ/DP5 Model	3-82
3.5.44	Measured and Calculated Detector Response EOC Cycle 5 CASMO/PDQ/DP5 Model Thimble D5	3-83
3.5.45	Measured and Calculated Detector Response EOC Cycle 5 CASMO/PDQ/DP5 Thimble H8	3-84

LIST OF FIGURES (Continued)

FIGURE	DESCRIPTION	PAGE
3.5.46	Measured and Calculated Integrated Detector Response BOC Cycle 6 CASMO/PDQ/DP5 Model	3-85
3.5.47	Measured and Calculated Detector Response BOC Cycle 6 CASMO/PDQ/DP5 Model Thimble G6	3-86
3.5.48	Measured and Calculated Detector Response BOC Cycle 6 CASMO/PDQ/DP5 Model Thimble J10	3-87
3.5.49	Measured and Calculated Integrated Detector Response MOC Cycle 6 CASMO/PDQ/DP5 Model	3-88
3.5.50	Measured and Calculated Detector Response MOC Cycle 6 CASMO/PDQ/DP5 Model Thimble G6	3-89
3.5.51	Measured and Calculated Detector Response MOC Cycle 6 CASMO/PDQ/DP5 Model Thimble G11	3-90
3.5.52	Measured and Calculated Integrated Detector Response EOC Cycle 6 CASMO/PDQ/DP5 Model	3-91
3.5.53	Measured and Calculated Detector Response EOC Cycle 6 CASMO/PDQ/DP5 Model Thimble G6	3-92
3.5.54	Measured and Calculated Detector Response EOC Cycle 6 CASMO/PDQ/DP5 Model Thimble K7	3-93
3.5.55	Observed Differences Density Function ECELL /PDQ/DP5 Model Comparison	3-94

LIST OF FIGURES (Continued)

FIGURE	DESCRIPTION	PAGE
3.5.56	Cumulative Distribution Function (CDF) ECELL /PDQ/DP5 Model Comparison	3-95
3.5.57	CDF in Region of 95th Percentile ECELL/PDQ/ DP5 Model Comparison	3-96
3.5.58	Observed Differences Density Function CASMO/PDQ/ DP5 Model Comparison	3-97
3.5.59	Cumulative Distribution Function (CDF) CASMO/PDQ/ DP5 Model Comparison	3-98
3.5.60	CDF in Region of 95th Percentile CASMO/PDQ/DP5 Model Comparison	3-99
3.5.61	Observed Differences Density Function Integrated Reaction Rates ECELL/PDQ/DP5 Model Comparison	3-100
3.5.62	Cumulative Distribution Function (CDF) for Integrated Reaction Rates ECELL/PDQ/DP5 Model	3-101
3.5.63	CDF in Region of 95th Percentile for Integrated Reaction Rates ECELL/PDQ/DP5 Model	3-102
3.5.64	Observed Difference Density Function Integrated Reaction Rates CASMO/PDQ/DP5 Model	3-103
3.5.65	Cumulative Distribution Function (CDF) for Integrated Reaction Rates CASMO/PDQ/DP5 Model	3-104

LIST OF FIGURES (Continued)

FIGURE	DESCRIPTION	PAGE
3.5.66	CDF in Region of 95th Percentile for Integrated Reaction Rates CASMO/PDQ/DP5 Model	3-105
3.5.67	Reliability Factor Versus Measured Instrument Response ECELL/PDQ/DP5	3-106
3.5.68	Reliability Factor Versus Measured Instrument Response CASMO/PDQ/DP5	3-107
3.6.1	Xenon Transient Test 9/5/74, Prairie Island Unit 1, Cycle 1	3-111
3.6.2	Xenon Transient Test 5/26/76, Prairie Island Unit 1, Cycle 2	3-112

1.0 INTRODUCTION

This report addresses the reactor model description, qualification and quantification of reliability factors, and applications to operations and reload safety evaluations of the Prairie Island Nuclear Reactors.

A summary description of the computer codes is given in Section 2. This report stresses the aspects of implementation of the NSP model, the individual code descriptions are referenced in Section 6.

Whenever possible, directly observable parameters (such as boron concentraton, incore detector fission rate and core exit thermocouples readings) are utilized. The PI1 data used in this evaluation span cycles 3 thru 6. In order to be completely objective in the choice of data to be used for the comparisons, all PI1 cycles 3 thru 6 measurements were reviewed and qualified prior to initiating the comparison calculations. Data rejection was based on the consistency of the data itself without prior knowledge of how it might compare to the model calculations.

After the measured data to be used in the benchmark process had been defined, the model calculations were performed and comparisons are presented in this report as part of the quantification of the NSP model calculational uncertainties and reliability factors. A statistical approach was used to derive the uncertainties. These uncertainties are consistent with the model application procedures and methodology.

The uncertainties are evaluated by direct comparison to experimental data.

In order to provide a continuing verification of the conservatism of the reliability factors determined by PI1 cycles 3 through 6 data, ongoing comparisons are made each cycle using the statistical methods described in this report. A discussion of the reliability factors is provided in Section 3.

The methods for use of the model and the reliability factors is described relative to reactor operation and reload safety evaluation in Sections 4 and 5.

2.0 GENERAL CHARACTERISTICS OF THE NSP CALCULATIONAL MODELS

Two calculational models have been used to analyze Prairie Island. The first model is a derivative of the Advanced Recycle Methodology Program[1] (ARMP) system developed under EPRI sponsorship by NAI. This model was normalized to cycles 3 through 6 for PI1. The second model is identical to the first with the exception that the EPRI-CELL program has been replaced with the CASMO II program developed by Studsvik Energiteknik AB[2]. This model was normalized to PI1 cycle 5 and 6 for continuity and is the model that will be used to analyze future cycles. These models are referred to as the ECELL/PDQ/DP5 model and the CASMO/PDQ/DP5 models respectively.

A flow diagram for the first model is shown in Figure 2.0.1. The spectral code, EPRI-CELL (ARMP, Part II, Chapter 5), produces initial nuclide concentrations, depletion and fission product chain data, and tables of microscopic and macroscopic cross sections varying with burn-up for input to the XY diffusion - depletion code, PDQ7/HARMONY[3,4]. Lumped absorber data for PDQ7/HARMONY are generated by a capture fraction matching procedure between PDQ7 and either EPRI-CELL (ARMP, PART I, Chapter 6, Section 4) for burnable poisons or CPM (ARMP, Part I, Chapter 6, Section 3) for control rods. PDQ7/HARMONY is run both in the quarter core mode and in the fuel type (color set) mode. The quarter core mode is used for nodal code normalization, local peaking factor generation, and for the establishment of assembly loading patterns.

In the color set mode, PDQ7/HARMONY supplies input data for NSP's nodal program, DP5, a derivative of the EPRI-NODE-P program (ARMP, Part II, Chapter 14). The DP5 program contains the following improvements over the NODE-P program:

- 24 axial nodes per assembly
- 4 radial nodes per assembly
- a nonlinear DOPPLER dependance with exposure

- a new parameter, LPF, has been added which is, in addition to the α and g parameters, used to normalize the nodal model to the more exacting PDQ representation. The LPF parameter is used as a multiplier on the assembly M^2.
- a routine has been added to calculate the parameters used in the transient analyses models (β, ℓ^*, etc.) for each time step.

Other minor changes have been made such as input and output edits, etc. but the primary calculational sequence and physics methodology have been preserved from the EPRI-NODE-P program.

A flow diagram for the second model is shown in Figure 2.0.2. The CASMO II program is a modified version of the CASMO[5] program distributed by EPRI. The major differences between CASMO II and CASMO are as follows:

- A non-symmetrically loaded fuel assembly can be represented. CASMO could only represent 1/8 of an assembly.
- Ability to shuffle fuel pins within an assembly in order to analyze fuel reconstitution.
- A two-dimensional diffusion theory routine (DIXY[6]) has been added to generate micro, macro, MND, IRT cross section, G-Factors, number densities integrated number of fissions, and a lumped fission product cross section for input into PDQ7/HARMONY.

The CASMO II program thus produces all of the input for PDQ7/HARMONY that was produced by the EPRI-CELL program for the previous model. The CASMO II program is also used to supply the input to the nodal program DP5. The PDQ7/HARMONY program is used for nodal program normalization, local peaking factor generation, for establishment of assembly loading patterns, and generation of detector constants.

It is recognized that the procedures used for the construction and application of the PI model are as much a part of the model definition as are the codes. It is essential, therefore, that the procedures used to calculate core safety margins be the same as those used in the model benchmarking and qualification process. This is particularly true in the calculation of core power distributions and local peaking factors in which the results are heavily dependent on the procedure used to normalize the nodal model. In view of the importance of model normalization, it is appropriate to identify the key aspects of the procedures used for Prairie Island and their application to future safety related calculations.

The Prairie Island nodal model has been normalized to both plant measurements and the PDQ model for cycles 3 thru 6. Those parameters that have been normalized to plant data have been constrained to retain a single set of values for all of the benchmark results presented in this document. These will also be used for future safety related calculations. The only normalization parameters that have been allowed to vary from cycle to cycle are those that have been analytically determined from the PDQ model. In such cases, the procedures used to derive these normalization parameters will also be used in performing future safety related calculations.

In addition to the main sequence computer codes, a number of auxiliary computer codes are employed to provide a user tailored code package. These auxiliary computer codes are not basic to the physics methodology, but are vital for automation and transformation of the large volume of calculated and measured parameters required for core analysis. The auxiliary computer codes are summarized in Appendix B.

FIGURE 2.0.1

EPRI - CELL/PDQ/DP5 MODEL

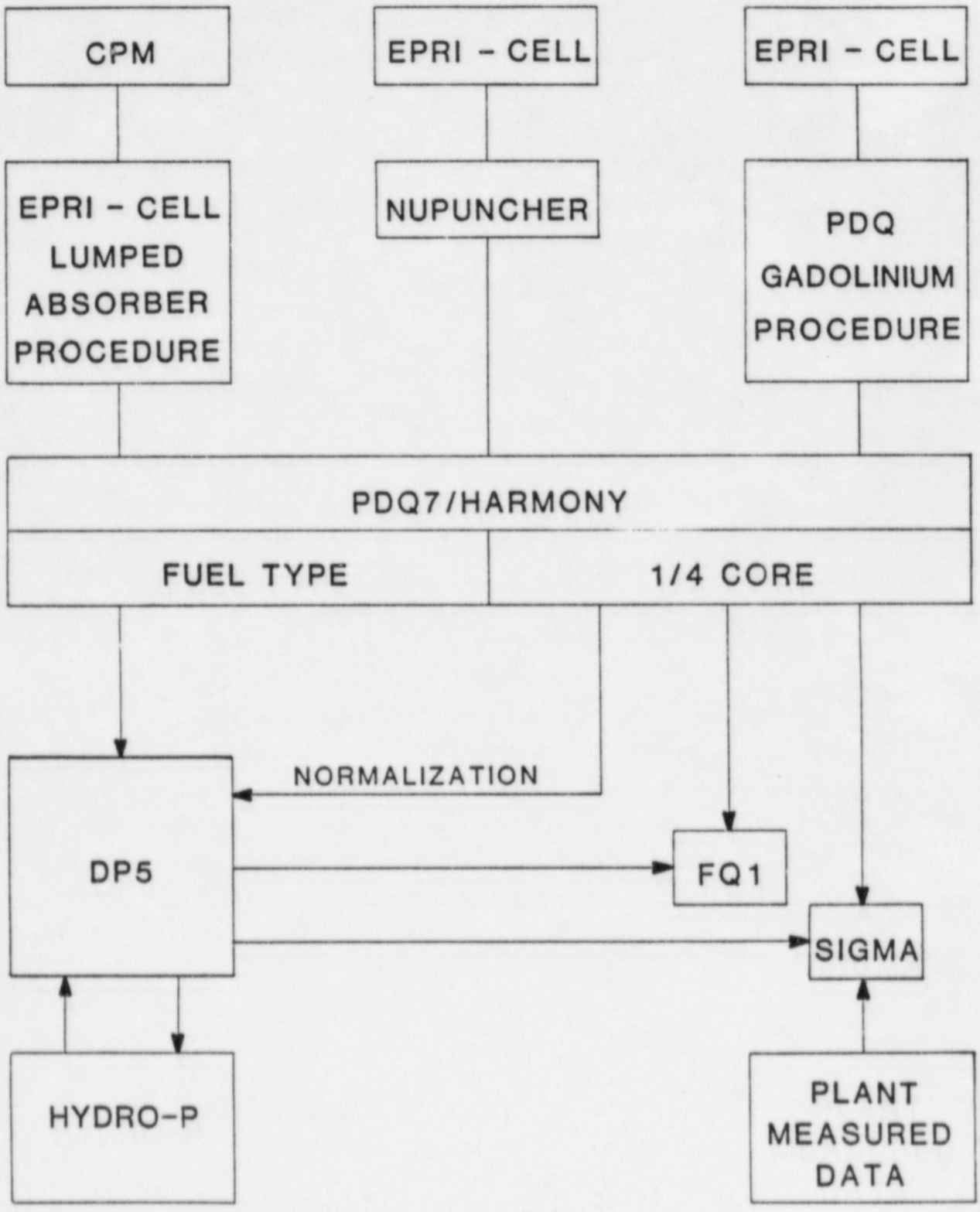
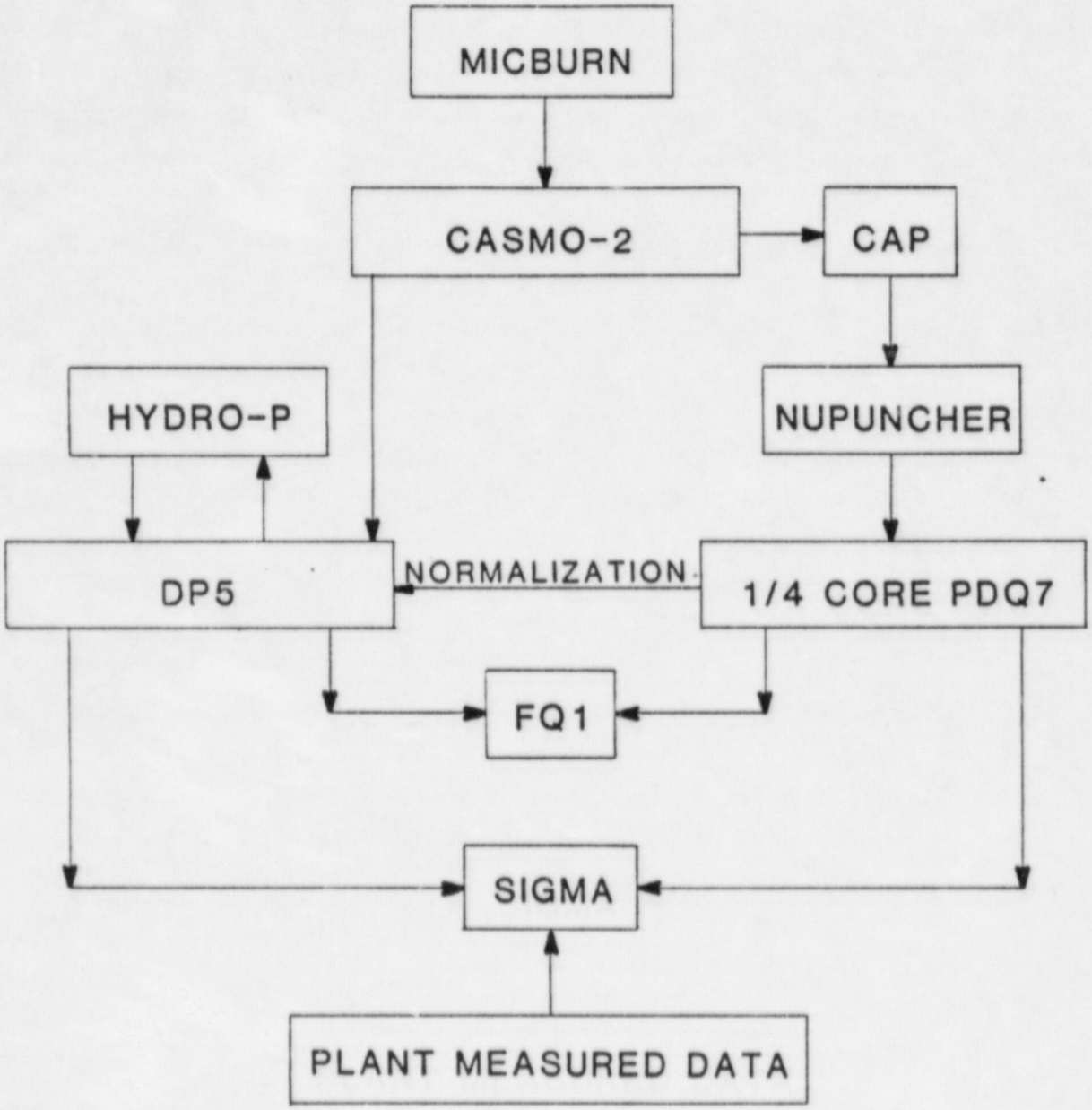


FIGURE 2.0.2

CASMO/PDQ/DP5 MODEL



3.0 MODEL VERIFICATION & RELIABILITY FACTOR DETERMINATION

The NSP models have been benchmarked against PI1 measurements made during cycles 3 thru 6 for the ECELL/PDQ/DP5 model and cycles 5 and 6 for the CASMO/PDQ/DP5 model to quantify the reliability factors to be used in safety related calculations. The resultant reliability factors and biases are summarized in Table 3.0.1. The remainder of this section is a detailed account of the derivation of these factors.

The term reliability factor (RF) is used to describe the allowances to be used in safety related calculations to assure conservatism. The uncertainty factor (1σ) is used to describe the actual model accuracy. The reliability factor is always larger than the uncertainty factor.

The term bias is used to describe the statistical difference between an observed or measured distribution and the calculated value.

Appendix A describes the statistical methods used in the evaluation of the uncertainties in the following sections.

During each cycle, measured and calculated parameters will be compared in order to verify and update the reliability factors determined in this section. Results of the verification and update for each parameter will be documented in the reload safety evaluation for the reload in which the updated values will be used. The updates to the reliability factors will be in accordance with the methods outlined in this section and in appendix A.

TABLE 3.0.1

Reliability Factors for Prairie Island

PARAMETER	ECELL/PDQ/DP5 RELIABILITY FACTOR	BIAS	CASMO/PDQ/DP5 RELIABILITY FACTOR	BIAS
F_Q^N	RF_{FQ} = 0.067	0.007	RF_{FQ} = 0.062	0.015
$F_{\Delta H}$	$RF_{F\Delta H}$ = 0.035	0	$RF_{F\Delta H}$ = 0.044	0
Rod Worth	RF_{Rods} =0.10	0	RF_{Rods} = 0.10	0
Temperature Coefficient(PCM/°F)	RF_M= 2.1	0.03	RF_M = 2.9	-0.03
Doppler Coefficient	RF_D = 0.10	0	RF_D = 0.10	0
Doppler Defect	RF_{DD} = 0.20	0	RF_{DD} = 0.20	0
Boron Worth	RF_B = 0.10	0	RF_B = 0.10	0
Delayed Neutron Parameters	RF_β = 0.04	0	RF_β = 0.04	0
	RF_{ℓ^*} =0.04	0	RF_{ℓ^*} =0.04	0

3.1 Rod Worth Benchmarking

Reactivity measurements made with the reactivity computer are interpretations of dynamic flux behavior based on a point kinetics model. Spatial flux redistributions cannot be isolated from reactivity effects. However, during the rod worth dilution measurements, critical boron concentrations can be measured at various stages of rod insertion. The accuracy of the boron concentration measurements is limited only by the titration accuracy which is estimated to be better than 2%. The approach taken is to benchmark the NSP models to the directly observable parameter, boron.

The data used in the benchmarking represent the actual measured critical statepoints without corrections to bank end points. All measured statepoints were included. The results are shown in Table 3.1.1 for ECELL/PDQ/DP5 followed by the CASMO/PDQ/DP5.

The standard deviation of the differences between measured and calculated boron end points is 1.0% for ECELL/PDQ/DP5 and is 1.0% for CASMO/PDQ/DP5. The boron measurement accuracy is less than or equal to 2%. Table 3.1.1 shows that the percent difference is of the same order as the measurement accuracy. For conservatism, the rod worth reliability factor (RF_{rods}) is defined as 10%. For consistency, the boron worth reliability factor is assumed to be of the same magnitude.

TABLE 3.1.1

MEASURED TO CALCULATED

BORON ENDPOINTS

ECELL/PDQ/DP5 MODEL

Cycle	Rod Position	BORON ENDPOINTS (PPM) Meas.	Calc.*	% Diff
3	D at 192	1444	1464	-1.4
	C at 219 D in	1372	1386	-1.0
	B at 213 D,C in	1264	1268	-0.3
4	D at 198	1455	1459	-0.3
	C at 210 D in	1388	1401	-0.9
	D at 211 D,C in	1261	1260	+0.1
5	D at 195	1496	1487	+0.6
	C at 211 D in	1436	1417	1.3
	B at 220 D,C in	1317	1293	1.9
	A at 25 D,C,B in	1028	1014	1.4
6	D at 213	1409	1406	0.2
	SDB at 191 D,C,B,A in	896	894	0.2

Bias = -3.9% σ = 1.0%

*Calc = DP5 calculated Boron Endpoint Times (1 + Bias/100%)

TABLE 3.1.1 (Continued)

CASMO/PDQ/DP5 MODEL

Cycle	Rod Position	BORON ENDPOINTS (PPM) Meas.	Calc.*	% Diff
5	D at 195	1496	1502	-0.4
	C at 211, D in	1436	1434	+0.1
	B at 220, C,D in	1317	1313	+0.3
	A at 25, B,C,D in	1028	1037	-0.9
6	D at 213	1409	1382	+1.9
	SDB at 191, A,B,C, D in	896	902	-0.7

Bias = -1.5% σ = 1.0%

* Calc = DP5 calculated Boron Endpoint t mes (1 + Bias/100%)

3.2 Temperature Coefficient Benchmarking

Measurements of the isothermal temperature coefficient (ITC) at HZP are adequately made with a reactivity computer as there is usually no rod motion. When there is rod motion, there is usually sufficient time to allow the flux to stabilize.

The comparisons of the measured ITC to the NSP models are summarized in Table 3.2.1. For the ECELL/PDQ/DP5 model the constant bias is 0.03 pcm/°F with a 1σ standard deviation of 0.65 pcm/°F. For the CASMO/PDQ/DP5 model the constant bias is -0.03pcm/°F with a 1σ standard deviation of 0.56pcm/°F.

The ITC reliability is defined as 2.1 pcm/°F for the ECELL/PDQ/DP5 model and 2.9pcm/°F for the CASMO/PDQ/DP5 model. This assures that the measured ITC will be bounded by the prediction including bias at a 95%/95% level of confidence (assuming normal distribution). These are absolute (measured-calculated) rather than relative ((measured-calculated)/(measured)) reliabilities because the relative reliability is undefined for an ITC value of 0.0 PCM/°F. The calculation is shown below (see Appendix A.1):

ECELL/PDQ/DP5 RF = $K_c(N)*\sigma$ = 3.19(.65) = 2.1pcm/°F

Bias = .03pcm/°F

CASMO/PDQ/DP5 RF = $K_c(N)*\sigma$ = 5.15(.56) = 2.9pcm/°F

Bias = -.03pcm/°F

TABLE 3.2.1

Measured and Calculated Isothermal Temperature Coefficients

BOC, HZP

ECELL/PDQ/DP5

CYCLE	ROD POSITION BANK	STEP	T_{MOD} (°F)	BORON (ppm)	ITC $\frac{(pcm)}{°F}$ Meas.	Calc.	Diff pcm/°F
3	D	192	544	1444	-2.70	-3.20	.50
	D	0					
	C	0					
	B	213	545	1264	-7.03	-7.55	.52
4	D	198	545	1455	-3.27	-3.15	-.12
	D	0					
	C	0					
	B	185	545	1253	-7.17	-8.30	1.13
5	D	200	545	1496	-2.75	-2.15	-.60
	D	0					
	C	211	545	1435	-4.44	-3.64	-.80
	D	0					
	C	0					
	B	220	545	1315	-6.70	-6.36	-.34
6	D	211	546	1403	-2.67	-2.62	-.05

Bias = .03 pcm/°F σ = .65 pcm/°F

TABLE 3.2.1 (Continued)

CASMO/PDQ/DP5

CYCLE	ROD POSITION BANK	STEP	T_{MOD} (°F)	BORON (ppm)	ITC (pcm/°F) Meas.	Calc.	Diff pcm/°F
5	D	200	545	1496	-2.75	-2.06	-.69
	D	0					
	C	211	545	1435	-4.44	-4.20	-.24
	D	0					
	C	0					
	B	220	545	1315	-6.70	-7.30	.60
6	D	211	546	1403	-2.67	-2.87	.20

Bias = -.03pcm/°F σ = .56pcm/°F

3.3 DOPPLER COEFFICIENT

Measurements can be made which are directed at determining the Doppler coefficient at various power levels. The uncertainty associated with such measurement (e.g., rod repositioning) and with the interpretation (e.g., reactivity inference by a reactivity computer) are such that results are not reliable for direct validation of the calculational model. Consequently, an indirect approach is taken.

For the ECELL/PDQ/DP5 model the primary variable in this calculation is the change in fuel temperature associated with the power change which results in a reactivity change due to the change in the resonance absorption (i.e., Doppler effects).

The algorithm in DP5 that determines the model change in reactivity due to the model fuel temperature change uses data calculated by EPRI-CELL, i.e., $\Delta\rho/^{o}F$. The approach is to determine the accuracy of EPRI-CELL in calculating the change in resonance integral (RI) due to a known fuel temperature increase, and to use engineering judgment to bound this uncertainty to assure conservatism. The results of these analyses are summarized in Tables 3.3.1 to 3.3.3 which are from the ARMP documentation, Part I, Chapter 4.

Comparisons of calculated and measured resonance integrals and fuel temperature coefficients are presented. In addition, the results in Table 3.3.1 can be utilized to compare the measured ΔRI due to a fuel temperature change with the calculated difference. In all cases, the calculated values from both EPRI-CELL and CPM are well within the quoted measurement uncertainty (4% on the resonance integrals and 10% on the coefficients). In view of this, a 10% reliability factor placed on the Doppler coefficient and a 20% reliability factor on the Doppler defect is judged adequate to assure a conservative value.

Comparisons of EPRI-CPM and CASMO calculations to experiments performed at the Kritz facility[9,10,11] in Sweden corroborate the 10% reliability factor on the Doppler coefficient for the CASMO/PDQ/DP5 model.

TABLE 3.3.1

RESONANCE INTEGRALS

Fuel Rod Radius(cm)	Temperature (°K)	Experiment	E≤0.821MeV		E≤2.2MeV	
			CPM	E-CELL	CPM	E-CELL
0.52	300	21.750	21.783	21.254	22.113	21.350
0.52	900	23.688	23.850	23.335	24.180	23.431
1.04	300	17.019	16.643	16.916	16.973	17.012
1.04	900	18.332	17.977	18.265	18.307	18.361

TABLE 3.3.2

RELATIVE DIFFERENCES IN RESONANCE INTEGRALS

$$RE = (RI - RI_{Exp})/RI_{Exp}$$

Fuel Rod Radius(cm)	Temperature (°K)	E≤0.821MeV		E≤2.2MeV	
		CPM	E-CELL	CPM	E-CELL
0.52	300	+.0015	-.0228	+.0167	-.0184
0.52	900	+.0068	-.0149	+.0208	-.0108
1.04	300	-.0221	-.0061	-.0027	-.0004
1.04	900	-.0194	-.0037	-.0014	+.0016

TABLE 3.3.3

TEMPERATURE COEFFICIENTS

$$\beta = \left[\frac{RI(T) - \delta}{RI(T_o) - \delta} - 1 \right] / \left[\sqrt{T} - \sqrt{T_o} \right]$$

$T = 900°K$ $\quad T_o = 300°K$ $\quad \delta = 1.558$ b

Fuel Rod Radius(cm)	Experiment	E≤0.821MeV CPM	E≤0.821MeV E-CELL	E≤2.2MeV CPM	E≤2.2MeV E-CELL
0.52	.0077	.0081	.0083	.0079	.0083
1.04	.0067	.0070	.0069	.0068	.0069

3.4 Isotopics

Isotopic compositions calculated by EPRI-CELL have been compared with spent fuel isotopic data obtained from Yankee Rowe fuel rods irradiated beyond 35 GWD/MTU. The reactor respresentation used for the EPRI-CELL and CASMO benchmarking in the calculations is described in the ARMP documentation (Part 1, Chapter 1, Section 4.0).

Experimental and analytic isotopic ratios for plutonium from the Yankee Rowe spent fuel are plotted versus accumulated fissions in Figures 3.4.1-3.4.3. The dots are experimental results and the line the EPRI-CELL results.

The agreement between calculated and experimental isotopic ratios is good. The calculated ratios Pu-239/Pu-240 and Pu-240/Pu-241 are within the scatter of the experimental results and the ratio Pu-241/Pu-242 is slightly over-predicted.

Calculated and measured isotopic compositions for MO_2 fuel (6.6 w/o) irradiated in the Saxton Core II (pellet, rod MY, zone 6) are compared in Table 3.4.1. The agreement is good for the most important uranium and plutonium isotopes as well as for americium and curium. The measured burnup ranged from 7 to 22 GWD/MTU. The reactor representation for the EPRI-CELL benchmarking is described in the ARMP documentation (Part 1, Chapter 3, Section 4).

Isotopic compositions calculated by CASMO have been compared with spent fuel isotopic data obtained from Yankee and Saxton. The reactor representation in the calculation is analogous to that used for the EPRI-CELL benchmarking above.

Isotopic ratios for plutonium in Yankee are compared in Figures 3.4.4 to 3.4.6. The abscissa is a fission product number density assuming a yield of unity and volume averaged over the pin cell. The corresponding burnup in MWd/kgU is also shown. The dots are experimental results and the line the CASMO results.

The agreement between calculated and experimental isotopic ratios is good. The calculated ratios Pu239/Pu240 and Pu240/Pu241 are within the scatter of the experimental results and the ratio Pu241/Pu242 is slightly overpredicated (by about 3% at 30 MWd/kgU).

Calculated and measured isotopic compositions for Saxton (pellet, rod MY, zone 6) are compared in Table 3.4.2. The agreement is good for the most important uranium and plutonium isotopes as well as for americium and curium. The concentrations of Np237, Pu238 and Pu242 are underestimated.

TABLE 3.4.1

COMPARISON BETWEEN EPRI-CELL AND SAXTON EXPERIMENTAL DATA

NUCLIDE	EXPERIMENT	EXPERIMENTAL UNCERTAINTY %	EPRICELL-EXP *100% Exp.
		ATOM %	
U-234	.00465	28.7	-3.7
U-235	.574	.9	+1.7
U-236	.0355	5.6	-7.6
U-238	99.386	0	0
Pu-238	.109	2.2	-32.1
Pu-239	73.77	0	+0.6
Ru-240	19.25	.2	-3.5
Pu-241	6.29	.3	-4.6
Pu-242	.579	.9	-11.7
		ATOM RATIOS	
Np-237/U-238	1.14×10^{-4}	15	-26.9
Pu-239/U-238	.04383	.7	+ 2.0
Pu-238/Pu-239	1.75×10^{-3}	.4	-17.6
Am-241/Pu-239	.0123	15	+ 2.4
Cm-242/Pu-239	1.05×10^{-4}	10	- 0.4
Cm-242/Pu-239	1.09^{-4}	20	- 3.2

TABLE 3.4.2

COMPARISON BETWEEN CASMO AND SAXTON EXPERIMENTAL DATA

Nuclide	Experiment	Experimental Uncertainty %	CASMO-exp *100% exp
		ATOM %	
U234	.00465	28.7	+15.9
U235	.574	.9	- 0.3
U236	.0355	5.6	- 2.8
U238	99.386	0	0
Pu238	.109	2.2	-11.4
Pu239	73.77	0	- 0.3
Pu240	19.25	.2	+ 1.6
Pu241	6.29	.3	+ 0.4
Pu242	.579	.9	-16.0
		ATOM RATIOS	
Np237/U238	$1.14.10^{-4}$	15	-26.4
Pu239/U238	.04383	.7	+ 0.2
Pu238/Pu239	$1.75.10^{-3}$	.4	- 9.8
Am241/Pu239	.0123	15	-10.6
Cm242/Pu239	$1.05.10^{-4}$	10	0
Cm244/Pu239	$1.09.10^{-4}$	20	0

FIGURE 3.4.1

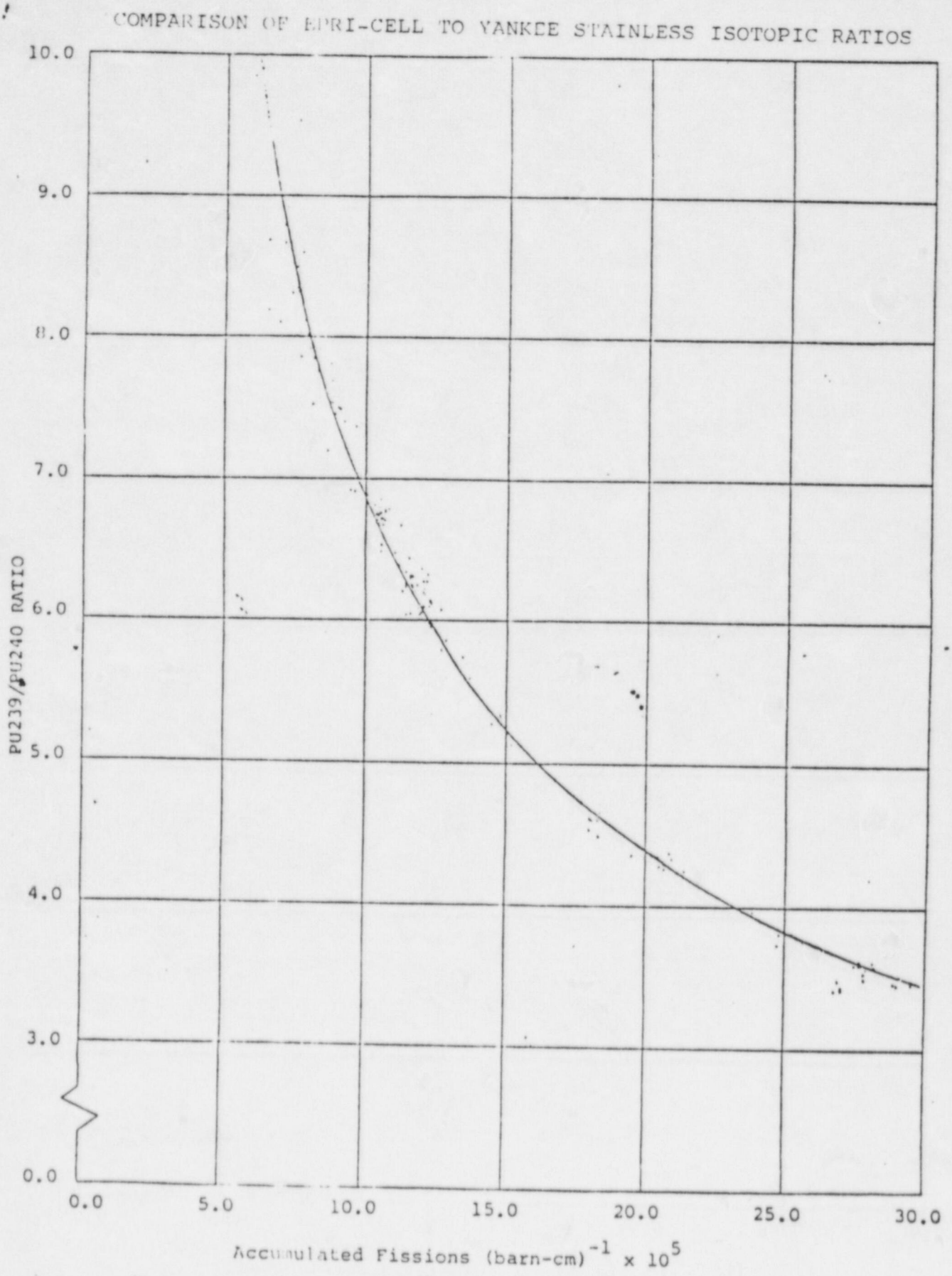

COMPARISON OF EPRI-CELL TO YANKEE STAINLESS ISOTOPIC RATIOS
PU239/PU240 RATIO
10.0
9.0
8.0
7.0
6.0
5.0
4.0
3.0
0.0
0.0
5.0
10.0
15.0
20.0
25.0
30.0
Accumulated Fissions (barn-cm)$^{-1}$ x 10^5

FIGURE 3.4.2

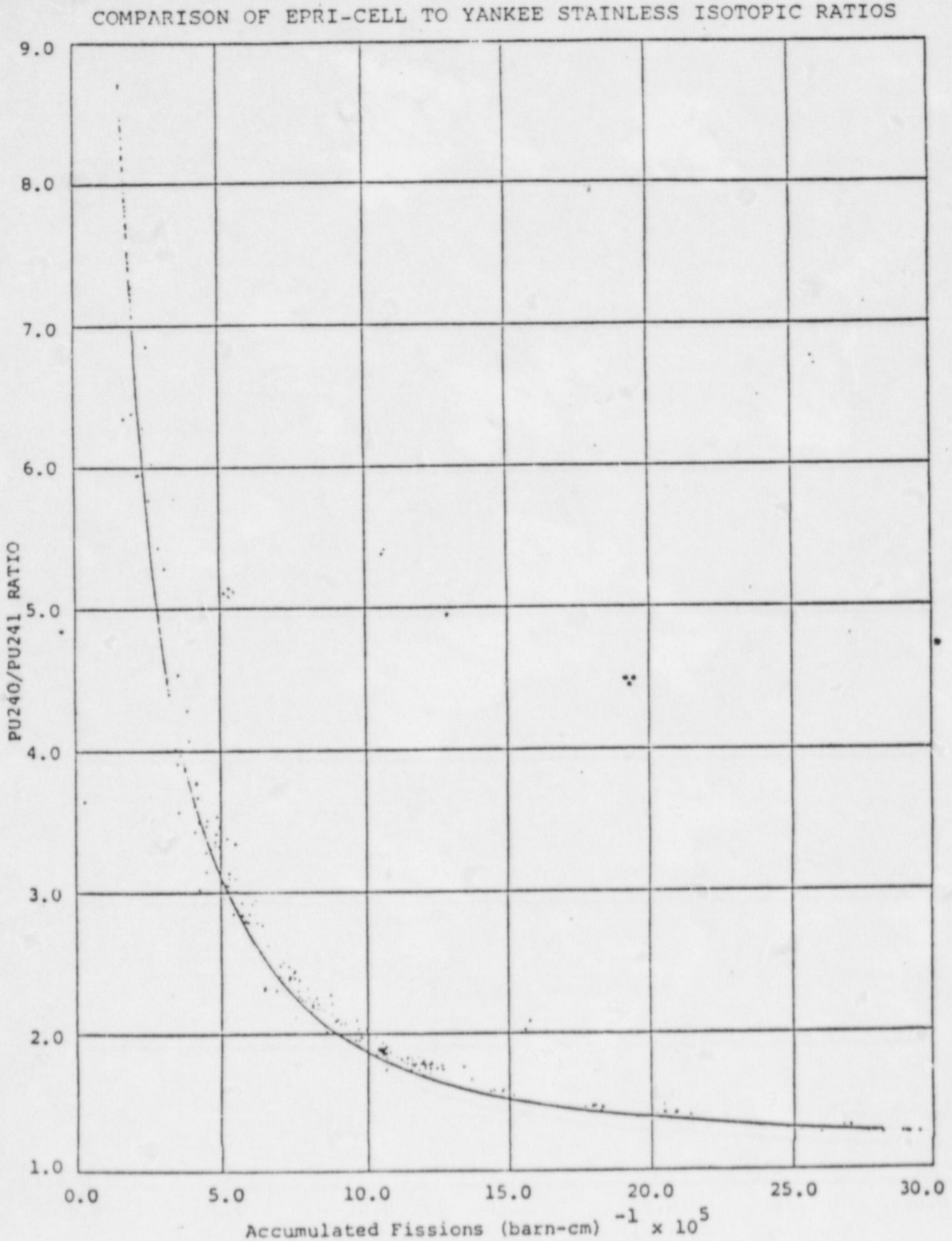

COMPARISON OF EPRI-CELL TO YANKEE STAINLESS ISOTOPIC RATIOS
PU240/PU241 RATIO
9.0
8.0
7.0
6.0
5.0
4.0
3.0
2.0
1.0
0.0
5.0
10.0
15.0
20.0
25.0
30.0
Accumulated Fissions (barn-cm) -1 x 10 5

FIGURE 3.4.3

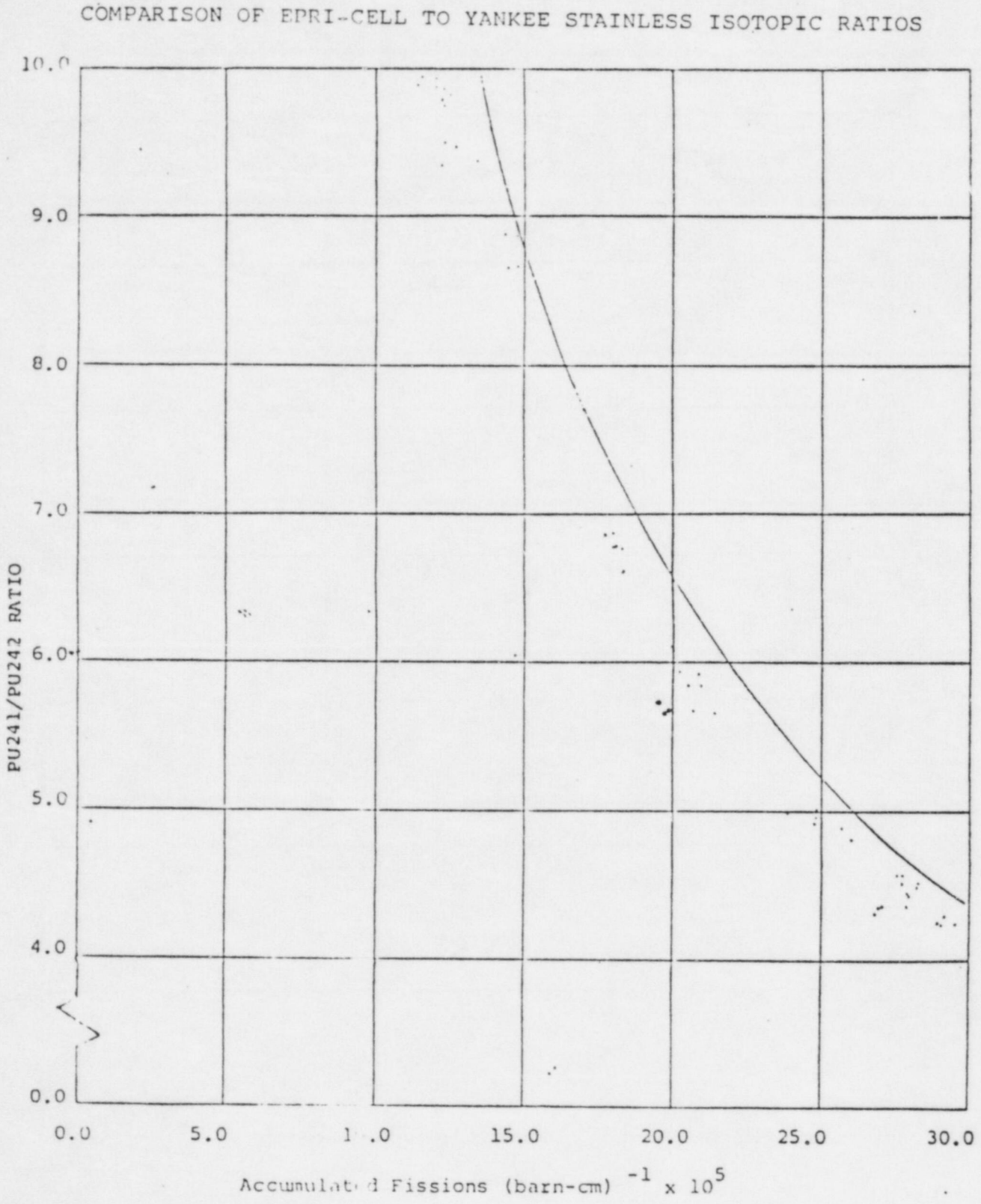

COMPARISON OF EPRI-CELL TO YANKEE STAINLESS ISOTOPIC RATIOS
PU241/PU242 RATIO
10.0
9.0
8.0
7.0
6.0
5.0
4.0
0.0
0.0
5.0
15.0
20.0
25.0
30.0
Accumulated Fissions (barn-cm) $^{-1}$ x 10^5

Figure 3.4.4 Yankee. The isotopic ratio Pu-239 / Pu 240
Comparison between CASMO and experiment

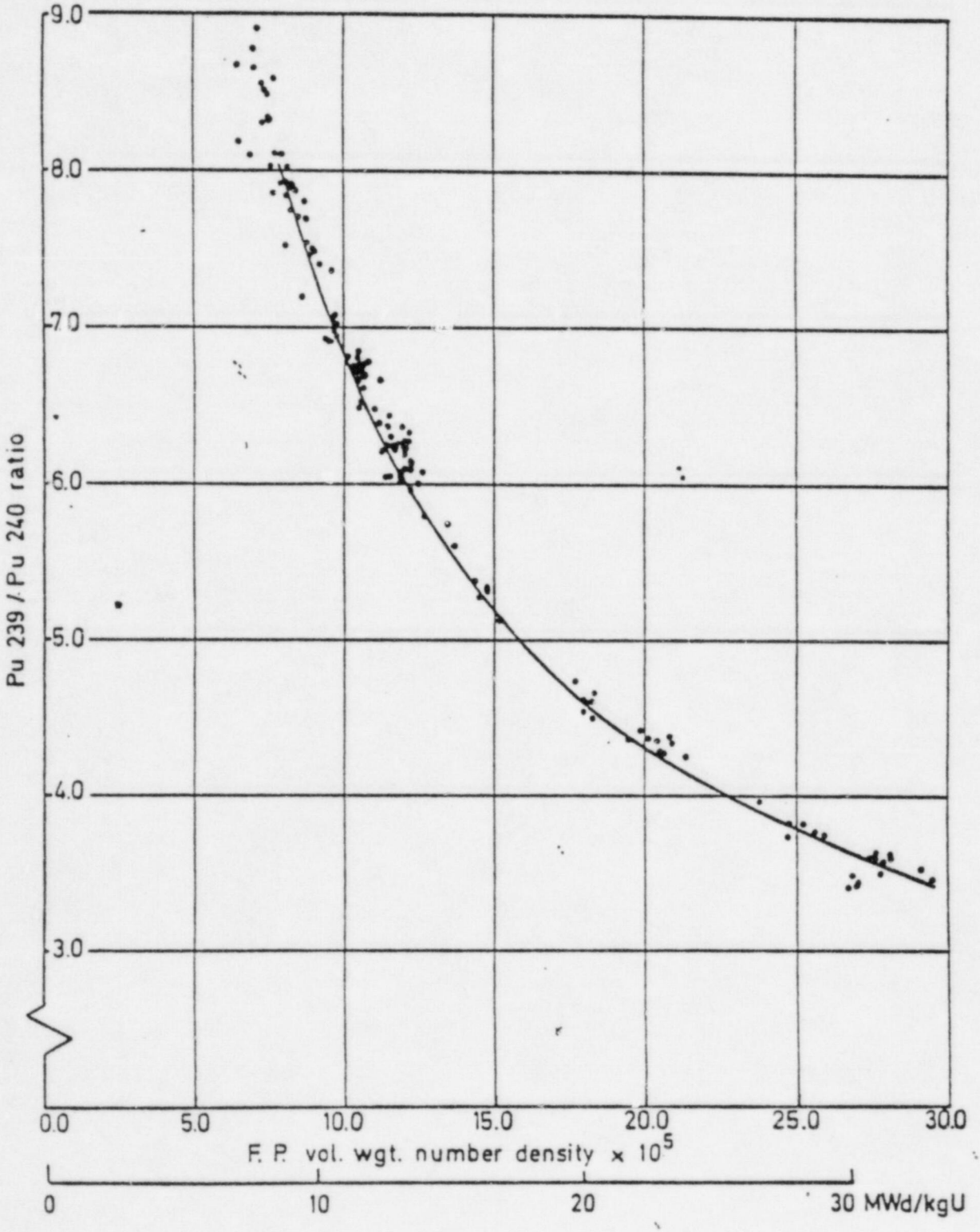


Figure 3.4.5 Yankee. The isotopic ratio Pu-240 / Pu 241
Comparison between CASMO and experiment

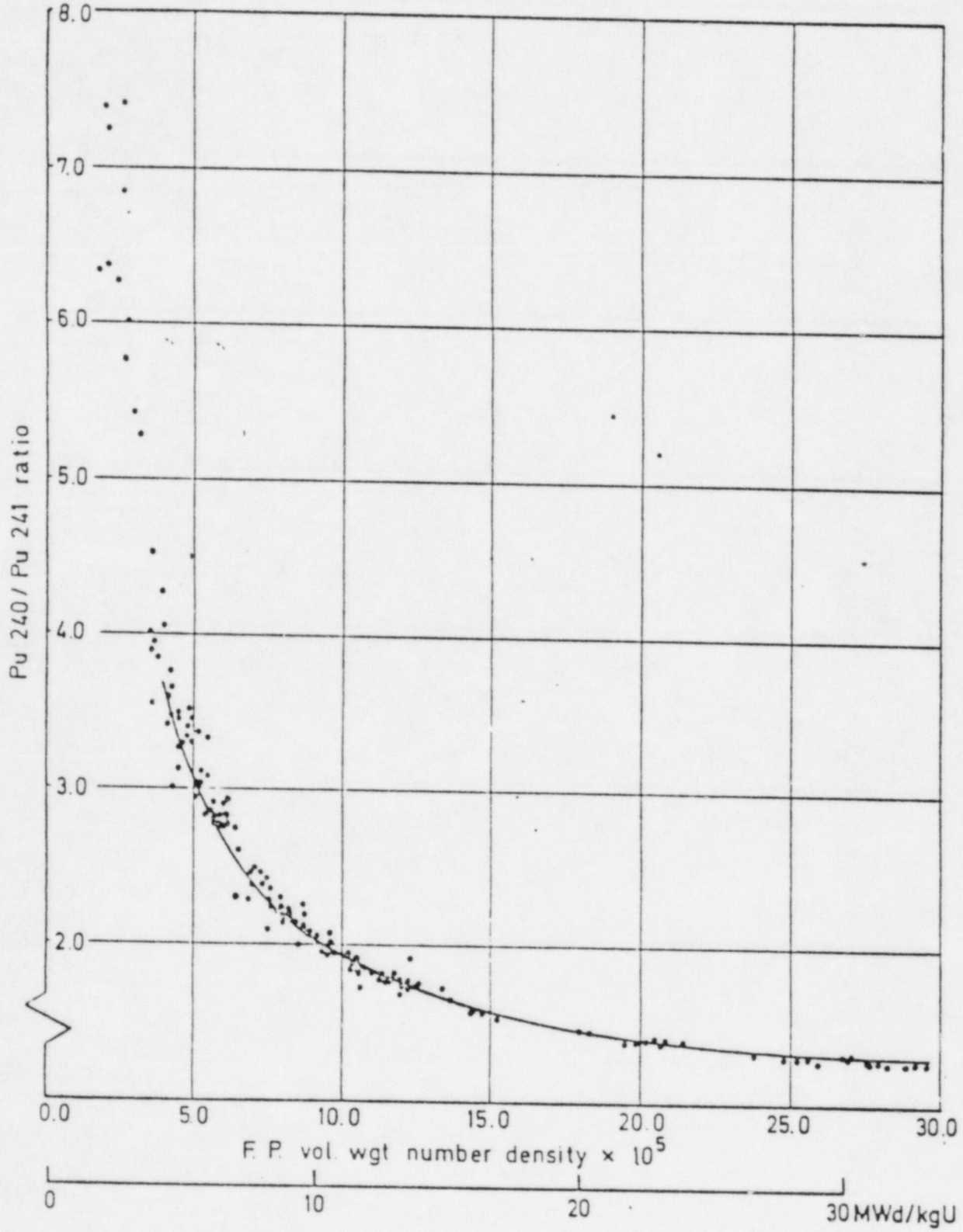
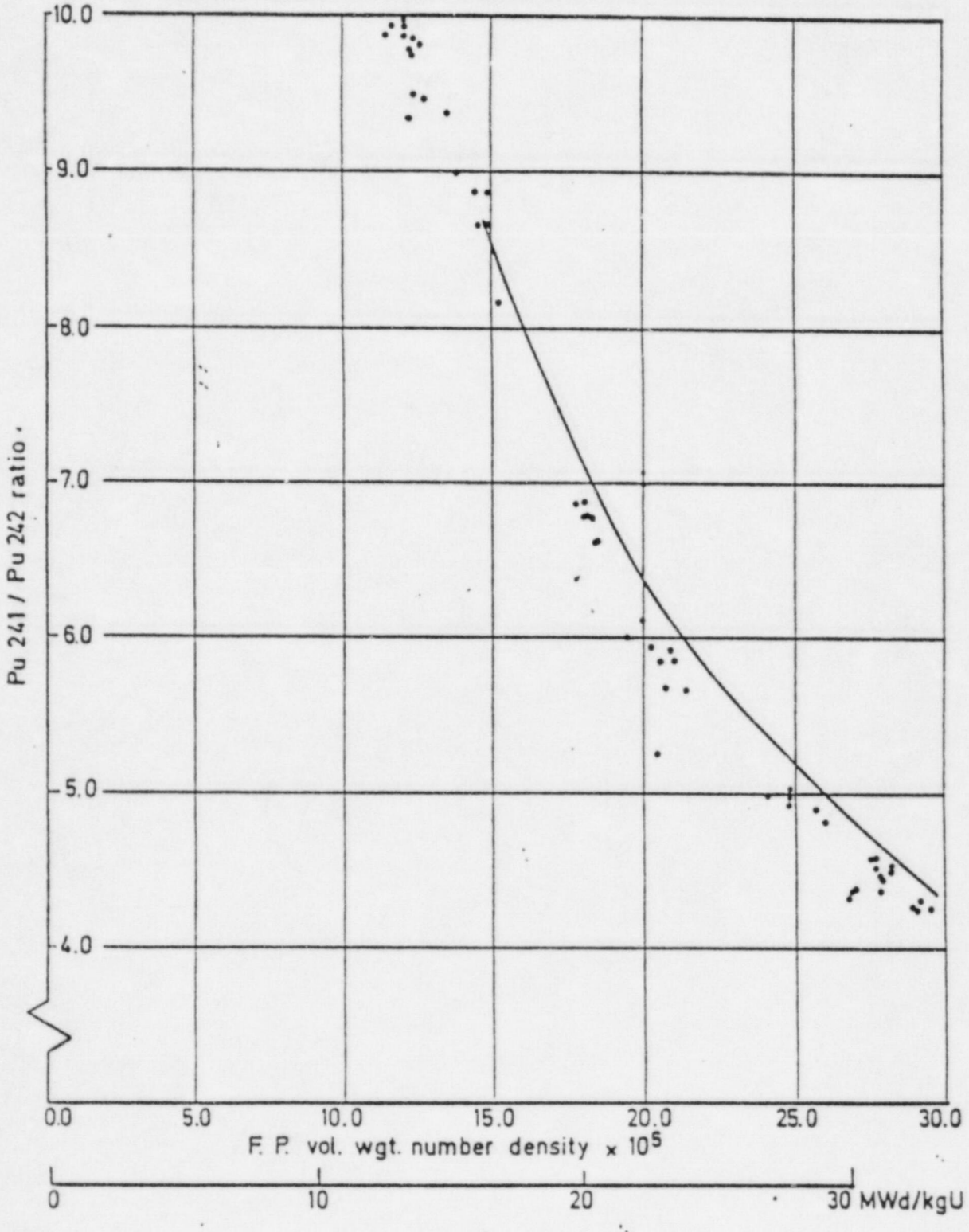


Figure 3.4.6 Yankee. The isotopic ratio Pu-241 / Pu 242
Comparison between CASMO and experiment



3.5 Power Distributions Reliability Factor Determination

The purpose of this section is to discuss the determination of the power distribution reliability factors. Section 3.5.1 discusses the local power distribution reliability factor determination on F_Q. Section 3.5.2 discusses the integrated local power distribution reliability factor on $F_{\Delta H}$.

3.5.1 Local Power Distribution Reliability Factor on FQ

The model reliability factor for calculating power distributions is based on comparisons of measured and predicted in-core flux detector signals for normal operating core conditions.

The signals from the detectors are corrected by the on-site process computer to account for such things as detector sensitivity, drift, and background. It is these corrected signals, or reaction rates, which have been compared to simulated reaction rates calculated with the NSP models in order to derive model reliability factors.

The reliability factor RF is defined as a single value of ΔF_Q such that F_Q (I,J,K) calculated plus ΔF_Q has a 95% probability at a 95% confidence level of being conservative with respect to the measured F_Q(I,J,K). The subscripts c and m will be used to denote calculated and measured values. F_Q(I,J,K) is the local pin peaking factor determined for all I,J,K locations in the core. This value cannot be measured directly. What is measured by the detector system is the reaction rate in the instrument thimble. This measured reaction rate is a local value. $RR_m = \phi\Sigma_f$ (measured). These values are measured at 61 axial locations in each thimble. The three-dimensional models ECELL/PDQ/DP5 and CASMO/PDQ/DP5

have been used to calculate the reaction rate in the instrument thimbles. $RR_c = \phi\Sigma_f$(calculated). The observed difference distribution (ODD) has then been calculated by simply taking the difference of these two values:

$ODD = RR_c - RR_m$ for all measured locations in the core.

It is important to note that the ODD is <u>not</u> the difference between nodal powers but rather is the difference between <u>local</u> values. It is assumed that the observed difference is equal to ΔF_Q between a measured and calculated local $F_Q(I,J,K)$. This is a good assumption since the calculated and measured reaction rates are also local values and are proportional to F_Q. The uncertainty determined from the above comparisons for the instrument thimble is the same as the uncertainty that would be determined in a fuel pin if that pin could be instrumented, except for a small self-shielding or flux depression in the pin which is not present in the fission chamber. The impact of this difference on the F_Q uncertainty is assumed to be negligible. To illustrate this mathmatically

$$RR = P\ (\text{Node})\ X\ PB_{IT}\ (\text{instrument thimble peaking factor})$$

$$F_Q = P\ (\text{Node})\ X\ PB_{FP}\ (\text{fuel pin peaking factor})$$

Therefore it is being assumed that the uncertainties of

$$PB_{IT} = PB_{FP}$$

The observed difference distribution determined above includes the uncertainties in the calculational model as well as the uncertainties in the measurement instrumentation. The calculational model uncertainty includes uncertainty in the calculation of the nodal powers as well as uncertainties in the local pin powers. Therefore the uncertainty in the local pin power can be written as follows:

$$RF_{FQ} = \sigma_{FQ.95}$$

where $\sigma_{FQ.95}$ is determined from the ODD.

It therefore is apparent that the reliability factor is appropriately applied as an addative factor to the calculated $F_Q(I,J,K)$ since it has been consistently derived from differences of absolute reaction rates.

The simulated detector signals are calculated in a manner which is consistent with the calculation of local power peaking factors for the purpose of safety evaluations. The first step is to compute the power distribution under consideration. The resolution used is four nodes per fuel assembly, with 24 axial levels.

The simulated detector signals are obtained by using the four nodes at each axial level to predict a signal power density for that assembly at the level. This power is then converted to a local relative reaction rate at the location of the detector. The conversion factors are calculated for each assembly location as a function of assembly exposure using a two-dimensional, quarter core PDQ7, fine mesh model. The 24 axial values in each detector location are then synthesized using a truncated Fourier sine series of the form:

$$P(Z) = A_o + \sum_{n=1}^{N} A_n \sin (n*\phi)$$

The grid flux depressions are then superimposed on the synthesized function using an empirical function designed to match the characteristics of flux depressions measured with in-core fission detectors. The effect of the grid flux depressions is to raise the flux level in the axial region between grids while depressing the flux in the grid region.

A total of 34 core state points, or flux maps, were chosen for the purpose of comparing measured and simulated in-core reaction rates for the ECELL/PDQ/DP5 model. These state points span operating cycles 3 thru 6 of Prairie Island. A total of 16 state points were chosen for the CASMO/PDQ/DP5 model spanning cycles 5 and 6. The specific core conditions for each of the state points are given in table 3.5.1.

Typical examples of the comparisons of measured and predicted rates are provided in Figures 3.5.1 through 3.5.54. The data is presented in sets of three figures, one set for each flux map, three maps per cycle (BOC, MOC, EOC). The first figure in each set presents the differences between the measured and predicted integral reaction rates for all instrumented locations. The instrumented core locations are indicated with circles in each of the figures. The second and third figures of each set present axial comparisons in two specific instrumented core locations. The measurements are shown as circles at the 61 axial levels. The predicted reaction rates are represented as triangles. The two core locations were chosen as typical of regions of high

power density. The cycle five and six data is presented using both models (i.e. the ECELL/PDQ/DP5 and CASMO/PDQ/DP5).

The method of normalizing the calculated and measured reaction rates is to adjust the average of all 36 detectors at 61 locations to one for each flux map. This normaliztion technique is used to put the measured and predicted values on a common basis which is consistent with the definition of F_Q and $F_{\Delta H}$. The measurement uncertainty in core thermal power is accounted for in the transient and LOCA analysis.

The distribution of observed differences between measured and calculated instrument signals for all 34 core state points was determined for the ECELL/PDQ/DP5 model comparison. For each trace, 23 values of the 61 axial values were excluded from consideration. Typically this included the top and bottom 3 points and 3 points in the vicinity of each grid. These are areas of steep flux gradients and small errors in instrument result in large differences in measured to calculated values. Since the reaction rates in these areas are always smaller than the between grid reaction rates (e.g., the high power point will never occur in top, bottom or grid location) these values were excluded from the determination of the observed differences density function. The total number of observations used was 43,358.

The observed differences density function was tested for normality using the chi-square test. The results demonstrated that this function differed significantly from a normal distribution. Therefore, all subsequent statistical analysis has been performed using the methods described in Appendix A.2. To ensure conservative reliability factor at all power levels the sample

was divided into subsamples as a function of power (see Figure 3.5.67). Each subsample contains 3500 observations. A reliability factor was calculated for each subsample using the methods described in Appendix A.2. Figure 3.5.67 shows a power dependence, therefore the most conservative subsample will be used. The following statistics represent the most conservative subsample. The distribution of observed differences is shown in Figure 3.5.55.

The first step using this method is to determine the mean of the measured to calculated values (μmc) and the standard deviation (σmc):

$$\mu mc = \sum_{\frac{i-1}{n}}^{n} e_i = 0.007$$

$$\sigma mc = \frac{\Sigma(e_i - \mu mc)^2}{n-1}^{\frac{1}{2}} = 0.038$$

where: e_i = ith observed difference
n = total number of observations

The second step is to transform the e_i to standard measure using the following formula:

$$Z_i = \frac{e_i - \mu mc}{\sigma mc}$$

and the resulting variates Z were then sorted into ascending order (see Figure 3.5.56). A value of Z was chosen as an estimate of the 95th percentile of the distribution, Z = 3,326. This gives the 95th percentile of Z to be

$$Z_{3326} = Q_{95} = 1.548$$

which implies that 95% of the errors are likely to be less than 1.548 standard deviations from the mean. It remains then to calculate a 95% confidence interval on Q_{95} using the following formula

$$\text{Var } Q_{95} = \frac{q(1-q)}{n\, f_1^2}$$

where: q = the quantile (.95)
n = number of independent observations in sample
f_1 = ordinate of the density function of the distribution function at the abscissa q

Due to the dependence of the observed differences with axial height, n was reduced by a factor of three. See Appendix A for the determination of the reduction factor.

It is necessary to obtain an estimate of $f_1(.95)$ and this was done by applying a linear regression analysis on a short interval of the cumulative distribution function (CDF) of Z in the region of the 95th percentile (see Figure 3.5.57). The estimated slope of the CDF (estimated from the straight line in Figure 3.5.57) is an estimate of the ordinate density function. The slope is calculated as .051.

This gives

$$\text{Var } Q_{95} = \frac{.95(1-.95)}{3500/3 \times .051^2} = .01565$$

and $\sigma_{Q95} = (\text{Var } Q_{95})^{\frac{1}{2}} = 0.12511$

The estimate of the upper limit on Q_{95} is

$$K_c \, \sigma_{Q95} = 1.645 * 0.1251 = 0.206$$

thus:

$$1.528 - .206 \leq Q_{95} \leq 1.528 + .206$$

The upper limit is then 1.528 + .206 = 1.734 which gives the following as the 95% confidence level that the calculated reaction rate (RRc) will be conservative with respect to the measured reaction rate (RRm).

$$RRm = RRc \pm 1.734 \, \sigma mc = RRc \pm 1.734 \, (.038)$$
$$RRm = RRc \pm 0.067$$
$$\text{therefore } \sigma_{FQ.95} = 0.067$$

Note that this value includes measurement error which adds to the conservativeness of the calculation.

The observed difference distribution for the 16 core state points (see Table 3.5.1) for the CASMO/PDQ/DP5 model was also tested for normality and was also found to vary significantly from a normal distribution. Therefore the methods used above and described in Appendix A.2 have been applied. To ensure a conservative reliability factor at all power levels the sample was divided into subsamples as a function of power (see Figure 3.5.68). Each subsample contains 3500 observations.

A reliability factor was calculated for each subsample using the methods described in Appendix A.2. Figure 3.5.68 shows a power dependence, therefore the most conservative subsample will be used. The following statistics represent the most conservative subsample. Again 23 values of the 61 axial values for each trace have been excluded as discussed above.

Figures 3.5.58, 3.5.59 and 3.5.60 give the density function, cumulative distribution function, and the CDF in the region of the 95th percentile respectively for the CASMO/PDQ/DP5 model comparisons. The significant parameters calculated for this distribution are as follows

$$\mu mc = .015$$
$$\sigma mc = 0.040$$
$$Q_{95} = 1.384$$
$$\sigma_{Q95} = .098$$
$$K_c\sigma_{Q95} = 0.16$$
$$RRm = RRc \pm 1.545\ (0.040)$$
$$\sigma_{FQ.95} = 0.062$$

Due to the dependence of the observed differences with axial height n was reduced by three. See Appendix A.2 for derivation of this reduction factor.

The uncertainties appropriate to the nodal model are then defined as the reliability factor

$$RF_{FQ} = \sigma_{FQ.95}$$

Therefore the RF_{Fq} for each model is as follows

$$RF_{FQ}(\text{ECELL/PDQ}) = .067$$

and RF_{FQ} (CASMO/PDQ) = .062

3.5.2 Integrated Power Distribution Reliability Factor on FΔH

The model reliability factor for calculating power distributions are based on comparisons of integrated measured and predicted in-core flux detector signals obtained from normal operating core conditions.

The reliability factor RF is defined as a single value of $\Delta F_{\Delta H}$ such that $F_{\Delta H}(I,J)$ calculated plus $\Delta F_{\Delta H}$ has a 95% probability at a 95% confidence level of being conservative with respect to the the measured $F_{\Delta H}(I,J)$. The subscripts c and m will be used to denote calculated and measured values. $F_{\Delta H}(I,J)$ is the integrated peaking factor determined for all I,J locations in the core. This value cannot be measured directly. What is measured by the detector system is the reaction rate in the instrument thimble. This measured reaction rate is a local value. $IRR_m = \phi\Sigma_f$ (measured). These values are determined at each thimble by integrating the 61 measured axial locations. The three-dimensional models ECELL/PDQ/DP5 and CASMO/PDQ/DP5 have been used to calculate the reaction rate in the instrument thimbles. $IRR_c = \phi\Sigma_f$ (calculated). The observed difference distribution (ODD) has then been calculated by simply taking the difference of these two values

$ODD = IRR_c - IRR_m$ for all measured locations in the core

It is important to note that the ODD is <u>not</u> the difference between nodal powers but rather is the difference between <u>local</u> values. It is assumed that the observed difference is equal to $\Delta F_{\Delta H}$ between a measured and calculated local $F_{\Delta H}(I,J)$. This is a good assumption since the calculated and measured reaction rates are also local values and are proportional to $F_{\Delta H}$.

The uncertainty determined from the above comparisons for the instrument thimble is the same as the uncertainty that would be determined in a fuel pin if that pin could be instrumented, except for a small self-shielding or flux depression in the pin which is not present in the fission chamber. The impact of this difference on the $F_{\Delta H}$ uncertainty is assumed to be negligible. To illustrate this mathmatically

$$IRR = \left(\sum_{i=1}^{61} P_N^i \times PB_{IT}^i\right) / 61$$

$$F_{\Delta H} = \left(\sum_{i=1}^{61} P_N^i \times PB_{FP}^i\right) / 61$$

where

P_N is the nodal power

PB_{IT} is the instrument thimble peaking factor

PB_{FB} is the fuel pin peaking factor

Therefore it is being assumed that the uncertainty of

$$PB_{IT} = PB_{FB}$$

The observed difference distribution determined above includes the uncertainties in the calculational model as well as the uncertainties in the measurement instrumentation. The calculational model uncertainty includes uncertainty in the calculation of the nodal powers as well as uncertainties in the local pin powers. Therefore the uncertainty in the local integrated pin power can be written as follows

$$RF_{\Delta H} = \sigma_{F\Delta H.95}$$

where $\sigma_{F\Delta H.95}$ is determined from the ODD

It therefore is apparent that the reliability factor is appropriately applied as an addative factor to the calculated $F_{\Delta H}(I,J)$ since it has been consistently derived from the differences of absolute reaction rates.

The distribution of observed differences between measured and calculated integrated instrument signals for all 34 state points was determined for the ECELL/PDQ/DP5 model and is shown in Figure 3.5.61. All 61 axial values are used to calculate the integrated value. The total number of integrated observations used was 1,139.

The observed difference density function was tested for normality using the chi-square test and was found to vary significantly from a normal distribution. Therefore, all subsequent statistical analysis has been performed using the methods described in Appendix A.2 on the entire sample. To ensure the use of the entire sample is conservative, the values were checked for a dependence on power. No dependence was found. The cumulative distribution function and the CDF in the region of the 95th percentile are given in Figures 3.5.62 and 3.5.63 respectively. The significant parameters calculated for this distribution are as follows:

$$\mu mc = 0.00006$$
$$\sigma mc = 0.0214$$
$$Q_{95} = 1.550$$
$$\sigma_{Q95} = 0.0465$$
$$K_c\sigma_{Q95} = 0.077$$
$$IRRm = IRR_c \pm 0.038$$
$$\sigma_{F\Delta H\cdot 95} = 0.035$$

where: IRRm = Integrated reaction rate measured
IRRc = Integrated reaction rate calculated

No dependence of the observed difference with position was found. Therefore, n was not reduced.

The distribution of observed differences between measured and calculated integrated instrument signals for all 16 state points was determined for the CASMO/PDQ/DP5 model and is shown in Figure 3.5.64. All 61 axial values are used to calculate the integrated value. The total number of integrated observations used was 542.

The observed difference density function was tested for normality using the chi-square test and was found to vary significantly from a normal distribution. Therefore, all subsequent statistical analysis has been performed using the methods described in Appendix A.2 on the entire sample. To ensure the use of the entire sample was conservative, the observed differences were checked for a dependence on instrument response. No dependence was found. The cumulative distribution function and the CDF in the region of the 95th percentile are given in Figures 3.5.65 and 3.5.66 respectively. The significant parameters calculated for this distribution are as follows.

$\mu_{mc} = -0.0000002$
$\sigma_{mc} = 0.0245$
$Q_{95} = 1.573$
$\sigma_{Q95} = 0.136$
$K_c\sigma_{Q95} = 0.22$
$IRRm = IRR_c \pm .044$
$\sigma_{F\Delta H} \cdot 95 = .044$

where:
IRRm = Integrated reaction rate measured
IRRc = Integrated reaction rate calculated

No dependence of the observed difference with position was found; therefore, n was not reduced.

The $F_{\Delta H}$ reliability factor ($RF_{F\Delta H}$) is defined as follows.

$$RF_{F\Delta H} = \sigma_{F\Delta H.95}$$

Therefore the $RF_{F\Delta H}$ for each model is as follows.

$$RF_{F\Delta H}(ECELL/PDQ) = .035$$

and

$$RF_{F\Delta H}(CASMO/PDQ) = .044$$

TABLE 3.5.1

FULL POWER STATEPOINTS

Cycle	Map	Exposure (GWD/MTU)	% of Full Power	Rod Bank D Position (Steps)	Boron Concen. (ppm)
3	10	1.161	100.0	218	888
	11	2.211	99.7	217	789
	12	3.465	100.0	218	676
	16	5.332	99.8	218	464
	17	6.295	99.1	218	378
	24	7.580	99.8	218	246
	26	9.322	99.7	218	88
	29	10.480	90.0	218	0
4	9	.179	99.8	208	999
	10	1.058	99.7	218	902
	11	1.825	100.0	218	816
	16	3.540	99.8	218	654
	17	4.511	99.8	218	553
	18	5.458	99.6	218	464
	21	6.420	99.5	218	368
	25	8.450	99.4	218	168
	26	9.400	99.4	218	75
	27	10.400	93.9	220	1
5	10	.831	99.8	190	969
	13	1.966	100.0	218	896
	16	3.026	99.6	218	809
	19	4.198	65.3	197	769
	23	5.919	99.5	218	515
	24	7.070	99.7	218	402
	28	8.880	99.6	218	232

TABLE 3.5.1 (Continued)

Cycle	Map	Exposure (GWD/MTU)	% of Full Power	Rod Bank D Position (Steps)	Boron Concen. (ppm)
	30	10.340	99.7	218	93
	34	11.653	93.0	218	1
6	15	.955	99.9	218	862
	16	1.474	99.6	218	823
	19	3.676	99.8	218	660
	21	4.512	99.5	218	567
	24	5.706	99.6	218	459
	25	6.918	99.6	218	341
	28	7.880	99.1	218	253

Measured and Calculated Integrated Detector Responses

PI 1 Cycle 3 HFP, 1.161 GWD/MTU, ARO, Eq Xenon

Absolute Differences

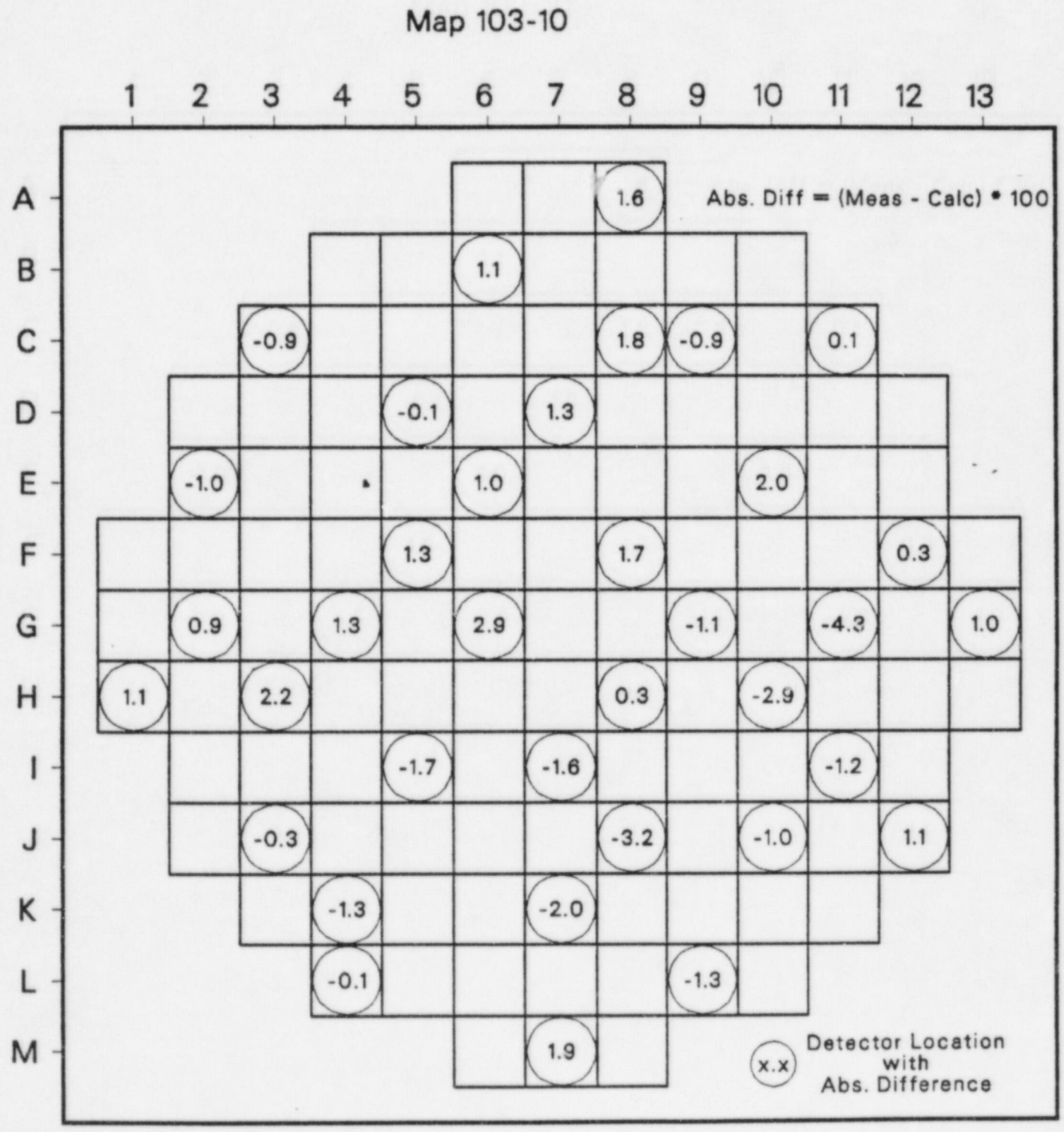


FIGURE 3.5.2

Measured and Calculated Detector Responses

PI 1 CYCLE 3 HFP, 1.161 GWD/MTU, ARO, EQ XENON

THIMBLE G6

MAP 103-10

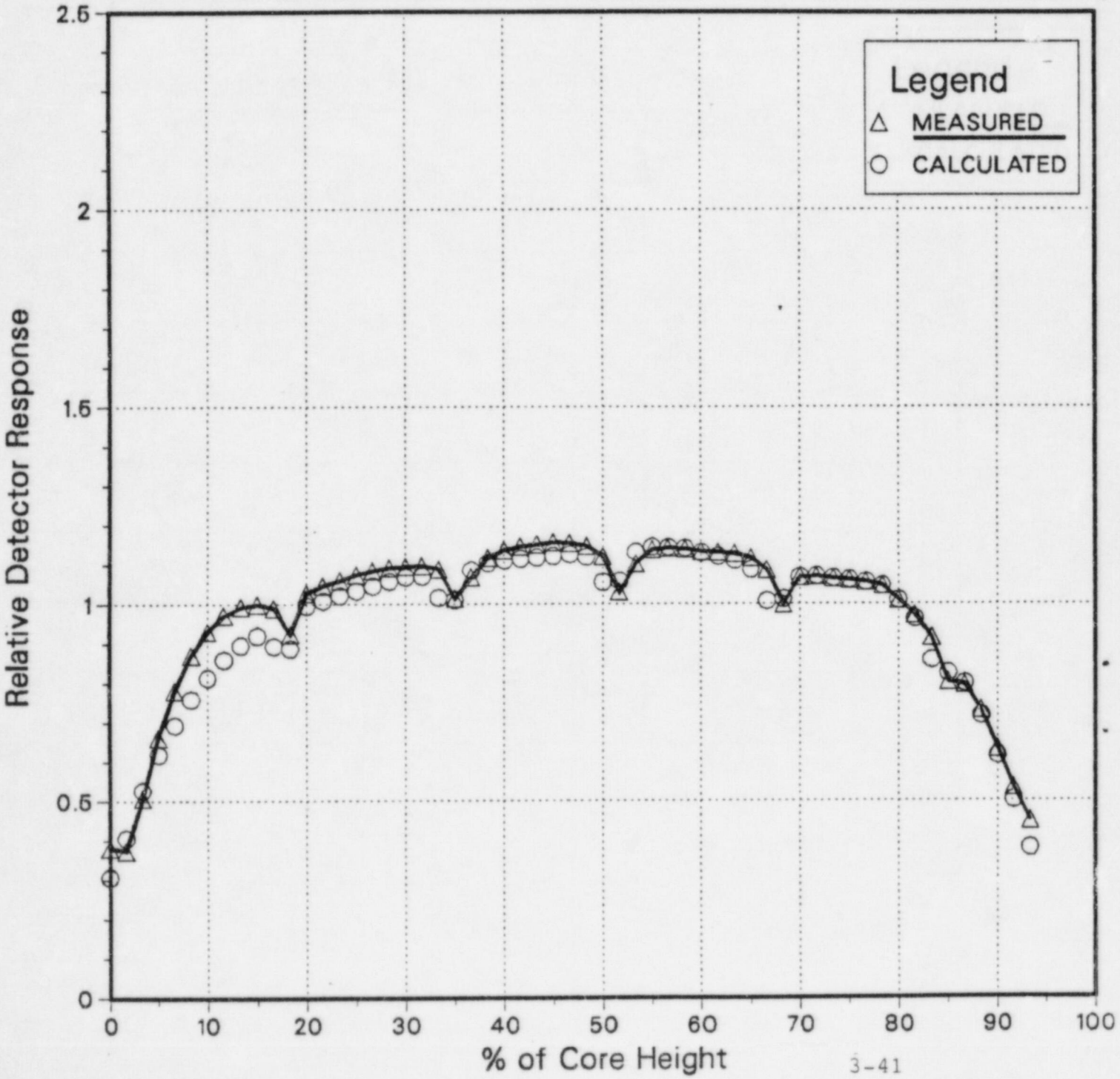


FIGURE 3.5.3

Measured and Calculated Detector Responses

PI 1 CYCLE 3 HFP, 1.161 GWD/MTU, ARO, EQ XENON

THIMBLE E6

MAP 103-10

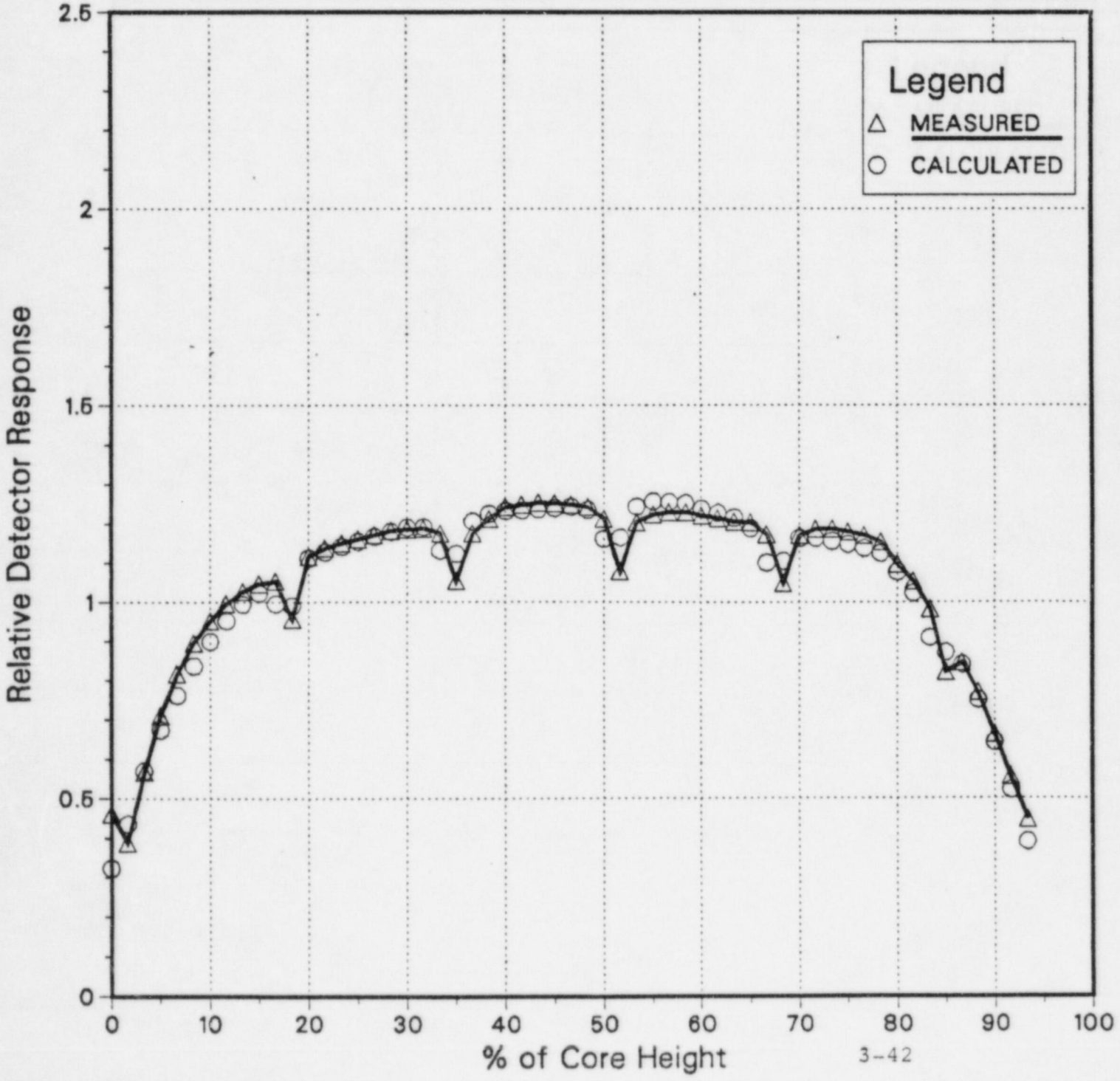


FIGURE 3.5.4

Measured and Calculated Integrated Detector Responses

PI 1 Cycle 3 HFP, 6.295 GWD/MTU, ARO, Eq Xenon

Absolute Differences

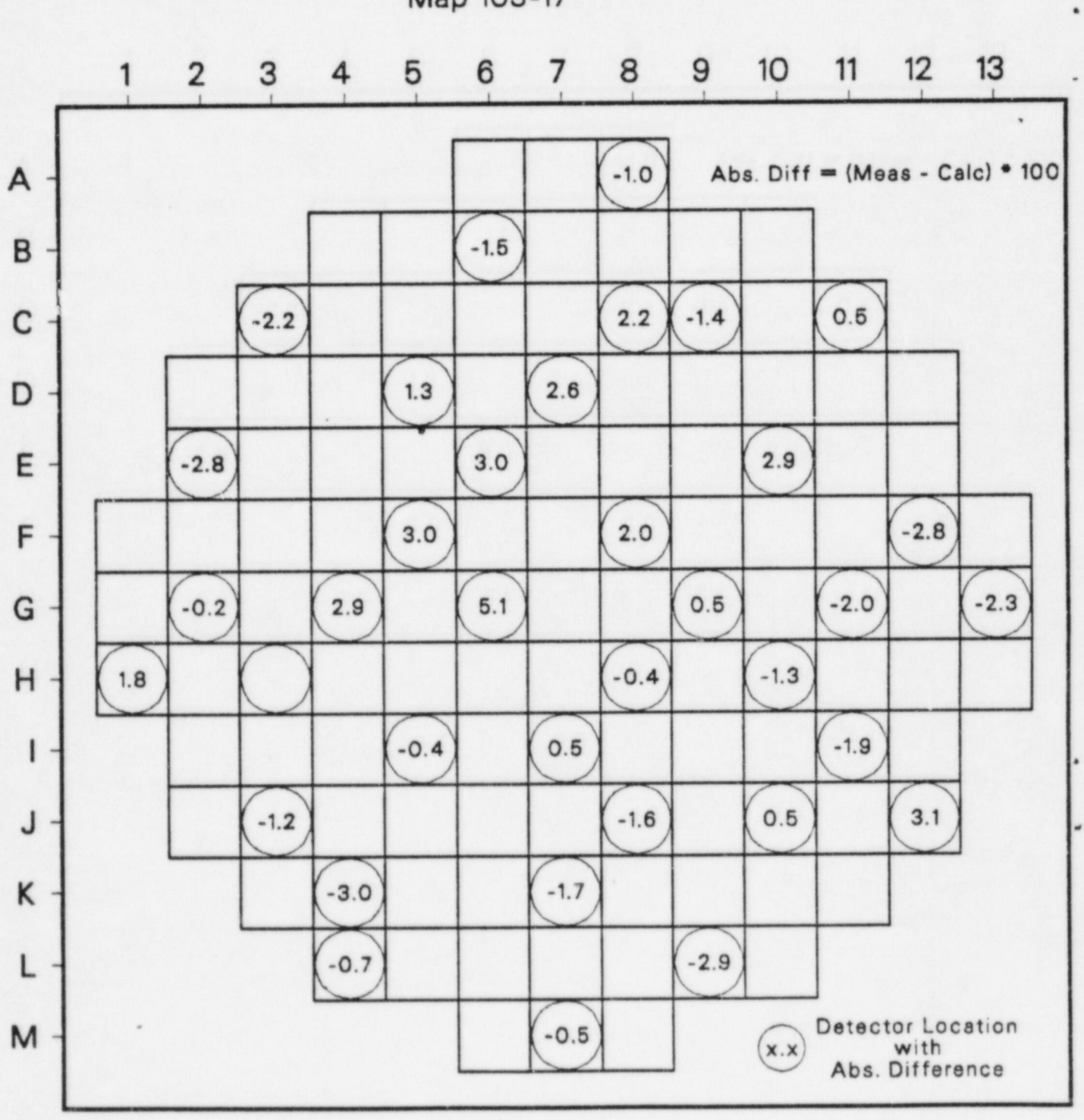


FIGURE 3.5.5

Measured and Calculated Detector Responses

PI 1 CYCLE 3 HFP, 6.295 GWD/MTU, ARO, EQ XENON

THIMBLE G6

MAP 103-17

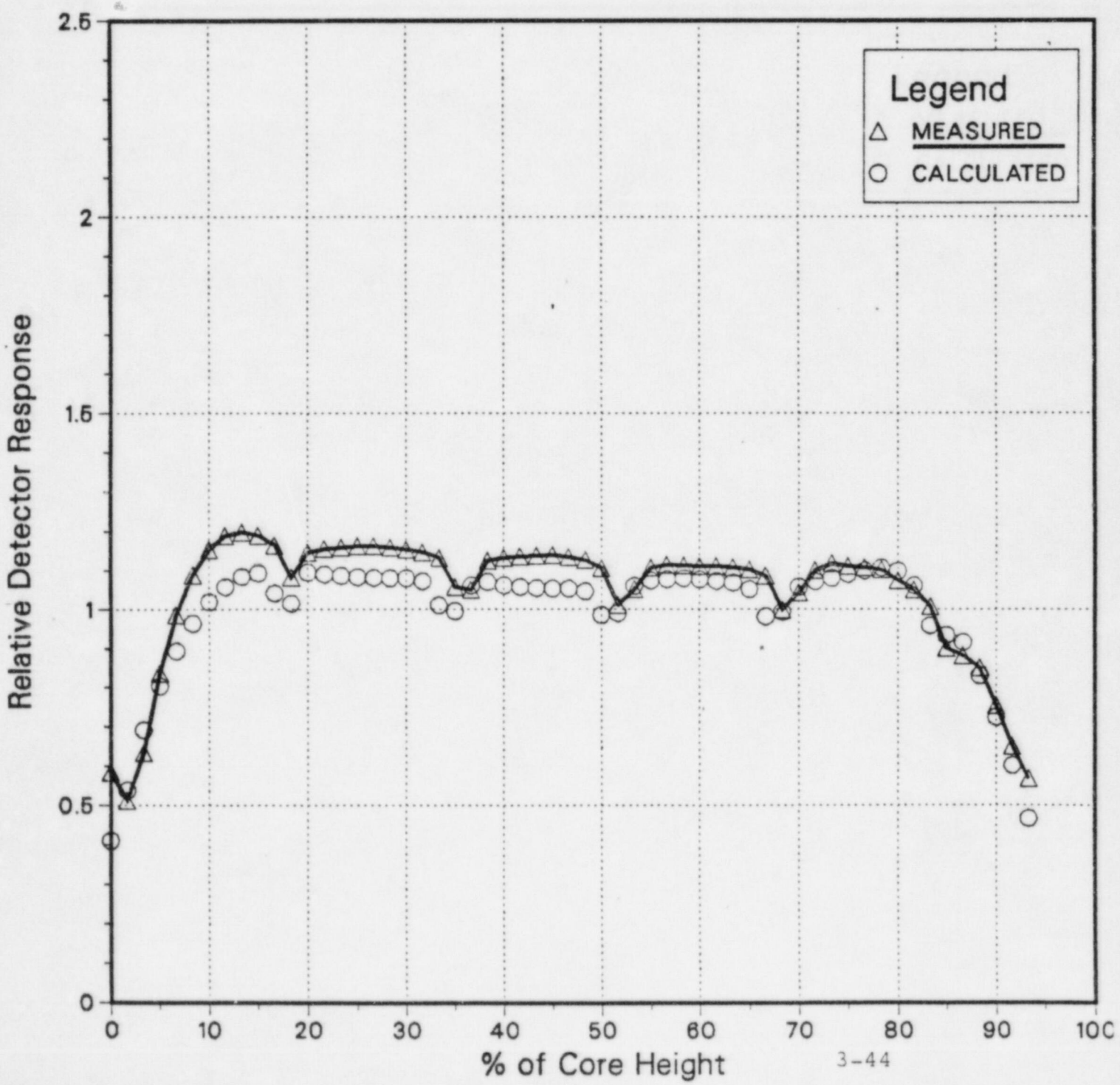


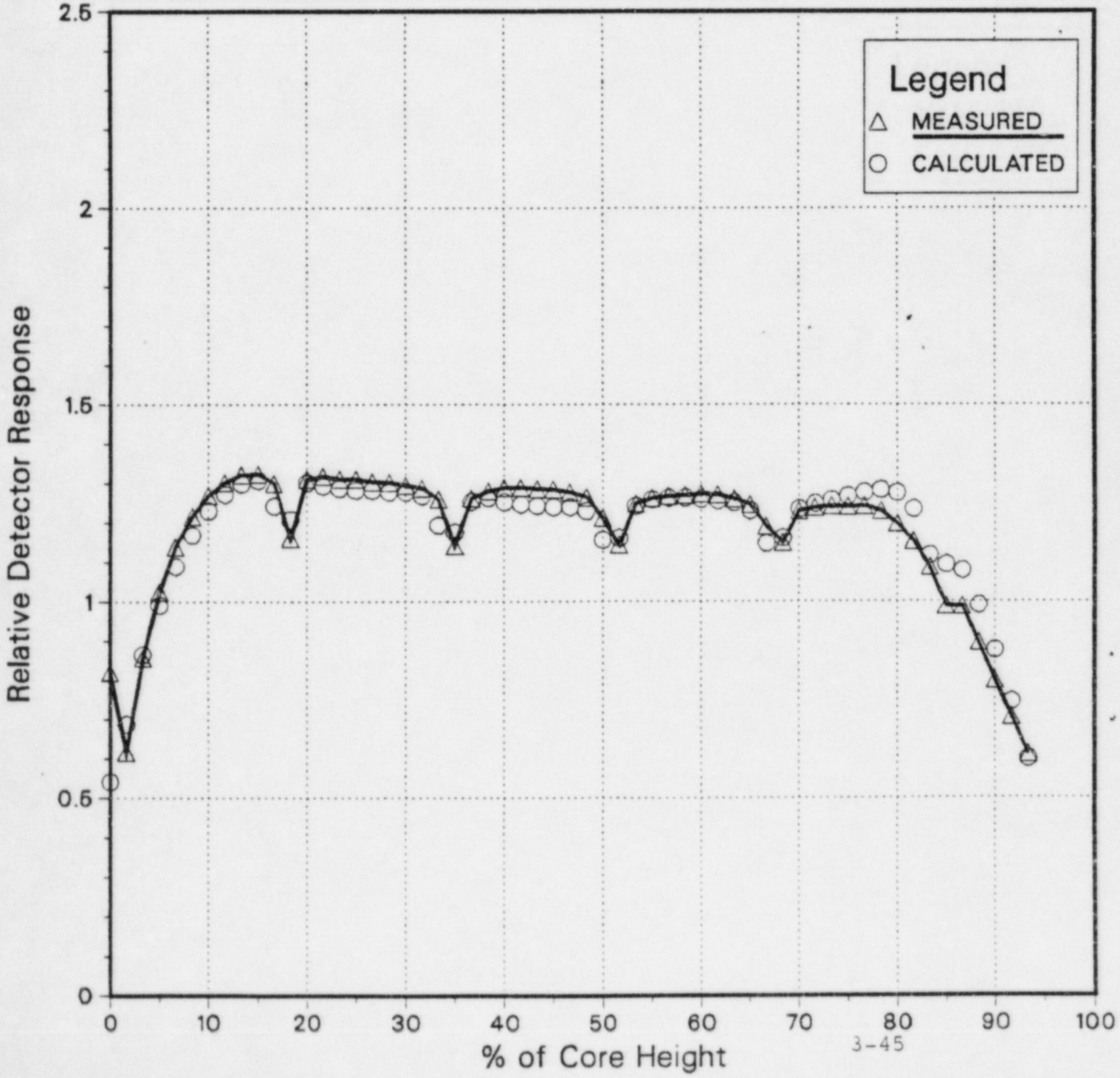
FIGURE 3.5.6

Measured and Calculated Detector Responses

PI 1 CYCLE 3 HFP, 6.295 GWD/MTU, ARO, EQ XENON

THIMBLE I7

MAP 103-17



Measured and Calculated Integrated Detector Responses

PI 1 Cycle 3 HFP, 10.480 GWD/MTU, ARO, Eq Xenon

Absolute Differences

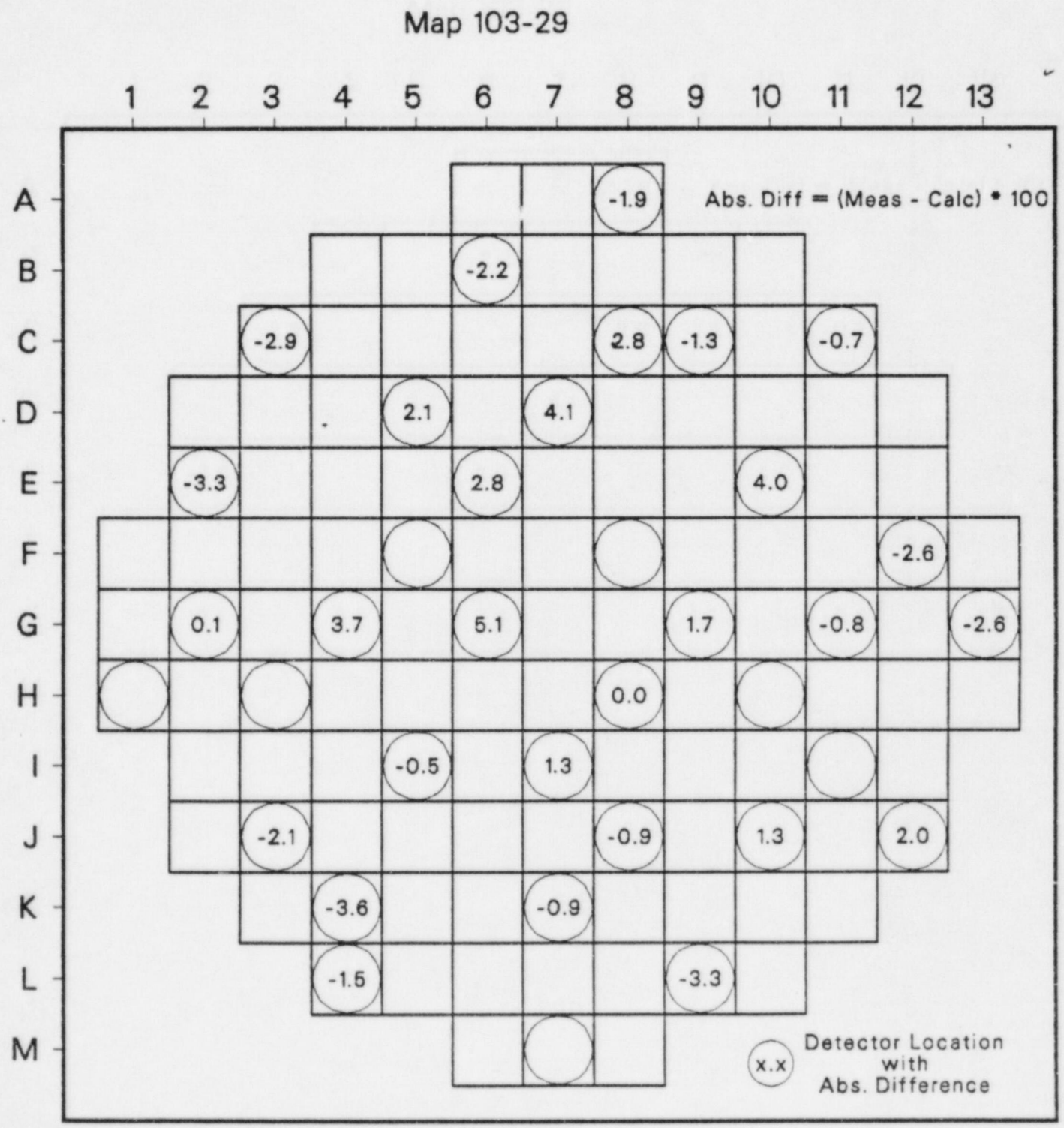


FIGURE 3.5.8

Measured and Calculated Detector Responses

PI 1 CYCLE 3 HFP, 10.480 GWD/MTU, ARO, EQ XENON

THIMBLE G6

MAP 103-29

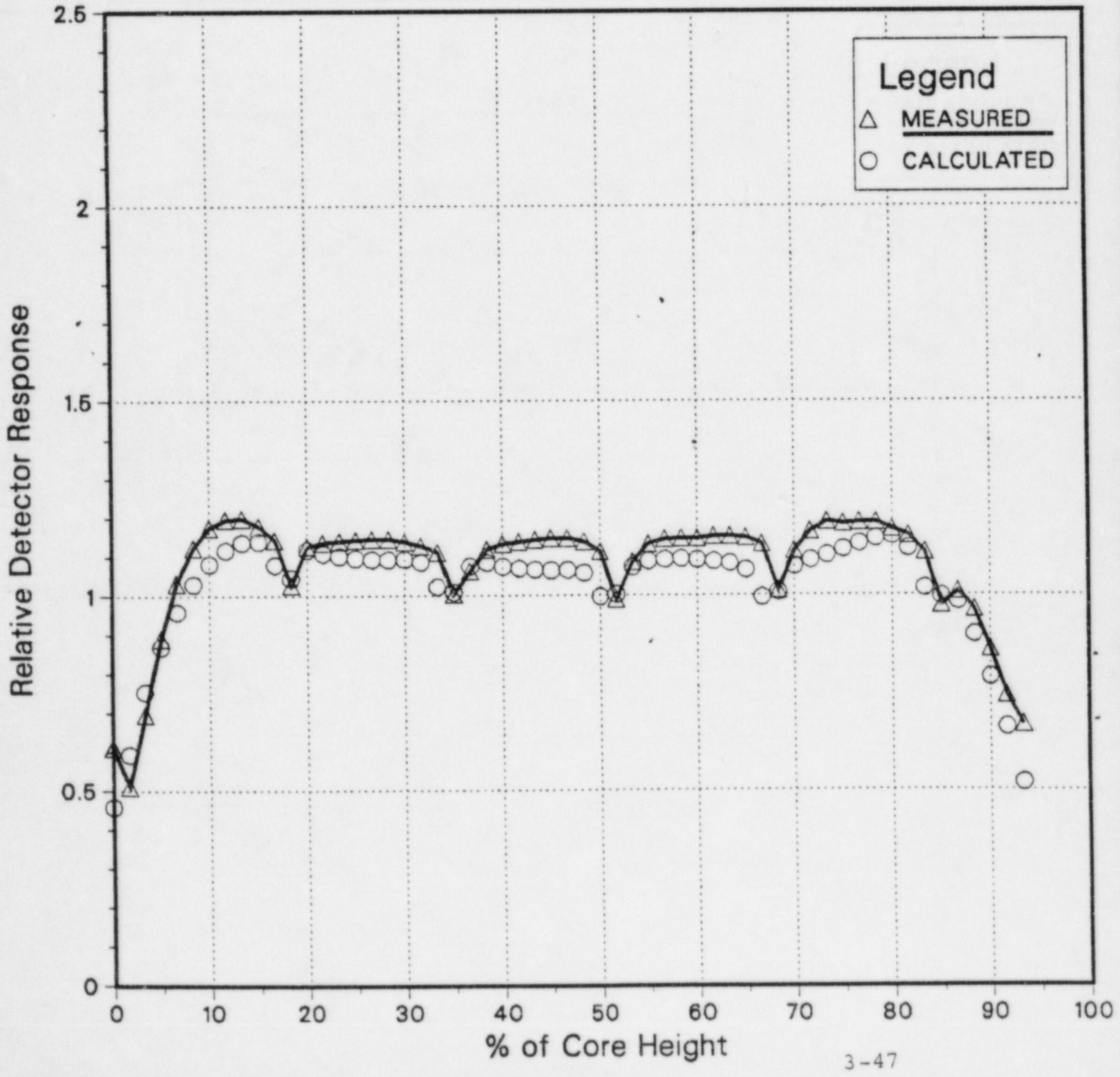


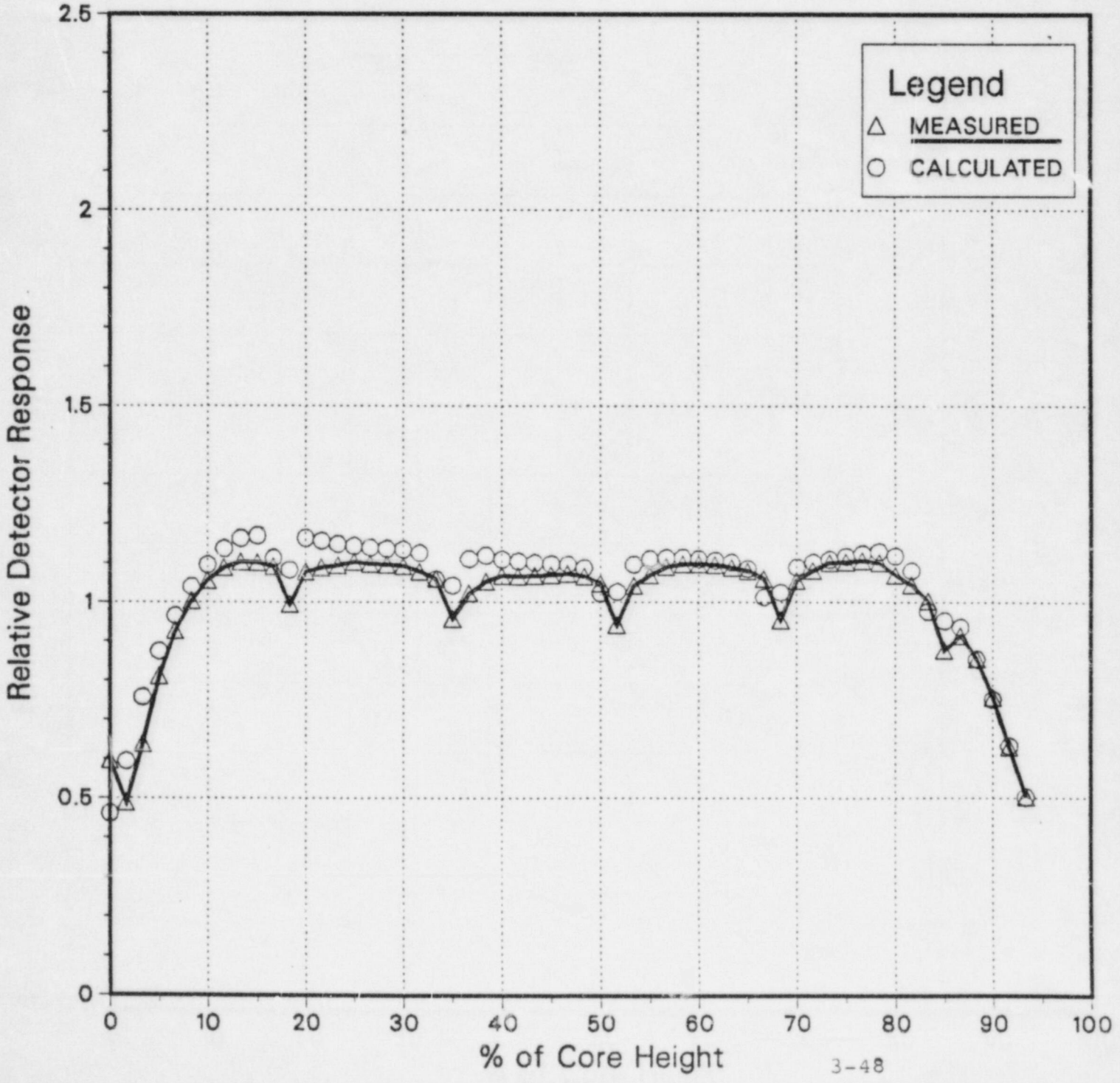
FIGURE 3.5.9

Measured and Calculated Detector Responses

PI 1 CYCLE 3 HFP, 10.480 GWD/MTU, ARO, EQ XENON

THIMBLE K4

MAP 103-29



Measured and Calculated Integrated Detector Responses

PI 1 Cycle 4 HFP, 1.058 GWD/MTU, ARO, Eq Xenon

Absolute Differences

Map 104-10

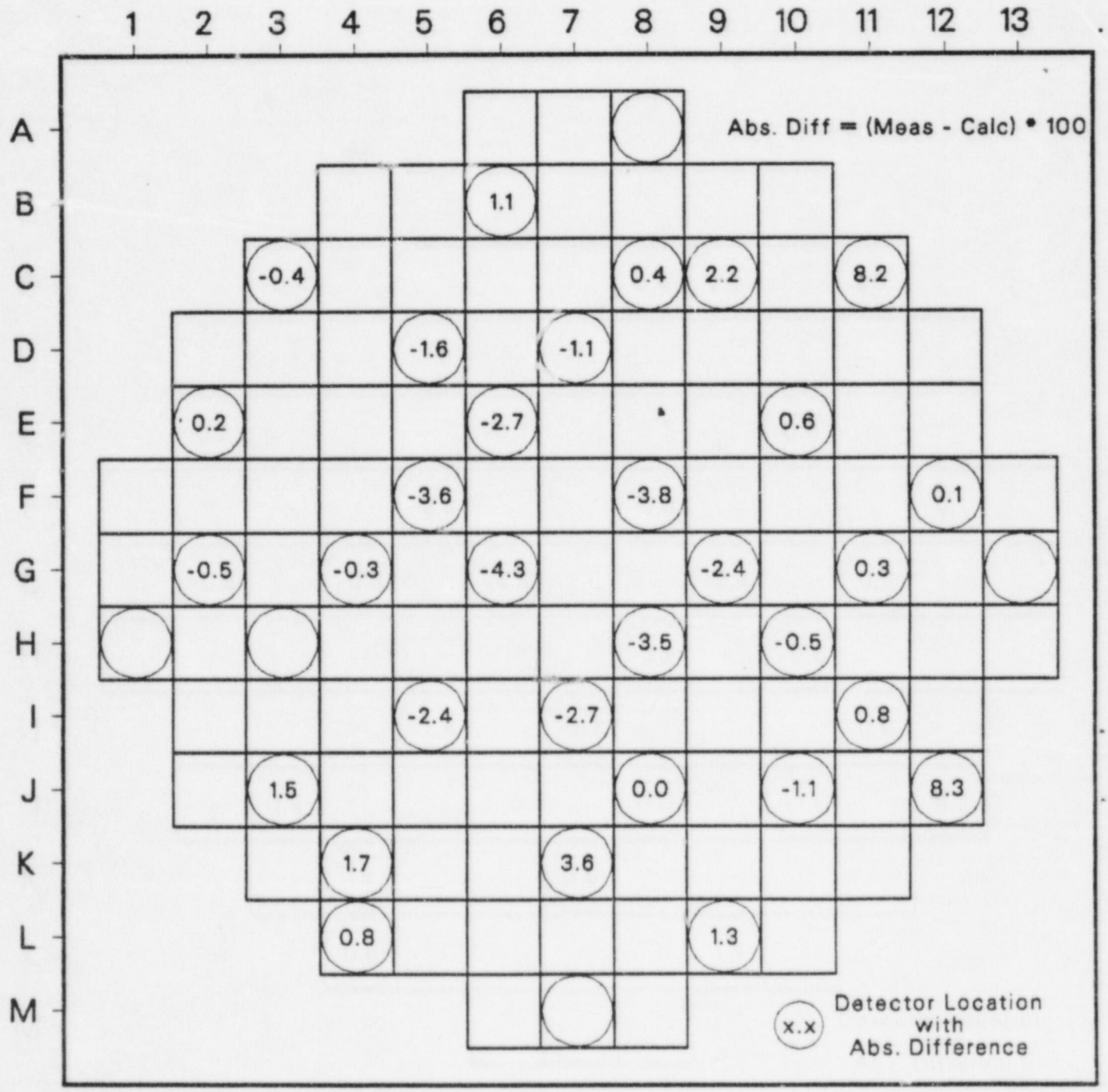


FIGURE 3.5.11

Measured and Calculated Detector Responses

PI 1 CYCLE 4 HFP, 1.058 GWD/MTU, ARO, EQ XENON

THIMBLE G6

MAP 104-10

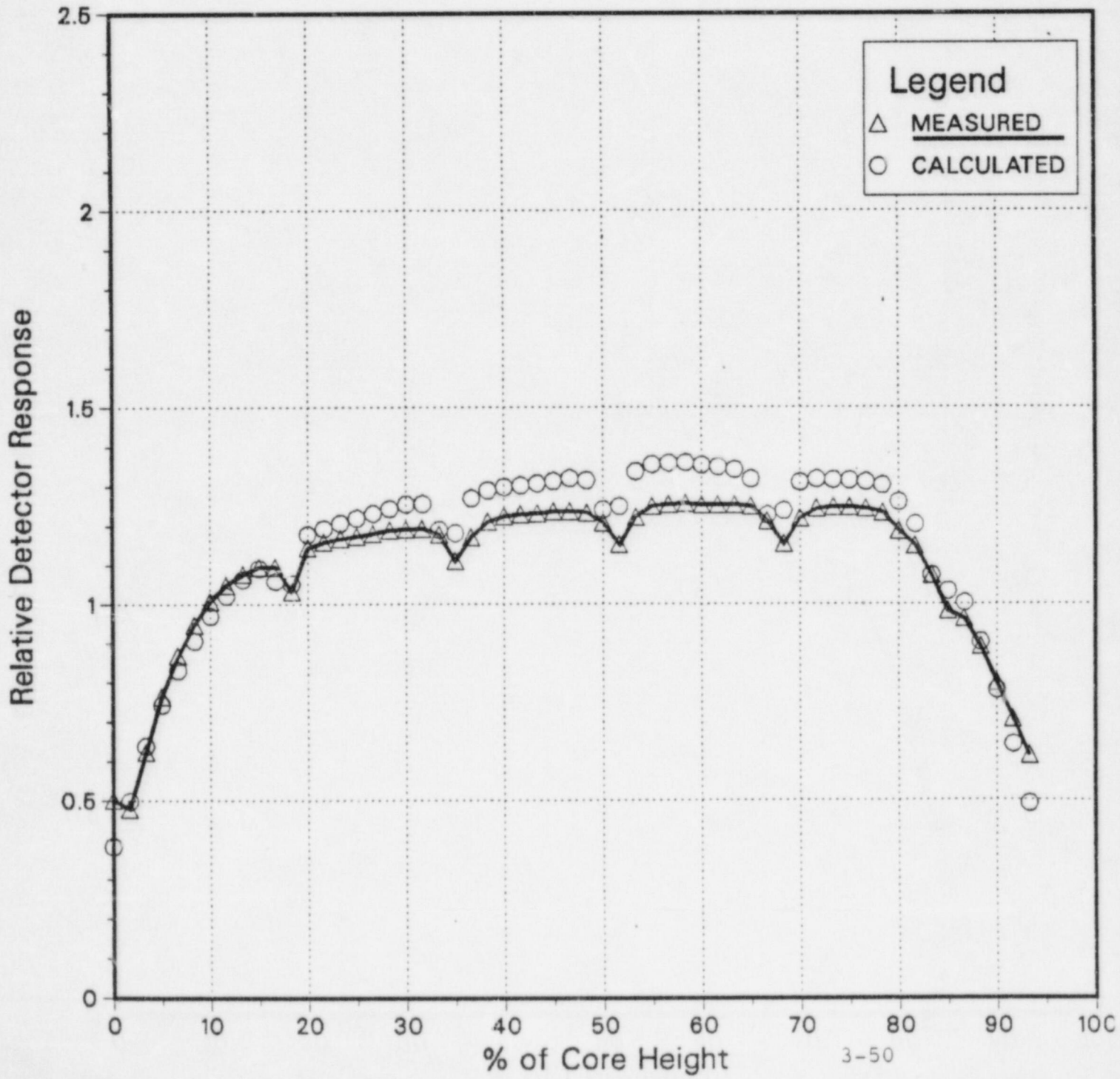


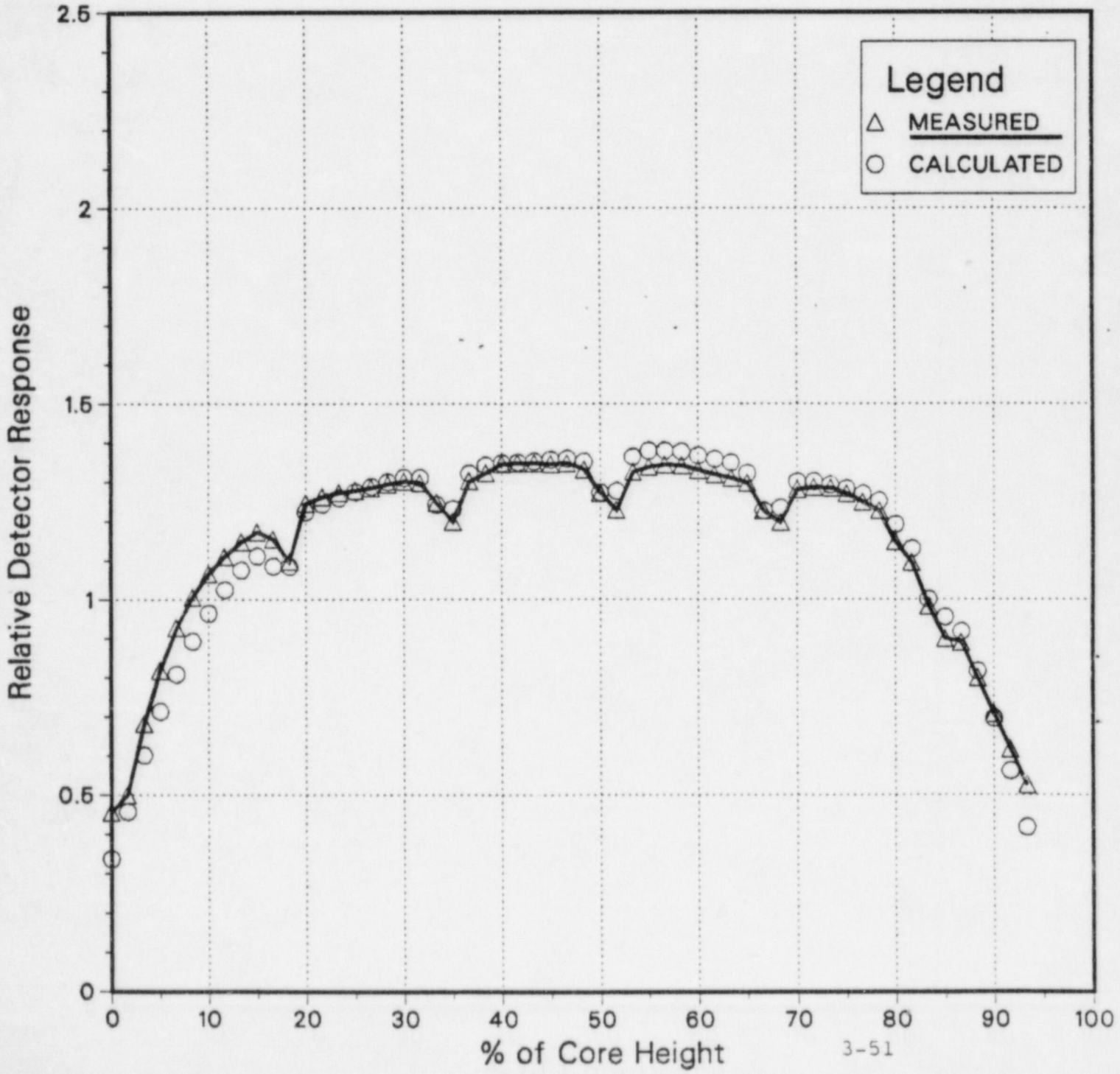
FIGURE 3.5.12

Measured and Calculated Detector Responses

PI 1 CYCLE 4 HFP, 1.058 GWD/MTU, ARO, EQ XENON

THIMBLE E10

MAP 104-10



Measured and Calculated Integrated Detector Responses

PI 1 Cycle 4 HFP, 5.458 GWD/MTU, ARO, Eq Xenon

Absolute Differences

Map 104-18

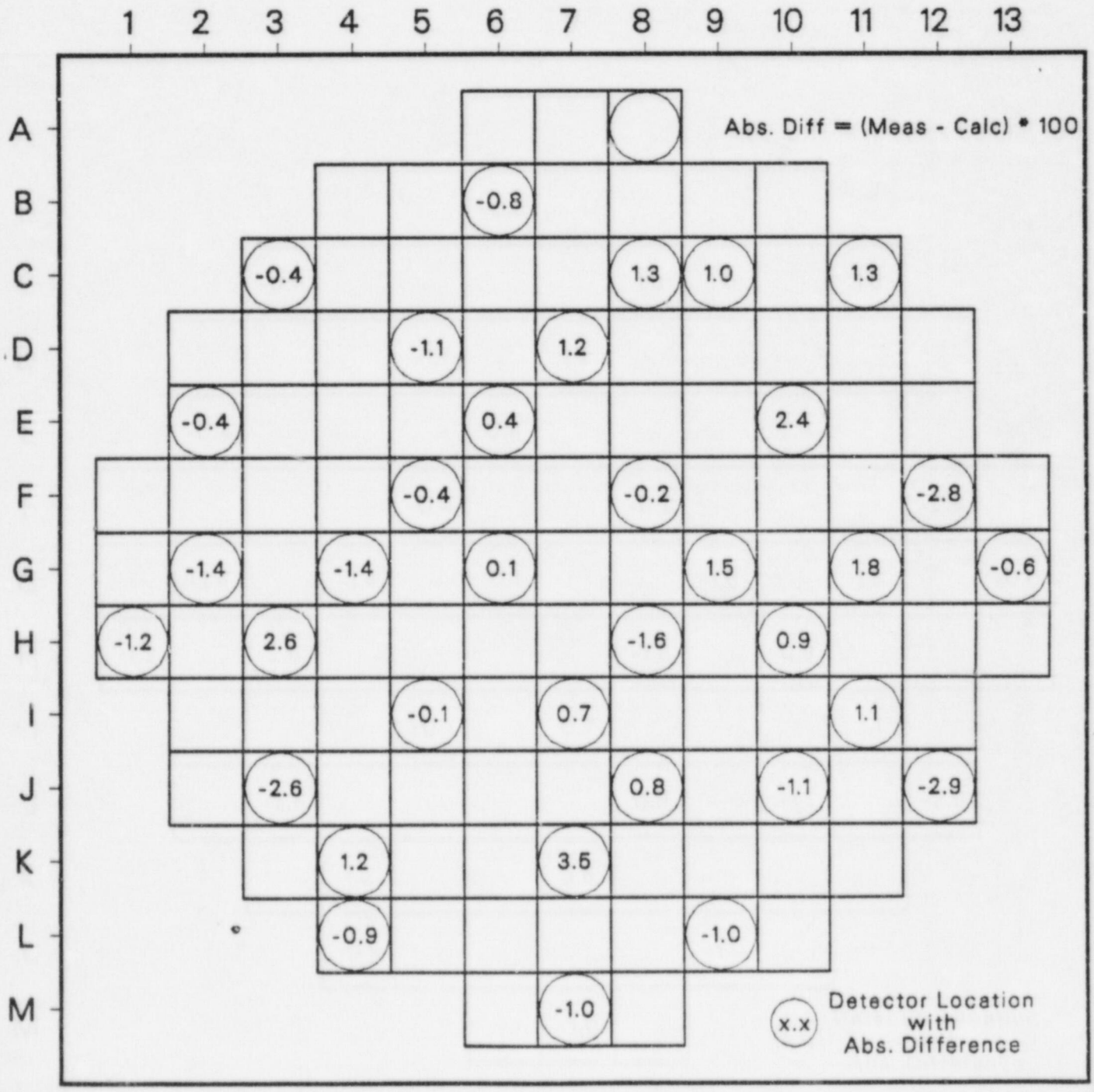


FIGURE 3.5.14

Measured and Calculated Detector Responses

PI 1 CYCLE 4 HFP, 5.458 GWD/MTU, ARO, EQ XENON

THIMBLE G6

MAP 104-18

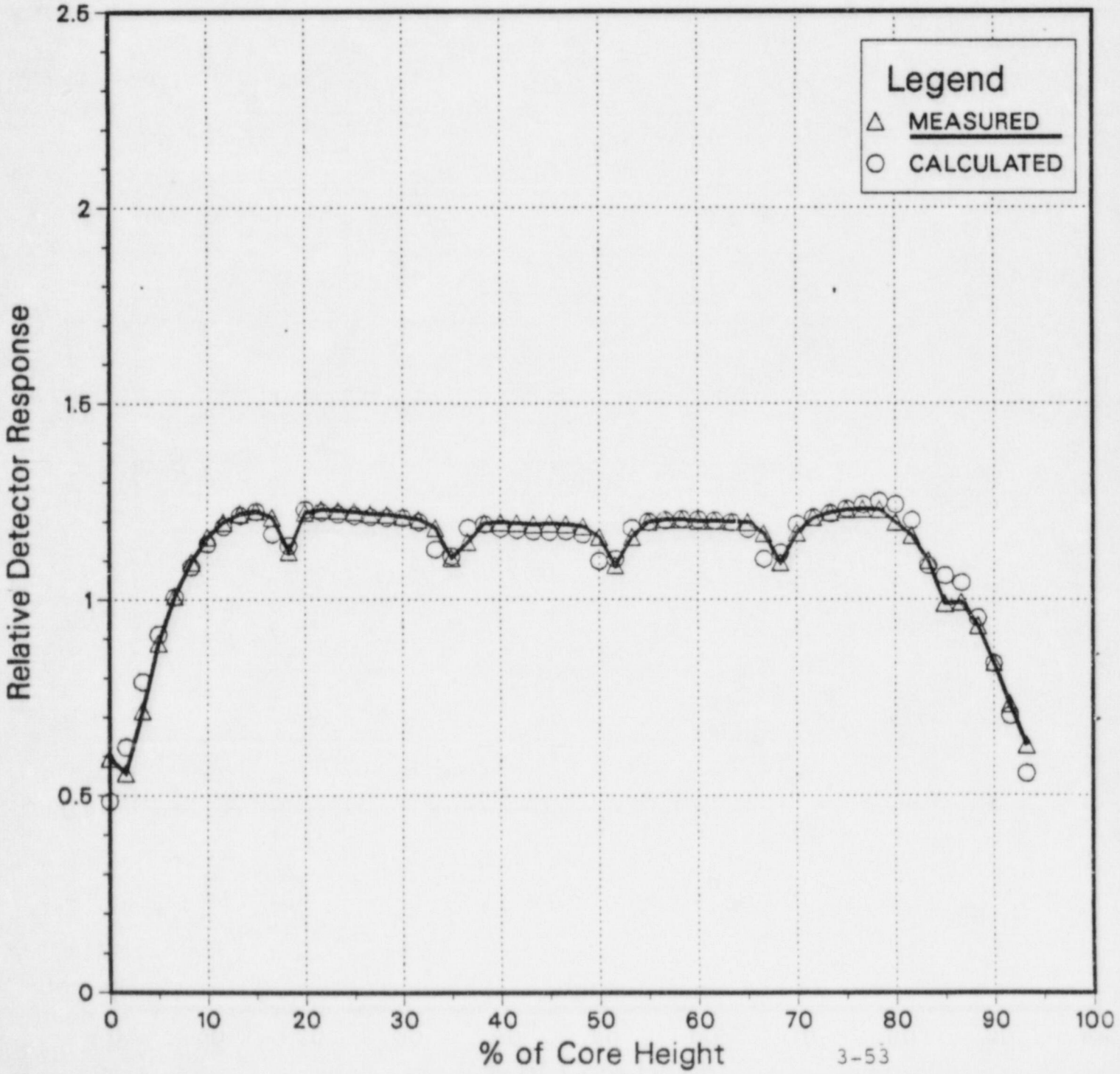


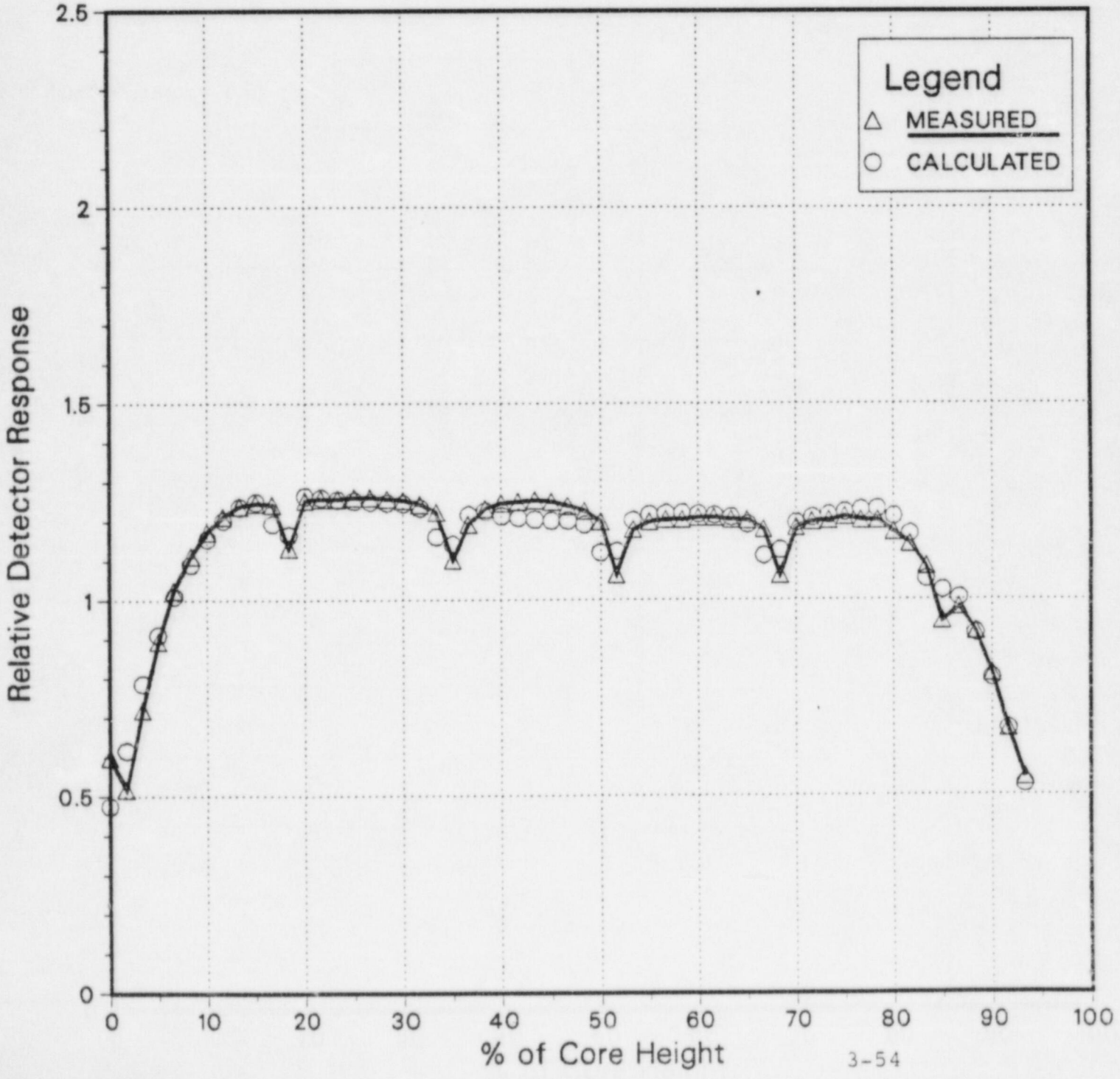
FIGURE 3.5.15

Measured and Calculated Detector Responses

PI 1 CYCLE 4 HFP, 5.458 GWD/MTU, ARO, EQ XENON

THIMBLE I5

MAP 104-18



Measured and Calculated Integrated Detector Responses

PI 1 Cycle 4 HFP, 10.400 GWD/MTU, ARO, Eq Xenon

Absolute Differences

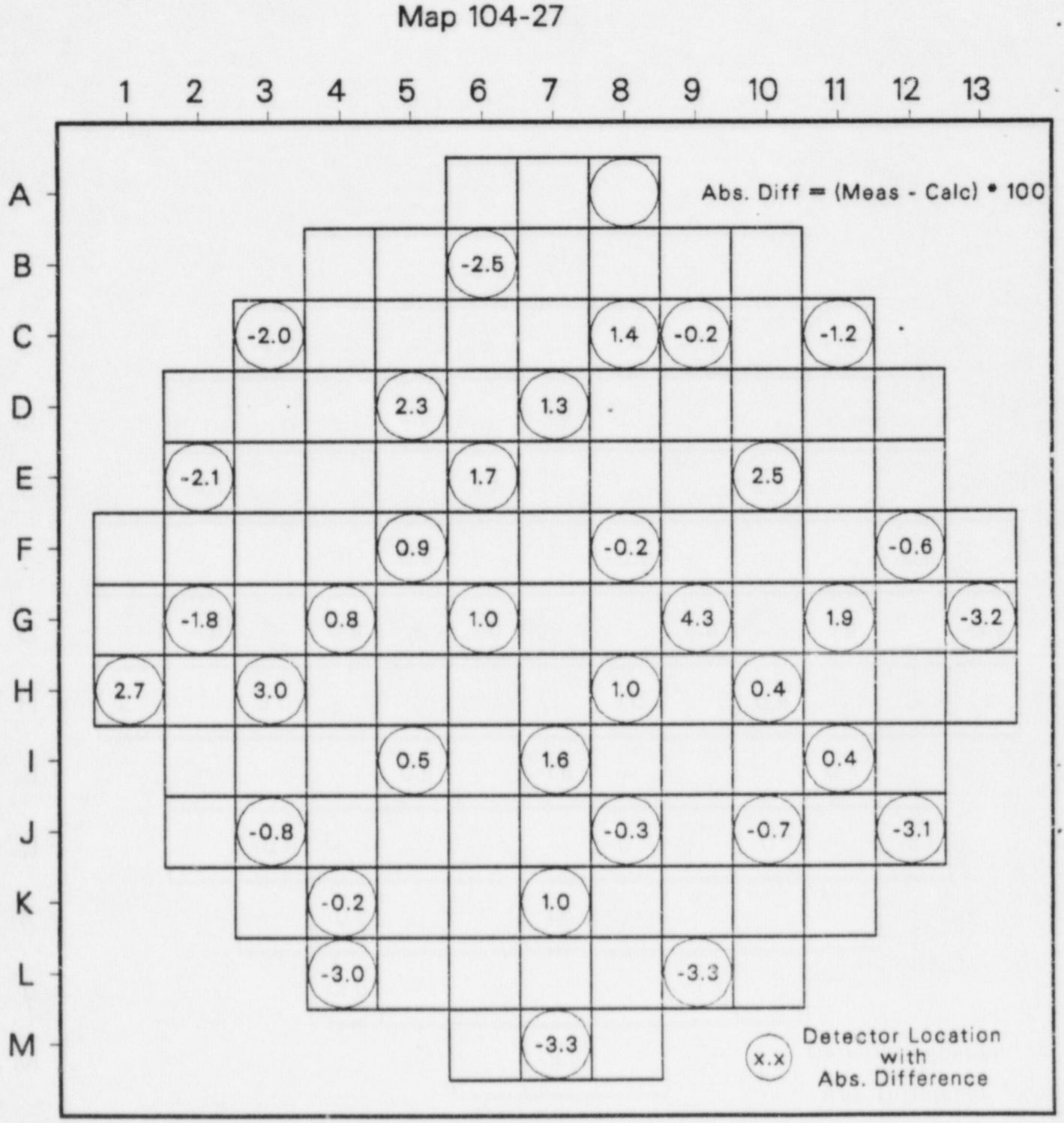


FIGURE 3.5.17

Measured and Calculated Detector Responses

PI 1 CYCLE 4 HFP, 10.400 GWD/MTU, ARO, EQ XENON

THIMBLE G6

MAP 104-27

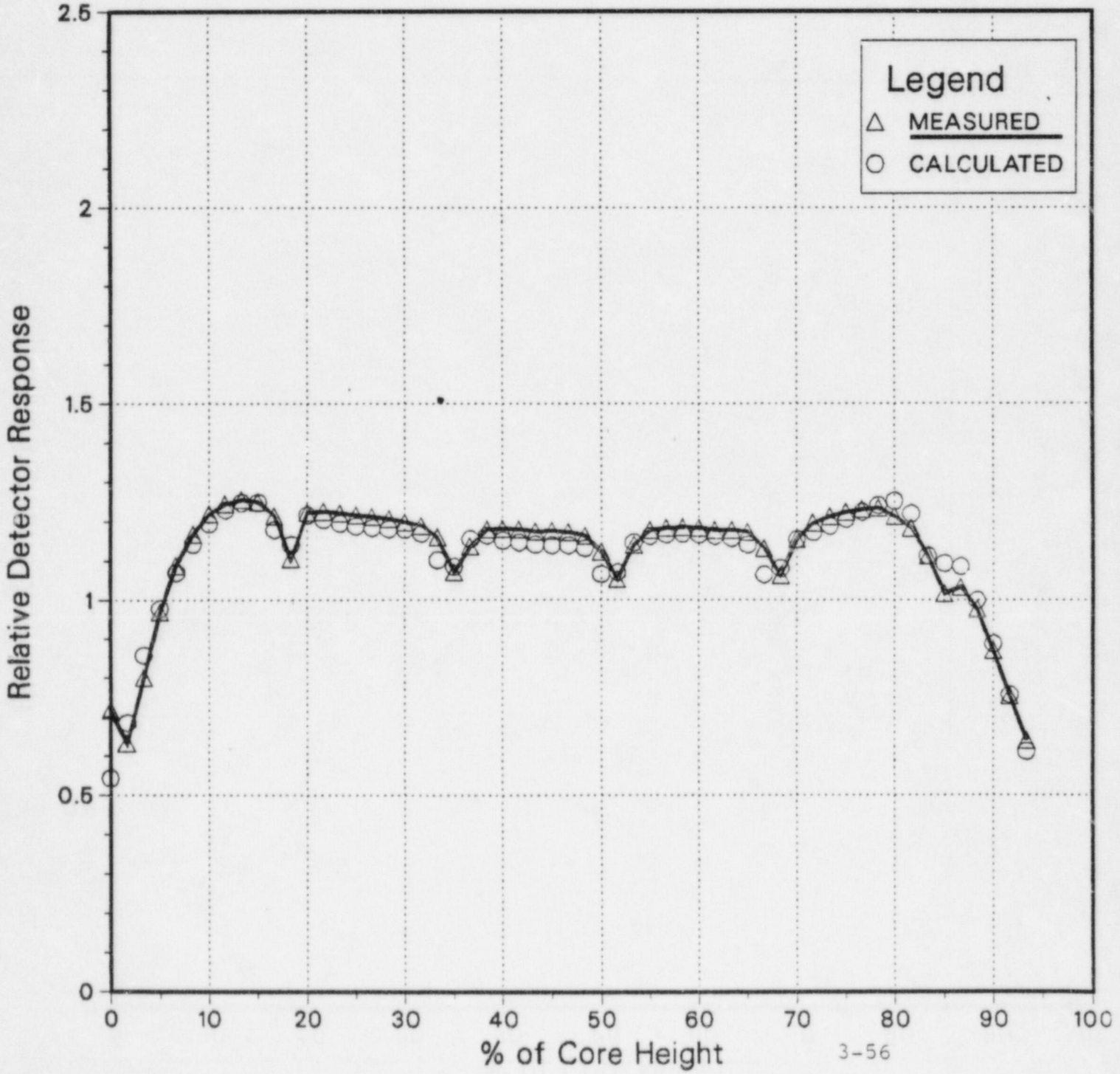


FIGURE 3.5.18

Measured and Calculated Detector Responses

PI 1 CYCLE 4 HFP, 10.400 GWD/MTU, ARO, EQ XENON

THIMBLE J8

MAP 104-27

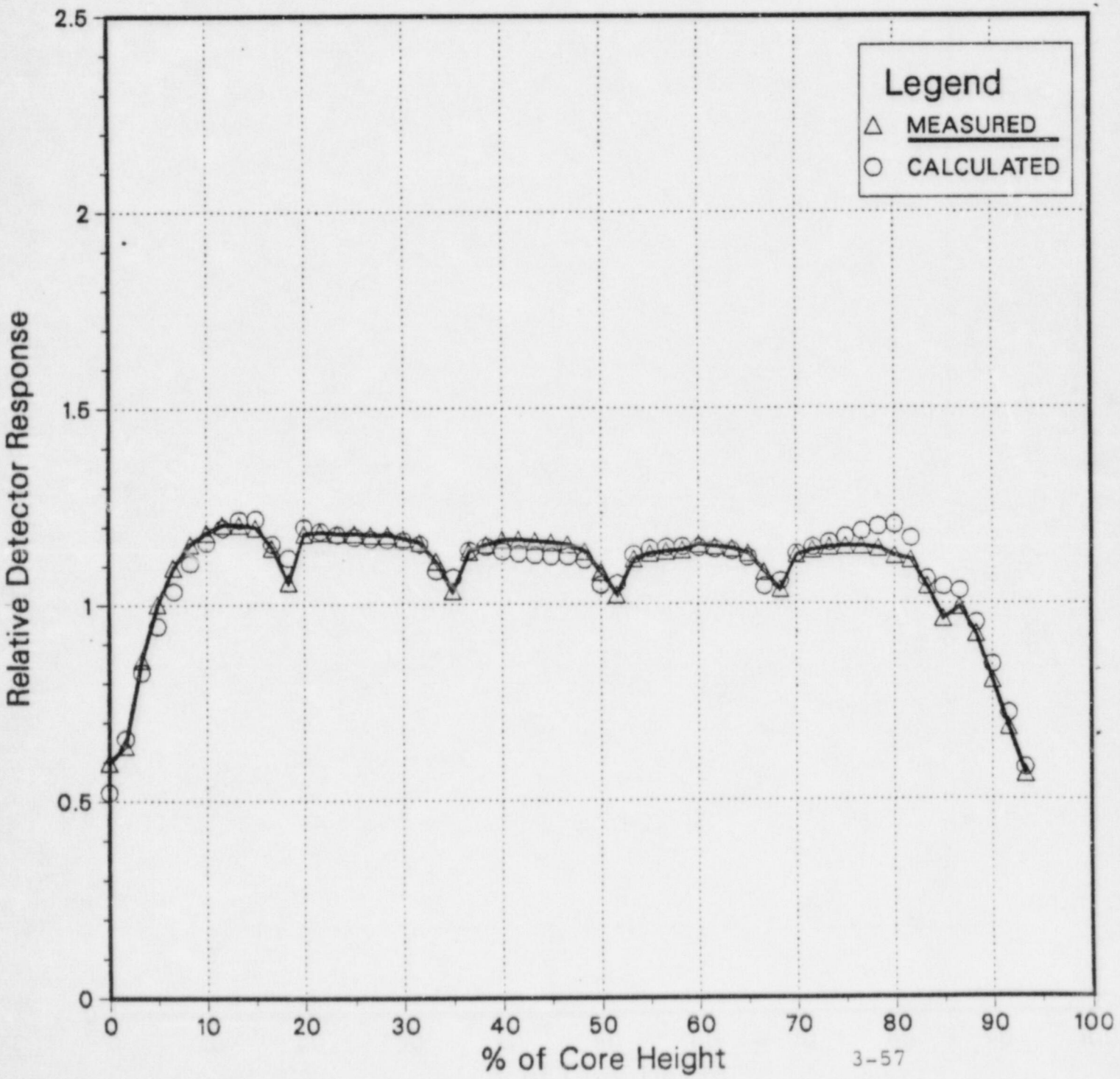


FIGURE 3.5.19

Measured and Calculated Integrated Detector Responses

PI 1 CYCLE 5 HFP, 0.831 GWD/MTU, ARO, EQ XENON

Absolute Differences

MAP 105-10

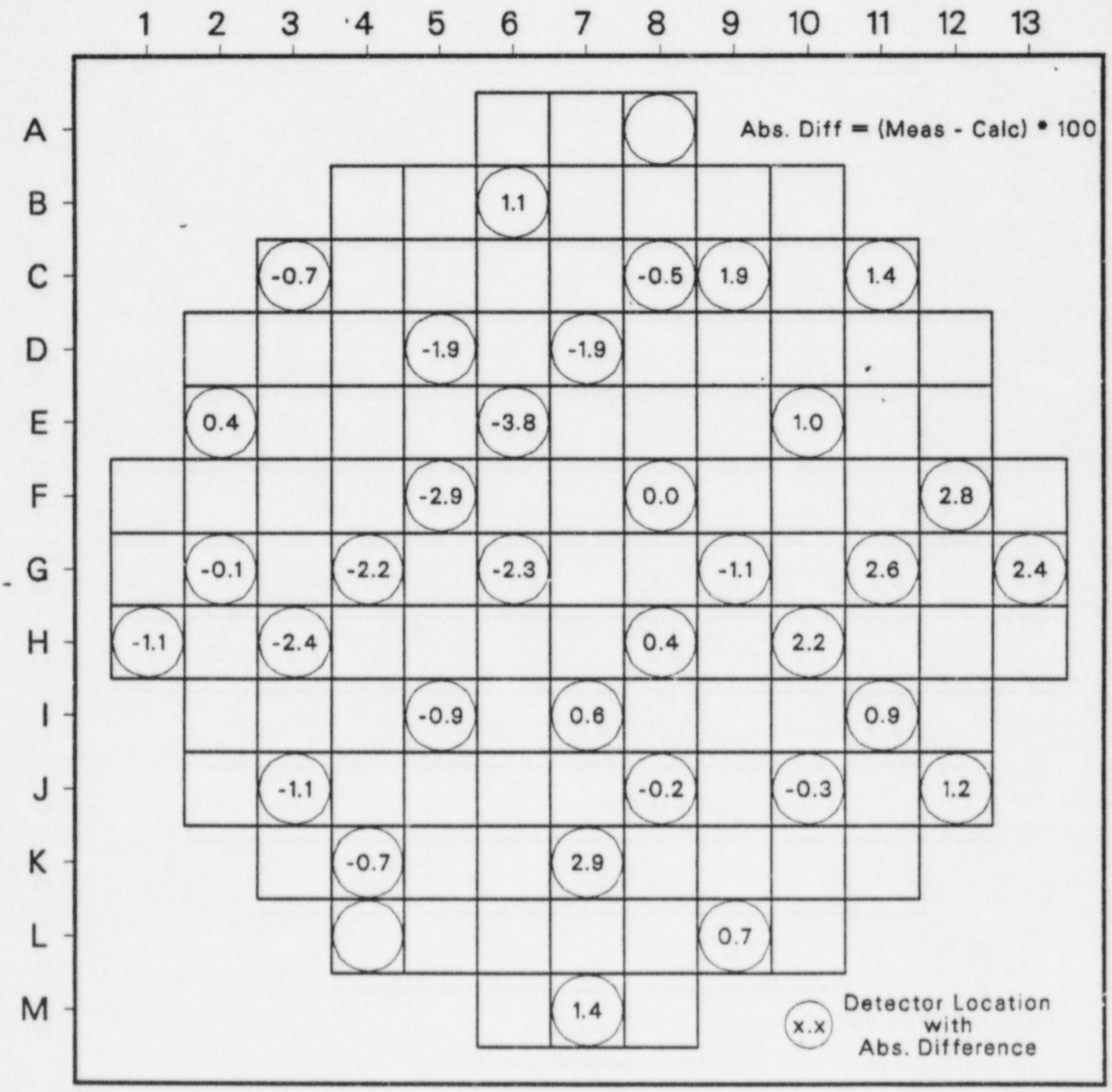


FIGURE 3.5.20

Measured and Calculated Detector Responses

PI 1 CYCLE 5 HFP, 0.831 GWD/MTU, ARO, EQ XENON

THIMBLE G6

MAP 105-10

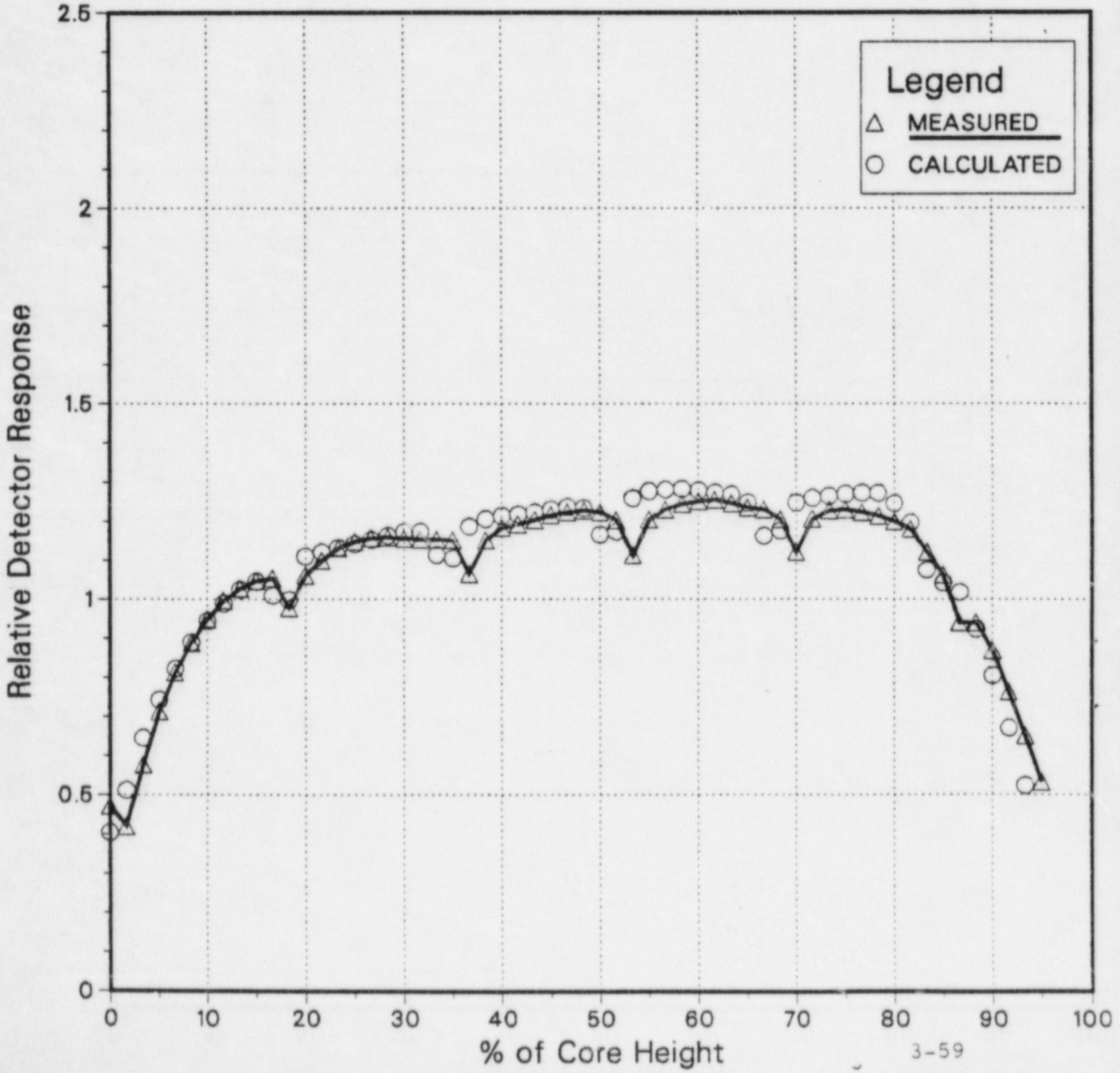


FIGURE 3.5.21

Measured and Calculated Detector Responses

PI 1 CYCLE 5 HFP, 0.831 GWD/MTU, ARO, EQ XENON

THIMBLE C8

MAP 105-10

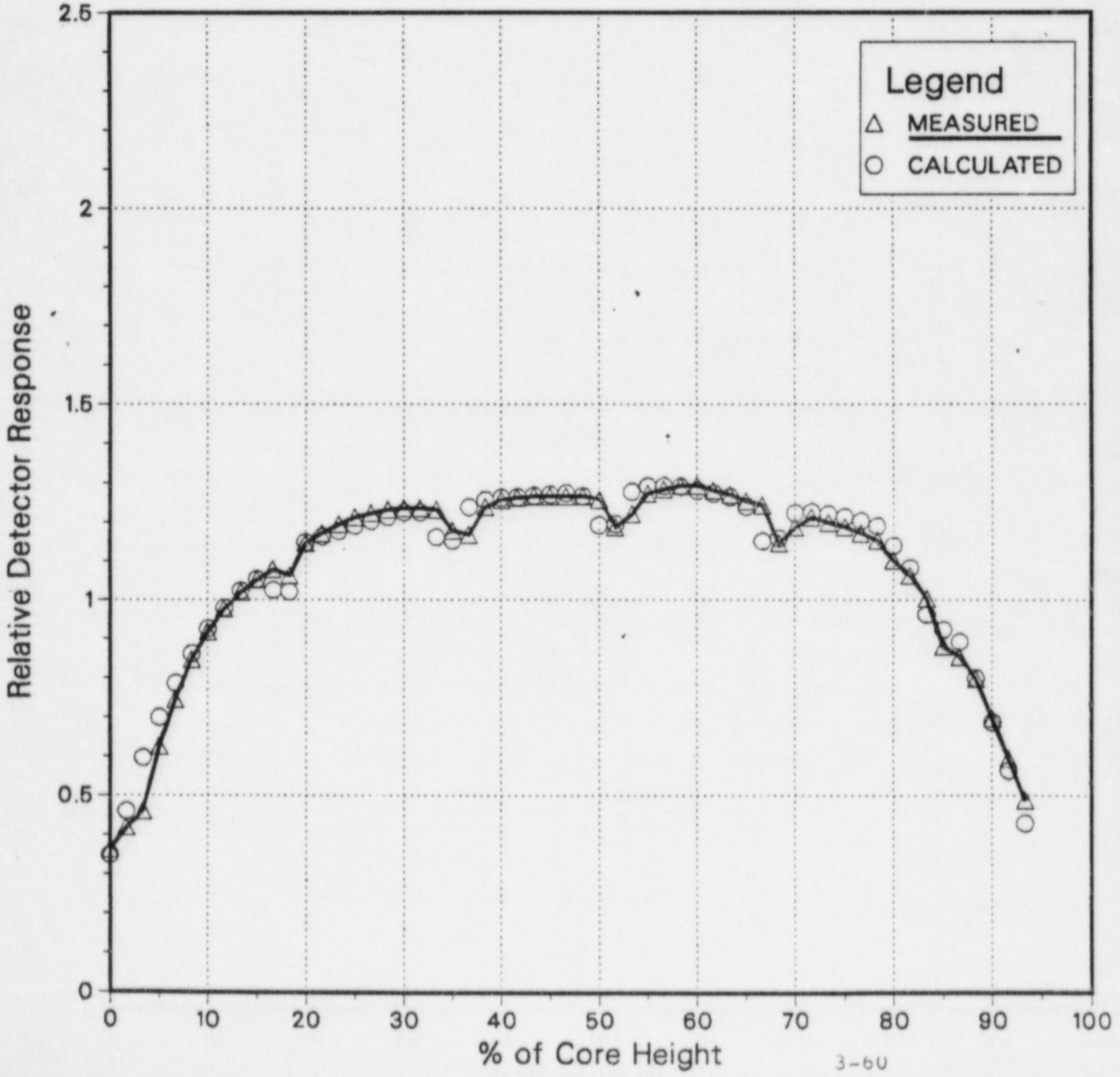


FIGURE 3.5.22

Measured and Calculated Integrated Detector Responses

PI 1 CYCLE 5 HFP, 5.919 GWD/MTU, ARO, EQ XENON

Absolute Differences

MAP 105-23

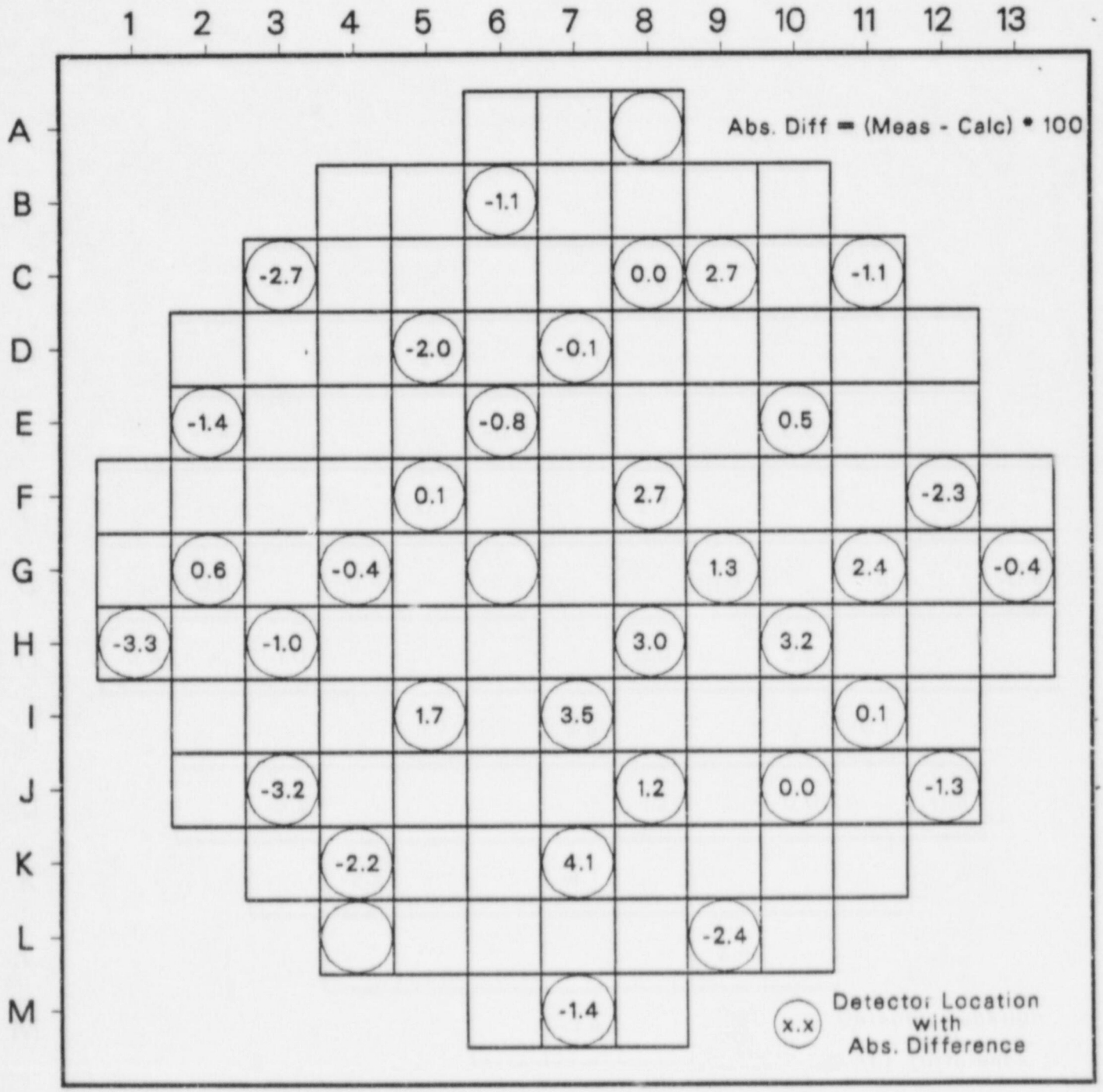


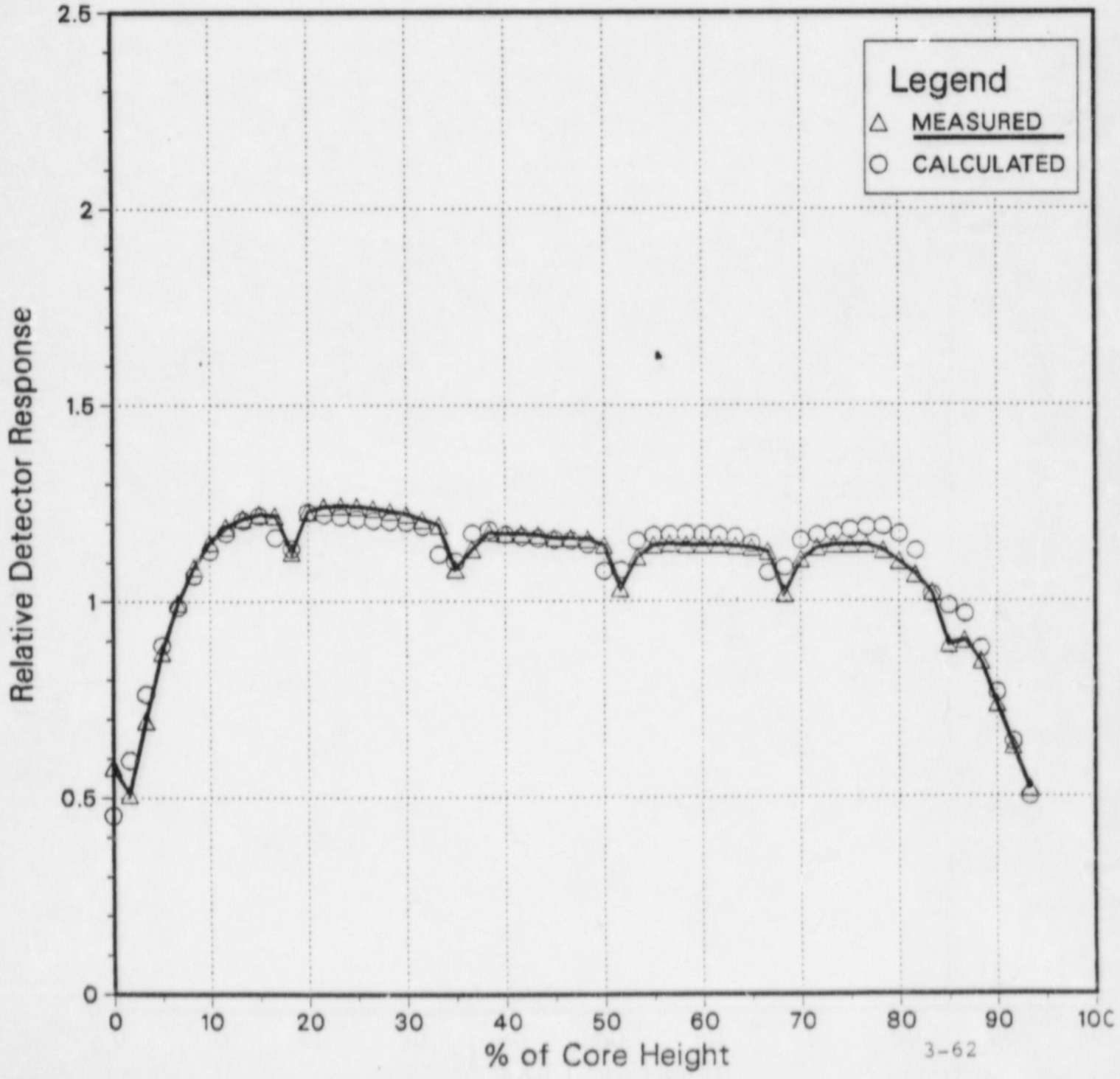
FIGURE 3.5.23

Measured and Calculated Detector Responses

PI 1 CYCLE 5 HFP, 5.919 GWD/MTU, ARO, EQ XENON

THIMBLE H3

MAP 105-23

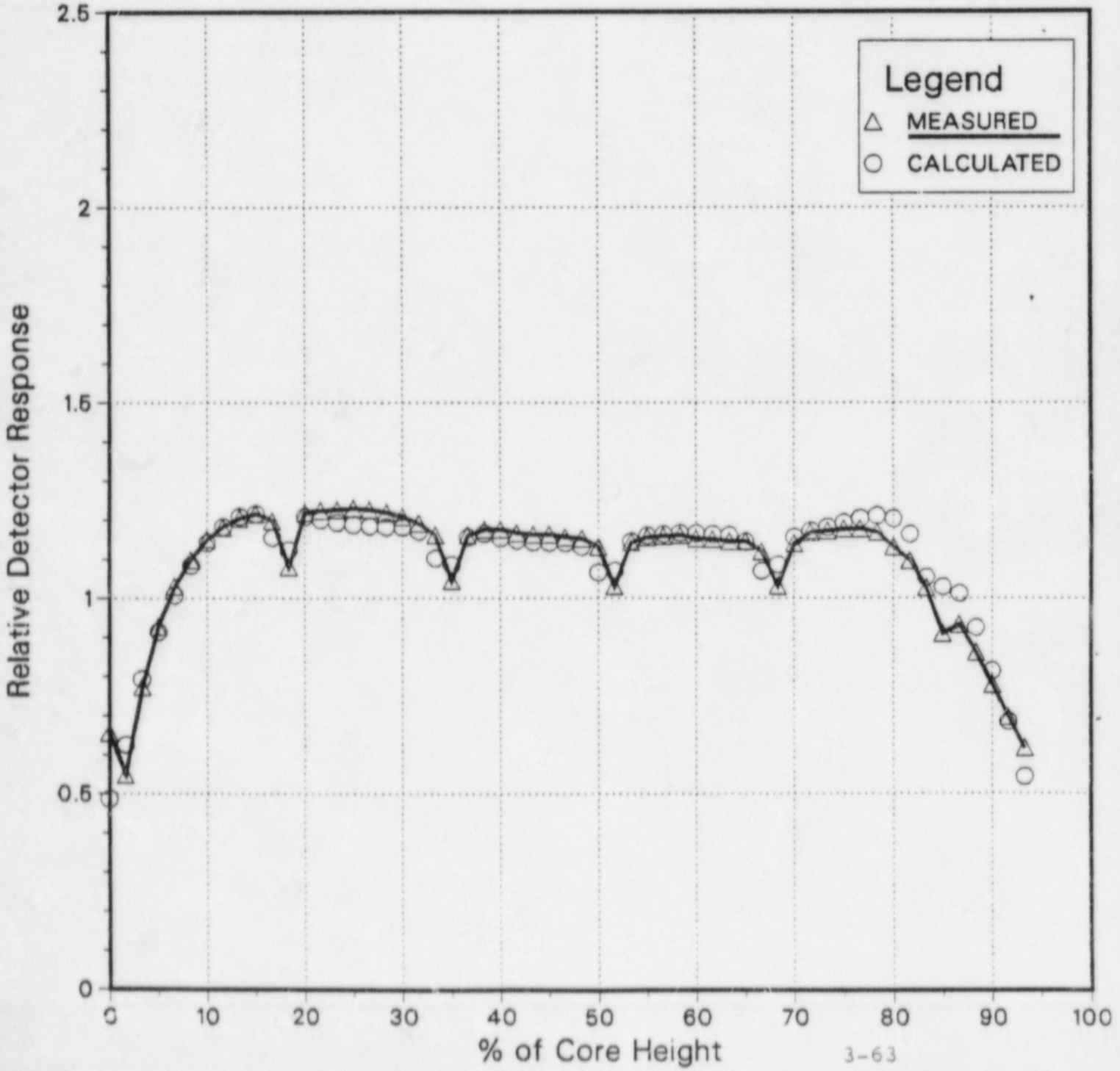


Measured and Calculated Detector Responses

PI 1 CYCLE 5 HFP, 5.919 GWD/MTU, ARO, EQ XENON

THIMBLE D7

MAP 105-23



Measured and Calculated Integrated Detector Responses

PI 1 CYCLE 5 HFP, 11.653 GWD/MTU, ARO, EQ XENON

Absolute Differences

MAP 105-34

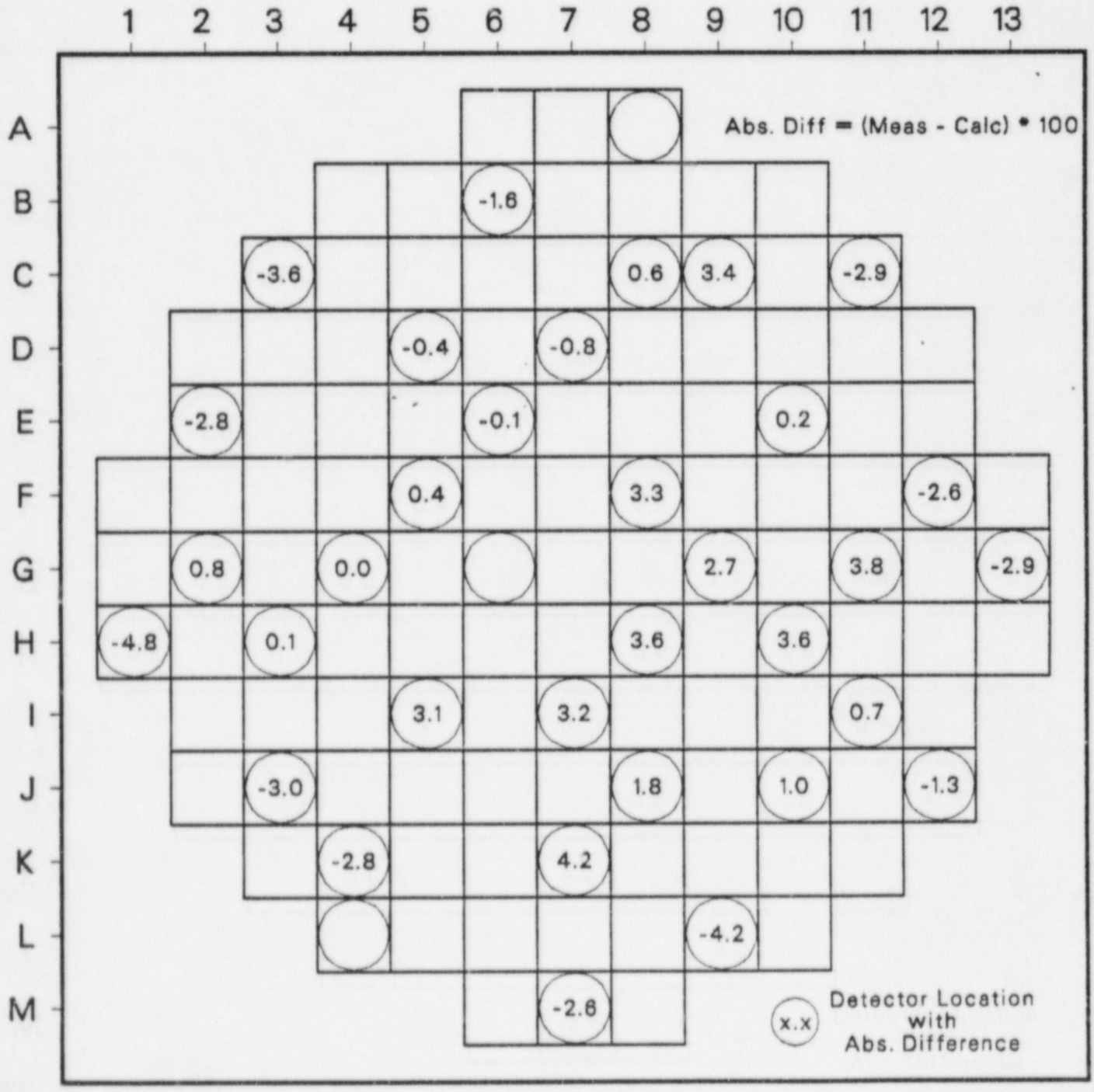


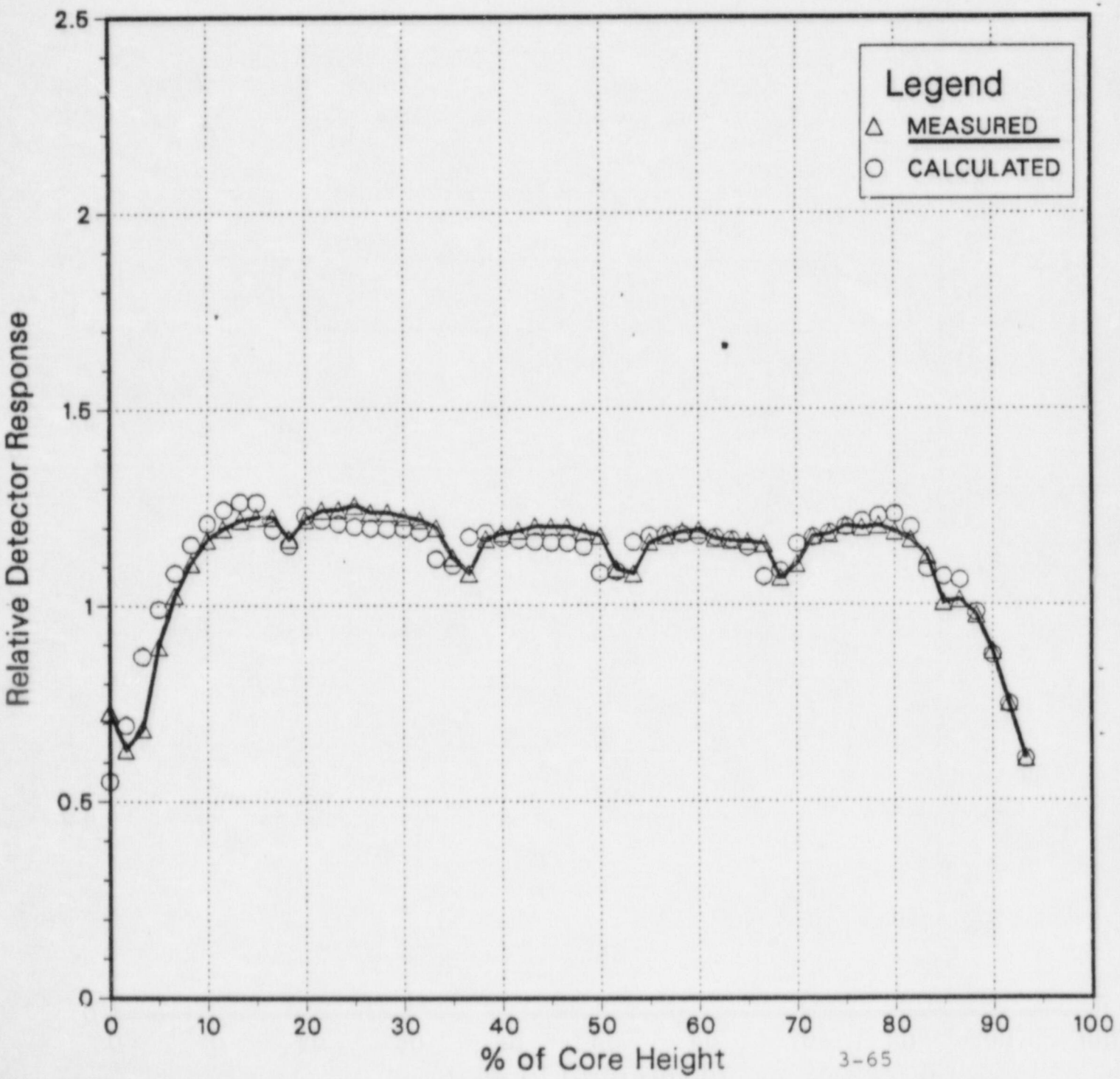
FIGURE 3.5.26

Measured and Calculated Detector Responses

PI 1 CYCLE 5 HFP, 11.653 GWD/MTU, ARO, EQ XENON

THIMBLE D5

MAP 105-34



Measured and Calculated Detector Responses

PI 1 CYCLE 5 HFP, 11.653 GWD/MTU, ARO, EQ XENON

THIMBLE H8

MAP 105-34

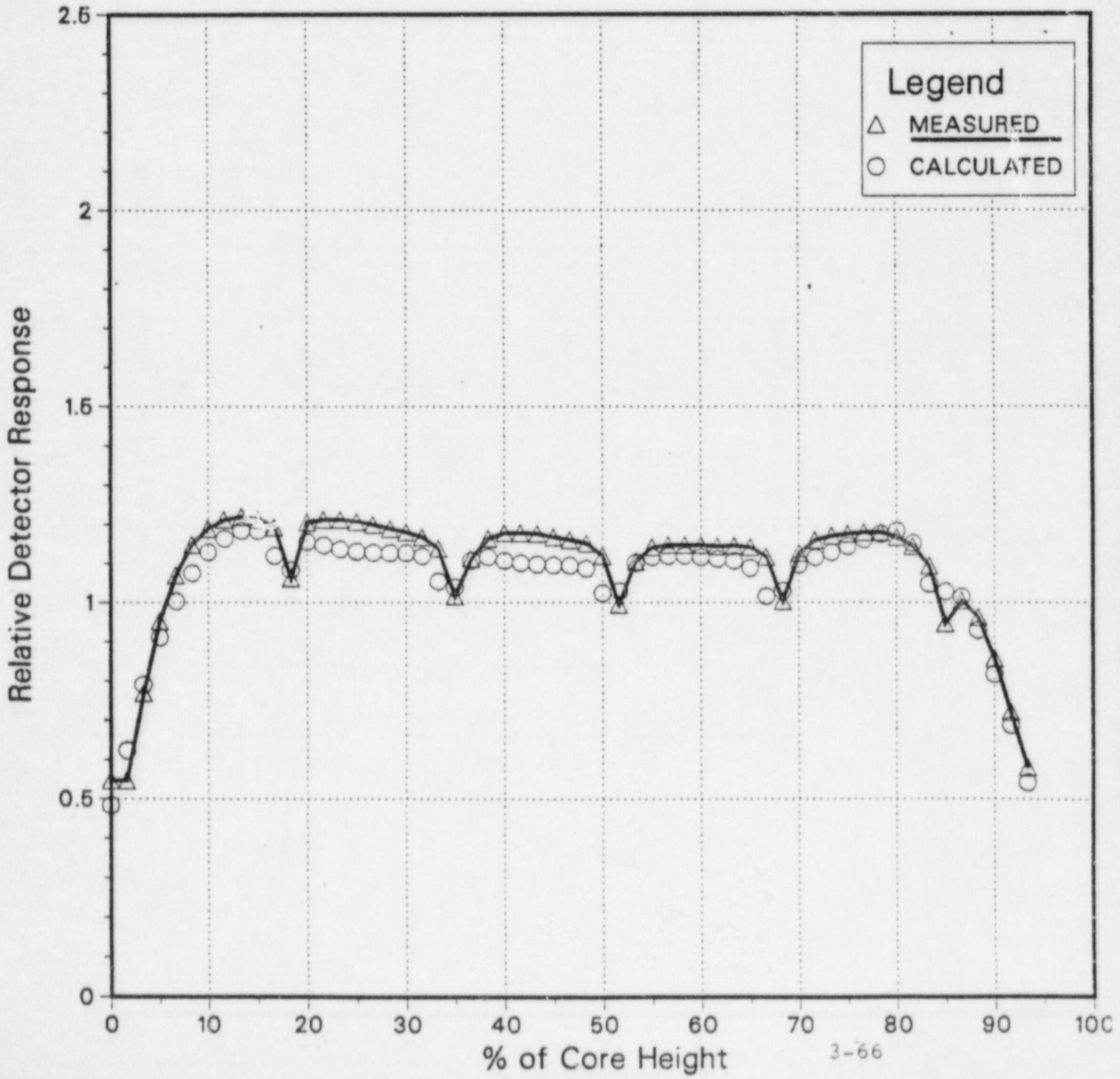


FIGURE 3.5.28

Measured and Calculated Integrated Detector Responses

PI 1 Cycle 6 HFP, 0.955 GWD/MTU, ARO, Eq Xenon

Absolute Differences

Map 106-15

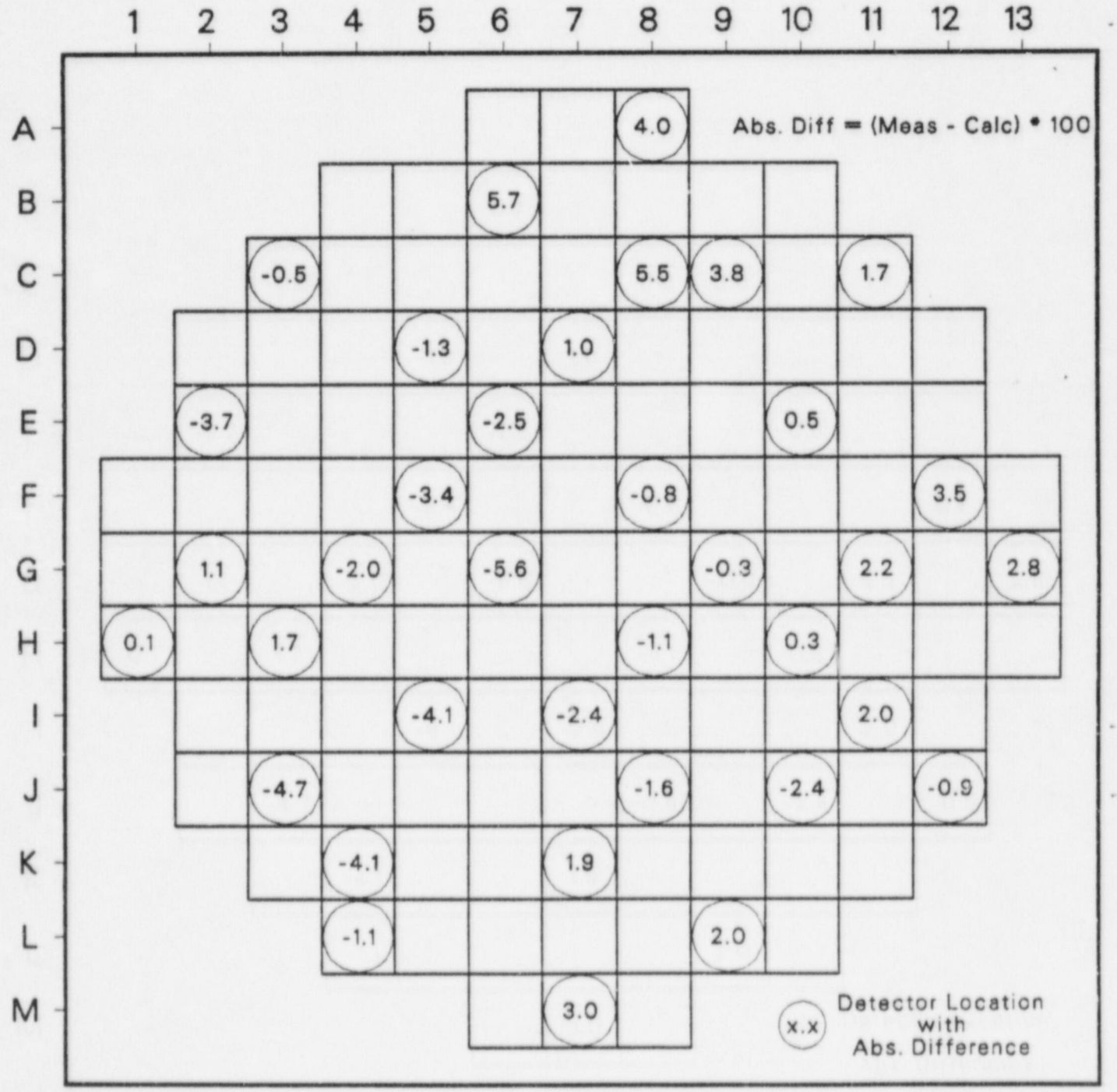


FIGURE 3.5.29

Measured and Calculated Detector Responses

PI 1 CYCLE 6 HFP, 0.955 GWD/MTU, ARO, EQ XENON

THIMBLE G6

MAP 106-15

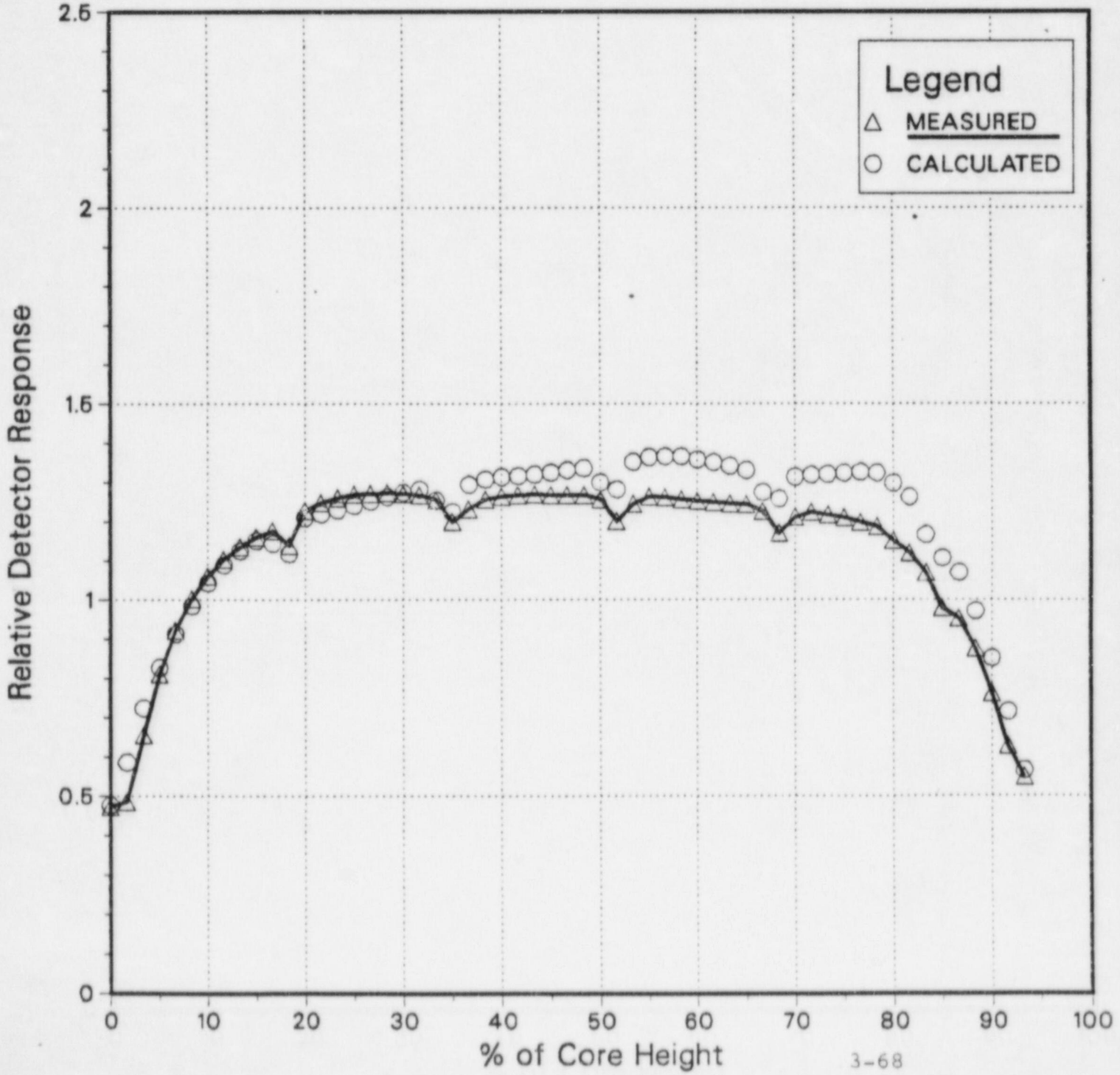


FIGURE 3.5.30

Measured and Calculated Detector Responses

PI 1 CYCLE 6 HFP, 0.955 GWD/MTU, ARO, EQ XENON

THIMBLE J10

MAP 106-15

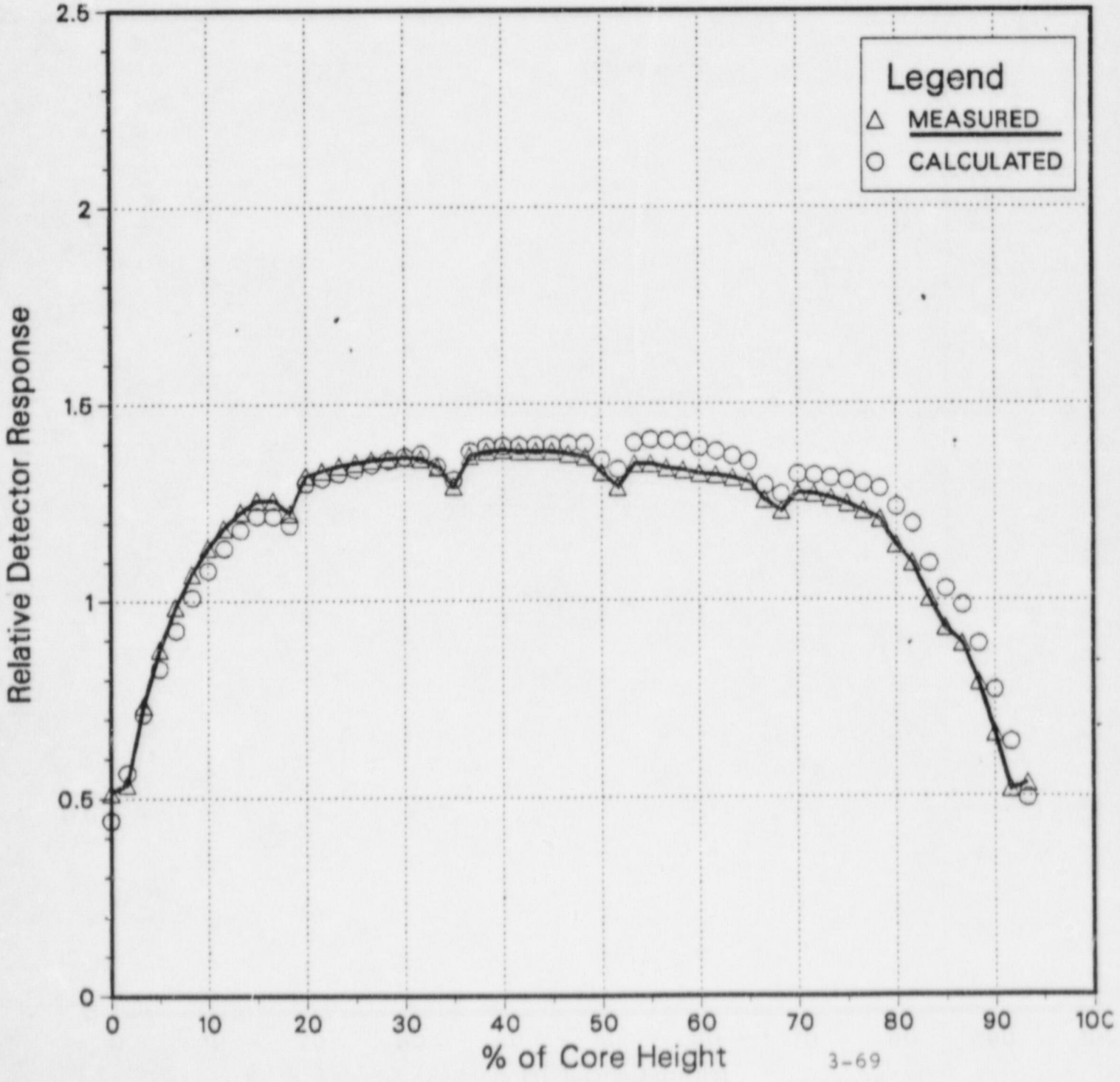


FIGURE 3.5.31

Measured and Calculated Integrated Detector Responses

PI 1 Cycle 6 HFP, 5.706 GWD/MTU, ARO, Eq Xenon

Absolute Differences

Map 106-24

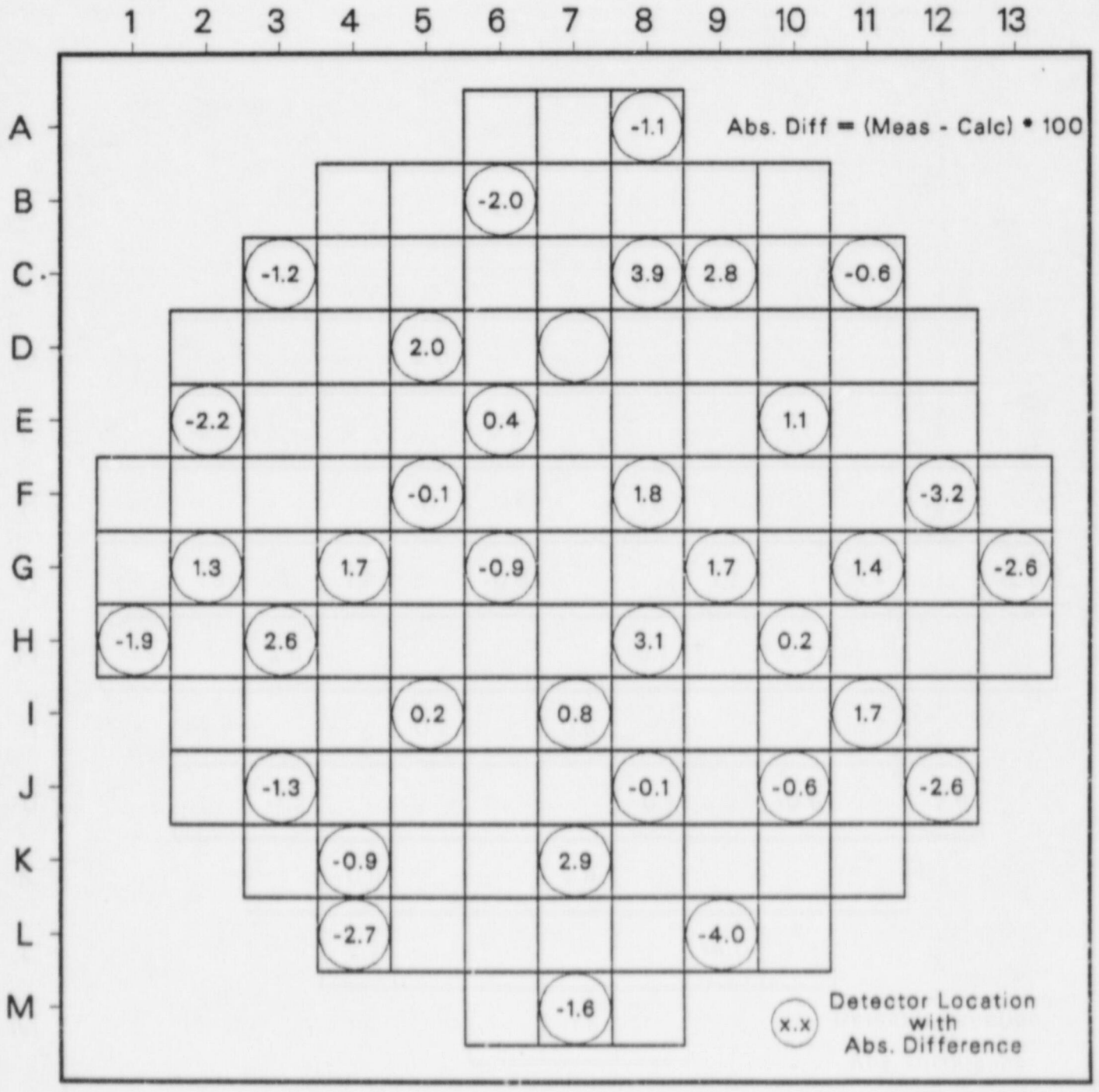


FIGURE 3.5.32

Measured and Calculated Detector Responses

PI 1 CYCLE 6 HFP, 5.706 GWD/MTU, ARO, EQ XENON

THIMBLE G6

MAP 106-24

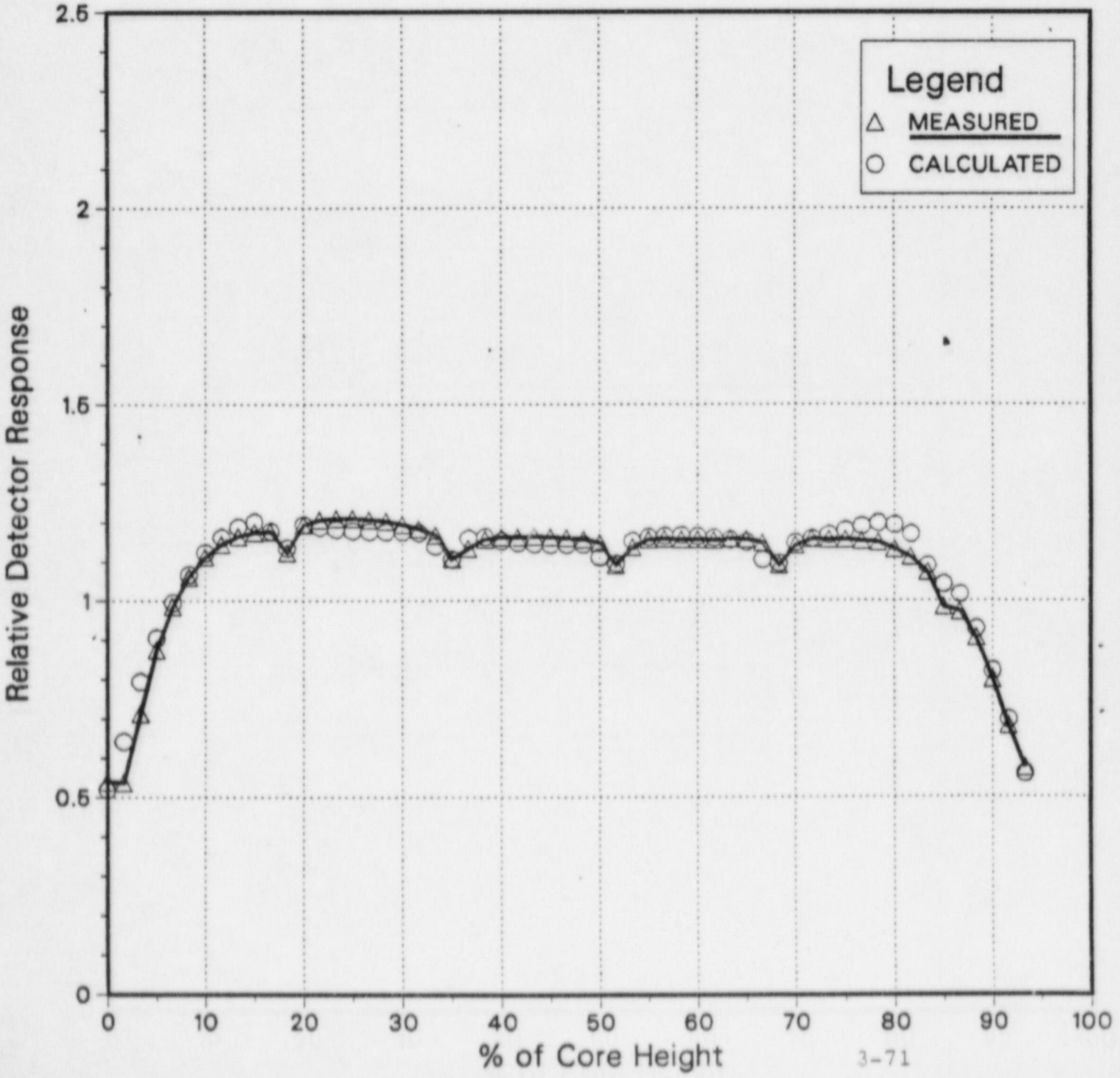


FIGURE 3.5.33

Measured and Calculated Detector Responses

PI 1 CYCLE 6 HFP, 5.706 GWD/MTU, ARO, EQ XENON

THIMBLE G11

MAP 106-24

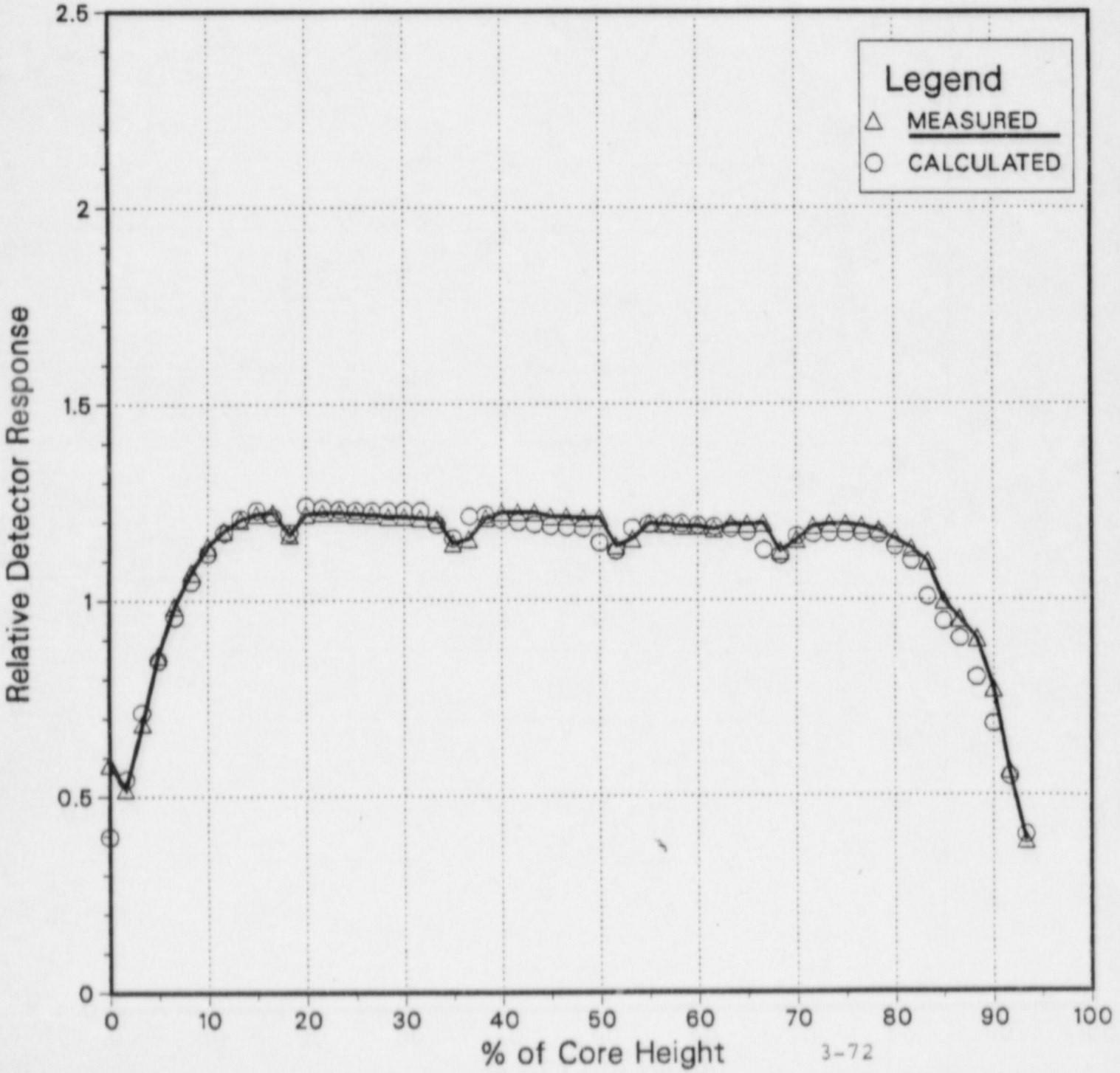


FIGURE 3.5.34

Measured and Calculated Integrated Detector Responses

PI 1 Cycle 6 HFP, 7.880 GWD/MTU, ARO, Eq Xenon

Absolute Differences

Map 106-28

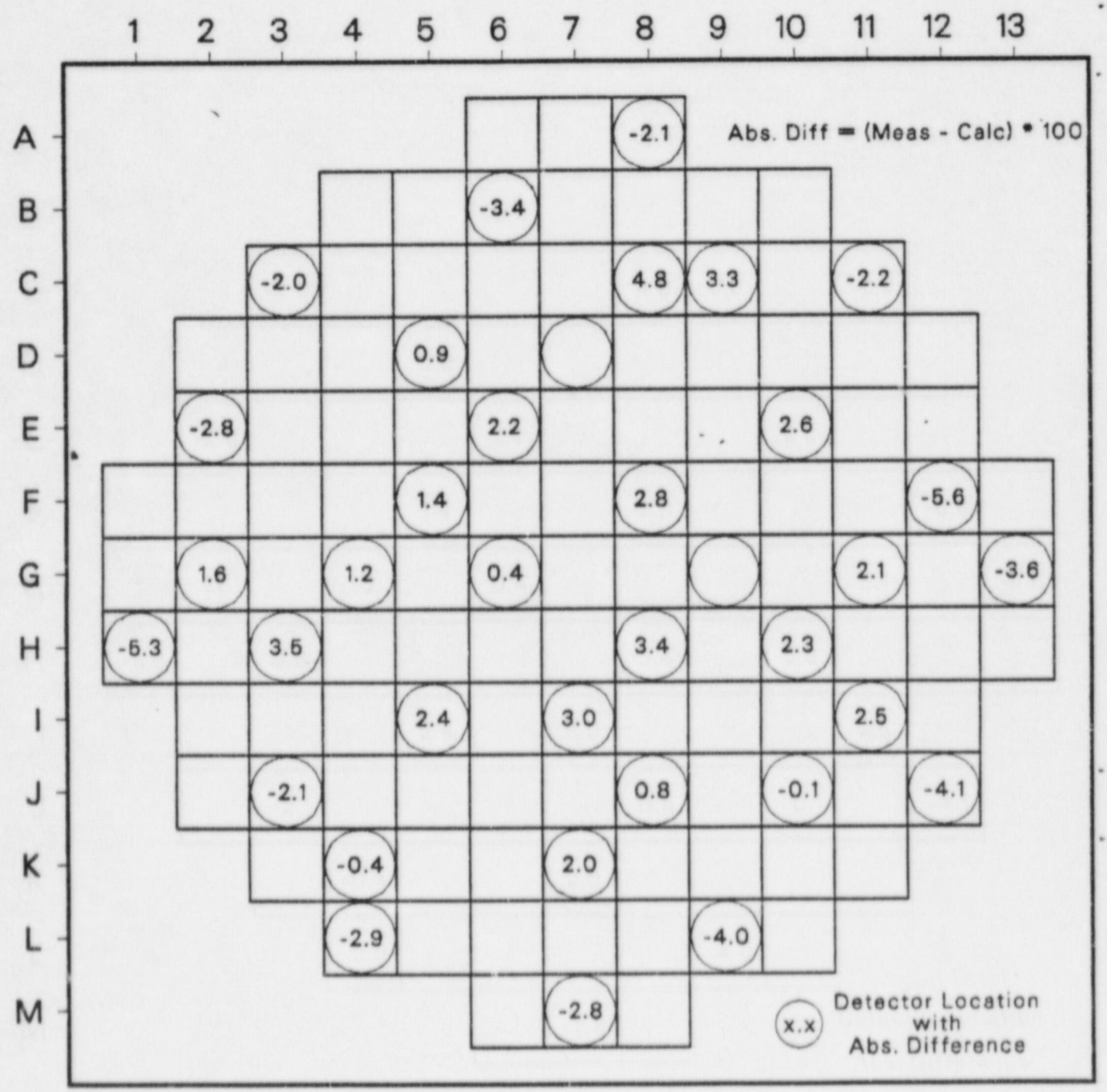


FIGURE 3.5.35

Measured and Calculated Detector Responses

PI 1 CYCLE 6 HFP, 7.880 GWD/MTU, ARO, EQ XENON

THIMBLE G6

MAP 106-28

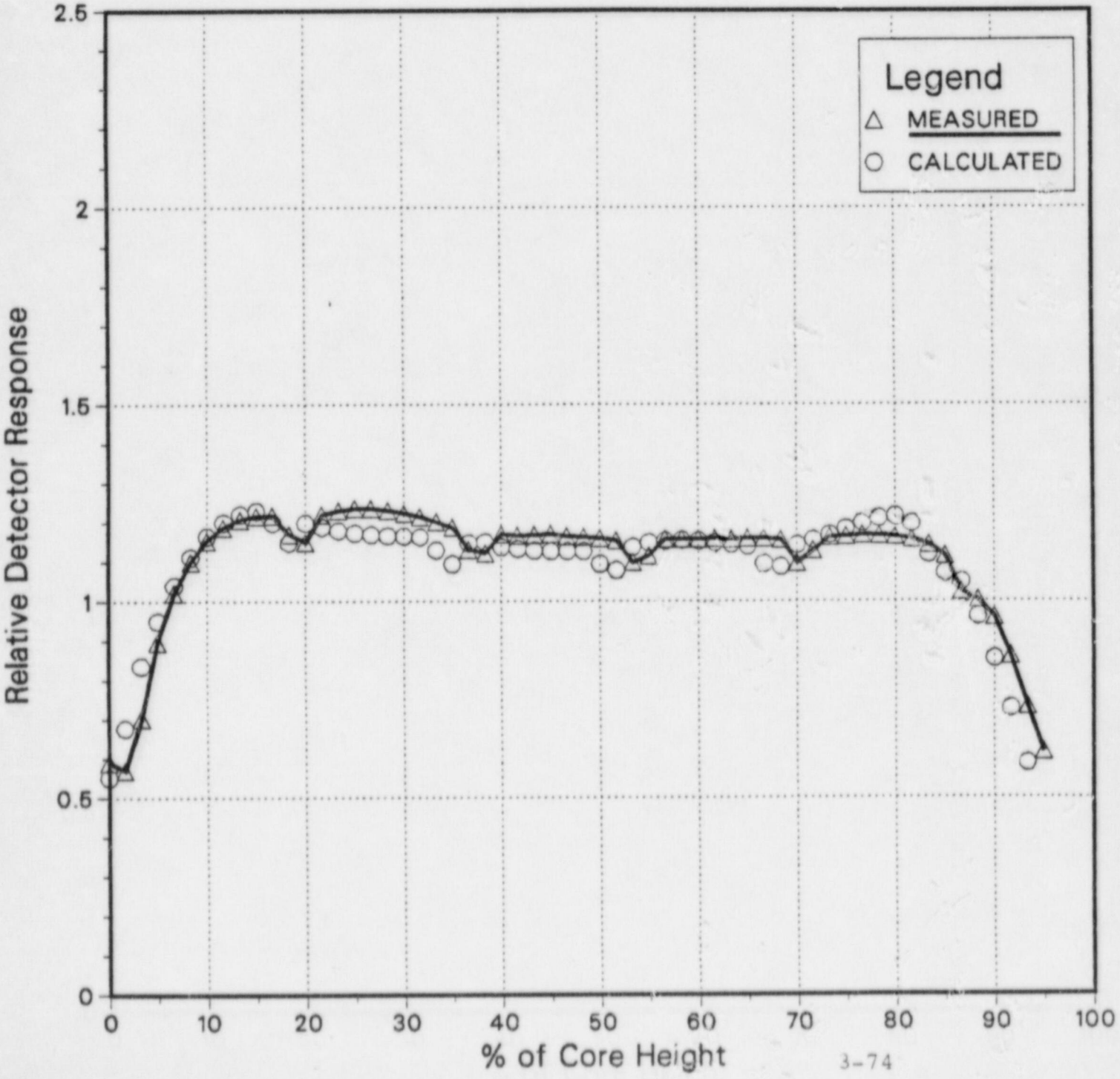


FIGURE 3.5.36

Measured and Calculated Detector Responses

PI 1 CYCLE 6 HFP, 7.880 GWD/MTU, ARO, EQ XENON

THIMBLE K7

MAP 106-28

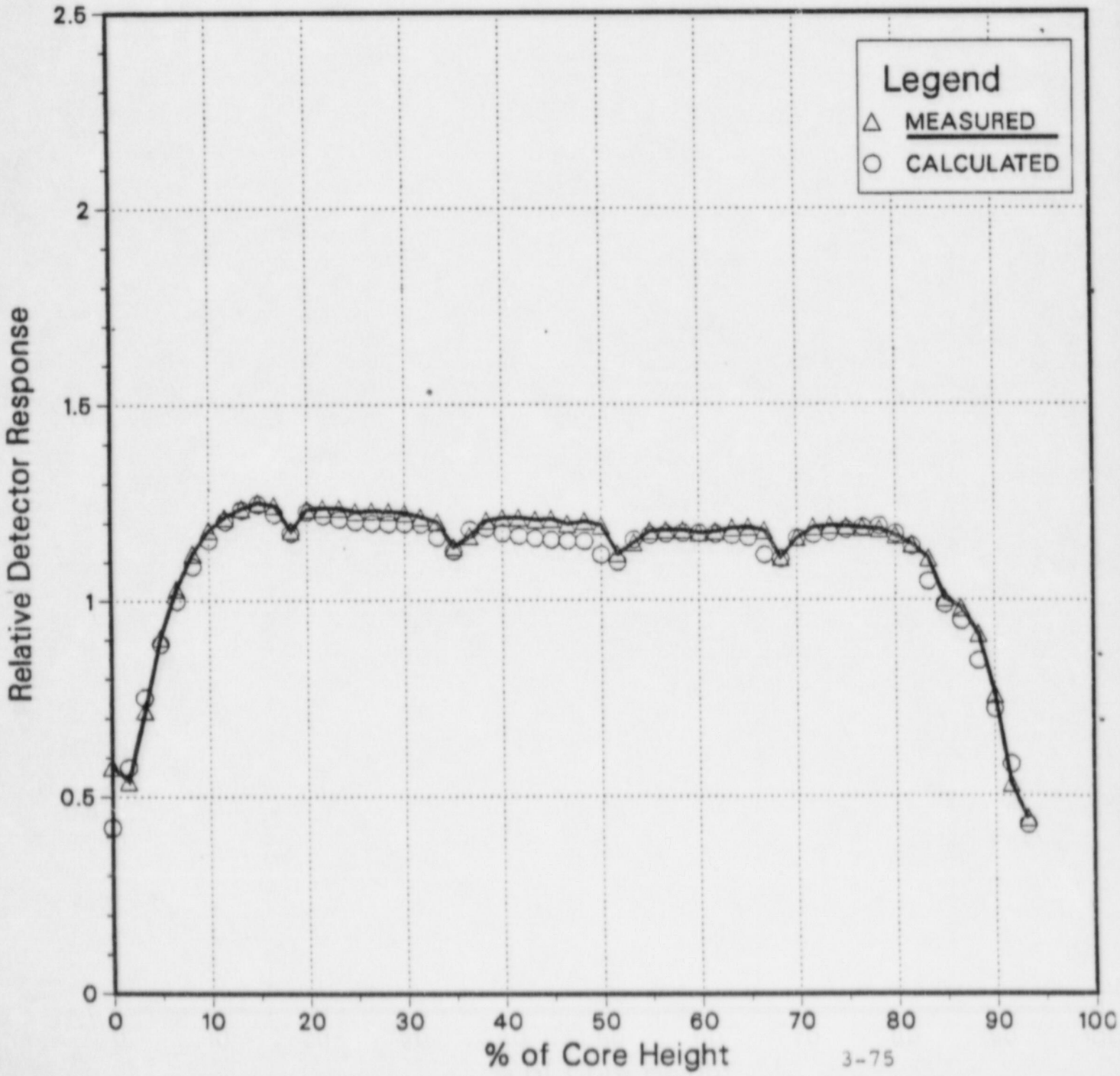


FIGURE 3.5.37

Measured and Calculated Integrated Detector Responses

PI 1 CYCLE 5 HFP, 0.831 GWD/MTU, ARO, EQ XENON

CASMO/PDQ/DP5 Model

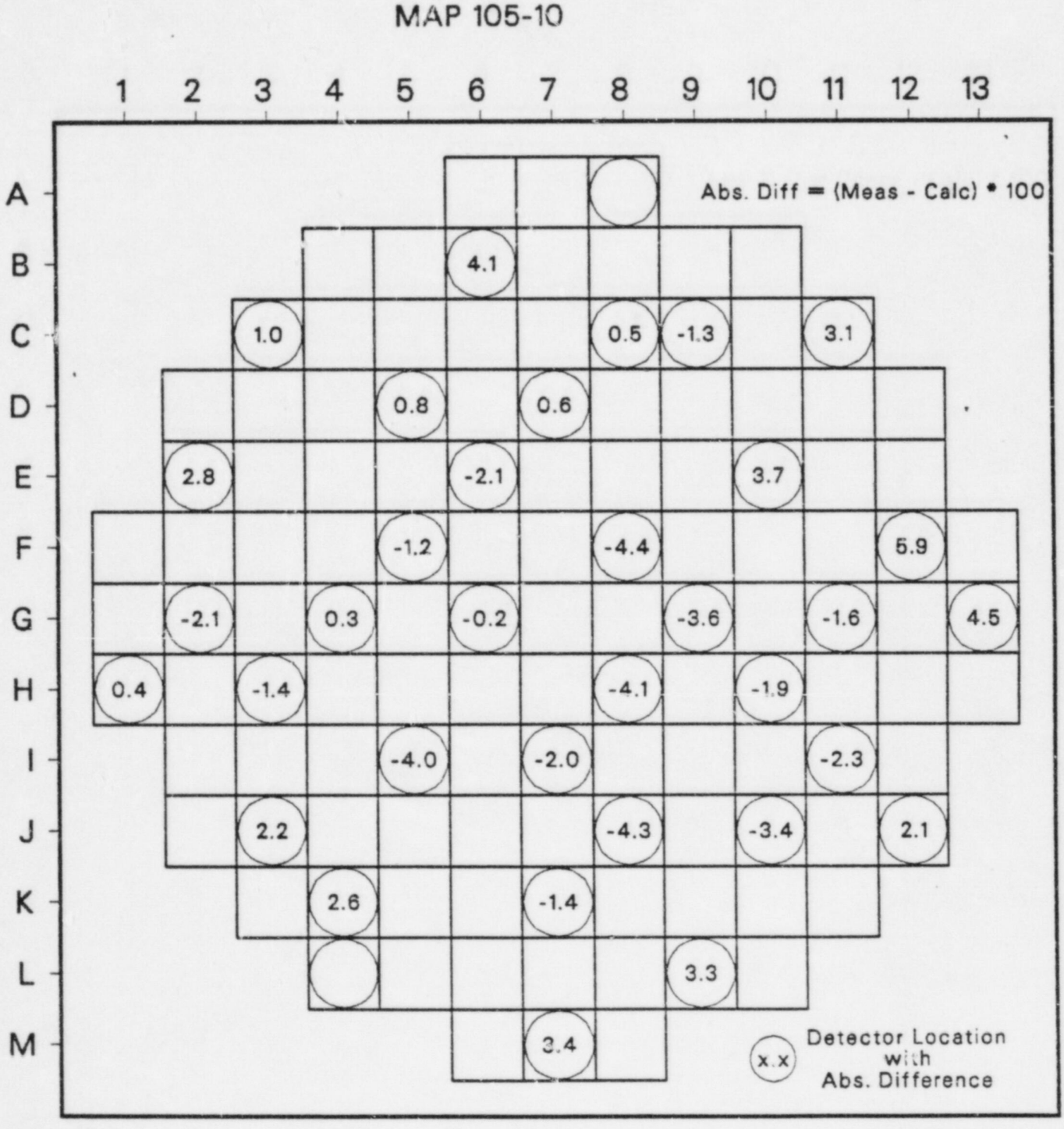


FIGURE 3.5.38

Measured and Calculated Detector Responses

PI 1 CYCLE 5 HFP, 0.831 GWD/MTU, ARO, EQ XENON

CASMO/PDQ/DP5 Model

THIMBLE G6

MAP 105-10

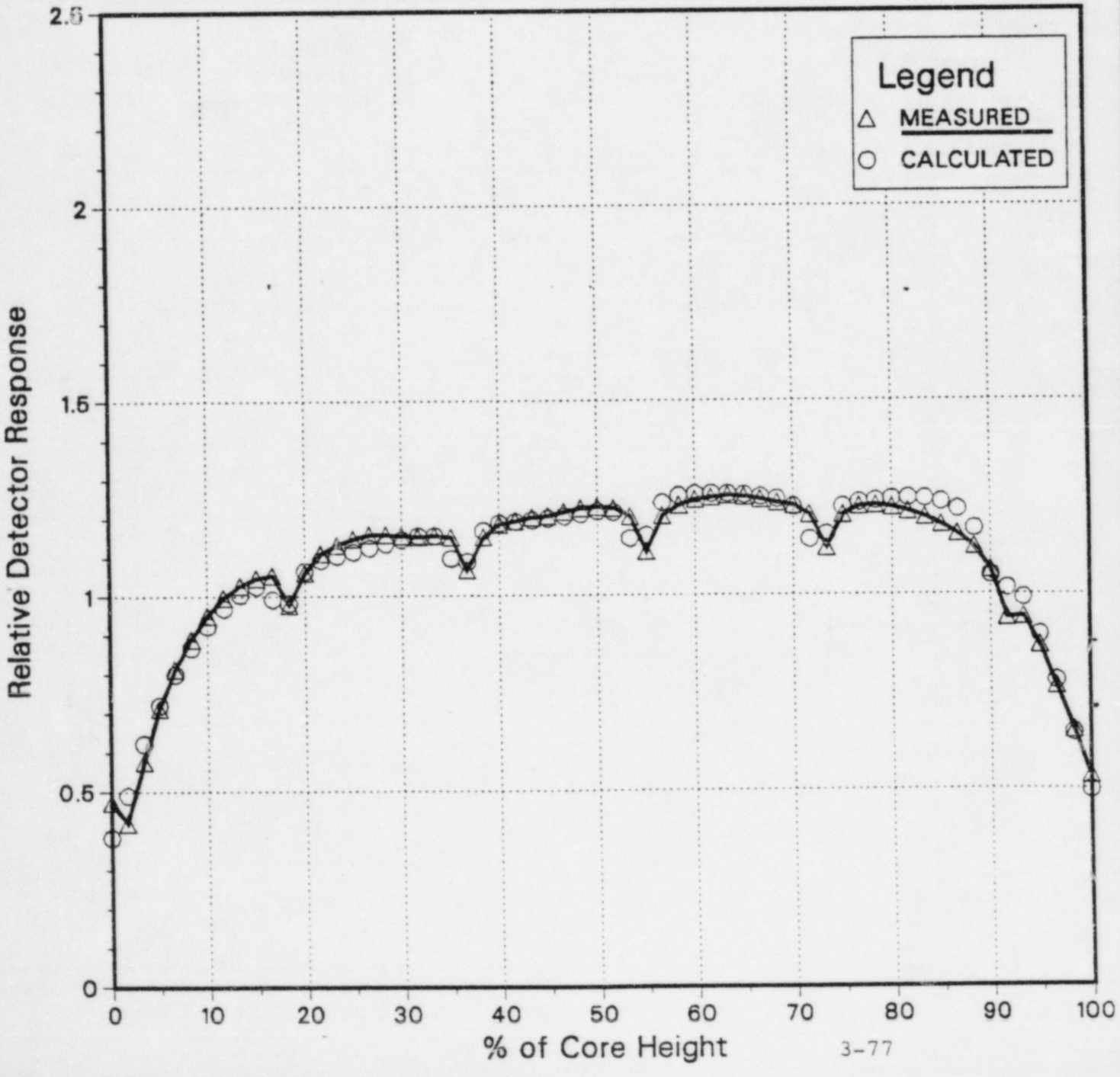


FIGURE 3.5.39

Measured and Calculated Detector Responses

PI 1 CYCLE 5 HFP, 0.831 GWD/MTU, ARO, EQ XENON

CASMO/PDQ/DP5 Model

THIMBLE C8

MAP 105-10

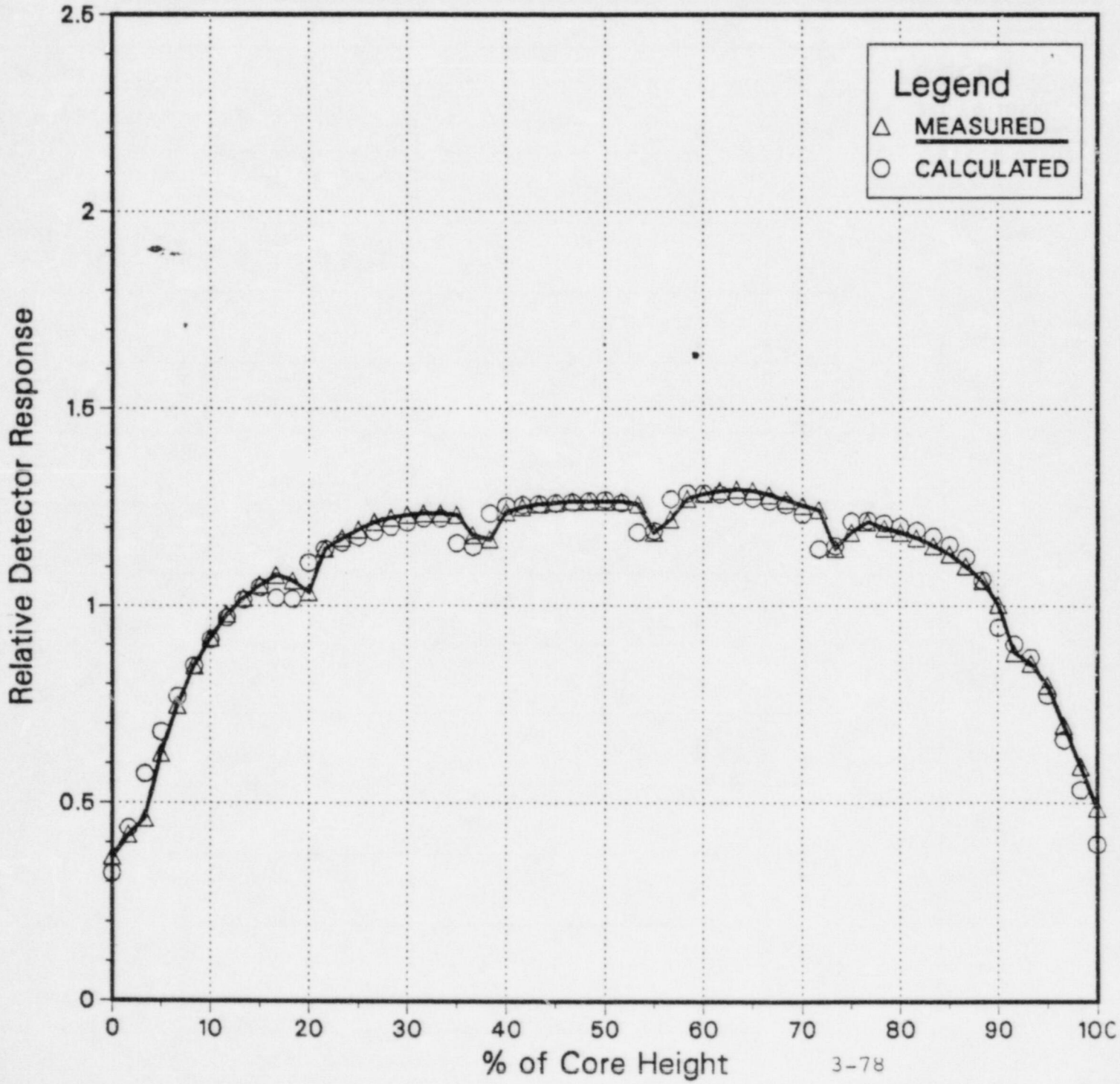


FIGURE 3.5.40

Measured and Calculated Integrated Detector Responses

PI 1 CYCLE 5 HFP, 5.919 GWD/MTU, ARO, EQ XENON

CASMO/PDQ/DP5 Model

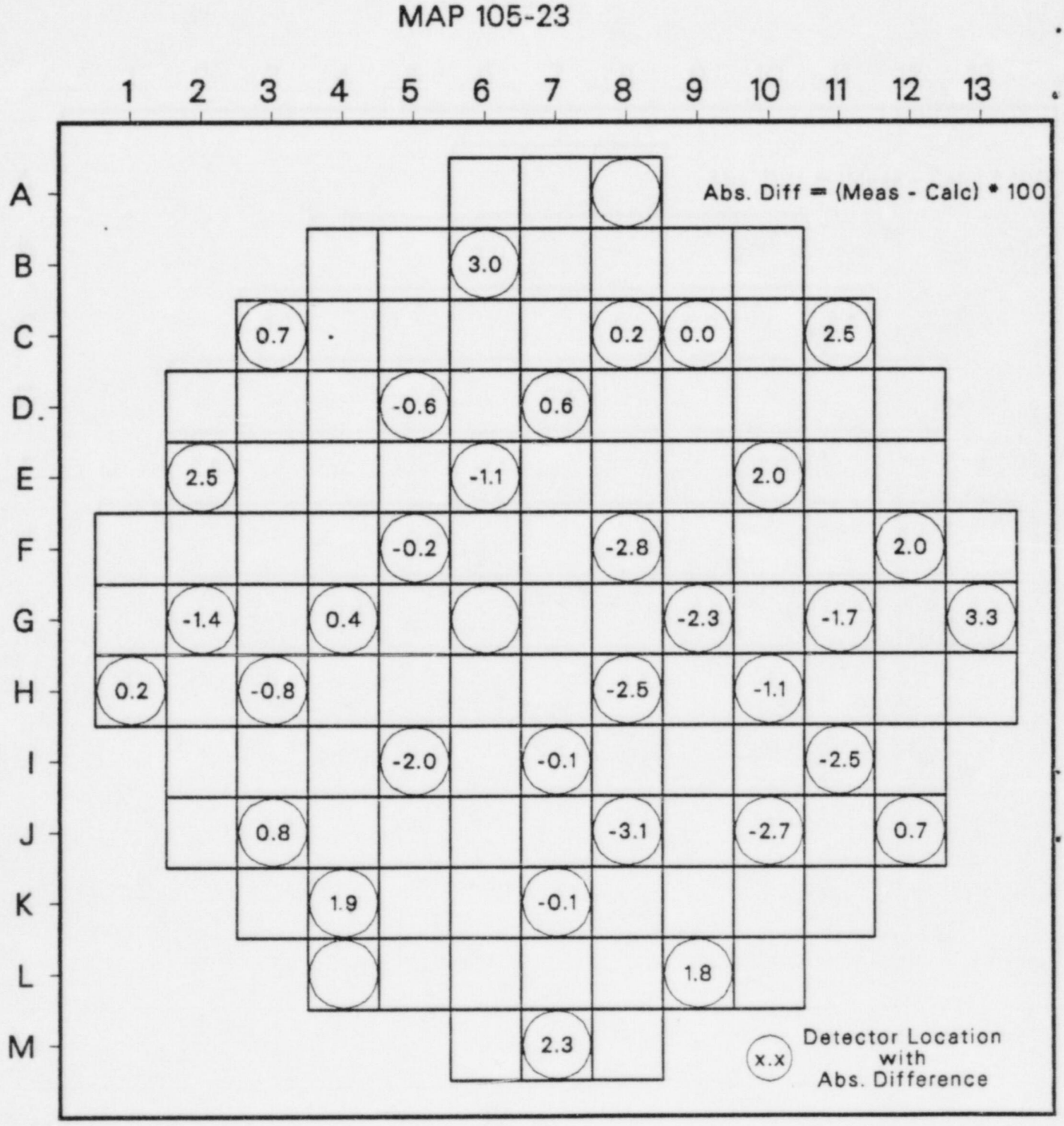


FIGURE 3.5.41

Measured and Calculated Detector Responses

PI 1 CYCLE 5 HFP, 5.919 GWD/MTU, ARO, EQ XENON

CASMO/PDQ/DP5 Model

THIMBLE H3

MAP 105-23

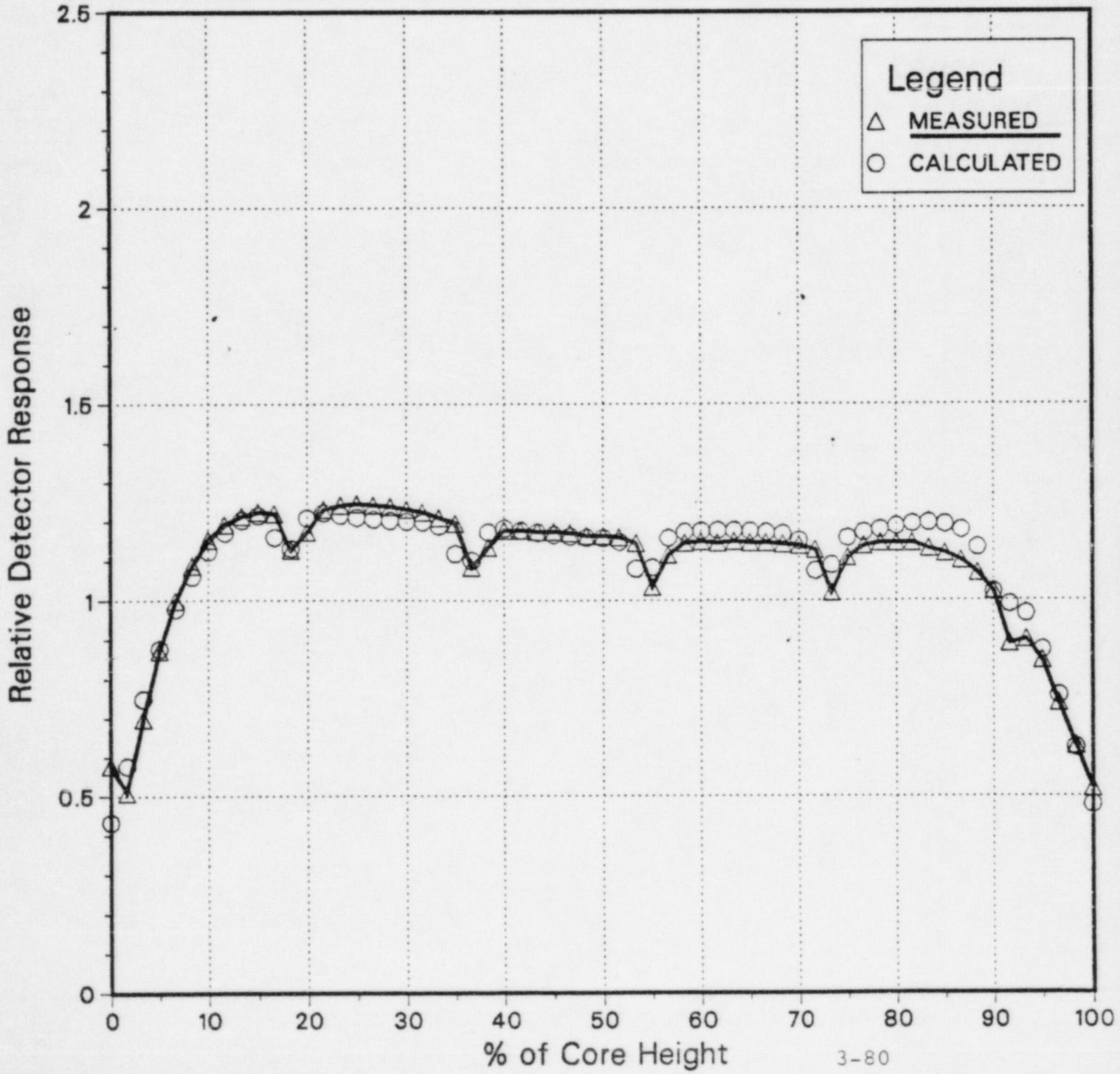


FIGURE 3.5.42

Measured and Calculated Detector Responses

PI 1 CYCLE 5 HFP, 5.919 GWD/MTU, ARO, EQ XENON

CASMO/PDQ/DP5 Model

THIMBLE D7

MAP 105-23

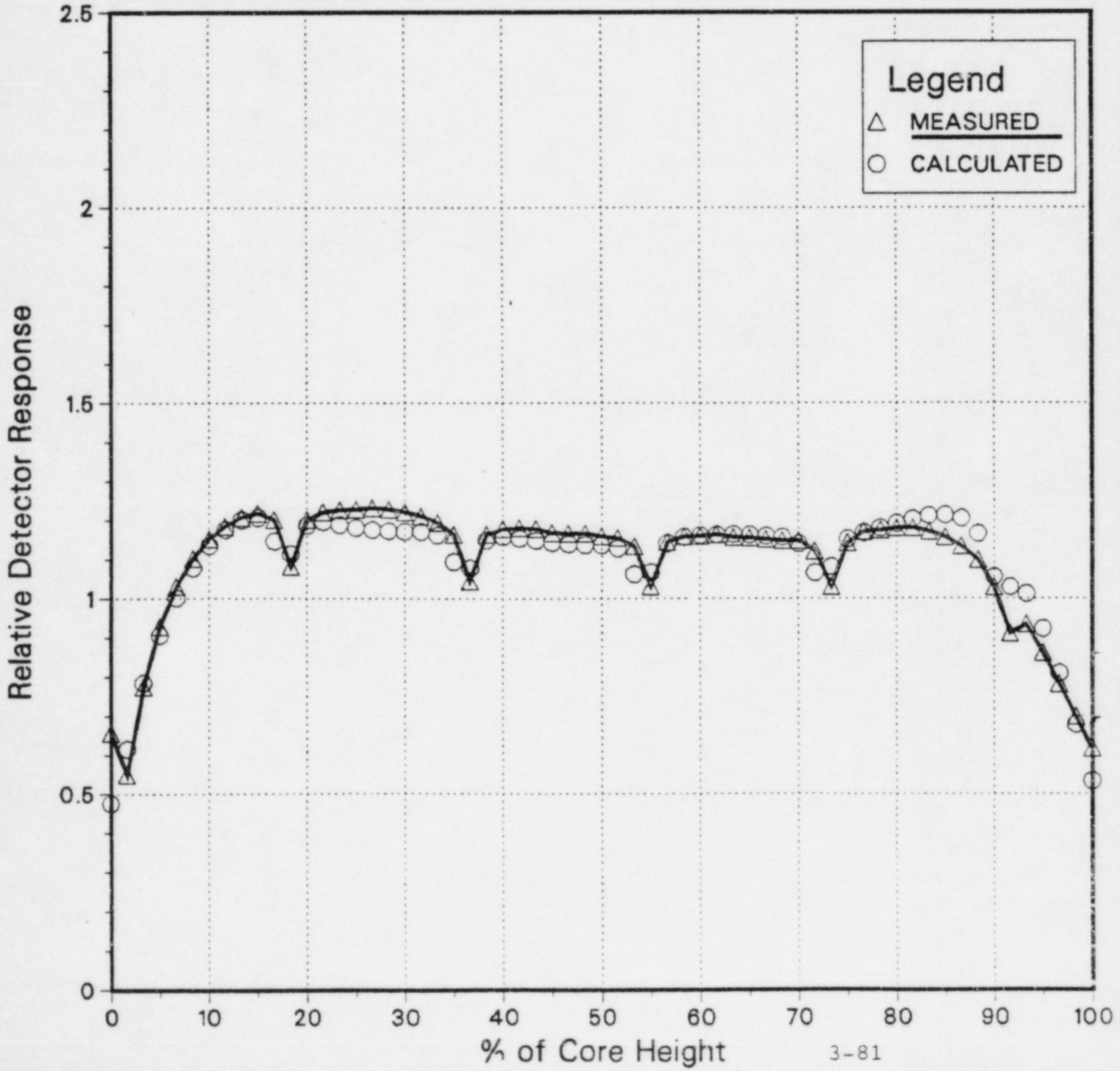


FIGURE 3.5.43

Measured and Calculated Integrated Detector Responses

PI 1 CYCLE 5 HFP, 11.653 GWD/MTU, ARO, EQ XENON

CASMO/PDQ/DP5 Model

MAP 105-34

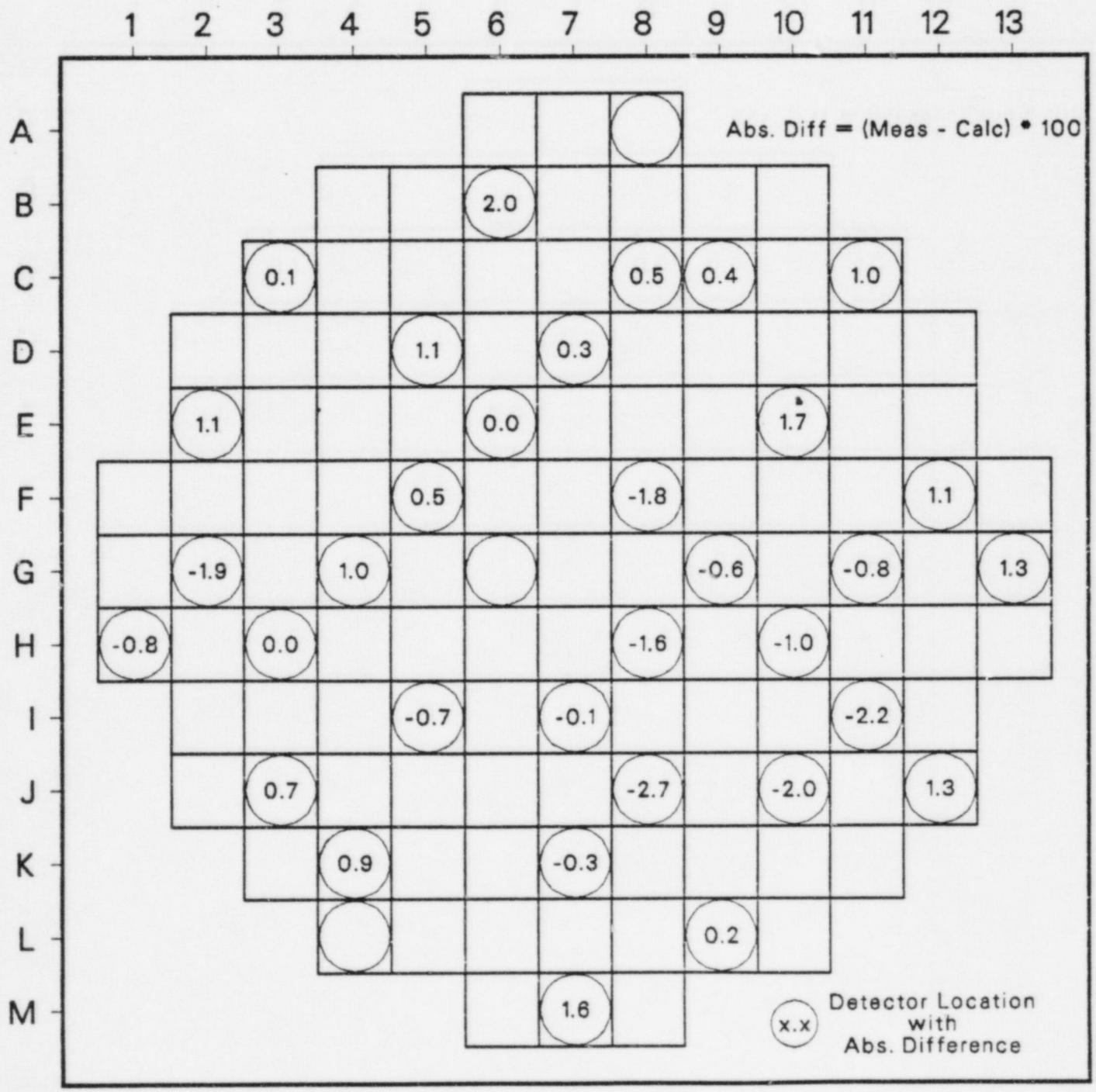


FIGURE 3.5.44

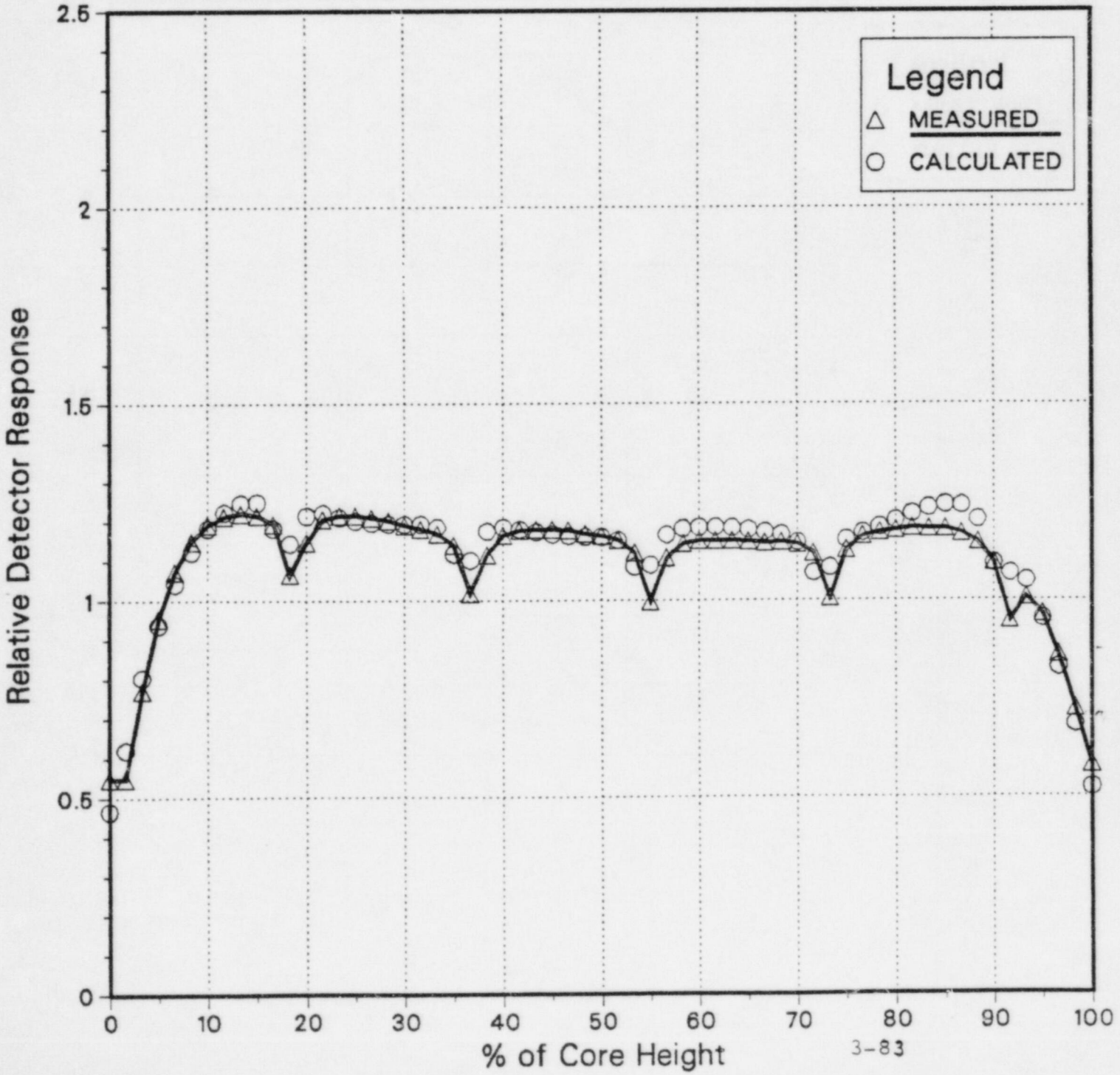
Measured and Calculated Detector Responses

PI 1 CYCLE 5 HFP, 11.653 GWD/MTU, ARO, EQ XENON

CASMO/PDQ/DP5 Model

THIMBLE D5

MAP 105-34



3-83

FIGURE 3.5.45

Measured and Calculated Detector Responses

PI 1 CYCLE 5 HFP, 11.653 GWD/MTU, ARO, EQ XENON

CASMO/PDQ/DP5 Model

THIMBLE H8

MAP 105-34

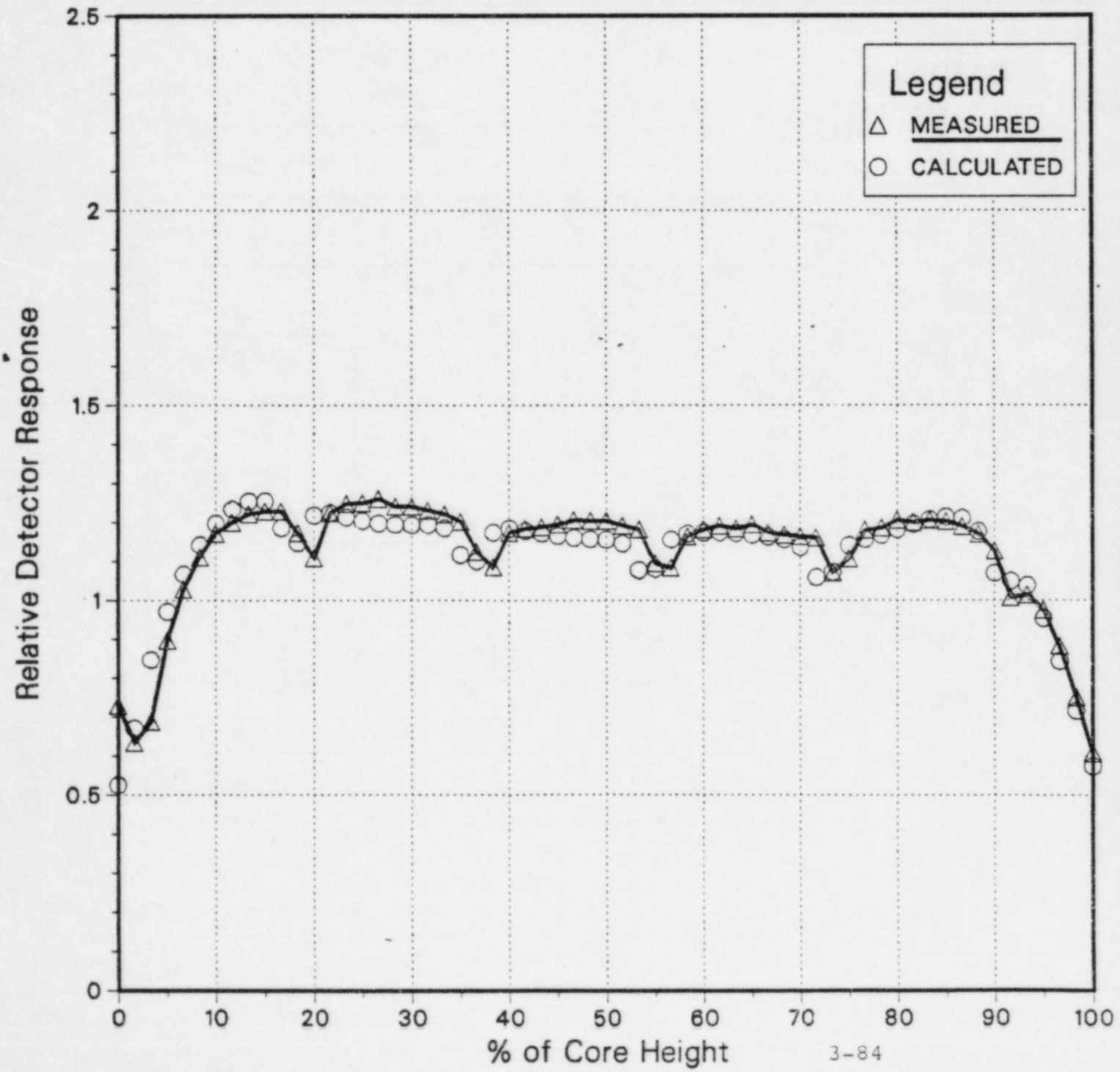


FIGURE 3.5.46

Measured and Calculated Integrated Detector Responses

PI 1 Cycle 6 HFP, 0.955 GWD/MTU, ARO, Eq Xenon

CASMO/PDQ/DP5 Model

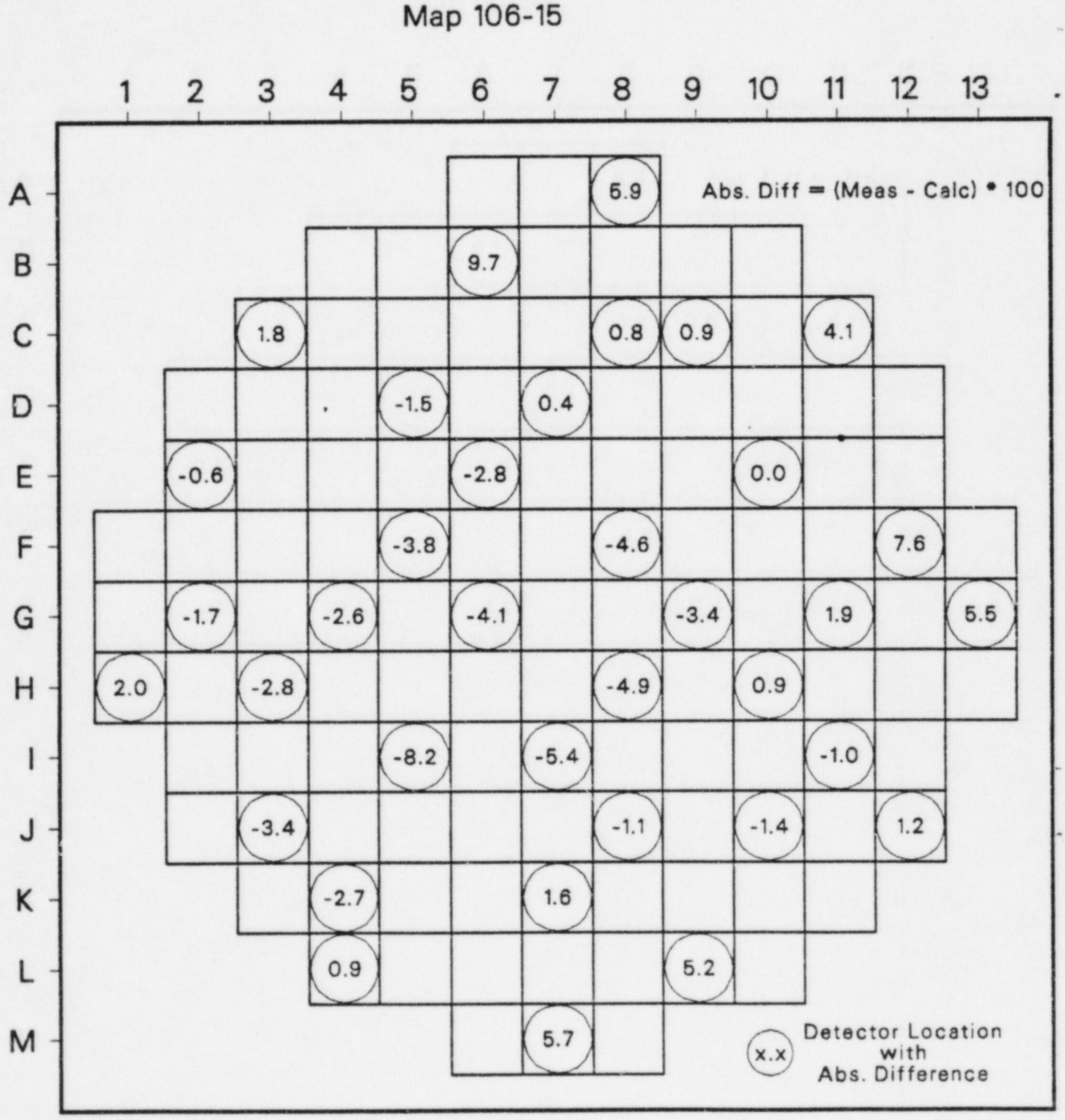


FIGURE 3.5.47

Measured and Calculated Detector Responses

PI 1 CYCLE 6 HFP, 0.955 GWD/MTU, ARO, EQ XENON

CASMO/PDQ/DP5 Model

THIMBLE G6

MAP 106-15

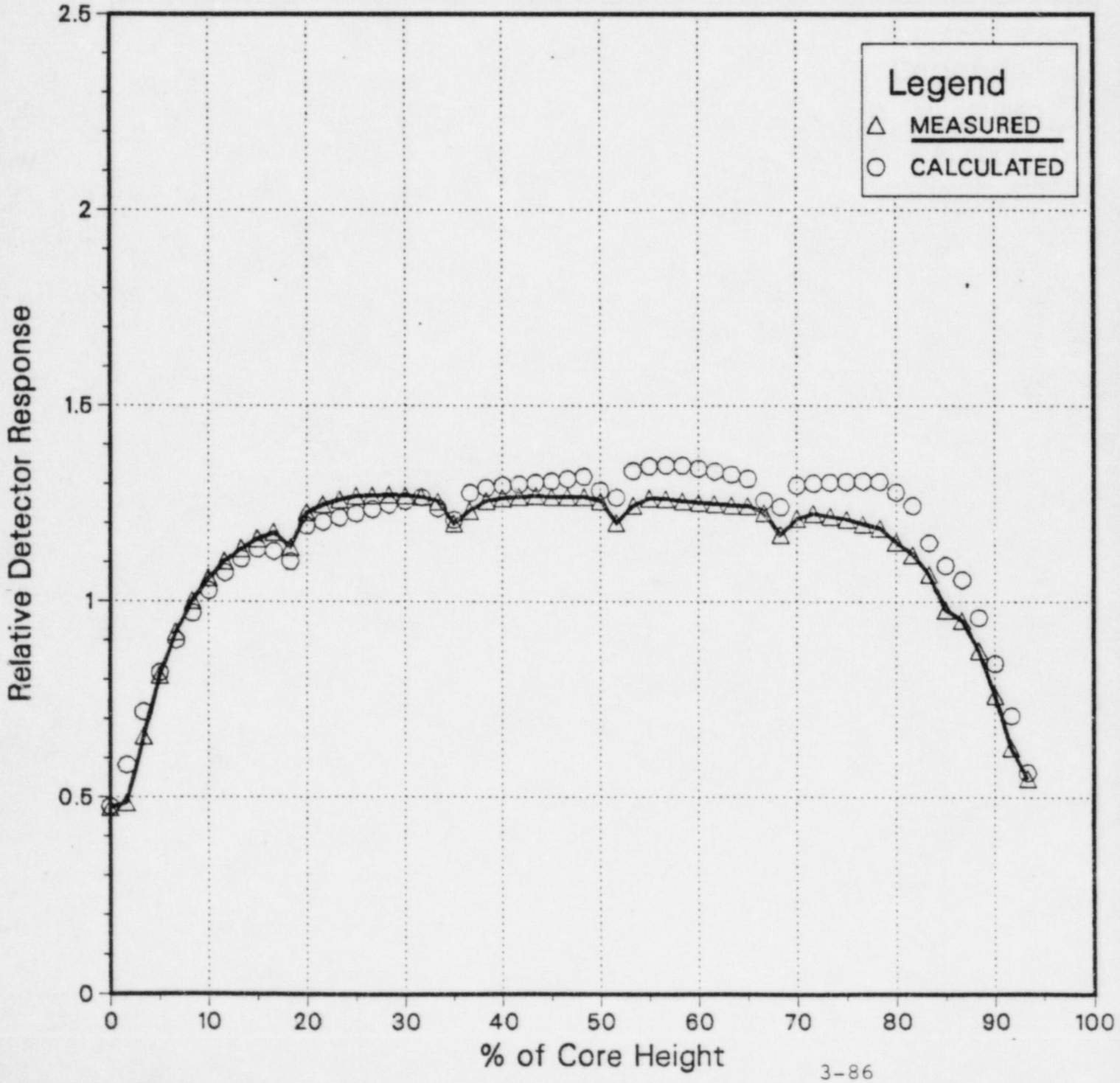


FIGURE 3.5.48

Measured and Calculated Detector Responses

PI 1 CYCLE 6 HFP, 0.955 GWD/MTU, ARO, EQ XENON

CASMO/PDQ/DP5 Model

THIMBLE J10

MAP 106-15

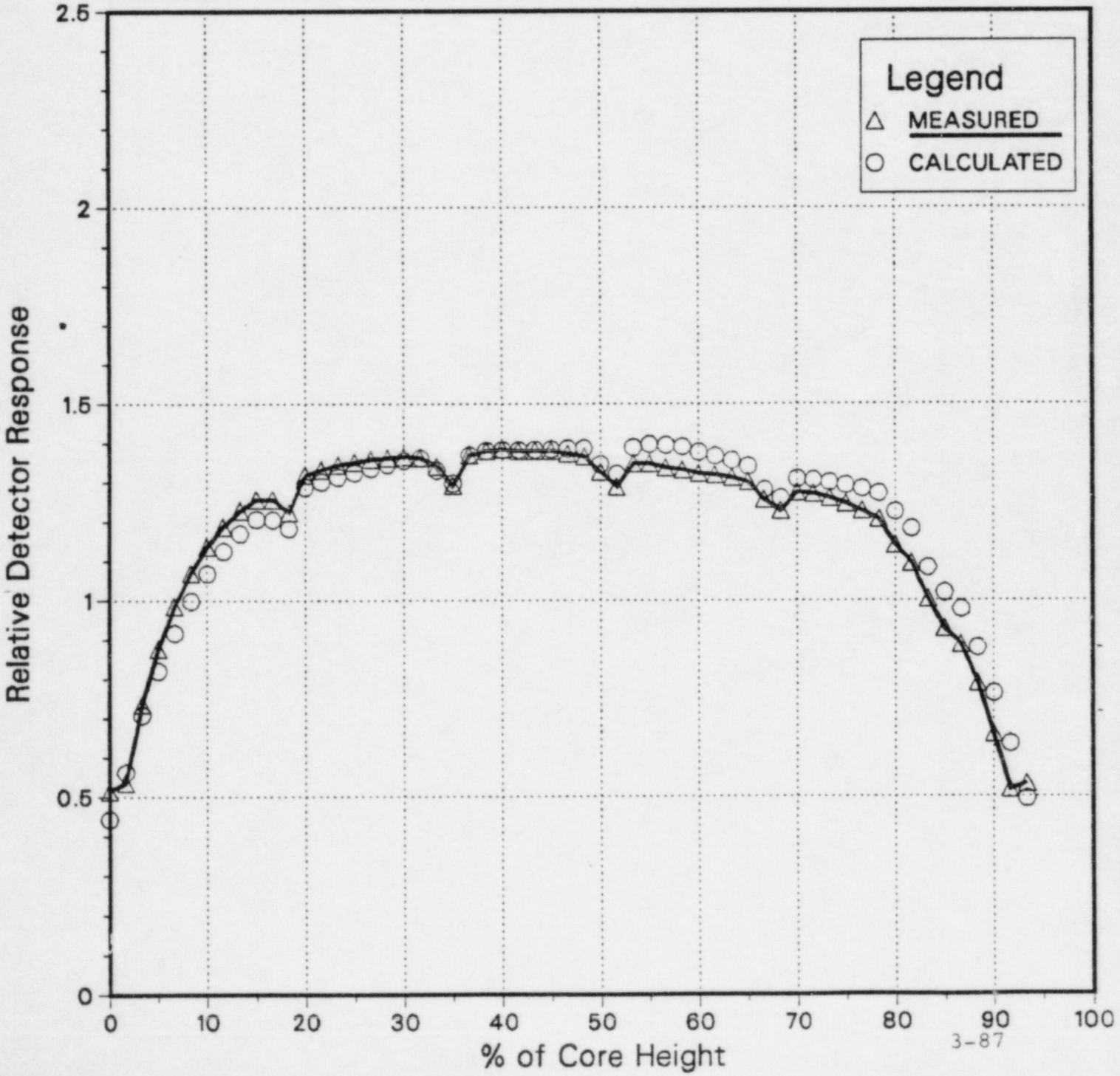


FIGURE 3.5.49

Measured and Calculated Integrated Detector Responses

PI 1 Cycle 6 HFP, 5.706 GWD/MTU, ARO, Eq Xenon

CASMO/PDQ/DP5 Model

Map 106-24

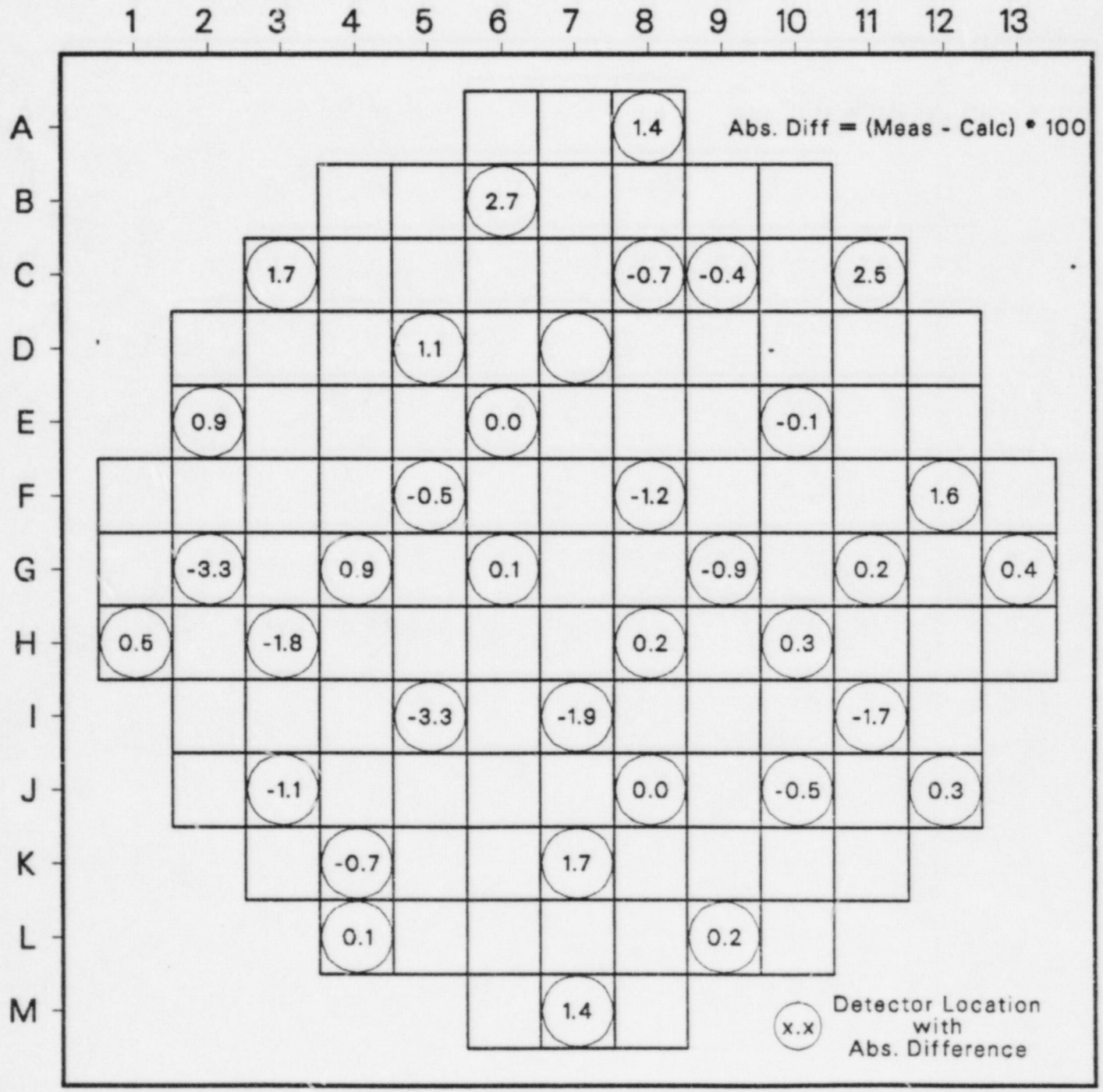


FIGURE 3.5.50

Measured and Calculated Detector Responses

PI 1 CYCLE 6 HFP, 5.706 GWD/MTU, ARO, EQ XENON

CASMO/PDQ/DP5 Model

THIMBLE G6

MAP 106-24

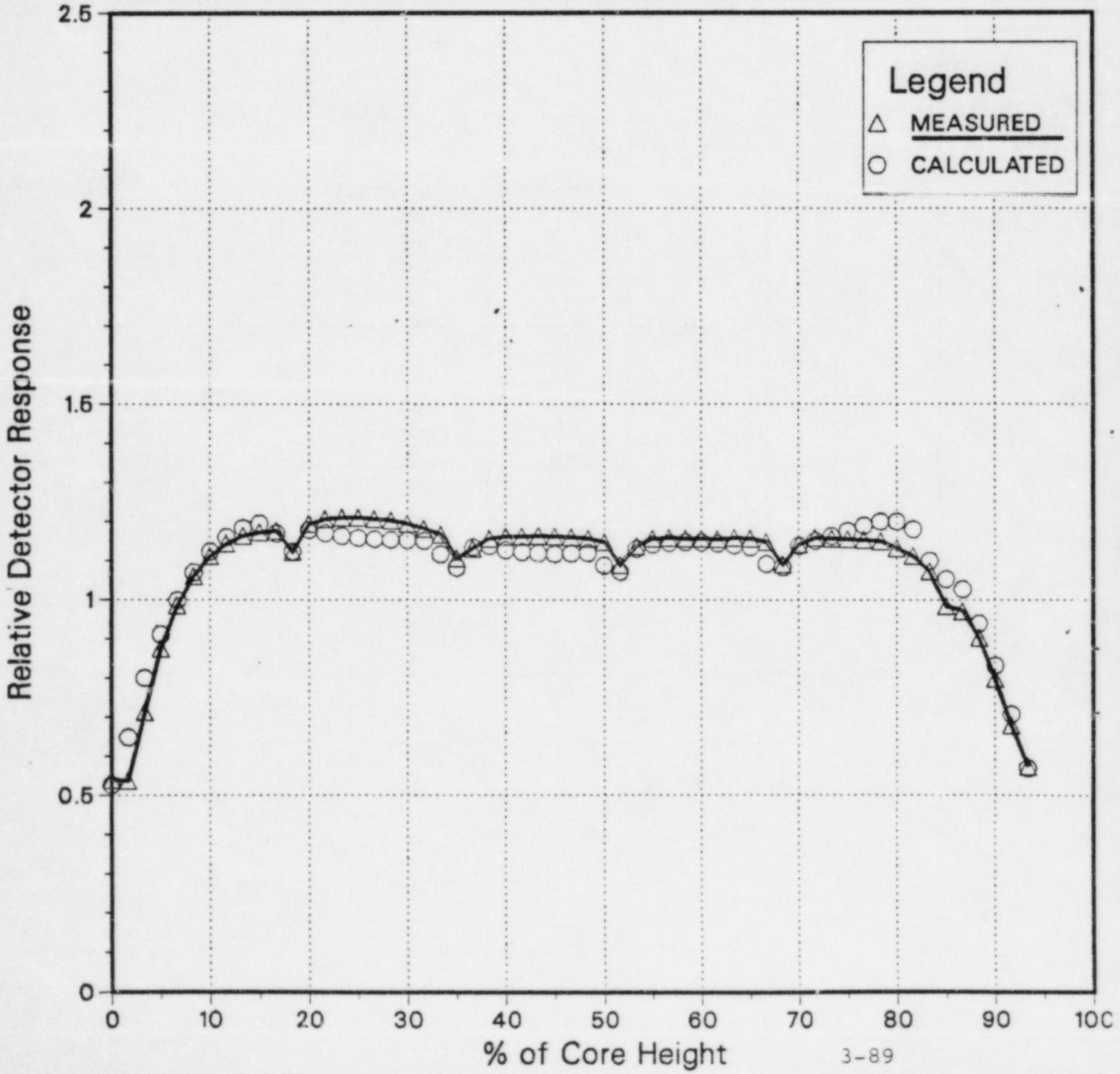


FIGURE 3.5.51

Measured and Calculated Detector Responses

PI 1 CYCLE 6 HFP, 5.706 GWD/MTU, ARO, EQ XENON

CASMO/PDQ/DP5 Model

THIMBLE G11

MAP 106-24

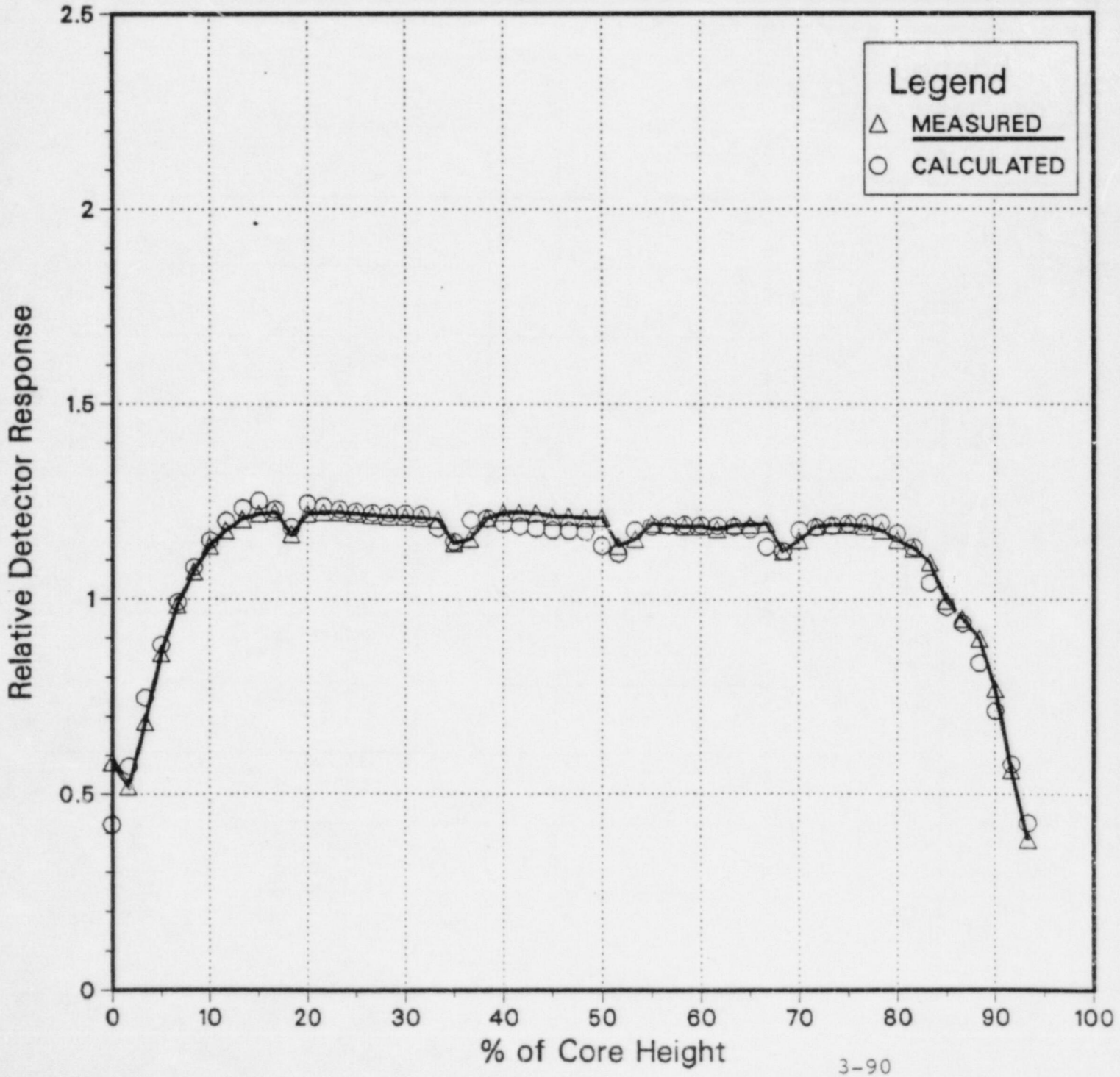


FIGURE 3.5.52

Measured and Calculated Integrated Detector Responses

PI 1 Cycle 6 HFP, 7.880 GWD/MTU, ARO, Eq Xenon

CASMO/PDQ/DP5 Model

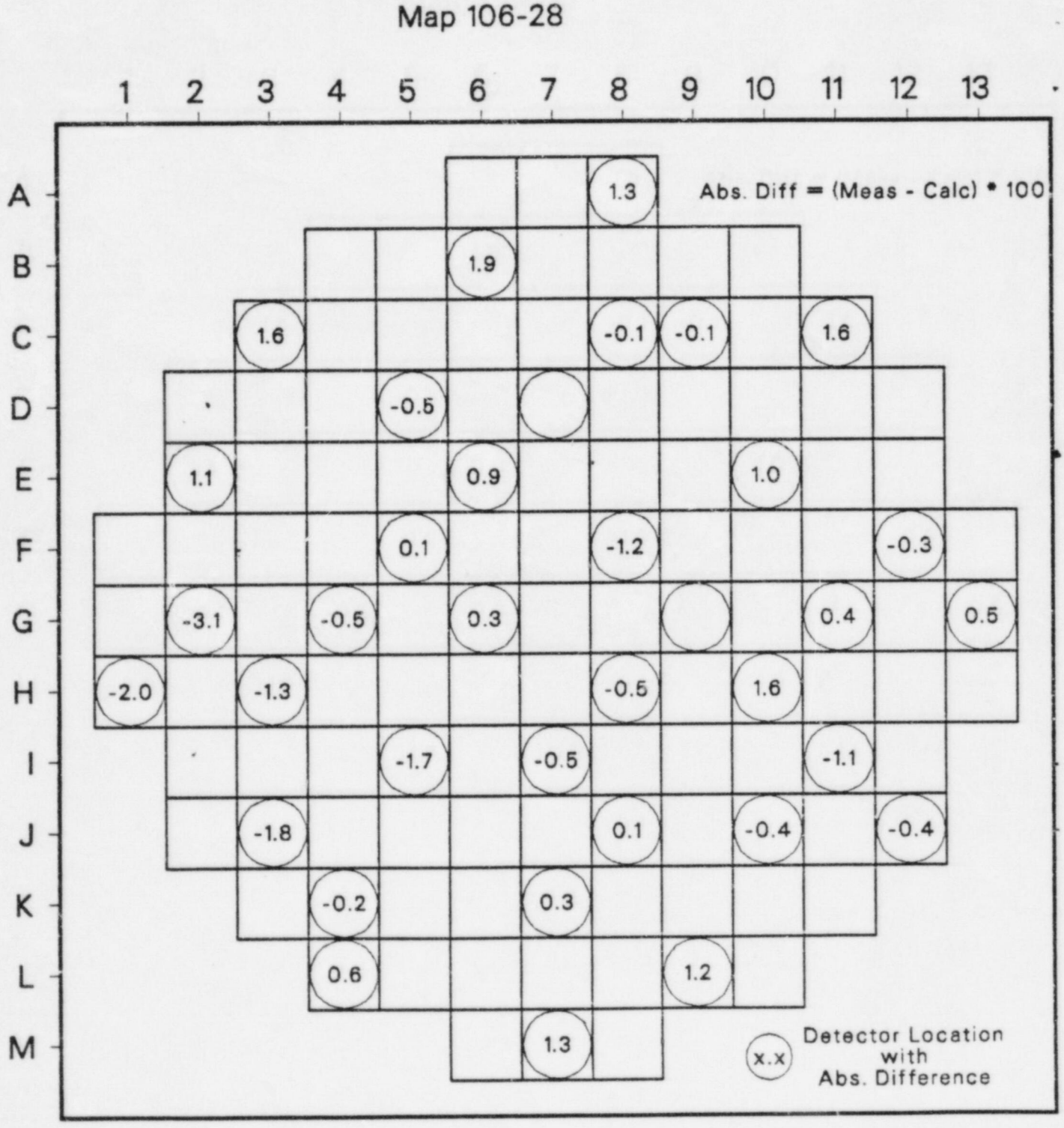


FIGURE 3.5.53

Measured and Calculated Detector Responses

PI 1 CYCLE 6 HFP, 7.880 GWD/MTU, ARO, EQ XENON

CASMO/PDQ/DP5 Model

THIMBLE G6

MAP 106-28

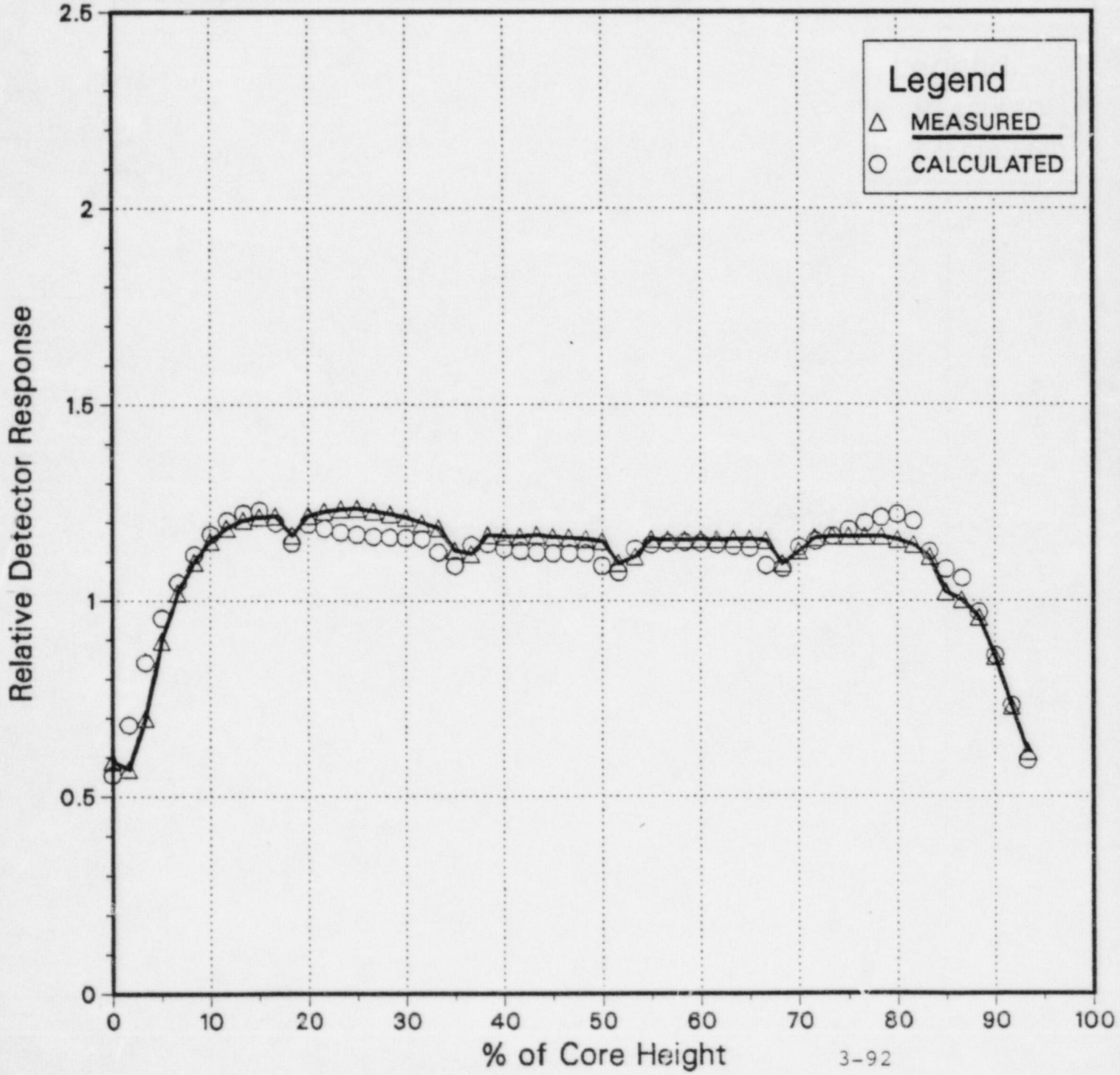


FIGURE 3.5.54

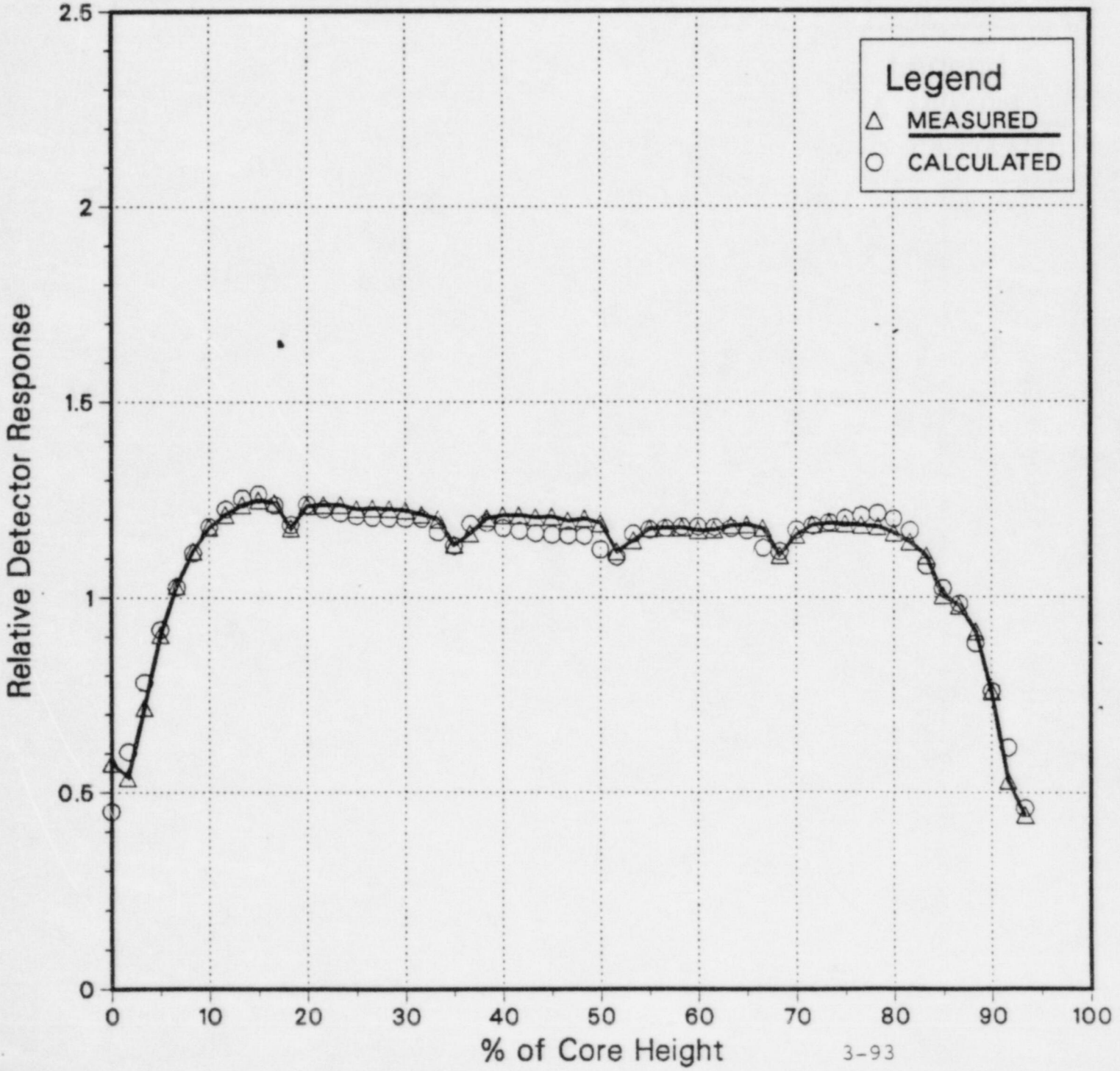
Measured and Calculated Detector Responses

PI 1 CYCLE 6 HFP, 7.880 GWD/MTU, ARO, EQ XENON

CASMO/PDQ/DP5 Model

THIMBLE K7

MAP 106-28



Observed Differences Density Function
ECELL/PDQ/DP5 Model Comparison

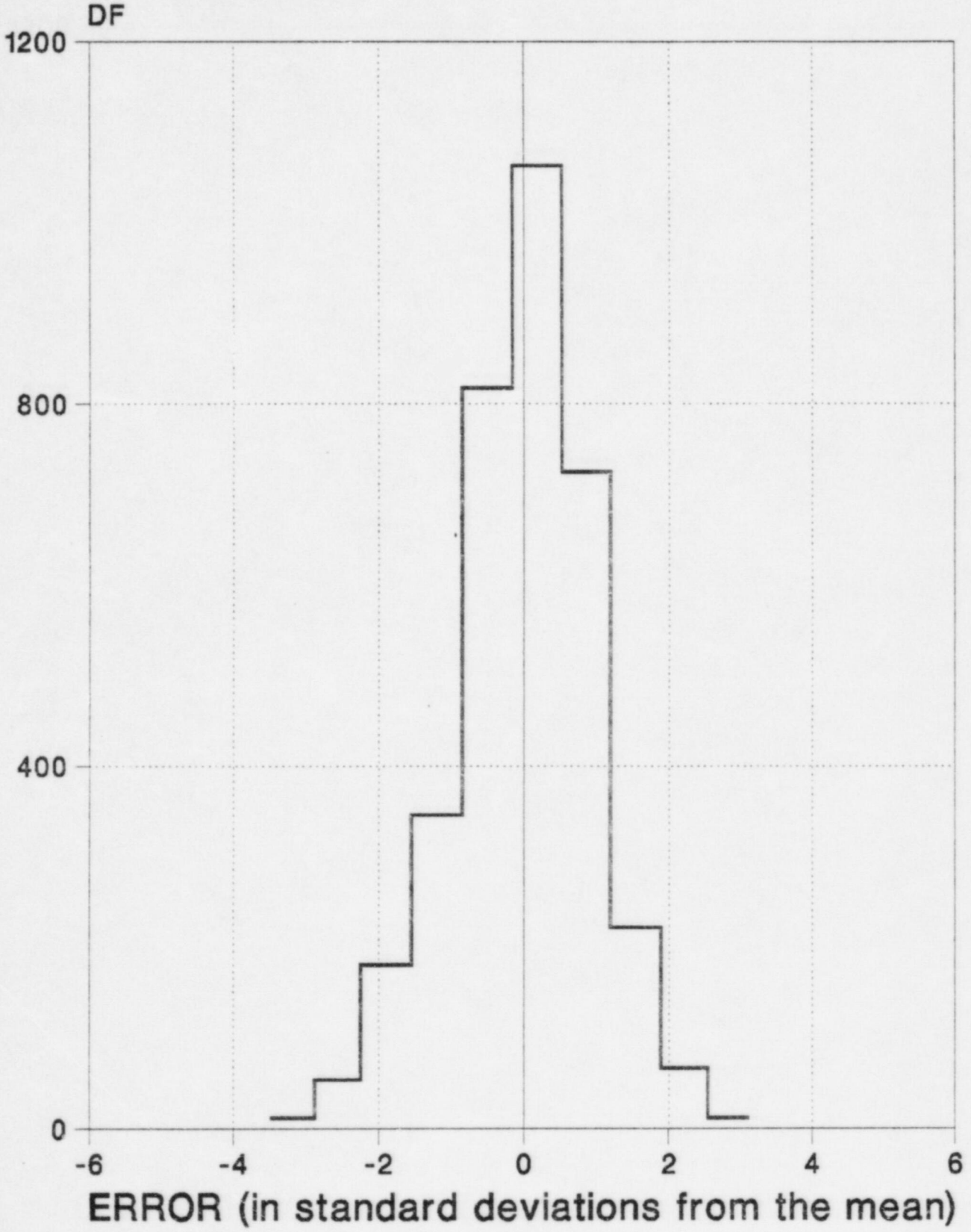


Figure 3.5.55

Cumulative Distribution Function
ECELL/PDQ/DP5 Model Comparison

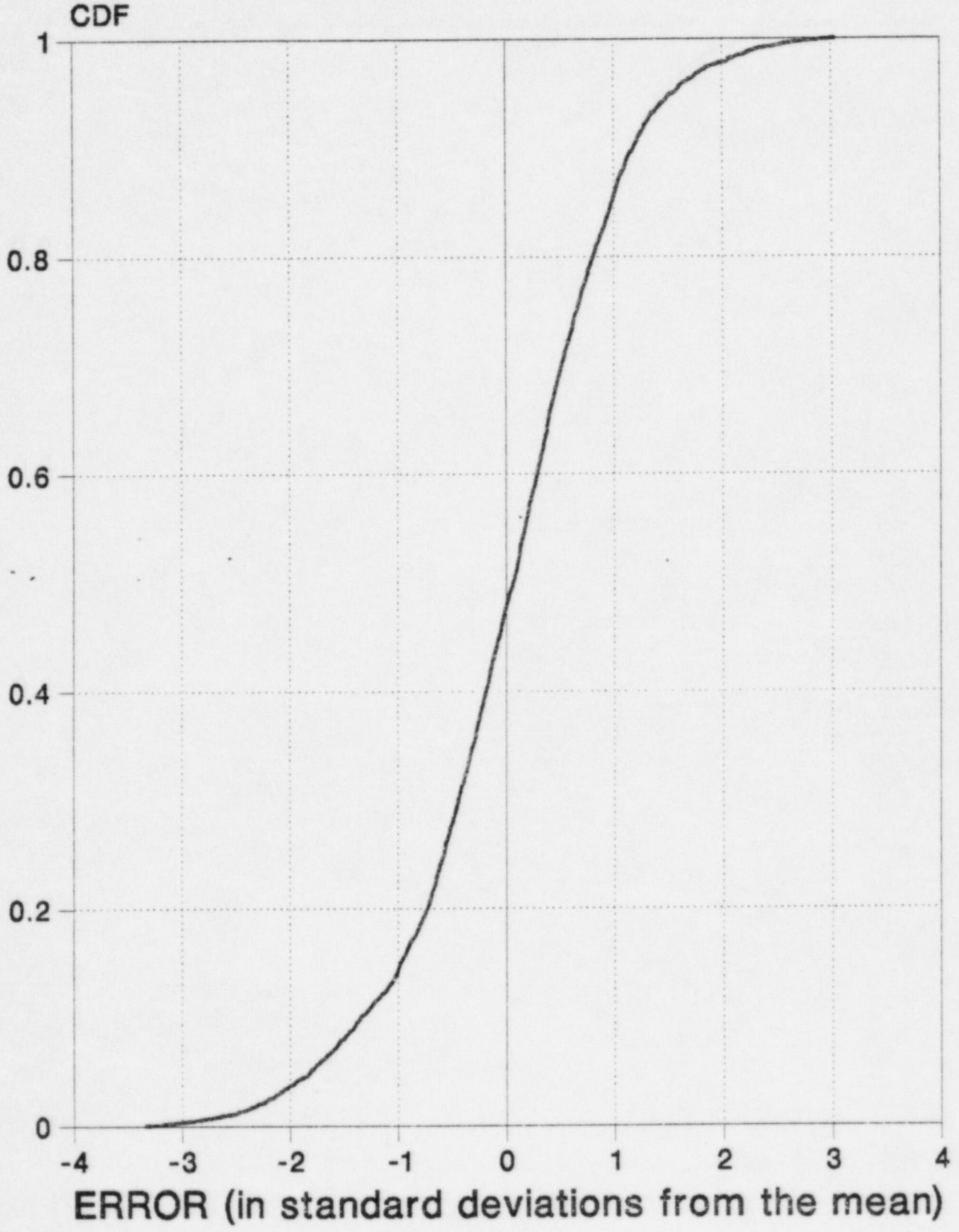


Figure 3.5.56

CDF in Region of 95th Percentile
ECELL/PDQ/DP5 Model Comparison

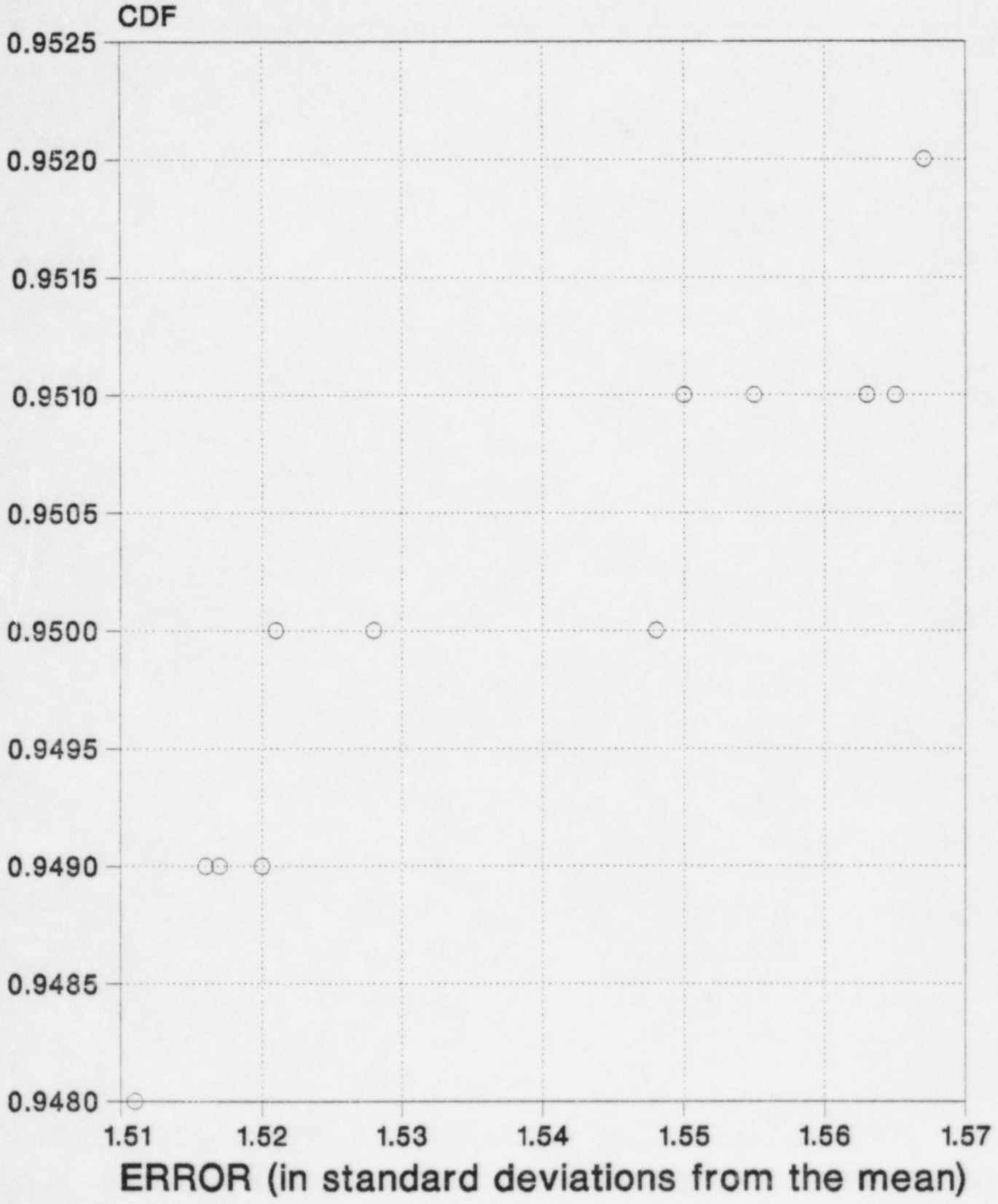


Figure 3.5.57

Observed Differences Density Function
CASMO/PDQ/DP5 Model Comparison

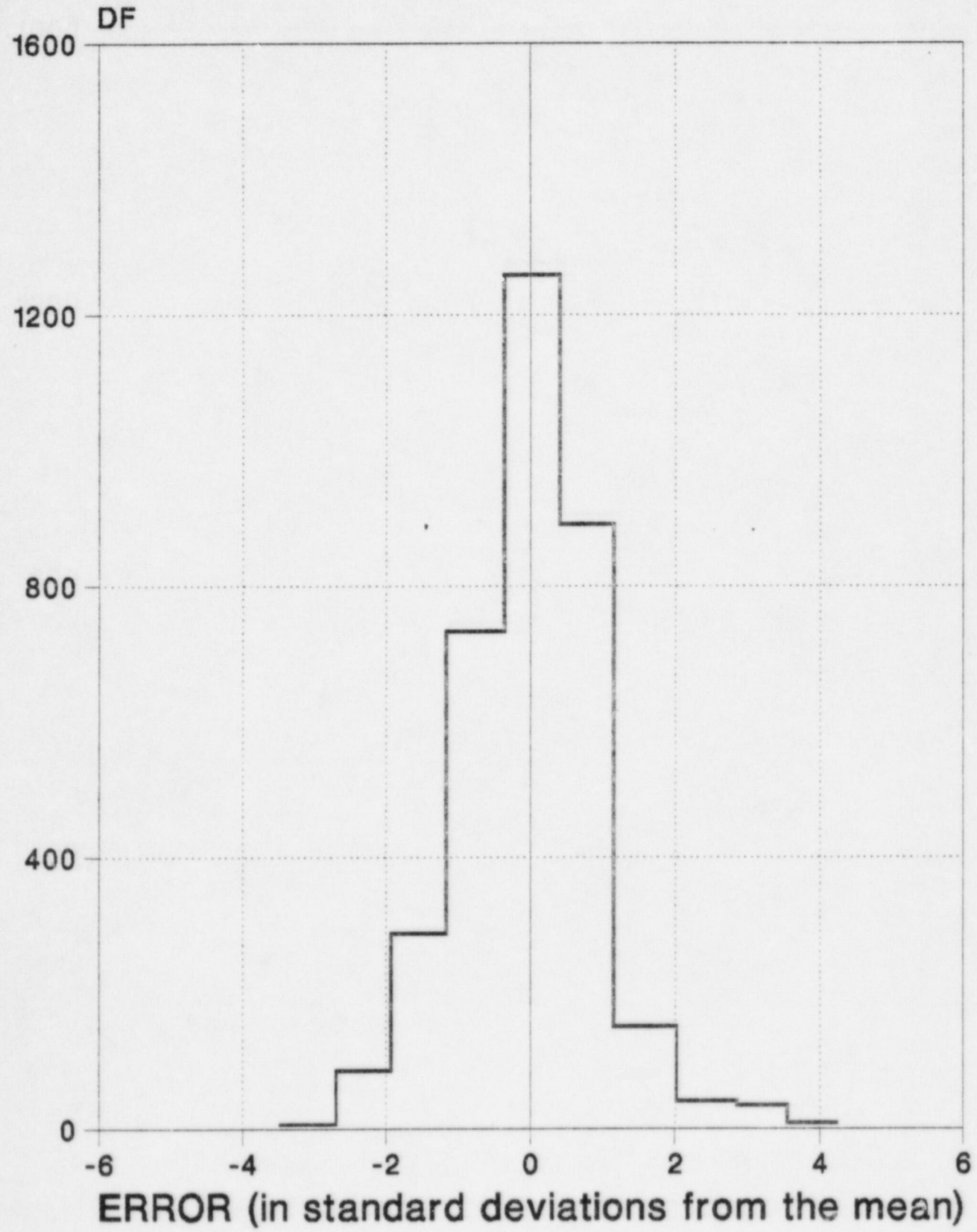


Figure 3.5.58

FIGURE 3.5.61

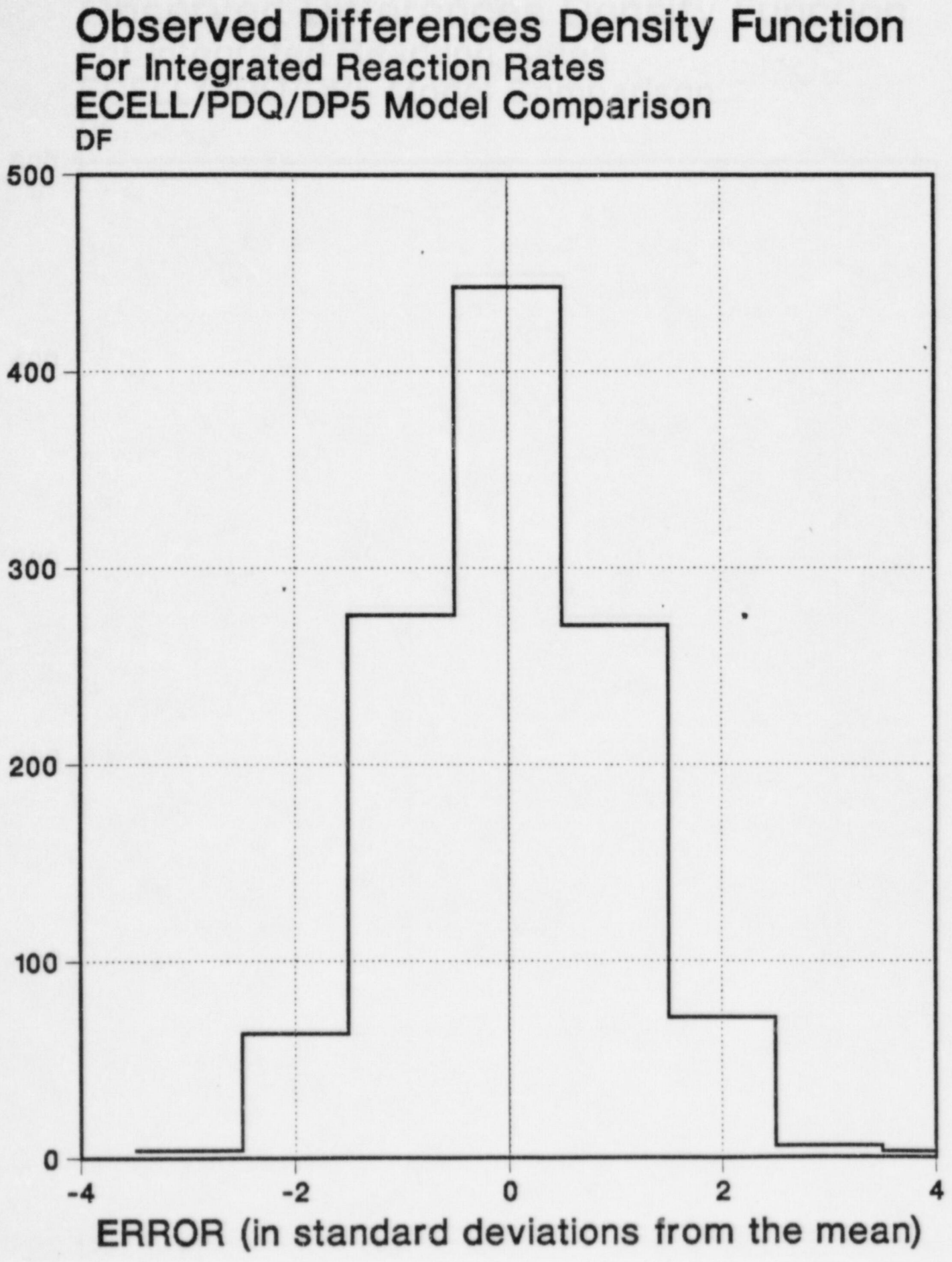

Observed Differences Density Function
For Integrated Reaction Rates
ECELL/PDQ/DP5 Model Comparison
DF
500
400
300
200
100
0
-4
-2
0
2
4
ERROR (in standard deviations from the mean)

FIGURE 3.5.62

CDF for Integrated Reaction Rates
ECELL/PDQ/DP5 Model Comparison

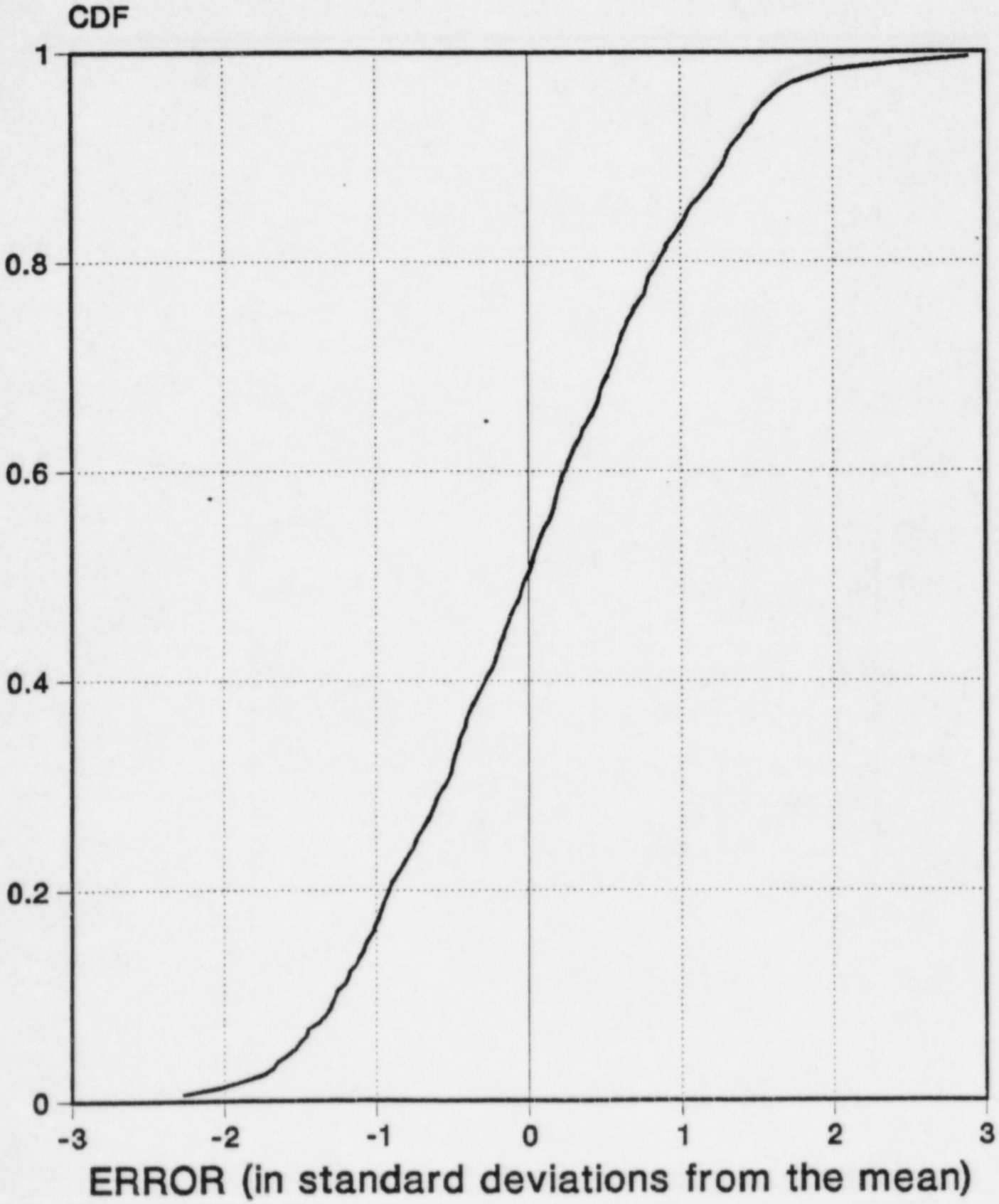


FIGURE 3.5.63

CDF in the Region of 95th Percentile
For Integrated Reaction Rates
ECELL/PDQ/DP5 Model Comparison

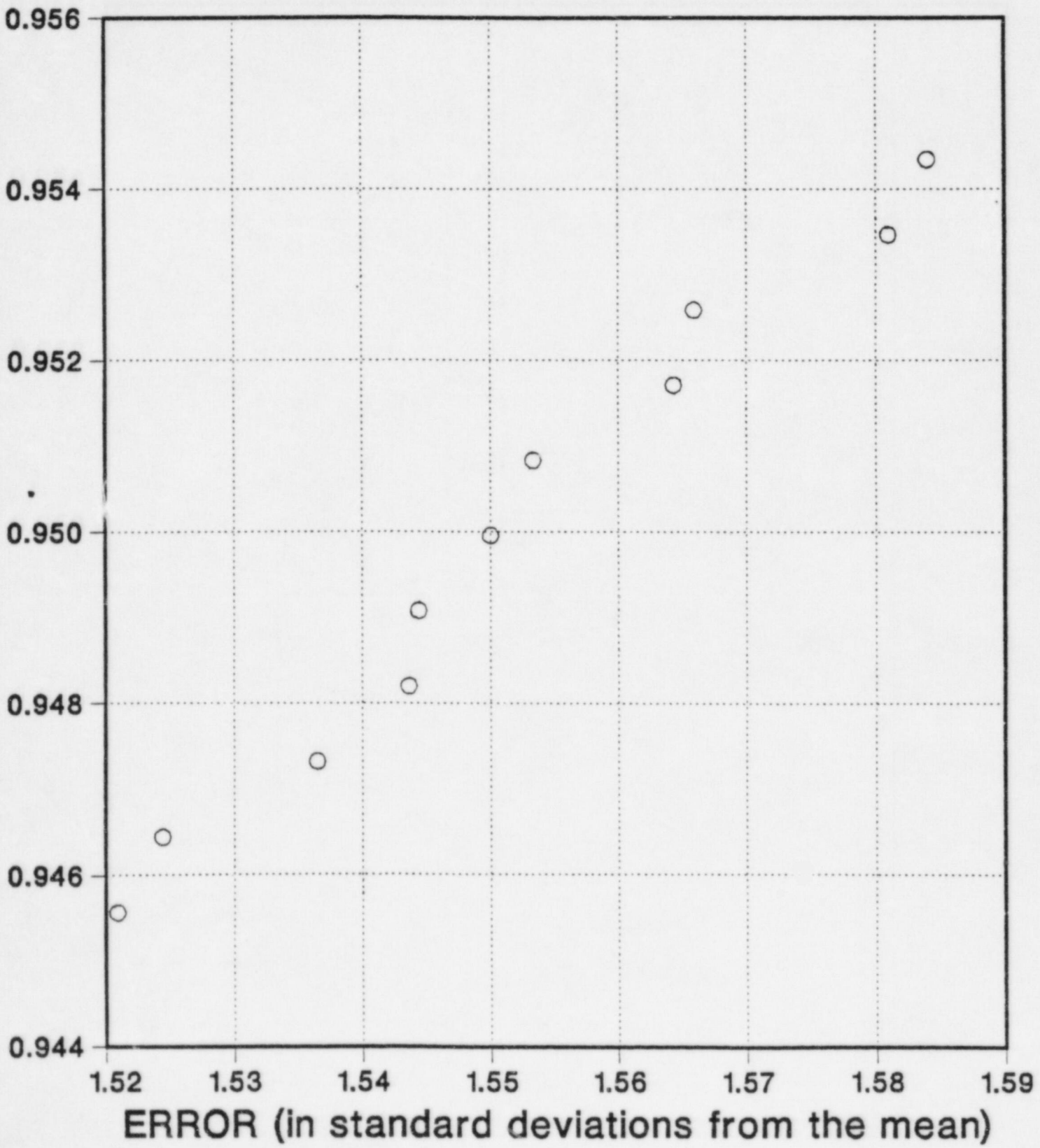


FIGURE 3.5.64

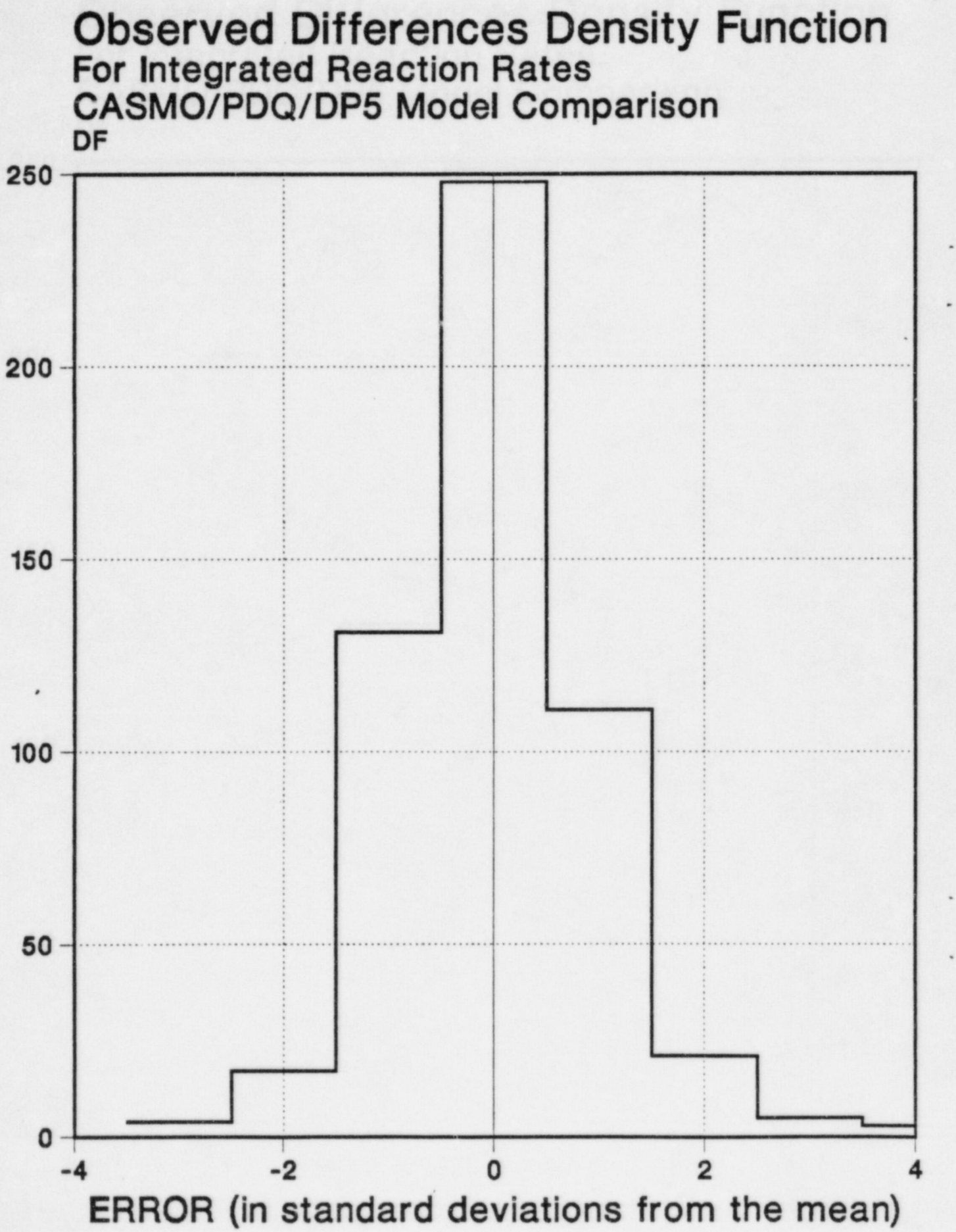

Observed Differences Density Function
For Integrated Reaction Rates
CASMO/PDQ/DP5 Model Comparison
DF
250
200
150
100
50
0
-4
-2
0
2
4
ERROR (in standard deviations from the mean)

FIGURE 3.5.65

CDF for Integrated Reaction Rates
CASMO/PDQ/DP5 Model Comparison

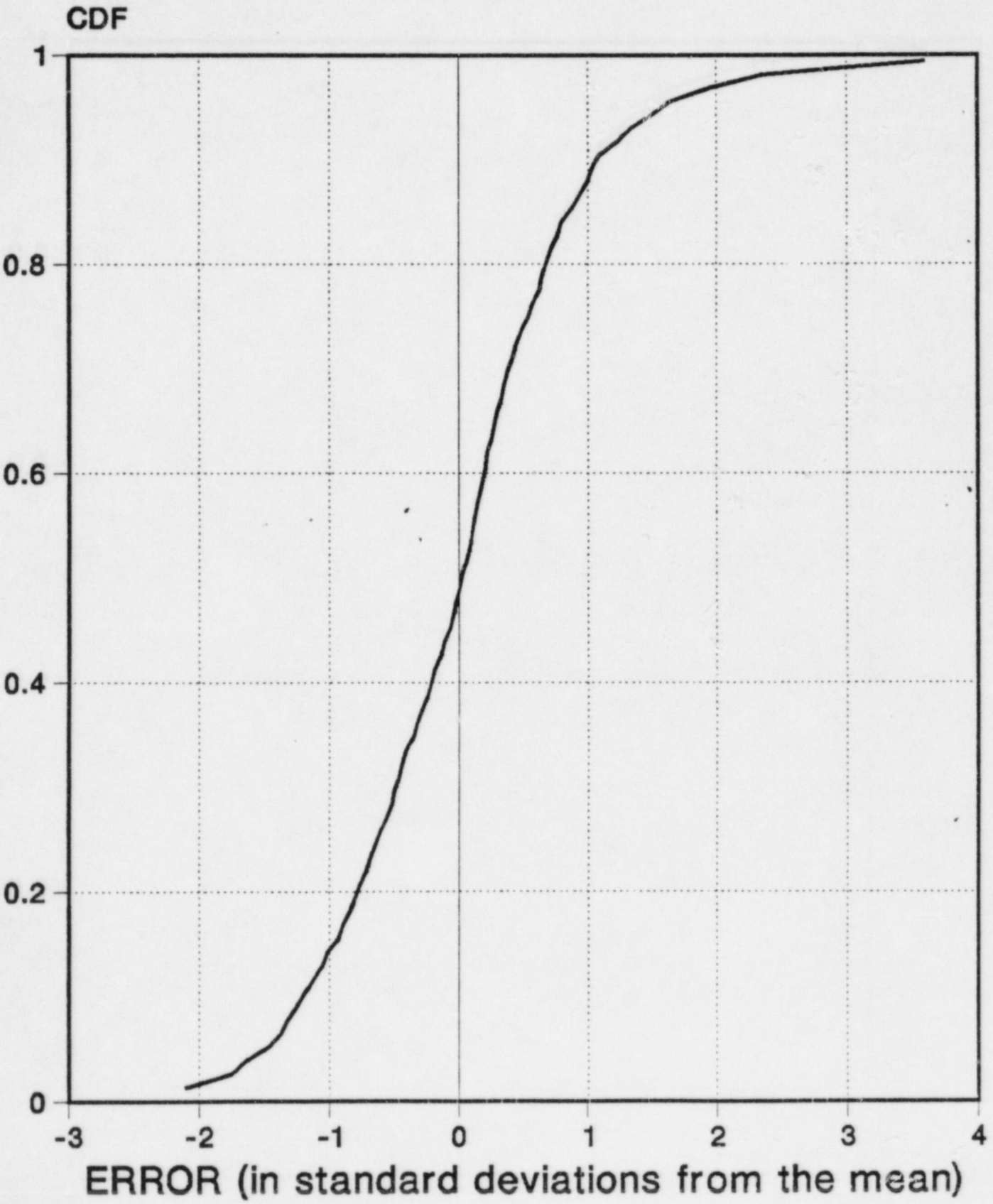
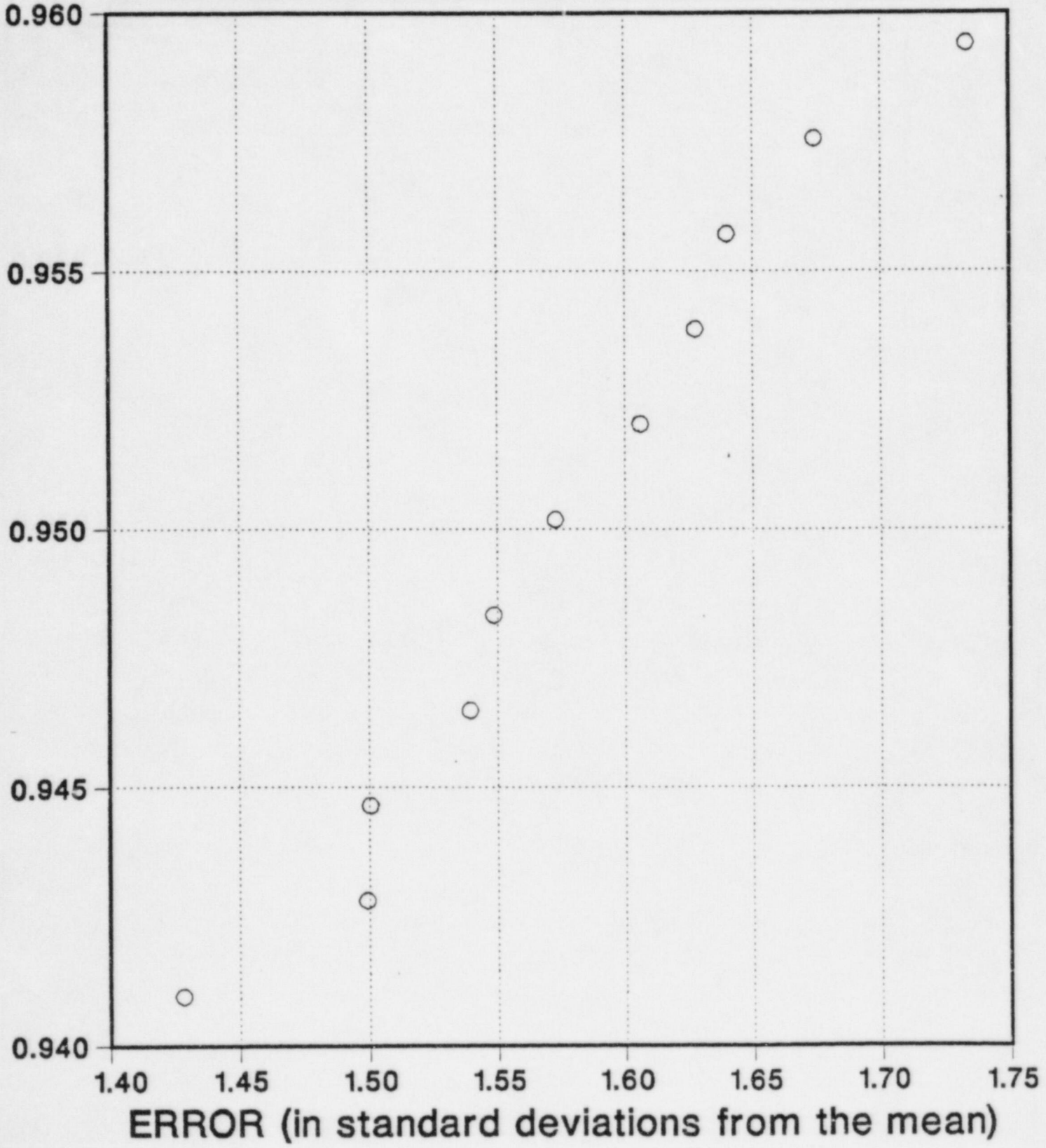


FIGURE 3.5.66

CDF in the Region of 95th Percentile
For Integrated Reaction Rates
CASMO/PDQ/DP5 Model Comparison



RELIABILITY FACTOR VERSUS MEASURED REACTION RATE ECELL/PDQ/DP5

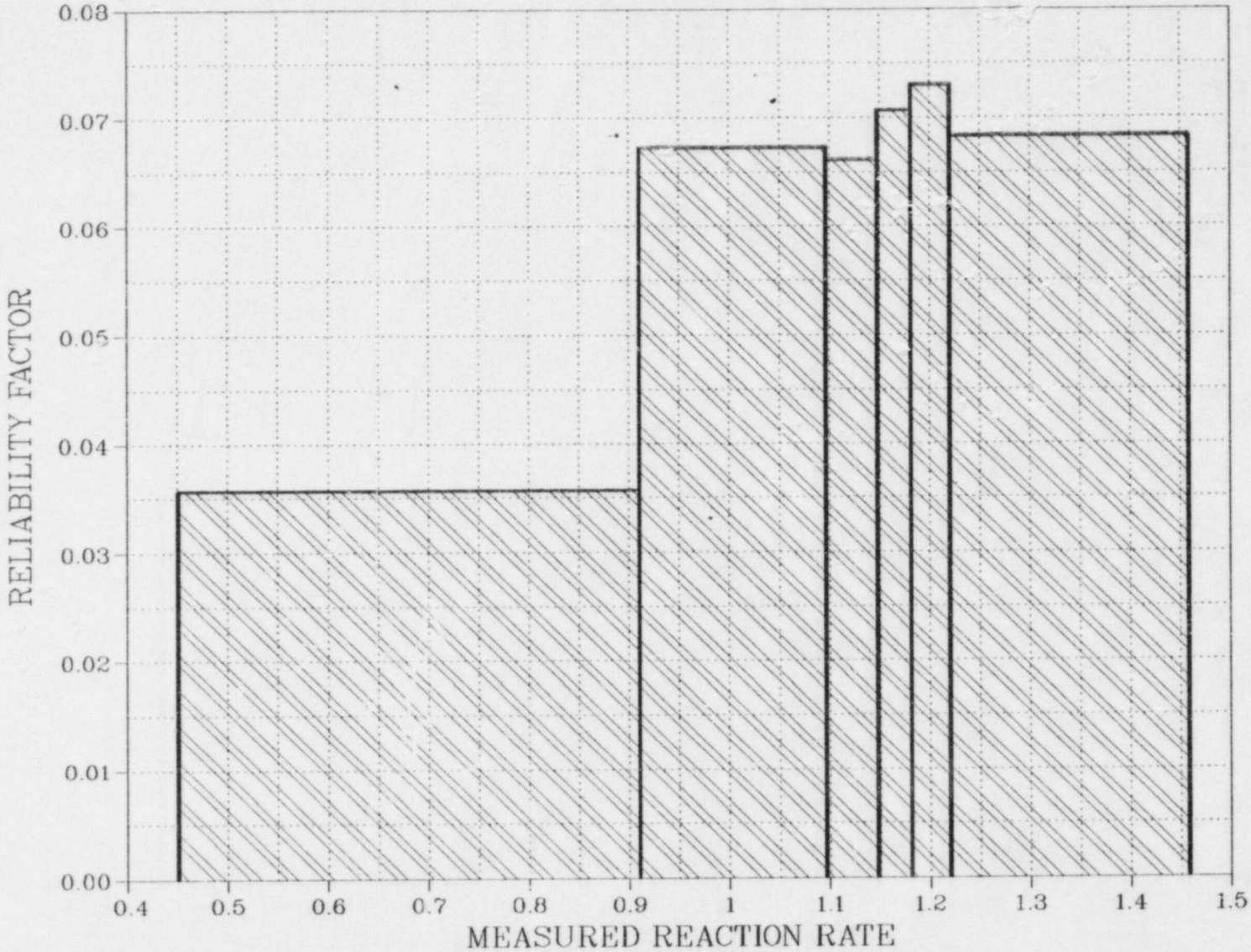


FIGURE 3-5-67
NSP-NUCLEAR ANALYSIS DEPARTMENT

3.6 Model Application to Plant Transient Tests

This section describes the application of the ECELL/PDQ/DP5 model to Prairie Island Unit 1 plant transient tests performed during cycles 1 and 2. The tests performed were the pseudo ejected rod, rod drop, and two xenon transients. Note that the model is being applied in a best estimate mode.

Table 3.6.1 gives the results of the pseudo ejected rod and rod drop tests.

The worth of the ejected rod K-7 was measured by increasing the boron concentration of the reactor coolant system and compensating for the reactivity decrease by withdrawing control rod K-7 while maintaining Tavg constant. The reactivity changes due to motion of K-7 was measured by the reactivity computer whose output was evaluated twice, yielding ejected rod worths of 57.2 pcm and 57.7 pcm or an average of 57.5 pcm.

The rod drop was performed as follows:

At 50% power, a base case flux map was taken with control bank D at 201 steps and all other rods withdrawn. A static drop of RCCA K-7 was performed by dilution and compensating for the dilution by insertion of RCCA K-7. During the insertion of RCCA K-7, at 25 step intervals, a partial flux map, a Thermocouple map and excore detector current readings were taken to demonstrate the ability of the incore and excore instrumentation systems to detect a RCCA below bank position. A flux map was taken with RCCA K-7 at zero steps in the dropped Rod configuration. RCCA K-7 was then borated back to its bank position. After the core power distribution and the reactor systems returned to equilibrium conditions, the entire procedure described above was repeated using RCCA H-8.

Figures 3.6.1 and 3.6.2 give the results of the measured to calculated comparisons for the two xenon transient tests.

The Cycle 1 test procedure was to establish steady-state, equilibrium Xenon conditions with nearly all rods out (ARO). Then the reactor was maintained in the ARO condition and shutdown as quickly as possible by increasing the boron concentration. As soon as the reactor power level reached the zero power physics testing range (about 50 minutes after the shutdown started), the reactor was maintained with the neutron flux at a nearly constant level for the next 30 hours, at all times in the nearly ARO condition. Criticality was maintained by varying the boron concentration. Bank D was the only control bank that was moved and at all times it was 180 or more steps out of the core out of its total travel of 228 steps.

A similar procedure was followed for the Cycle 2 tests. The results given in Figures 3.6.1 and 3.6.2 show only the zero power transient period.

TABLE 3.6.1

COMPARISON OF FSAR, MEASURED, AND CALCULATED

PARAMETERS FOR ROD DROP AND EJECTED ROD TESTS

PRAIRIE ISLAND UNIT 1, CYCLE 1

TRANSIENT	PARAMETER	FSAR**	CALCULATED	MEASURED
Ejected Rod				
2% Power	F_Q	6.26*	5.19	5.34
K-7	$F_{\Delta H}$	3.53***	3.48	3.51
	Worth	730* pcm	603 pcm	720 pcm
Ejected Rod				
30% Power	F_Q	4.34*	2.15	2.10
K-7	$F_{\Delta H}$	2.45***	1.60	1.56
	Worth	460* pcm	55 pcm	57.5 pcm
Rod Drop				
50% Power	F_Q	2.51	2.24	2.27
K-7	$F_{\Delta H}$	1.84+	1.63	1.66
Rod Drop				
50% Power	F_Q	2.51	2.11	2.16
H-8	$F_{\Delta H}$	1.74+	1.56	1.59

* FSAR Table 14.2-2

\+ FSAR Amendment #24, supplementary information for WCAP-8090

** FSAR values used in safety analysis

*** Estimated Values

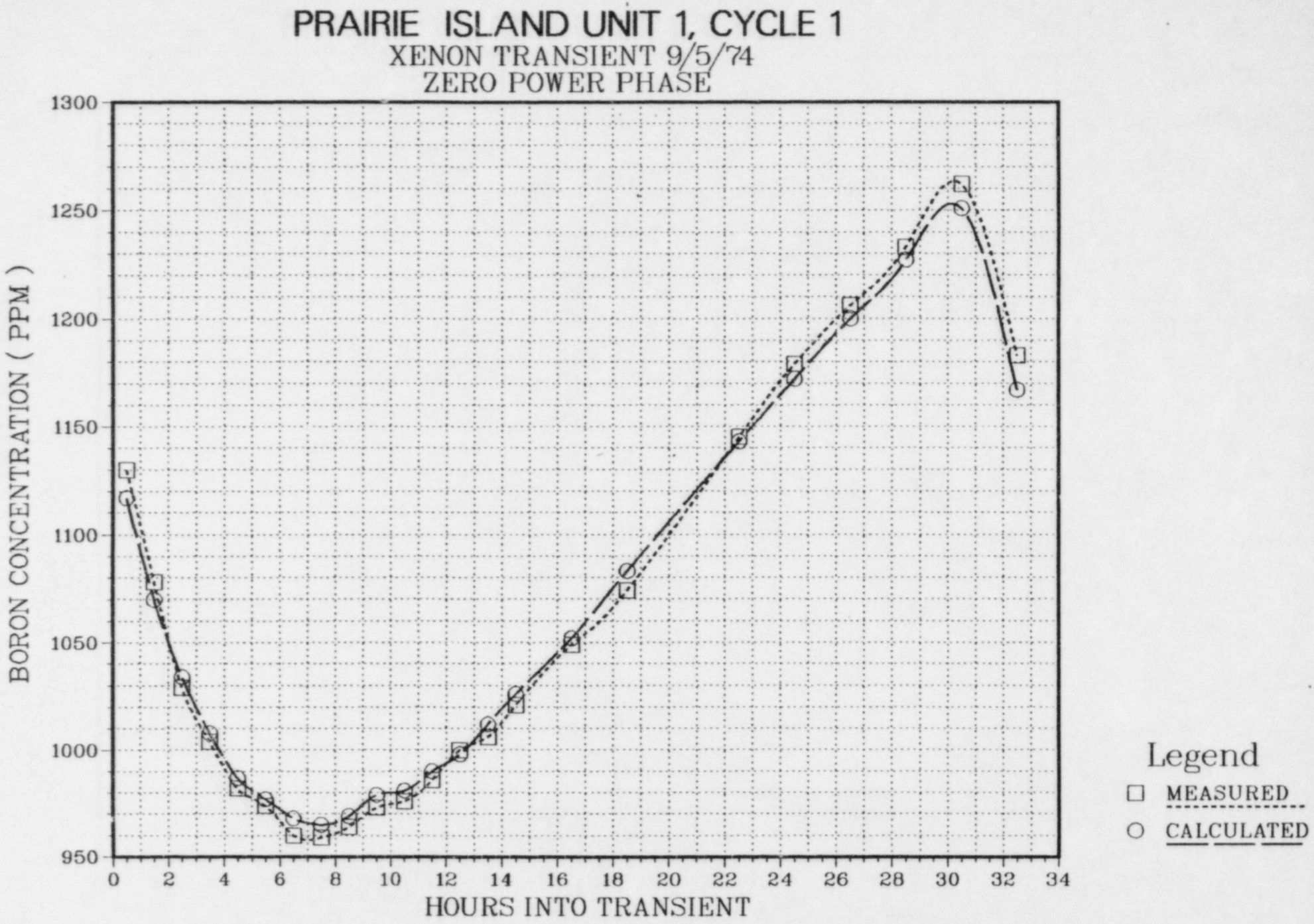


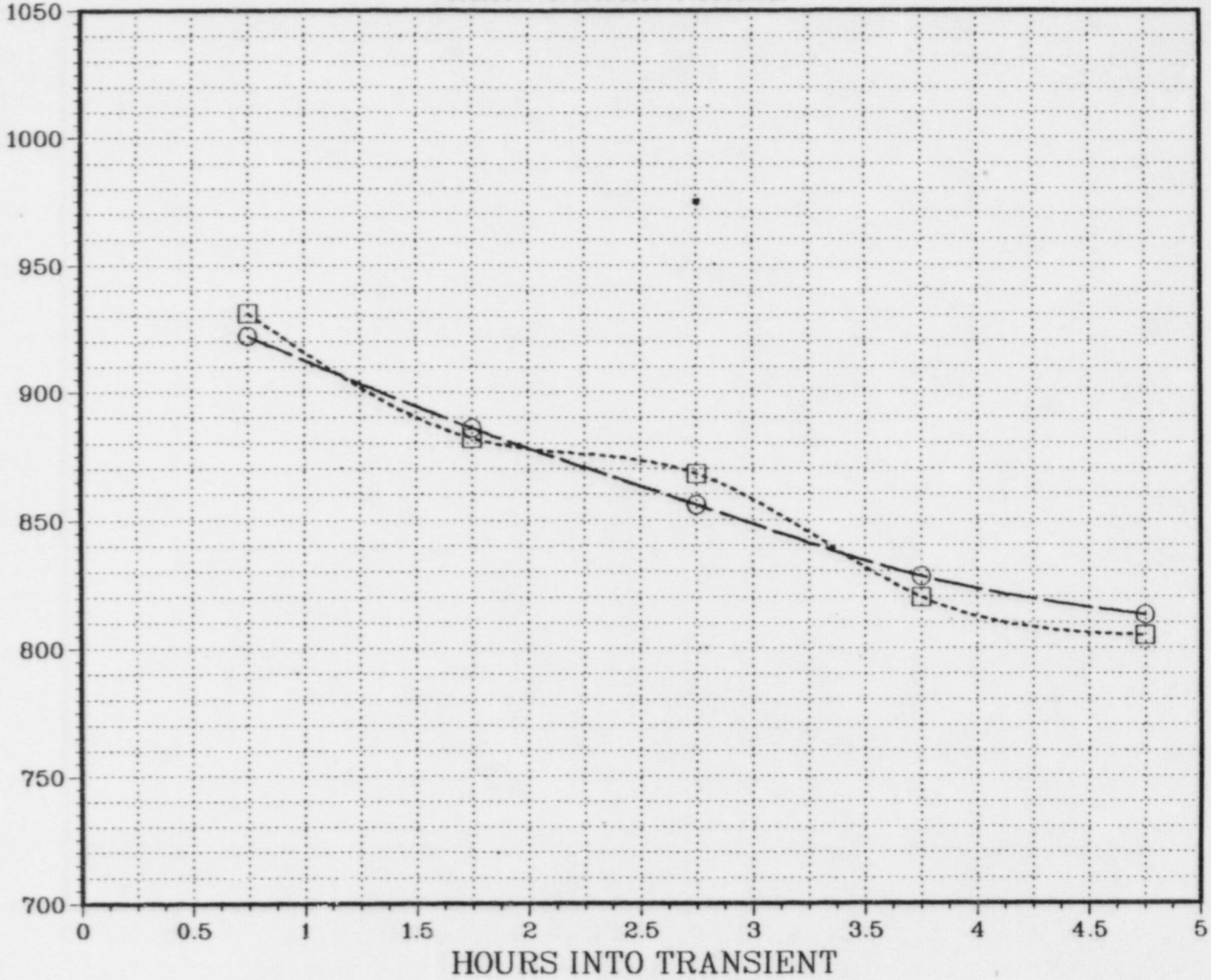
FIGURE 3.6.1

NUCLEAR ANALYSIS DEPT.

PRAIRIE ISLAND UNIT 1, CYCLE 2

XENON TRANSIENT 5/26/76

ZERO POWER PHASE



Legend

□ MEASURED

○ CALCULATED

FIGURE 3.6.2

NUCLEAR ANALYSIS DEPT.

3.7 Reliability Factors for Delayed Neutron Parameters

This section deals with determining reliability factors for values which can be calculated but not measured. In these cases, an argument may be made for the general magnitude of the reliability factor without making direct comparisons between measured and predicted values.

The importance of the reliability of the calculated values of the delayed neutron parameters is primarily associated with the core β_{eff}. The uncertainties in the calculation of β_{eff} are composed of several components, the most important of which are listed below:

a. Experimental values of β, and λ, by nuclide;
b. Calculation of the spatial nuclide inventory;
c. Calculation of core average β as a flux weighted average over the spatial nuclide inventory;
d. Calculation of β_{eff} from the core average as $\beta_{eff} = I*\beta$, where I = importance factor.

The experimental determination of the β's and λ's are assumed to be accurate to within 1%. The most important nuclide concentrations with respect to core β are U^{238}, U^{235} and Pu^{239}. Tables 3.4.1 and 3.4.2 inidcate that the uncertainty in the calculation of these parameters is about 1.7% for ECELL and -0.3 for CASMO. Therefore, components a) and b) above are combined as 2.7% for ECELL and 1.3% for CASMO.

The uncertainty in the calculation of a core average β depends on the relative flux weighting of the individual assemblies in the core. For demonstration purposes, consider a three region core, each with a different average burnup and average β. This is typical of advanced PWR cycles in that about a third of the core

has seen two previous cycles, a third only one previous cycle and a third is the feed fuel. Typical regional β's are given below:

Region 1 (third cycle fuel) β = 0.005
Region 2 (second cycle fuel) β = 0.006
Region 3 (feed fuel) β = 0.007

The effect of errors in the calculated flux distribution can be evaluated in terms of the effect on the core average β. As a base case, flux weighting factors (FWF) are all set to 1.0. In this case, the core average β = 0.006. Using a maximum error in the regional flux weighting of 7.0%, the worst error in the calculation of the core average β is obtained by increasing the weight of the Region 1 fuel and decreasing the weight of the Region 3 fuel. It should be noted that the average relative weighting factor is unity. The revised β is calculated as follows:

β(1) x 1.07 = .00535
β(2) x 1.0 = .0060
β(3) x 0.93 = .00651
β = .00595, which yields a -0.8% error for component c) above.

The last uncertainty component, d), concerns the reduction of core average β to obtain β_{eff} by using the importance factor. Since this reduction is computed to be about 3 to 4%, an error of 10% in this computation would lead to an error in β_{eff} of less than 0.5%.

The sum of the errors for these four factors for ECELL and CASMO are as follows:

$$\text{ECELL} - 2.7\%(a+b) + 0.8\%(c) + 0.5\%(d) = 4.0\%$$
$$\text{CASMO} - 1.3\%(a+b) + 0.8\%(c) + 0.5\%(d) = 2.6\%$$

So the reliability factor for delayed neutron parameters is set at 4%.

3.8 Effective Neutron Lifetime

An argument similar to the delayed neutron parameter argument is applied to the determination of the effective neutron lifetime (ℓ^*) uncertainty. The uncertainty components which go into the calculation of ℓ^* are as follows:

(a) Experimental values of microscopic cross sections;
(b) Calculation of the spatial nuclide inventory; and
(c) Calculation of the core average effective neutron lifetime, ℓ^*, as a flux weighted average over the spatial nuclide inventory which includes the effects of leakages.

Uncertainties for components (a) and (b) are assumed to be the same as described for the calculation of β_{eff}, that is, 1% uncertainty in the experimental determination of nuclear cross section and 1.7% uncertainty in the determination of the spatial nuclide inventory for ECELL and -0.3% for CASMO. The core average neutron lifetime depends on flux weighting of local absorption lifetimes ℓ^*. If a conservative estimate of the error in regional power sharing (7%) is used in determining the impact on the core average lifetime (ℓ^*), the error in lifetime is on the order of 1.0%. Combining all of these uncertainties linearily results in a total uncertainty of 3.7% for CPM and 2.3% for CASMO. Therefore, a 4% reliability factor will be applied to the neutron lifetime calculation when applied to safety related calculations.

4.0 Model Applications to Reactor Operations

This section describes the methods used in applying the reliability factors and biases to reactor operations. It is not the intent of this section to define the procedures used. However, some aspects of these procedures are presented in order to clarify the approach taken in applying the model reliability factors and biases.

4.1 Power Distributions

Two categories are considered for application of calculated power distributions to reactor operations, predictive and monitoring. In the case of the predictive calculation, a best estimate of a future core state is desired and therefore only the power distribution biases in Table 3.0.1 are applied to the predicted distributions.

In the case of the monitoring application, the intent is to supply design input data to the flux map code. NSP intends to continue using the Exxon DETECTOR code for this purpose. The use of the current F_Q and $F_{\Delta H}$ measurement uncertainties were evaluated by comparing predicted versus measured integrated detector responses. This was done by comparing the results of the Detector program from two cases, one with Detector PDQ constants from the NSP model and the other using EXXON PDQ data. The results of these comparisons are shown in Table 4.1.1. The results show that the standard deviations calculated using NSP supplied data are less than those calculated using EXXON data. Therefore the current technical specification measurement uncertainties will be used.

4.2 Isotopic Inventory

The calculation of the isotopic inventory for Prairie Island

is based upon two-dimensional, CASMO calculation. This is the same model as is used to calculate the flux map design input. Therefore, the accuracy of the burnup distribution can be verified by the agreement of the measured and calculated reaction rates which is used to evaluate the measurement uncertainties in Section 4.1 above. The accuracy of the isotopics versus local exposure is described in Section 3.4 above based on measurements at Saxton and Yankee.

TABLE 4.1.1

STANDARD DEVIATION OF RELATIVE DETECTOR RESPONSE ERRORS

AXIAL LEVEL 2 (MIDDLE 11 FEET)

MAP	σ(NSP) NSP INPUT PDQ DECK	σ (ENC) EXXON INPUT PDQ DECK
107-23	2.01	3.17
107-26	1.97	3.32
107.27	1.99	3.67
107-28	2.01	3.86
107-29	1.98	4.13
107-30	2.08	4.05

σ (M-C/M * 100)

M = Measured Detector Response

C = Calculated Detector Response Input from PDQ Deck

5.0 Model Applications To Safety Evaluation Calculations

This section describes the methods used in applying the reliability factors and biases to the results of safety related physics calculations. It is not the intent of this section to define the procedures to be used in performing the physics calculations. However, some aspects of these procedures are presented in order to clarify the approach taken in applying the model reliability factors and biases.

In such applications the question is generally: Will the reload core maintain a safe margin to established safety limits (i.e., peak linear heat rate, minimum DNBR, shutdown margin, etc.) under normal and non-normal or accident conditions? The question is usually answered by comparing the calculated kinetics, reactivity, and power distribution parameters of the reload core to those used in the analysis of each accident/occurrence described in a reference safety analysis - usually the Final Safety Analysis Report.

For each parameter of interest, RF_X and $Bias_X$ are given in Table 3.0.1. The application of the RF_X and $Bias_X$ for each parameter of interest is shown below.

5.1 Nuclear Heat Flux Hot Channel Factor, F_Q^N

The nuclear heat flux hot channel factor, F_Q^N, is defined as the maximum local fuel rod linear heat generation rate (LHGR) divided by the average fuel rod LHGR, assuming nominal fuel pellet and rod parameters. Calculations of F_Q^N are performed using the three-

dimensional power distribution obtained from the nodal code coupled with local peak pin to assembly power ratios obtained from the quarter core PDQ model. The general approach is as follows:

$$F_Q^N(i,j,k,m,n) = F_{assy}(i,j,k)*F_{pin}(i,j,k,m,n)$$

where:

i,j are discrete assembly coordinates

k is a continuous axial coordinate

m,n are discrete pin coordinates within a given assembly

$F_{assy}(i,j,k)$ is the relative power density in an axial slice of assembly i,j

$F_{pin}(i,j,k,m,n)$ is the ratio of the power density in pin m,n at level k to the average pin power density at level k, within assembly i,j

The model reliability factor and bias listed in Table 3.0.1 are then applied as follows:

$$F_Q^N = (F_Q^N(MODEL)+RF+Bias\ F_Q)*(1+T)$$

where T is azimuthal Tilt.

5.2 Nuclear Enthalpy Rise Hot Channel Factor, $F_{\Delta H}$

The nuclear enthalpy rise hot channel factor is defined as the ratio of the integral of linear power along the rod on which the minimum DNBR occurs to the core average integral power. Calculations of $F_{\Delta H}$ are based on three dimensional power distributions obtained with the nodal code coupled with local peak

pin to assembly power ratios obtained from the quarter core PDQ model. The general approach is given in Section 3.5.2.

The model reliability factor and bias listed in Table 3.0.1 are then applied as follows:

$$F_{\Delta H} = (F_{\Delta H}(MODEL)+RF_{\Delta H} + Bias\ F_{\Delta H}) * (1+T)$$

5.3 Rod Worths

Rod worths are calculated using the three-dimensional nodal model. Worths are determined by varying the rod position while the independent core parameters such as core power and boron are held constant.

The model reliability factor and bias listed in Table 3.0.1 are then applied as follows:

$$\Delta\rho_{ROD} = (\Delta\rho_{ROD}(MODEL)+Bias)*(1\pm RF_{ROD})$$

The reliability factor is either added or subtracted, whichever is most conservative for each particular application.

5.4 Moderator Coefficient (α_m)

The moderator coefficient is a measure of the change in reactivity due to a change in specific coolant density parameters such as density, temperature, and pressure.

The moderator temperature coefficient is obtained by varying the core average temperature in nodal calculations while holding all other parameters constant.

The model reliability factor and bias listed in Table 3.0.1 are applied as follows:

$$\alpha_m = \alpha_m(\text{MODEL}) + \text{Bias}_m \pm RF_m$$

The reliability factor is either added or subtracted, whichever is most conservative for each particular application.

5.5 Fuel Temperature (Doppler) Coefficient (α_D)

The Doppler coefficient is a measure of the change in core multiplication associated with a change in fuel temperature. Core reactivity is changed mainly due to Doppler broadening of the U_{238} parasitic resonance absorption cross section due to increases in fuel temperature. This effect is calculated by first calculating the power coefficient. This is the change in core reactivity associated with a change in power, and is composed of changes due to moderator and fuel temperature changes. The 3D nodal code is used to calculate power coefficients as a function of power and exposure. The Doppler coefficient is then calculated by removing the moderator temperature coefficient component from the power coefficient.

The model reliability factor and bias listed in Table 3.0.1 are then applied as follows:

$$\alpha_D = (\alpha_D(\text{MODEL}) + \text{Bias}_D) * (1 \pm RF_D)$$

The reliability factor is either added or subtracted, whichever is most conservative for each particular application.

5.6 Boron Concentration Coefficient (α_B)

The boron concentration coefficient is a measure of the change in core neutron multiplication factor associated with a change in boron concentration. Calculations of α_B are performed in three dimensions with the nodal code.

The model reliability factor and bias listed in Table 3.0.1 are then applied as follows:

$$\alpha_B = (\alpha_B(\text{MODEL}) + \text{Bias}_B) * (1 \pm RF_B)$$

The reliability factor is either added or subtracted, whichever is most conservative for each particular application.

5.7 Effective Delayed Neutron Fraction (β_{eff})

Average delayed neutron fractions are determined by weighting local values from each fissile nuclide by the appropriate fission sharing as determined from PDQ. This result is then reduced by the importance factor, I, to account for the effects of reduced fast fissioning, increased resonance escape, and decreased fast leakage. Finally, the reliability factor listed in Table 3.0.1 is applied as shown below.

$$\beta_{eff} = (1 \pm RF_\beta) * \beta_{eff}(\text{MODEL})$$

5.8 Prompt Neutron Generation Time (ℓ^*)

The prompt neutron generation time is calculated as a function of core exposure from two-dimensional PDQ calculations. This is

accomplished by using two-group flux weighted PDQ parameters to compute the slowing down time and the thermal diffusion time, based on the 1/v nature of the boron cross section. Finally, the reliability factor listed in Table 3.0.1 is applied as shown below:

$$\ell^* = (1 \pm RF_{\ell^*})^* \ell^*(MODEL)$$

5.9 Shutdown Margin (SDM)

Upon receiving a signal for reactor trip, the control rods are allowed to free fall into the active core. Consistent with NRC General Design Criteria 27, the highest worth control rod is assumed to remain untripped in its full out position. This negative reactivity insertion caused by the rods entering the core is offset in part by positive insertions due to decreases in fuel temperature (Doppler defect), moderator temperature, and flux redistribution. The resulting net reactivity is the shutdown margin. In evaluating the negative reactivity used for a reactor trip in the safety accident analyses, shutdown margin calculations are performed using the 3D nodal model.

The calculation is performed at both BOL and EOL and consists of determining the highest worth stuck rod and shutdown reactivity. Consideration is given to the range of initial power, xenon distributions and control rod initial positions consistent with the power dependent insertion limits. The first case is performed at the power, xenon, and control rod positions being considered. The second case is performed at HZP with all rods in except the stuck rod. The third case is performed at HZP conditions with the rod positions from case 1. The shutdown margin is computed as the change in core reactivity between case one and two. The shutdown margin is conservatively adjusted using model reliability factors

and biases applied to the inserted rod worth, the moderator temperature defect, and the Doppler defect as discussed in Section 5.3, 5.4, and 5.5 as follows:

	BOC	EOC
1. Reactivity required for shutdown		
Case 1 (K_{eff})		
Case 3 (K_{eff})		
.. Power defect (moderator and doppler)	(pcm)	(pcm)
where defect = (Case 3 - Case 1)		
$+(RF_D * \rho_D) + (RF_M * \Delta T)$		
Required shutdown margin	1000 pcm	2000 pcm
Total reactivity required for shutdown	(pcm)	(pcm)
2. Reactivity available for shutdown		
Case 1 (K_{eff})		
Case 2 (k_{eff})		
N-1 Rod Worth	(pcm)	(pcm)
where worth = (Case 1 - Case 2) * $(1-RF_{Rods})$		
3. Excess shutdown margin		

5.10 Scram Worth Versus Time

Scram worth insertion rates used in safety analyses are evaluated for conservatism in two components. First, empirical data relating rod position to time after rod release is normalized such that the total time is equal to or greater than the limits defined by the technical specification. Secondly, the 3D nodal model is then used to obtain reactivity insertion versus rod position. This positional insertion dependence is converted into a time dependent function using the position versus time curve.

The model reliability factor and bias are applied in the same manner as for rod worth, described in Section 5.3.

6.0 REFERENCES

1. Advanced Recycle Methodology Program (ARMP) System Documen-tation, EPRI CCM-3 Research Project 118-1, September, 1977.

2. M. Edenius, A. Ahlin, H. Haggblom "CASMO-2 Users Manual," Studsvik Energiteknik AB, Studsvik/NR-81/3.

3. Cadwell, W.R., "PDQ-7 Reference Manual," WAPD-TM-678, Westinghouse Electric Corporation (January, 1967).

4. R. Breen, O. Marlowe, C. Pfeifer, "Harmony: System for Nuclear Reactor Depletion Computation," WAPD-TM-478, Westinghouse Electric Corporation (January, 1965).

5. M. Edenius, A. Ahlin, H. Haggblom, "CASMO, A Cell and Assembly Spectrum Code," Studsvik Energiteknik AB, Studsvik/RF-77/6276. See also A. Ahlin, M. Edenius, H. Haggblom, "CASMO, A Fuel Assembly Burnup Program," Studsvik Energiteknik AB (Formerly AB Atomenergi), AE-RF-76-4158 (rev. ed.).

6. A. Ahlin, "DIXY-A Two Dimensional Diffusion Theory Code," Studsvik Energiteknik AB. See also ARMP Documentation (Ref. 1 above), Part 1, Chapter 5.

7. Bevington, Phillip, R., "Data Reduction and Error Analysis for the Physical Sciences." McGraw-Hill Book Company, New York, 1969.

8. D.B. Owen, "Factors for One-Sided Tolerance Limits and for Variables Sampling Plans" Sandia Corporation, March 1963.

9. M. Edenius, "Studies of the Reactivity Temperature Coefficient in Light Water Reactors," AE-RF-76-3160, AB Atomenergi, 1976.

10. M. Edenius, "Seminar on U-238 Resonance Capture," S. Pearlstein, Editor, P. 87, BNL-NCS-50451, 1975.

11. M. Edenius, "Temperature Effects in Thermal Reactor Analysis," Internal Report presented to Oskarshamnuerkets Kraftgrupp AB(OKG), Stockholm, Sweden, employed by AB Atomenergi Studsvik, Sweden.

12. M.G. Kendall, A. Stuart "The Advanced Theory of Statistics" Vol. 1, 3rd Ed., Hafner Publishing Co., N.Y., 1969.

APPENDIX A

STATISTICAL METHODS FOR THE DETERMINATION

AND APPLICATION OF UNCERTAINTIES

The purpose of using statistical methods is to determine the value X_c (calculated) such that there is a 95% probability at the 95% confidence level that X_c will be conservative with respect to X_t (true value) when applying the calculational methods to safety related reactor analyses.

The first step is to determine whether or not a distribution is normal. If it is, the methods described in Section A.1 are used. If the distribution cannot be treated as normal, but the distributions are known, then the methods described in Section A.2 are used.

If neither of the above methods apply then the parameter in question is conservatively bounded.

A.1 Application of Normal Distribution Statistics

Separation of Measurement and Calculational Uncertainties

Comparison of measured and calculated reactor parameters include the effects of both the measurement and calculational uncertainties. Methods used in this report to isolate the calculational uncertainties are described below in terms of the following definitions:

X_T = true reactor parameter

X_M = measured reactor parameter

X_C = calculated reactor parameter

$e_M = X_M - X_T$ = measurement error

$e_C = X_C - X_T$ = calculation error

$e_{MC} = X_M - X_C$ = observed differences

$\mu_i = e_i$ = mean error

$$\sigma_i = \left(\left[\frac{1}{(N-1)}\right]\Sigma(e_i-\mu_i)^2\right)^{\frac{1}{2}} \quad = \text{standard deviation}$$

$$m^2_{i(A)} = \frac{1}{(N-1)}\ \Sigma(e_i - A)^2 = \text{second moment about an arbitrary origin A}$$

If e_M and e_C are independent, then the following relationships exist.[7] (Note that these relationships apply for non-normal distributions as well).

$$\sigma_c^2 = \sigma^2_{MC} - \sigma_M^2$$

$$\mu_c = \mu_M - \mu_{MC}$$

Once the σ_C and μ_C have been calculated from historical data, they could be used to apply conservatism to future calculations of reactor parameters, X_C, as follows:

$$X_C = X_C - \mu_C + K_c\sigma_c$$

The factor K_c is defined as described in Table A.1.[8] to provide a 95% probability at the 95% confidence level that X_C is conservative with respect to the true value, X_T.

Reliability Factors

It is the objective to define reliability factors which are to be used to increase/decrease calculated results to the point where there is a 95% probability at the 95% confidence level that they are con-servative with respect to actual reactor parameters.

For any given application, we are only concerned with one side of the component; that is, if the calculated value is too large or too small. We may therefore use one-sided tolerance limits based on normal distributions to find a K_c which will give a 95% probability at the 95% confidence level to the reliability factor defined by

$$RF = K_c * \sigma_c$$

Numerical values of K_c for various sample sizes used to calculate σ_c are provided on Table A.1.[8]

TABLE A.1

SINGLE-SIDED TOLERANCE FACTORS

n^1	k_c
2	26.26
3	7.66
4	5.15
5	4.20
6	3.71
7	3.40
8	3.19
9	3.03
10	2.91
11	2.82
12	2.74
15	2.57
20	2.40
25	2.29
30	2.22
40	2.13
60	2.02
100	1.93
200	1.84
500	1.76
∞	1.645

1 n = Number of data points used for σ

If n falls between two numbers on the table, the larger of the k_c's should be used.

A.2 Application of Non-Normal Distribution Statistics

If a distribution is determined to be other than normal the requirement is that there is a 95% confidence level that X_c will be conservative with respect to the true value X_m. (In the following, the notation used is consistent with that defined in Section A.1). It is thus required that a 95% upper confidence limit be determined for the 95th percentile of the distribution of errors.

In the calculation, a set of error observations (e_i) are determined. The mean (μ_m) and the standard deviation (σ_{mc}) are calculated using the following formulation:

$$\mu_{mc} = \frac{\sum_{i=1}^{n} e_i}{n}$$

$$\sigma_{mc} = \left[\frac{\sum_{i=1}^{n} (e_i - \mu_{mc})^2}{n-1}\right]^{\frac{1}{2}}$$

Note that the e_i above are determined from the following:

$$e_i = e_{mc} = X_m - X_c = \text{observed differences}$$

Generally, the e_{mc} are taken from several cycles of operation thus they represent the true distribution. The e_i are then transformed to standard measure by the following formula:

$$Z_i = \frac{e_i - \mu_{mc}}{\sigma_{mc}}$$

and the resulting variates (z) are sorted into ascending order and the kth (such that K≥.95n) variate is chosen as an estimate of the 95th percentile of the distribution (See reference 12, page 40-41). This gives a 95th percentile of z to be Q_{95}. This implies that 95% of the errors are likely to be less than Q_{95}.

It remains to calculate a 95% confidence interval on Q_{95}. (The formula for this calculation is taken from reference 12 page 236-243.):

$$\text{Var } Q_{95} = \frac{q(1-q)}{n f_1^2}$$

where: q = the quantile (.95)
n = number of independent observations in the sample
f_1 = ordinate of the density function of the distribution of observed differences at abscissa q

It is necessary to determine if the observations are independent. If they are not independent, it is necessary to reduce the sample size to account for the dependence in the determination of the 95% confidence level.

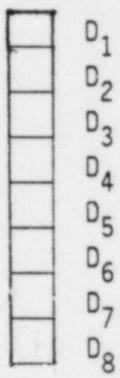


Figure 1. Differences for Nearby Positions

To set notation, let $\delta_{.95}$ be the population 95th percentil for the observed differences, that is $P[D_i \leq \delta_{.95}] = .95$. We wish to determine a 95% upper confidence limit for $\delta_{.95}$ when some of the differences are dependent. For differences observed at adjacent positions, the appropriate measure of association for our analysis can be shown to be

$$C(1) = P[D_1 \leq \delta_{.95} \text{ and } D_2 \leq \delta_{.95}] - (.95)^2$$

We also consider the association of differences observed at locations two apart

$$C(2) = P[D_1 \leq \delta_{.95} \text{ and } D_3 \leq \delta_{.95}] - (.95)^2$$

and, more generally,

$$C(k) = P[D_1 \leq \delta_{.95} \text{ and } D_{1+k} \leq \delta_{.95}] - (.95)^2$$

for k = 1,2,3,4,5,6,7 locations apart. In this example, there are 8 differences D_i, 7 adjacent pairs (D_i, d_{i+1}), 6 pairs with indicies two apart (D_i, D_{i+2}) ..., 1 pair $D_1 D_8$.

Let $d_{(s)}$ be the sample 95th percentile with s selected to be the smallest integer not less than .95n. The large sample distribution of $d_{(s)}$ depends on that of

$$T(x) = \text{number of differences, } D_i, \text{ that are less than or equal x.}$$

Even with dependence among the D_i,

$$\frac{T(x)-nF(x)}{\text{s.d.}[T(x)]} = \frac{\frac{1}{\sqrt{n}}(T(x)-nF(x))}{\frac{1}{\sqrt{n}}\,\text{s.d.}[T(x)]}$$

will be approximately standard normal. Here $F(x) = P[D_i \le x]$ and $f(x)$ is the probability density function for the observed differences.

It follows that

$$P[\sqrt{n}(d_{(s)}-\delta_{.95}) \le z] = 1 - P[T(\delta_{.95} + n^{-\frac{1}{2}}z) \le s-1]$$

$$\sim 1 - \Phi\left[\frac{-f(\delta_{.95})z}{\frac{1}{\sqrt{n}}\text{s.d.}[T(\delta_{.95})]}\right]$$

where

$$\left[\frac{1}{\sqrt{n}}\text{s.d.}[T(\delta_{.95})]\right]^2 = \frac{1}{n}\left[n(.95)(.05)+2\tfrac{7}{8}nC(1)+2\tfrac{6}{8}nC(2)+\ldots+\tfrac{2}{8}nC(7)\right]$$

$$= (.95)(.05)+\tfrac{14}{8}C(1)+\tfrac{12}{8}C(2)+\tfrac{10}{8}C(3)+\ldots+\tfrac{2}{8}C(7).$$

Under independence $0 = C(1) = C(2) = \ldots = C(7)$ and this expression reduces to its customary value $(.95)(.05)$. If the differences are dependent, the variance of $d_{(s)}$ is

$$\frac{1}{n}\frac{(.95)(.05)}{f^2(\delta_{.95})}\left[1 + \sum_{k=1}^{7}\frac{2(8-k)C(k)}{8(.95)(.05)}\right]$$

In order to apply this result, we estimate $C(1)$ by

$$\hat{C}(1) = \frac{\#\text{ adjacent pairs } (D_i, D_{i+1}) \text{ where both} \le d_{(s)}}{\text{Total \# of adjacent pairs}} - (.95)^2.$$

The estimate of C(2) is

$$\hat{C}(2) = \frac{\#\text{ pairs } (D_i, D_{i+2}) \text{ where both} \le d_{(s)}}{\text{Total \# of pairs } (D_i, D_{i+2})} - (.95)^2$$

and

$$\hat{C}(k) = \frac{\#\text{ pairs } (D_i, D_{i+k}) \text{ where both} \le d_{(s)}}{\text{Total \# of pairs } (D_i, D_{i+k})} - (.95)^2$$

for k = 3,4,5,6,7. The value of $f^2(\delta_{.95})$ can be estimated as previously suggested. Then, the large sample upper 95% confidence limit for $\delta_{.95}$, adjusted for dependence among differences by location is given by

$$d_{(s)} + \frac{1.645}{\sqrt{n}} \left[\frac{(.95)(.05)}{f^2(\delta_{.95})} \left(1 + \sum_{k=1}^{7} \frac{2(8-k)\hat{C}(k)}{8(.95)(.05)} \right) \right]^{\frac{1}{2}}.$$

One interpretation of this confidence limit, or the variance expression, is that the total sample size n is effectively reduced by the dependence. We estimate the effective sample size to be

$$\frac{n}{1 + \sum_{k=1}^{7} \frac{2\,(8-k)\hat{C}(k)}{8(.95)(.05)}}$$

If only two terms are used, the effective sample size is estimated to be

$$n \left[\frac{(.95)(.05)}{(.95)(.05) + \frac{14}{8}\hat{C}(1) + \frac{12}{8}\hat{C}(12)} \right]$$

It is necessary to obtain an estimate of f_1 (.95) on a short interval of the cumulative distribution function of z in the region of the 95th percentile. The slope of the cumulative distribution function is an estimate of the ordinate of the density function since the density function is simply the derivative of the cumulative distribution function. Thus

$$\sigma Q_{95} = \text{Var } Q_{95}$$

This value then allows an estimate of the 95% confidence limit on Q_{95}. Even though nothing is known about the distribution of Q_{95}, the distribution can be shown to be normal using the following derivation.

$$P[D_1 \leq \delta_{.95} \text{ and } D_2 \leq \delta_{.95}]$$

where $\delta_{.95}$ is the 95th percentile of the distribution of differences. If the differences D_1 and D_2 are independent

$$P[D_1 \leq \delta_{.95} \text{ and } D_2 \leq \delta_{.95}] = P[D_1 \leq \delta_{.95}] \text{ and } P[D_2 \leq \delta_{.95}]$$

$$= (.95)(.95) = (.95)^2.$$

The difference

$$P[D_1 \leq \delta_{.95} \text{ and } D_2 \leq \delta_{.95}] - (.95)^2$$

is a measure of association (dependence) from position to adjacent position.

Note that if

$$I(D_1 \leq \delta_{.95}) = \begin{cases} 1 \text{ if } D_1 \leq \delta_{.95} \\ 0 \text{ if } D_1 > \delta_{.95} \end{cases}, \quad I(D_2 \leq \delta_{.95}) = \begin{cases} 1 \text{ if } D_2 \leq \delta_{.95} \\ 0 \text{ if } D_2 > \delta_{.95} \end{cases}$$

then the covariance is

$$C(1) = \mathrm{Cov}(I(D_1 \le \delta_{.95}), I(D_2 \le \delta_{.95})) = P[D_1 \le \delta_{.95} \text{ and } D_2 \le \delta_{.95}] - (.95)^2.$$

We assume the same covariance for $I(D_2 \le \delta_{.95})$ and $I(D_3 \le \delta_{.95})$

... $I(D_7 \le \delta_{.95})$ and $I(D_8 \le \delta_{.95})$. There are about n 7/8 such pairs among the whole set of n observed differences.

Let $d_{(s)}$ be the sample 95th percentile where s is the smallest integer not less than n(.95). When n is large

$$\hat{C}(1) = \frac{\#\text{ pairs } (D_i, D_{i+1}) \text{ both} \le d_{(s)}}{\text{Total number of pairs } (D_i, D_{i+1})} - (.95)^2$$

is a good estimate of C(1). Similarly, for the approximately 6n/8 pairs $(D_i, , D_{i+2})$

$$C(2) = \mathrm{Cov}[I(D_1 \le \delta_{.95}),\ I(D_3 \le \delta_{.95})]$$

is estimated by

$$\hat{C}(2) = \frac{\#\text{ pairs } (D_i, D_{i+2}) \text{ both} \le d_{(s)}}{\text{Total number of pairs } (D_i, D_{i+2})} - (.95)^2$$

and

$$\hat{C}(k) = \frac{\#\text{ pairs } (D_i, D_{i+k}) \text{ both} \le d_{(s)}}{\text{Total number of pairs } (D_i, D_{i+k})} - (.95)^2$$

Let us now see how to modify the proof that $d_{(s)}$ is asymptotically normal in order to account for the dependence among adjacent differences. It is still true that

(A1) $$P[d_{(s)} \le x] = 1 - P[d_{(s)} > x] = 1 - P[s-1 \text{ or fewer } D_1 \le x]$$

$$= 1 - P[T(x) < s]$$

where $T(x) = \sum_{i=1}^{n} I(D_i \le x) = \#$ differences $D_i \le x$. Moreover, $T(x) - nF(x)$ has mean 0 and, for large samples, is approximately normal under a wide range of dependence structures. Consequently, the sums $\sum_{i=1}^{8} I(D_i \le x)$ are independent of one another and each has the same distribution. Since $T(x)$ is just the sum of these group sums, the central limit theorem gives

$$\frac{T(x) - nF(x)}{\text{s.d.}[T(x)]} \text{ is approximately standard normal.}$$

Consequently, from (A1) and the normal approximation

$$P[\sqrt{n}(d_{(s)} - \delta_{.95}) \le Z] = P[d_{(s)} \le \delta_{.95} + n^{-\frac{1}{2}}z]$$

$$= 1 - P[T(\delta_{.95} + n^{-\frac{1}{2}}z) < s]$$

$$= 1 - \Phi\left[\frac{s - nF(\delta_{.95} + n^{-\frac{1}{2}} z)}{\text{s.d.}[T(\delta_{.95} + n^{-\frac{1}{2}} z]}\right]$$

Now, note that

$$\frac{1}{\sqrt{n}}\left(s - nF(\delta_{.95} + n^{-\frac{1}{2}} z)\right) = \frac{1}{\sqrt{n}}\left(s - nF(\delta_{.95}) - nf(\delta_{.95})n^{-\frac{1}{2}} z + O(1)\right)$$

$$= \frac{1}{\sqrt{n}}\left(s - n(.95) - n^{\frac{1}{2}} zf(\delta_{.95})\right) + O(1)$$

$$= -zf(\delta_{.95}) + O(1).$$

Furthermore,

$$\frac{1}{n}\text{Var}[T(\delta_{.95} + n^{-\frac{1}{2}}z)] = \text{Var}[I(D_1 \le \delta_{.95} + zn^{-\frac{1}{2}})]$$

$$+ \sum_{k=1}^{7} \frac{2(8-k)}{8} \text{Cov}[I(D_1 \le \delta_{.95} + n^{-\frac{1}{2}} z), I(D_{1+k} \le \delta_{.95} n^{-\frac{1}{2}} z)$$

which converges to

$$F(\delta_{.95}) - F^2(\delta_{.95}) + \sum_{k=1}^{7} \frac{2(8-k)}{8} \{P[D_1 \le \delta_{.95}, D_{1+k} \le \delta_{95}] - (.95)^2\}$$

$$= (.95)(.05) + \sum_{k=1}^{7} \frac{2(8-k)}{8} C(k) = \lim \frac{1}{n} \text{Var}[T(\delta_{.95})].$$

Therefore, by (A2),

$$P[\sqrt{n}(d_{(s)} - \delta_{.95}) \le z] \sim 1 - \Phi\left[\frac{-zf(\delta_{.95})}{\frac{1}{\sqrt{n}} \text{s.d.}[T(\delta_{.95})]}\right]$$

or $\sqrt{n}(d(s) - \delta_{.95})$ is approximately normal with mean 0 and variance

$$\frac{1}{n}\left[\frac{(.95)(.05) + \sum_{k=1} 2(8-k)C(k)/8}{f^2(\delta_{.95})}\right]$$

As we have indicated above, the C(k) may be estimated by $\hat{C}(k)$ and the large sample normality will still hold. Therefore using Table A.1 to obtain K_c:

$$\sigma Q_{95} = K_c \, (\text{Var } Q_{95})^{\frac{1}{2}}$$

Thus it is 95% certain that Q_{95} lies in the interval

$$Q_{95} - \lambda\sigma Q_{95} \leq Q_{95} \leq Q_{95} + \lambda\sigma Q_{95}$$

therefore it is safe to say that we are 95% confident that

$$Q_{95} \leq (Q_{95} + \lambda\sigma Q_{95})\sigma_{mc}$$

APPENDIX B

COMPUTER CODE SUMMARY DESCRIPTION

COMPUTER CODE	DESCRIPTION
CAP	Reformats CASMO-II output to match NUPUNCHER input to produce HARMONY input for PDQ.
CASMO-II	CASMO-II is a multigroup two-dimensional transport theory code for depletion and branch calculations for a single assembly. It calculates K_∞'s, M^2's and delayed neutron constants used to calculate input to the DP5 program and generates cross sections used by PDQ. Some of the characteristics of CASMO-II are: 1. 69 energy group cross section library 2. 12 energy groups are used during the two-dimensional transport calculations. 3. Gadolinium effective cross sections are generated by the MICBURN program. 4. A fundamental mode calculation is performed to account for leakage effects. 5. The predictor-corrector approach is used for depletion. 6. Effective resonance cross sections are calculated individually for each pin.

COMPUTER CODE	DESCRIPTION

7. A two-dimensional diffusion theory routine is used for automatic generation of effective cross sections for PDQ.

8. Simple user oriented input.

References 2, 5, and 6

CPM — CPM is a multigroup two-dimensional collision probability code for depletion and branch calculations for a single assembly.

Reference 1

DP5 — DP5 is a modified version of the EPRI-NODE-P computer program. The following is a list of improvements made:

1. Doppler reactivity Effect

EPRI-NODE-P uses:

$$\Delta\rho_{Dop}=B_{17}(1+B_{20}E)[(P_{ijk}\frac{P_{th}}{P_{rated}}(T_{Ave}^{UO_2}-T_{Ave}^{H_2O})+T_{Ave}^{H_2O})^{.5}-(T_{Ave}^{UO2})^{.5}]$$

DP5 uses:

For $E \leq DOP_1$

$$\Delta\rho_{Dop}=[DOP_2+DOP_3E+DOP_4E^2+DOP_5E^3][(DOP_{12}P_{ijk}\frac{P_{th}}{P_{rated}}(T_{Ave}^{UO_2}-T_{Ave}^{H_2O})+T_{Ave}^{H_2O})^{.5}-(T_{ave}^{UO_2})^{.5}]$$

COMPUTER CODE	DESCRIPTION

DP5 (Cont.)

For $E > DOP_1$

$$\Delta\rho_{DOP}=[DOP_6+DOP_7E+DOP_8E^2+DOP_9E^3][(DOP_{12}P_{ijk}\frac{P_{th}}{P_{rated}}(T_{Ave}^{UO_2}-T_{Ave}^{H_2O})+T_{Ave}^{H_2O})^{.5} - (T_{Ave}^{UO_2})^{.5}]$$

2. Xenon Reactivity Effect

EPRI-NODE-P uses:

$$\Delta\rho xe_{/Nxe} = B_{14}$$

DP5 uses:

$$\Delta\rho xe_{/Nxe} = B_{14}+B_{32}E+B_{59}E^2+B_{60}E^3$$

3. Reactivity Effect of Soluble Boron

EPRI-NODE-P uses:

$$\Delta\rho_{CB/N_{CB}} = B_{21}(1+B_{22}+B_{38}E^2)$$

DP5 uses:

$$\Delta\rho_{CB/N_{CB}} = B_{21}+B_{22}E+B_{38}E^2+B_{39}E^3+B_{40}E^4+(400-PPM)B_{31}$$

4. Reactivity Effect of Exposure

EPRI-NODE-P uses:

COMPUTER CODE	DESCRIPTION

DP5 (Cont.)

$$\Delta\rho_{exp} = B_{54} + B_{33}(E + B_{34}\ V) + B_{35}E^2 + B_{36}E^3 + B_{37}E^4$$

DP5 uses:

For $E \leq F_1$

$$\Delta\rho_{exp} = F_2 + F_3E + F_4E^2 + F_5E^3 + F_6E^4 + F_3F_7V$$

For $E > F_1$

$$\Delta\rho_{exp} = F_8 + F_9E + F_{10}E^2 + F_{11}E^3 + F_{12}E^4 + F_9F_{13}V$$

5. Reactivity Effect of Control Rod

EPRI-NODE-P uses:

$$\Delta\rho_{rod} = \Delta\rho^{rod}_{E=0}[(B_{31} - 1.0)\bar{E}B_{32} + 1.0]$$

DP5 uses:

$$\Delta\rho_{rod} = \Delta\rho^{rod}_{E=0}\ [B_{55} + B_{56}E + B_{57}E^2 + B_{58}E^3]$$

6. Treatment of Migration Area

EPRI-NODE-P uses:

$$M^2 = B_1 + B_2T + B_3T^2$$

COMPUTER CODE	DESCRIPTION

DP5 (Cont.)

DP5 uses:

$$M^2 = LPF(B_1+B_2T+B_3T^2)$$

Where LPF is a multiplier to M^2 for each I, J location as a function of core average exposure. It is calculated during the normalization procedure.

7. Delayed Neutron Constants

EPRI-NODE-P does not calculate delayed neutron constants.

DP5 calculates the core average delayed neutron constants.

8. Maximum Number of Axial Nodes

EPRI-NODE-P has a maximum of 12 axial nodes.

DP5 has a maximum of 24 axial nodes.

9. DP5 Additional Output Edits

- Axial offset - K_∞ - Power tilts - Xenon and iodine array edits - Core average delayed neutron constants

Reference 1

COMPUTER CODE	DESCRIPTION
	10. DP5 allows a different fuel type to be used at the top and bottom nodes.
EPRI-CELL	EPRI-CELL computes the space, energy and burnup dependence of the neutron spectrum within cylindrical cells of light water reactor fuel rods. It is used to generate cross sections for PDQ on a ECDATA file. Reference 1
FQ1	Calculates F_Q and $F_{\Delta H}$ using DP5 output nodal power distribution and PDE output pin powers from one or more 1/4 core PDQ.
HYDRO-P	HYDRO-P is the same program as EPRI-THERM-P and is used to calculate the power to flow relationship used by DP5. Reference 1
MICBURN	MICBURN calculates the burnup of a fuel pin containing gadolinium and generates 69 group effective cross sections as a function of number density for gadolinium to be used as input to CPM or CASMO-II. Reference 1
NUPUNCHER	NUPUNCHER prepares HARMONY cross section tables from cross section data on an ECDATA file. Reference 1
PDE	Reads PDQ output files and calculates pin powers used by the FQ1 program.

COMPUTER CODE	DESCRIPTION
PDQ7/HARMONY	PDQ7/HARMONY is a nuclear reactor analysis program which solves the neutron diffusion equations and preforms depletion calculations. References 1, 3
SHUFFLE	SHUFFLE is the same as EPRI-SHUFFLE and will read a PDQ7 concentration file and write a new updated concentration file. It is used to simulate assembly movement between cycles. Reference 1
SIGMA	SIGMA calculates the predicted detector reaction rates using DP5 nodal power distribution and 1/4 core PDQ7 detector reaction rate to assembly power factors. The predicted detector reaction rates are then compared to measured detector reaction rates.